Sliceforms

Deployable structures from interlocking slices

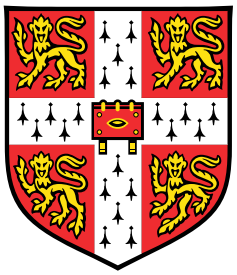

Timothy James Marvin Watson

Supervisor: Professor Keith A. Seffen

Department of Engineering
University of Cambridge

This dissertation is submitted for the degree of
Doctor of Philosophy

Corpus Christi College April 2021

Declaration

I hereby declare that except where specific reference is made to the work of others, the contents of this dissertation are original and have not been submitted in whole or in part for consideration for any other degree or qualification in this, or any other university. This dissertation is my own work and contains nothing which is the outcome of work done in collaboration with others, except as specified in the text and Acknowledgements. This dissertation contains fewer than 65,000 words including bibliography, footnotes, and equations and has fewer than 150 figures.

Timothy James Marvin Watson
April 2021

Abstract

A sliceform is a volumetric, honeycomb-like structure assembled from an array of cross-sectional planar slices that are interlocked via pairs of complementary slots placed along each intersection. If the slices are *thin*, these slotted intersections function as revolute joints, and the sliceform is foldable if the geometry of the embedded spatial linkage permits it, for example a *lattice sliceform* (LS) is bi-directionally flat-foldable. This thesis concerns a study of such sliceforms toward the design of novel deployable structures.

A sliceform torus, composed of two sets of inclined slices arranged at regular intervals about a central axis of symmetry, has been discovered to exhibit a surprising and intriguing folding action whereby its incomplete form can be collapsed to a flat-folded stack of coplanar slices. On deployment, the assembly expands smoothly about an arc until the slices have rotated to their design inclination, then, without reaching any apparent physical limit, abruptly 'locks out'. With a full complement of slices, the outermost intersections can be interlocked to complete and rigidify the ring. The torus is an example of a *rotational sliceform* (*RS*), and analysis of these structures proceeds by noting that their structural geometry comprises an array of pyramidal cells that is commensurate to a spherical scissor grid. The conditions for flat-foldability are determined by examination of the intrinsic geometry of each cell; the incompatibility of the slices with apparent rigid-folding revealed by assessment of the extrinsic motion of the slices. Investigation of their compliant kinematics reveals the articulation to be a bistable transition admitted by small transverse deflections of the slices.

This structural form is generalised by development of a technique for generating sliceforms along a smooth spatial curve – *curve sliceforms* (*CS*). Their synthesis is more involved than for an RS, but a range of sliceform 'tubes' are generated and manufactured. Each example retains the flat-foldable, deployable characteristic of an RS, despite the apparent intrinsic rigidity of each constituent *skew cell*. Examination of the small-scale models indicates that deployable motion is achieved via imperfect action of the slots, and a simple model of the articulation of a single cell is constructed to investigate how this proceeds, verifying that motion is kinematically admissible via local deformations.

Keywords: Deployable structures, Sliceforms, Slices, Interlocking, Flat-folding, Compliant-folding, Bistability

Acknowledgements

First and foremost, my deepest gratitude goes to my supervisor Professor Keith Seffen for his guidance, mentorship and friendship. His genuine interest in the principles and science of structural mechanics, keen eye for an unusual or interesting problem, and passion for teaching have been an inspiration, and it is no exaggeration to say that I have always left our meetings with a renewed enthusiasm. Thank you for your unwavering belief in me, it has been a privilege to be your student.

I also extend my thanks to all of my colleagues in the Advanced Structures Group and wider Structures Research Group from whom I have learnt so much and enjoyed sharing so many friendships and memorable occasions over these last few years. It has been a pleasure to work alongside you all.

To the students, fellows and staff of Corpus Christi College and the MCR for the truly special community of which I have been privileged to be a part.

And to the many friends, both near and afar, with whom I have immensely enjoyed these last years. A special mention goes to my many housemates, Sam Wimpenny, Tudor Ilca, Michael Tomaszewski, Thomas Fryer, Will Hawkins, Will Tebbut, Millie Hood and Simon Copley, for many enjoyable evenings and weekends, to George Roberts and Cora Olpe for many hours shared in the gym and at the pool, and to Pedro Magalhães de Oliveira, Alex Sigston, Matt Bergin, Giles Harper-Donnelly, and Spencer Wilson for your friendship and many stimulating and lively discussions over coffee, beer, or, better yet, fish and chips on a Friday lunchtime.

Financial support has been received from the Engineering and Physical Sciences Research Council from whom I received a doctoral training grant (#10361473), travel grants from the Department of Engineering and Corpus Christi College, and funding to enable me to complete this work from the Cambridge Philosophical Society (#S52/023/19).

Finally, I am ever grateful for the constant support, encouragement, and love of my family. Thank you to my parents and sisters (Helen, Elizabeth and Rebecca) for everything you've done for me and for always being there for me when I needed it most. And to Rosalie, for your friendship and companionship.

To my grandparents...

Table of contents

List of figures

Chapter 1

Introduction

In the last 40 years, papercraft-derived structures have provided a rich source of inspiration, insight and innovation toward the design of new active, transformable, and deployable structures. This thesis concerns an investigation of deployable 'sliceforms' formed from a volumetric assembly of planar slices interlocked via pairs of complementary slots placed along their intersections. Subject to the spatial arrangement of slices, rotation about these intersections enables global folding of the structure (the slices themselves do not fold) to a flat-folded stack of coplanar slices. This dissertation concerns an investigation of the kinematics of such sliceforms and exploration of this technology toward the design of new deployable structures.

1.1 Deployable structures

A *deployable structure* is a structure which can undergo a large shape change, *deploying* to its operating configuration from some compact *collapsed* configuration (and *vice-versa*). The compactness of the collapsed geometry and capability to be rapidly deployed on-demand makes them valuable in a wide variety of engineering scenarios, perhaps due to restricted access for in-situ assembly or construction, transportation limitations, or an intermittent and/or time-critical demand. They are distinct from *morphing structures* – which change shape through multiple (or continuous) operating geometries to improve or modify performance in response to different operating or loading conditions – though they share many common technologies, and also from *demountable structures* – which are rapidly assembled and disassembled from a kit of parts – though some components of such a system may be deployable.

Engineered examples are found throughout the artificial world, from 'low-tech' pop-up greetings cards to precision-engineered solar arrays and dish antenna for spacecraft. The classic example is of the umbrella, which can be rapidly unfurled when needed (*i.e.* when raining) but otherwise collapses to a compact configuration for storage and transport (*i.e.* when it might rain later!). Deployable structures are also found in nature, particularly in plants, where complex geometric forms are first grown as a compact bud before unfurling, and flying animals where large wings are folded away for protection from damage and to improve overall mobility when not in use.

The deployment process is usually reversible and may be enacted by mechanical linkage, elastic and/or plastic deformation, shape-changing material, or any combination of these. Most deployable structures are deployable systems with multiple highly integrated subsystems accounting for load-bearing, definition of external shape, actuation between configurations, for example, and requiring a highly multidisciplinary design process.

Due to the often contradictory design requirements – mobility during deployment but rigidity in the final configuration, low weight but high stiffness, low volume for maximum compactness but large deployed dimension – most deployable systems are inherently high-performance structures and rapid developments in design, materials and manufacturing capabilities over recent decades – particularly 3D printing technologies and composite materials – have greatly increased their capabilities and utility, thereby expanding the range of useful and viable applications.

1.2 Papercraft engineering

Provided as examples above, the contrast between a low-tech pop-up greetings card and a high-tech satellite antenna is particularly pertinent because in 1985 Koryo Miura presented a concept for packaging large membranes for space applications using his developable double corrugation surface (DDC, first described in 1970[57], now known as the *Miura-ori* pattern), in doing so applying membrane-folding principles – which he observes relate directly to "folding a Sunday edition of the New York Times" – to a solution for an engineering problem[58]. Since then, the field of papercraft engineering has blossomed as researchers and designers appeal to papercraft for insights and inspiration to the design of novel "structures-from-sheets"[64, 46, 91].

The appeal is obvious; in the hands of a skilled artist, a humble, two-dimensional sheet of paper can be transformed out-of-plane to form a profusion of geometric shapes, detailed static models and intriguing kinematic action toys. For the artist, the challenge is

Fig. 1.1 A selection of paper sliceforms built by María García Monera and Juan Monterde.

Source: María García Monera (2012). Sliceforms. *Flickr.com*, https://www.flickr.com/photos/mgmonera/albums/72157632885563751

typically the generation of complex curved geometries from flat or developable patches by careful combinations of folds, cuts and glued seams, inspiring architectural and industrial designs for facades and surfaces. Though a high in-plane stiffness relative to a low out-of-plane bending stiffness is inherent to all thin sheets, the addition of structural depth and curvature embeds these structures with new structural and kinematic characteristics that are dominated by geometric effects. Furthermore, with creases in paper acting as hinges, folded designs form simple mechanical linkages providing them with morphing or deployable capabilities. Additionally, many patterns are created from an initially planar sheet by a series of consecutive 180-degree folds to build a 'base' before partially re-opening to reveal the final three-dimensional form, thereby forming a ready-made deployable, flat-foldable structure. By formalising the underlying geometric principles, the insights and ideas developed through centuries of art and craft can now be translated directly to the design of new functionally enhanced deployable structures at a large range of length scales using conventional engineering materials (metals, composites, polymers) and mechanical joints[64, 91, 86].

1.3 Sliceforms

Instead of folding a sheet of paper to raise it out-of-plane, a volumetric structure can be generated by slotting multiple sheets together via pairs of complementary slots. This is the basic principle of a *sliceform* which comprises a honeycomb-like array of interlocking planar slices, each shaped to form a cross-section of an inscribed volume. These visually striking structures are lightweight, simple to manufacture from stock materials and do not require any adhesives to assemble. Some examples are shown in Figure 1.1.

(a.i)

(a.ii)

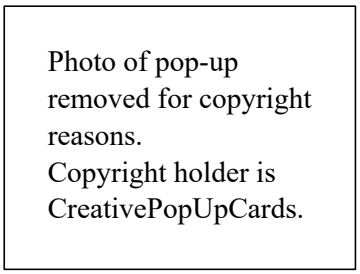

(b)

Fig. 1.2 Many sliceforms are flat-foldable, (a), and this is often used to produce novelty 'pop-up' cards, (b).

Sources: (a) Cheng, K. (2007) V Canyon. *Flickr.com*, https://www.flickr.com/photos/86062931@N00/albums/72157615496032473
(b) 3D Heart Pop Up Card Template. *creativepopupcards.com*, https://www.creativepopupcards.com/store/anniversary/3d-heart-pop-up-card-template/

The edge of each slice is an exact contour of the surface geometry with the inscribed volume is discretised by the array of cross-sectional slices to a series of plane faced cells. The simplicity and accuracy of this approach makes 'sliceforming' a powerful tool for manufacturing physical reconstructions of complex three-dimensional forms, useful for making simple sculptures, modelling mathematical surfaces, and in the generation of templates to guide non-developable forming processes, *e.g.* in coachbuilding.

With slices cut from thin material, or with sufficiently wide slots, each intersection forms a rudimentary revolute hinge. The sliceform then embeds a spatial mechanism whose kinematics are derived directly from the geometric arrangement of the slices. With two sets of parallel slices, a *lattice sliceform* embeds an array of parallel linkages and is bi-directionally flat-foldable via a global shear mode, Fig. 1.2(a), a feature commonly exploited in the design novelty 'pop-up' greetings cards in which an initially flat-folded sliceform is deployed automatically as the card is opened, Fig. 1.2(b).

On first impression, it appears that only a lattice sliceform could be foldable, but it was recently discovered that a particular sliceform torus, Fig. 1.3 – designed independently by Yoshinobu Miyamoto and María García Monera – also exhibits a foldable characteristic. The complete torus is kinematically rigid but, at mid-assembly, an incomplete ring of slices is readily expanded and collapsed about the axis of revolution. This partial assembly has an unusual mobility, expanding smoothly to-and-from a flat-folded compact-stack of coplanar slices but abruptly 'locking-out' once the design expansion is reached (as if excised perfectly from a complete ring), Fig. 1.4. The source of this limit is not readily apparent. There is no internal collision between slices and no intersection has reached its natural rotational limit,

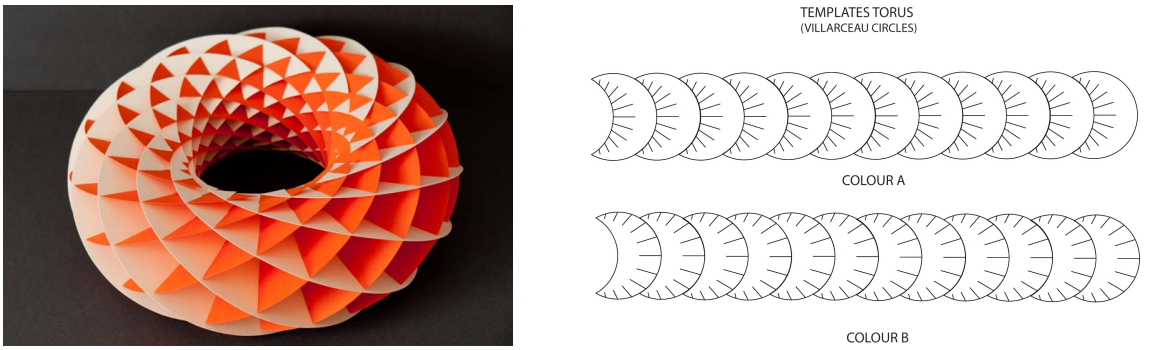

(a) (b)

Fig. 1.3 A sliceform torus built from Villarceau circles. The assembled sliceform, (a), and crescent-shaped slice templates, (b), each bounded by the pair of overlapping Villarceau circles found on a torus' double-tangent plane, (b).

Source: María García Monera (2012). Torus. *Flickr.com*, https://www.flickr.com/photos/mgmonera/albums/72157632885563751

the array apparently ceases to be mobile and cannot be expanded further without visible distortion (bending) of the slices.

This deployable action is highly intriguing, with the smoothness of initial expansion belying the abruptness of locking-out. It is immediately apparent that a mechanism with this characteristic and inherent limitation to its range of motion could be useful as a functional, load-bearing deployable structure, motivating an investigation to resolve the nature of the folding action. Furthermore, the discovery that this design is foldable also suggests that other non-lattice, deployable sliceforms might be designed. To date, the design and use of sliceforms has been limited to sculptural functions, and the design space for 'deployable structures from slices' has not been explored.

1.4 Thesis overview

1.4.1 Objectives

The overall objective of this thesis is to investigate the folding action of sliceforms to explore the potential of this technology for the design of novel deployable structures. The simplicity of their construction from interlocking planar slices is appealing in terms of both the ready manufacture of each component by cutting from a sheet of stock material and the intrinsic constraints this sets on their design.

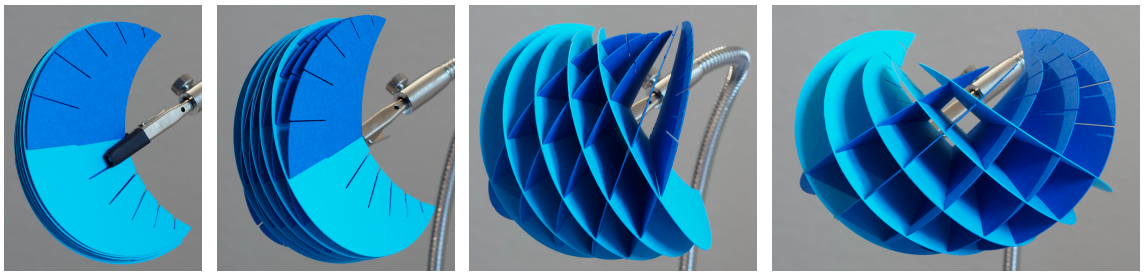

(a) (b) (c) (d)

Fig. 1.4 A partially assembled sliceform torus exhibits a surprising deployable action, expanding and contracting about an arc. From flat-folded, (a), the sliceform deploys smoothly and without resistance until the design configuration is reached, (d) – as if excised from the complete ring, whereupon it abruptly 'locks-out' and cannot be over-expanded without deformation of the slices.

The torus sliceform serves as a starting point for exploring this design space, and an investigation of its unusual folding characteristic – which is shown to apparently contradict the expectation set by conventional kinematic analyses – is pursued. This is approached without specific applications in mind but with the broad intention to develop insights into the function and limitations of this structural form which might also be translated to the design of deployable structures in more conventional form. Of primary concern, therefore, is capture of the underlying principles of action via simple models to derive insights and understanding into their folding behaviour.

Following this, an investigation of the wider design space of deployable structures from interlocking slices is pursued. The objective here is to determine whether the arrangement of slices underlying the torus can be generalised whilst retaining a similar deployable action, and, if so, to explore the range of variations that can be generated and formulate a generalised model of their behaviour.

Throughout this work, the intention is to pursue simple geometric models where possible, supported by informal observations obtained from small-scale physical prototypes, to derive generalised insights and relationships; seeking to develop analogous analytical approaches to those used in models of more conventional folding structures rather than pursuing numerical simulations of specific examples. It is also intended to remain material and scale 'agnostic' in the sense that specific material properties and absolute dimensions are of secondary importance to the functional behaviour of the structures, the investigation focusing instead on the role played by the geometric form.

1.4.2 Outline

The first chapters of this thesis detail the background of this investigation. In Chapter 2 the synthesis and properties of a sliceform are described, establishing some basic principles for the design of a viable structure, along with a comprehensive overview of previous research into this type of 'structure-from-slices'. To inform the investigation of these structures, Chapter 3 introduces some key concepts for kinematic mechanisms and a survey of the treatment of scissor structural mechanisms and of origami structures – with which sliceforms share the fundamental kinematic component with embedded revolute joints, and a similar hinged-plate form, respectively – is conducted.

The research undertaken is then presented in two parts:

Part I concerns an investigation of the geometry and folding action of deployable sliceforms constructed according to the layout of slices in the torus, a *rotational sliceform*, or *RS*. Their design and synthesis is formalised in Chapter 4, establishing the underlying spherical form of their *structural geometry* and presenting a range of example structures to explore the limits of this formulation. Chapter 5 deals exclusively with the deployable action of an incomplete RS, examining this unusual articulation from both an *intrinsic* and *extrinsic* perspective to establish its nature. A simple model of the overall articulation as a spherical linkage is developed to capture the key characteristics of their motion in a general form.

In Part II the basic technology of an RS is generalised by development of a technique for synthesising sliceforms according to a prescribed smooth spatial curve – so-called *curve sliceforms*, or *CS* – and analysis of their geometry and folding characteristics. This novel formulation is introduced and developed in Chapter 6 with a range of representative examples designed and manufactured to illustrate the scope and flexibility of this technique for the synthesis of deployable structures. In Chapter 7 their structural geometry is examined and a framework for description of their intrinsically localised form is developed. This informs an analysis of their deployable action in Chapter 8 where the imperfect action of their interlocking slots is captured.

1.4.3 Contribution

This work is a first investigation of the structural mechanics of non-trivial (*i.e.* non-lattice-style) sliceform structures, firstly through investigation of the folding action of rotational sliceforms and then the design of more generalised folding sliceforms from a range of spatial curves.

These elegant structures are intriguing in their own right and the understanding of their unusual folding action developed in this work adds directly to the growing body of literature concerning the real-world performance of folding structures whose behaviour is significantly influenced by elastic deformations of the components.

A purely geometric model of the folding behaviour of rotational sliceforms is constructed by analysing a simplified, functional dual of each class of sliceform structure in which the dominant mode of compliance of the slices is explicitly included in a representative form. This extends the work of other researchers in developing tools for analysing complex folding systems that cannot be captured by conventional rigid kinematics. Such structures are often challenging to model because of the complex nature of the compliances which affect their functional behaviour, in particular their effect on the geometry of the system, and it can be tempting to look to numerical analyses to capture a realistic model of the structural response. However, this investigation serves to demonstrate that through careful modelling choices the real-world behaviour of such structures may still be adequately captured through analytical methods.

Exploration of the wider design space for sliceforms is approached by generalisation of the RS technique and development of a comprehensive and novel design protocol for generating sliceform structures from an input basis curve. This robust tool can be used to generate folding sliceforms whose deployed shapes conform to a large variety of smooth spatial curves, with a set of striking examples synthesised in the course of this investigation.

This work also demonstrates the use of a highly integrated approach to the design, manufacture and analysis of these sliceform structures, with insights gained at each stage informing development of the others throughout. Using software which allows for an algorithmic approach to design enables a wide variety of examples to be synthesised alongside detailed interrogation of their common geometric form, whilst the use of digital tools for rapid manufacture of small-scale physical prototypes supplements this, with insights generated through informal observations of their behaviour directly informing both improvements to the design methodology and also the development of analytical models of their behaviour. This results in a deep understanding of these novel deployable structures, both in terms of their geometric form and structural behaviour, and also in developing principles for their design, an approach which could readily be extended to other structural technologies.

Chapter 2

Sliceforms: An overview

2.1 Introduction

Briefly described in the introduction, a sliceform is a volumetric, honeycomb-like array of planar, cross-sectional slices interlocked via pairs of complementary slots placed along each line of intersection – detailed in Fig. 2.1(a). This simple technique enables complex three-dimensional models to be constructed from two-dimensional slices, which are compact for storage and transport, without the need for additional joints or adhesives. Once a suitable set of templates has been designed, the slices are cut directly from sheet material, preferably using a computer-controlled cutting machine, with assembly of the final sliceform proceeding by hand.

2.1.1 Chapter outline

In this chapter the history and design features of a general sliceform structure are described and some broad principles of their structural mechanics are introduced, particularly pertaining to the slot details. A survey of prior research into sliceforms is conducted, the majority of which focuses on their automatic synthesis as a minimal geometric proxy, along with a brief overview of some related slot-together structures.

2.2 History of sliceforms

An early description of 'structures-from-slices' appears in the 1957 textbook "Mathematical models" by Cundy and Rollet who describe a method for constructing models of binary function surfaces from "cardboard sections which are interlocked in the same manner as

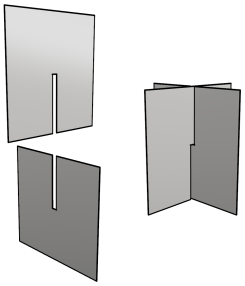

Photo of book and sliceform models removed for copyright reasons.
Copyright holder is Ivars Peterson.

Photo of sliceform removed for copyright reasons.
Copyright holder is Richard Sweeney.

(a) (b) (c)

Fig. 2.1 (a) Detail of interlocking slots along intersection lines. (b) Sliceforms exhibited by John Sharp at the Second Annual Conference of the International Society of the Arts, Mathematics and Architecture (ISAMA 2000, University at Albany, New York, 2000). (c) 'Void' sliceform by Richard Sweeney.

Sources: (b) Peterson, I (2016). Sliceforms. *The Mathematical Tourist, Mathtourist.Blogspot*, https://mathtourist.blogspot.com/2016/02/sliceforms.html
(c) Sweeney, R (2006). sliceform. *flickr.com*, https://www.flickr.com/photos/richardsweeney/331359084/.

partitions in an egg-box"[12]. When the sections are oriented "horizontally and vertically" each corresponds to a contour of each variable making their shape easy to design. They also suggest that the interior cells of the final structure be filled with clay or concrete with the sections acting as templates to guide the formation of a solid model, if desired.

The term "sliceform" was coined more recently by the mathematician John Sharp, who attributes their inception to the mathematician Olaus Henrici. He notes that they were popularised by Alexander von Brill who exhibited several 'continuously deformable' models (likely manufactured in collaboration with Felix Klein and students at workshops at the University of Munich) at an exhibition of scientific apparatus in 1876[80, 59]. Sharp himself noted that though these examples tended to be limited to models of quartic surfaces, many more shapes could be constructed according to the same principle. He designed many new sliceforms, a selection of which are shown in Fig. 2.1(b), describing them as a "Bridge between Art and Mathematics"[78] and authored a series of books containing templates for readers to make their own[79, 81].

Versus more conventional papercraft techniques – in which a geometric surface is discretised to a series of patches, with a folded model often requiring extensive 'pleating' to effectively add or remove surface area to approximate a non-developable surface[85] – the key advantage of this slice-based approach is that a sliceform model tends to be much more straightforward to design and manufacture whilst achieving a similar overall impression. Typical applications range from the pop-up greetings cards mentioned previously to quirky

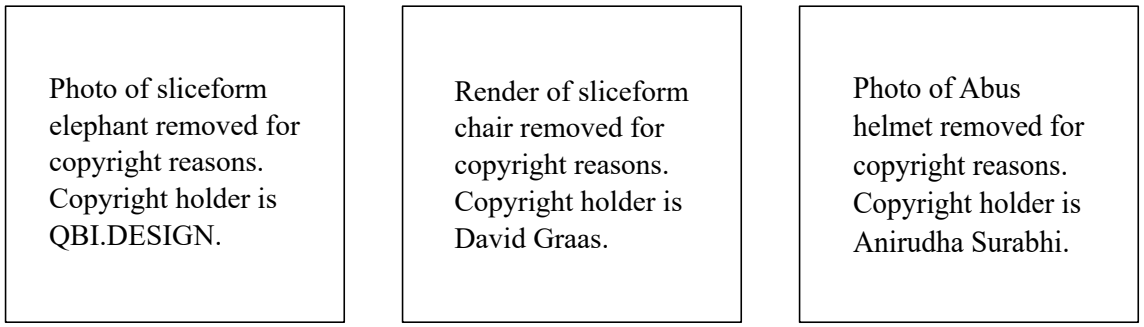

Fig. 2.2 Sliceform products: (a) Cardboard elephant by QBI.design, (b) Cardboard chair by David Graas, (c) Kranium/Abus Performance helmet by Anirudha Surabhi.

Sources: (a) Frank – cardboard elephant figure. *QBI.design*, http://qbi.design/shop/frank-cardboard-elephant/
(b) Graas, D. Cardboard Lounge. *designboom.com*, https://www.designboom.com/design/david-graas/
(c) Image by Surabhi, A., in Chappel, B. (2012). A Cardboard Helmet, To Go With Your Cardboard Bike. *The Two-Way by npr.org*, https://www.npr.org/sections/thetwo-way/2012/12/12/167111810/a-cardboard-helmet-to-go-with-your-cardboard-bike

home decorations, Fig. 2.2(a), but the honeycomb-like form is also suited to functional, load-bearing applications, such as recyclable furniture, (b), and impact-absorption structures such as in the "Kranium" bicycle helmet by Anirudha Surabhi, (c), which is claimed to absorb three times the energy of conventional polystyrene helmets whilst being more robust (conventional polystyrene designs are readily cracked, *e.g.* by dropping, compromising their safety without the user realising)[82].

By discretising the target volume to an array of plane-faced cells, each slice-edge contour may precisely trace the surface of the inscribed volume. This type of 'sectioning' technique is often used in the construction of accurate volumetric templates in manufacturing – such as 'body bucks' used to guide metal forming for coachbuilding and formwork to support the construction of masonry shells and tiled vaults – 'waffle' strucutures for rapid prototyping of architectural models, and, occasionally, as visually striking but easy to manufacture architectural facades, Fig. 2.3.

Sliceforms have also been proposed as an approach to rapid-prototyping for testing object geometries in industrial design[43], but this has largely been negated by recent advances in the availability and accessibility of low-cost 3D printing.

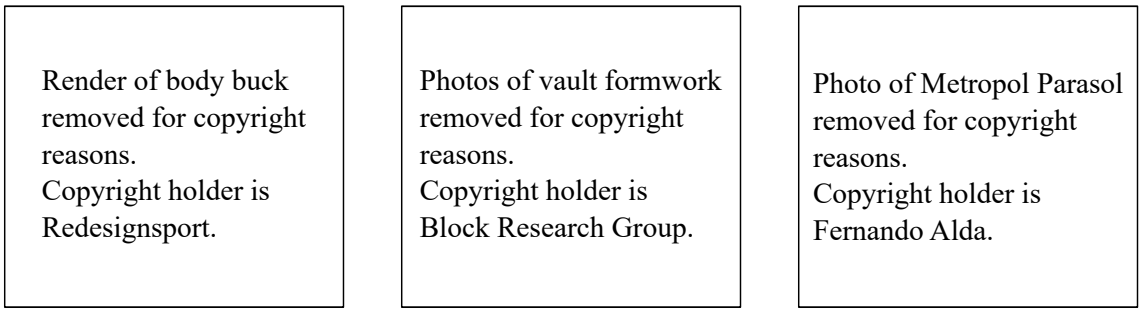

(a) (b) (c)

Fig. 2.3 Engineering 'structures from sections': (a) Slot-together 'body buck' template to guide metal forming in coachbuilding; Cardboard formwork for tile vaulting (Using an array of shaped boxes, rather than interlocking slices)[13]; (c) Facade of J Mayer H's "Metropol Parasol" (2011) in Plaza de la Encarnacion, Seville, Spain.

Sources: (a) Cobra body buck (render). *Redesign Sport LTD.*, https://www.redesignsport.com/projects-1
(c) Photo by Alda, F. in Metropol Parasol: The World's Largest Wooden Structure, *yatzer.com*, https://www.yatzer.com/Metropol-Parasol-The-World-s-Largest-Wooden-Structure-J-MAYER-H-Architects

2.3 Geometry and synthesis of a sliceform

The geometry of a sliceform has an intriguing threefold geometric hierarchy consisting of the *global volume* inscribed by the assembled structure; the spatial arrangement of the array of slice planes – the *structural architecture*; and the local, in-plane shape of each slice – the *slice geometry*.

The design of a sliceform follows this hierarchy: first the global volume is defined, then a suitable structural architecture generated, and finally the cross-sectional planforms are excised for each slice plane – hence a '*slice-form*'. The slice templates are completed by furnishing pairs of complementary slots along each intersection line, usually to the midpoint, Fig. 2.4.

Generation of cross-sectional slice templates from a given volumetric geometry is readily accomplished in modern 3D modelling packages[48]; indeed, rudimentary plug-ins for generating 'waffle' structures complete with slots are widely available for many of the major suites.

In the manufacture of a sliceform, the slices are cut from a sheet of stock material, either by hand using a craft knife or using a CNC (computer-numerical-control) cutting machine with either a sharpened blade or a laser, and then assembled according to the structural architecture to form a mutually self-supporting structure. Depending on the structural architecture, the assembly sequence may or may not be important.

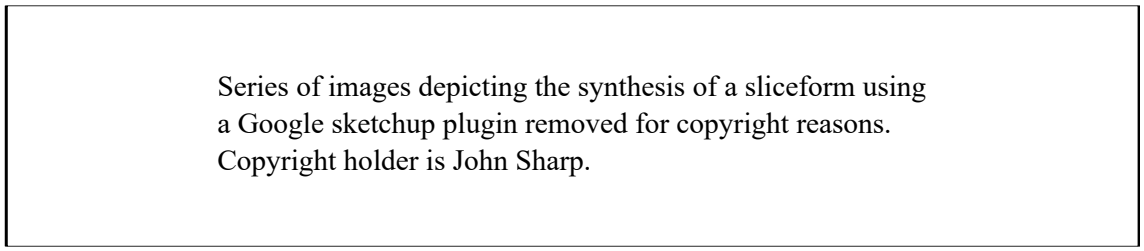

Fig. 2.4 Design of a sliceform torus with a lattice-style structural architecture using a plugin for the Google Sketchup modelling package. (a) Definition of the volumetric geometry (an inclined torus), (b) slicing the volumetric model to excise a series of planar cross-sections, (c) array of cross-sectional slices in two sets, (d) one set of slice templates with slots placed along and to the midpoint of each intersection.

Source: Sharp, J. (2010) Creating Sliceforms with Google SketchUp. *Sliceforms.wordpress.com*, https://sliceforms.wordpress.com/2010/12/03/sketchup-sliceform-using-the-sliceform-plugin/

2.4 Structural architecture of a sliceform

The sliceform designer's usual objective is to find an arrangement of slice planes (*i.e.* the structural architecture) which provides a visually effective and aesthetically pleasing impression of the surface geometry of global volume, whilst reducing the 'resolution' of the sliceform (*i.e.* total number of slice planes) for efficiency. Though a minimal geometric representation might be best achieved by independently orienting slice planes to capture each geometric feature, care must be taken to ensure that the final arrangement of slices is *geometrically feasible – i.e.* that a valid arrangement of slots can be formulated to enable the slices to pass through one another without becoming discontinuous – and that the slices can also be physically assembled.

Geometric feasibility requires that the array of slices can be interlocked via complementary pairs of slots without splitting any slice into two parts, whilst also preserving separability so that the sliceform can be completely disassembled into a set of independent slices (i.e. No interlinked loops).

Consider a pair of interlocking slices, it is straightforward to place complementary slots along their line of intersection, as illustrated previously in Fig. 2.1(a). If a third slice is added it may interlock with one or both existing slices provided that the new intersection lines do not pass through the existing line of intersection. If they do (in which case all three intersection lines will necessarily meet at a point) then slots placed along these lines of intersection will split the slices into two parts, Fig. 2.5(a). Topologically viable solutions to such a triple-intersection point which maintain the contiguity of each slice do exist , Fig. 2.5(b)&(c),

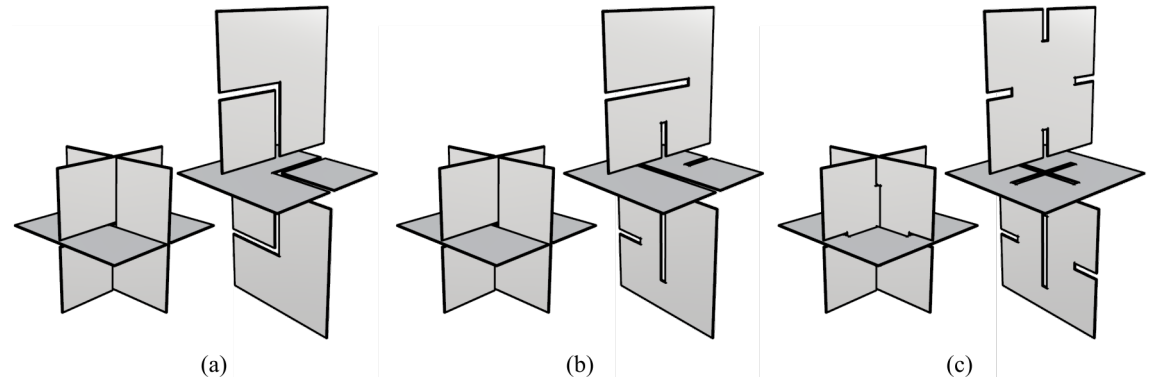

Fig. 2.5 If three slices are arranged such that their intersection lines themselves intersect, the usual approach of placing slots along and to the midpoint of each intersection will cause a portion of each slice to become separated, (a). This can be resolved in isolated cases by adjusting the slots so that either: the slots in each slice span complementary, unequal portions of each intersection so that each slice remains contiguous with the segment joining the previously disconnected portion now enclosed between the other pair of slices once assembled, (b); the slots span the central half and outer quarters of each intersection line so that the first slice (top) is inserted into the central slot in the second (bottom), and the third (middle) then encloses both, (c). However, these solutions require significant flexibility from the slices to permit assembly and cannot be transposed across multiple such points without the slices becoming interlinked and inseparable. It follows that intersections between lines of intersection are not geometrically feasible in general.

however these solutions require significant flexibility to assemble in practice and are only viable in isolation: transposing these solutions across a volumetric array containing multiple such points causes the slices to become interlinked. It therefore follows that a key principle in the design of volumetric sliceform structures is that no pair of intersection lines should themselves intersect.

The second constraint, assemble-ability, places a further restriction on the domain of possible structural architectures. There are two distinct contexts in which to evaluate this: when the slices are rigid, and when the slices are flexible. If the slices are rigid a rigid assembly path is required in which the slots being engaged at each step are parallel. More complex designs may require a specific slice-by-slice assembly sequence, or even the construction of separate assemblages of slices which are mated together at a later stage. If the slices are flexible – as is usually the case for craft models cut from thin sheets of paper or card – it is possible to simultaneously engage non-parallel pairs of slots by carefully twisting and bending the slices to overcome the wedge spanned between them[1]. The assemble-ability of a

[1]The triple intersections illustrated in Fig. 2.5(b-c) would require that the slices be rolled or folded in order to insert portions through contained slots, only possible with very flexible slices

given design now depends on the geometric misalignment of the intersections which must be interlocked at each step, and the range of elastic deformation that the slices can accommodate without tearing, creasing or otherwise plastically deforming. Resolution of this for a given design is much more involved and usually verified by experimental means, *i.e.* simply trying to construct the sliceform. Nonetheless, it is immediately apparent that even some slight flexibility greatly increases the design space of possible structural architectures.

2.4.1 Lattice sliceforms

The consequence of these requirements is that the design of a bespoke arrangement of slice planes which remains valid is often non-trivial. The most straightforward approach is to simply use two (usually orthogonal) sets of parallel slices forming a rectilinear lattice-style grid. All intersection lines are now parallel, thereby satisfying both requirements regardless of overall shape, and thus forming a *lattice sliceform*, or *LS*, *e.g.* the examples in Figs. 1.1, 1.2 & 2.1.

The slice spacing (which may be non-uniform) is selected for best coverage of the geometric features, and the grid can also often be aligned to some intrinsic feature of a model, such as the axes of a binary function[2] or the skeleton of an animal. For sculptural models, an improved visual impression can often be achieved by the addition or adjustment of a few slice planes 'off-axis' to refine the sliceform once the basic grid layout has been generated. Collapsing the silhouette of any prominent features onto the nearest slice plane also enables improved visual interpretation without increasing the number of slices at the expense of geometric accuracy. Manufacturing the two sets of slices from two contrasting colours emphasises the continuity of each slice and provides additional visual impact.

Many other non-lattice designs are based on an underlying grid but without globally parallel intersection lines, such as the examples in Figure 2.2. In (b) one set of slices are parallel, ensuring that the slots in the other set of slices are parallel and can be engaged simultaneously for rigid-assembly, in (c) the slices are rotated so that each is broadly perpendicular to the wearer's head and are not compatible with rigid-assembly. These illustrate again that the intersection lines do not need to be parallel for a geometrically feasible set of slots to be rendered provided that their intersection points lie outside the global volume.

[2]With mathematical surfaces a volumetric geometry is generated by extruding from some reference plane so that the surface is the interface between the filled domain and the empty space above it.

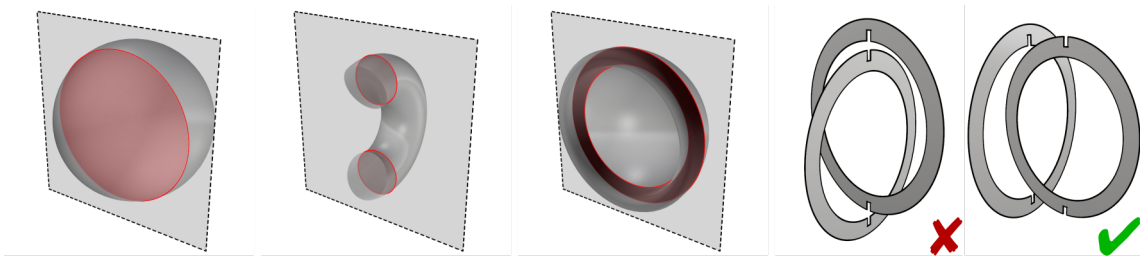

(a) (b) (c) (d)

Fig. 2.6 A selection of possible cross-section topologies. A planar section of a smooth, convex volumetric solid is also smooth and convex, (a). If the volumetric surface is convex a section may consist of multiple parts, (b), or contain a hole, (c). Careful slot placement can enable the realisation of non-standard sliceforms. For example, if a pair of cross-sections intersect across a hole consistently oriented slots will result in a pair of interlinked loops: this is resolved by re-orienting one pair of slots so that one slice fits within the other, (d).

2.5 Slice topology

Whilst synthesis of a sliceform is generally robust, when excising a cross-sectional slice from the global volume there are various topological possibilities. For a simple convex volume, each cross-section will be singular and bounded by a convex curve, Fig. 2.6(a). Any sharp edges or vertices in the global surface will translate to kinks in the bounding curve. If the surface of the global volume is concave, the cross-section will be concave but may also consist of multiple distinct parts or contain a topological hole, Fig. 2.6(b) & (c). Likewise, multiple parts may result if the global volume is genus non-zero, and a hole may result if the global volume features an internal void.

A convex, non-singular or hole-containing cross-section may split an intersection into two collinear segments. Whilst it is usually straightforward to place pairs of slots in the same sense along each segment, the slices will become interlinked if both contain a hole. A valid set of slots are generated by re-orienting one pair so that they face ‘inward’ in one slice and ‘outward’ in the other, which may be assembled if the hole is sufficiently large and the slices are sufficiently flexible, Fig. 2.6(d).

2.6 Slot details

Further considerations must be given to the geometry of the slots along each line of intersection. They must be oriented in concordance with the assembly path – for instance, in lattice sliceforms (and derivatives with two dominant sets of slices) it is usually safe to orient slots in one consistent ‘sense’ in one set and the opposing sense in the other. The slot width must

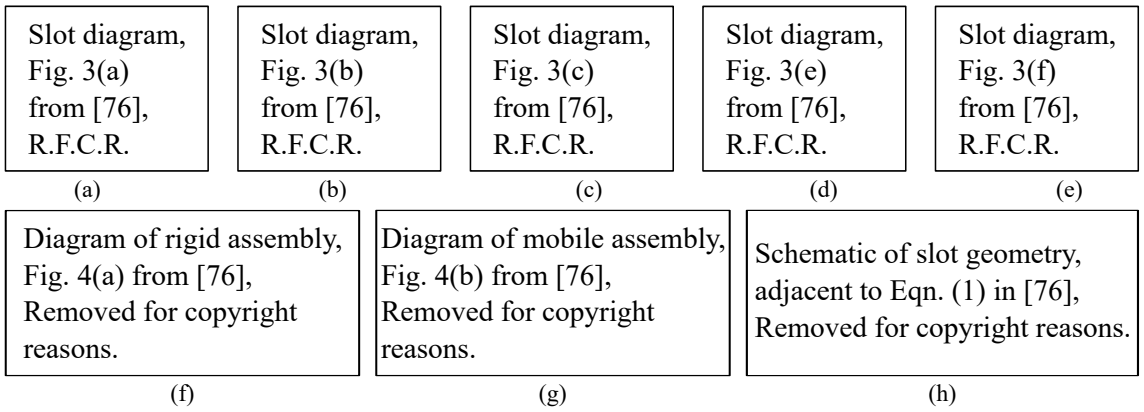

Fig. 2.7 Slot geometries and mobility with thick slices (adapted from [76]). (a) Orthogonal intersections with slots of material-thickness width are tight and rigid; (b) non-orthogonal intersections may be tight and rigid if the slots are cut by an inclined blade, but must be non-tight if the slots are orthogonal, (c). Non-tight intersections may be non-rigid hinges, (d), or rigidified by a closed cycle, (e); though note that a closed cycle may be rigid, (f), or mobile, (g), depending on its geometry and other slot mobilities. (h) A comprehensive geometric definition of a minimum width, non-tight, non-orthogonal slot for a non-orthogonal intersection.

be at least the thickness of the material from which the slices are cut, but depends on the whether the slices are thick and rigid, or thin and flexible.

Orthogonal intersections can be formed with slots of width equal to the material thickness, forming a *tight fit*. Such slots are rigid if the slices themselves are rigid, Fig. 2.7(a).

For non-orthogonal intersections the slots may be cut at material width thickness with an inclined blade, Fig. 2.7(b), preserving tightness of fit at the expense of significant additional manufacturing complexity, or the slot width may be increased in accordance with the dihedral angle between the slices to form a non-tight, contact fit, Fig. 2.7(c). Tight slots prevent rotation, maintaining rigidity of the intersection, whilst wide slots are unstable, permitting the slices to rotate toward orthogonal and becoming loose when this is so, Fig. 2.7(d). When a slice with non-tight slots forms part of a cycle, *i.e.* a closed chain of slices, its mobility depends on the spatial geometry of the assembly and other slot mobilities, Fig. 2.7(e-g).

Formally, the minimum slot width required for an intersection of dihedral angle α_{ij} with slice thickness σ and cut at incline t_α (see Fig. 2.7(h) for schematic) is ([76])

$$h_{ij} = \sigma / \sin\alpha_{ij} + \max(\sigma/\tan\alpha_{ij} - \sigma\tan t_\alpha, 0)$$

If the slices are flexible the slots must still be at-least material-thickness width for orthogonal intersections, but their low bending stiffness allows additional relative rotation

about their line of intersection than their tight-ness predicts, enabled by the slots becoming prised apart. It follows that material-thickness width slots are also sufficient to accommodate non-orthogonal intersections, which remain free to rotate, though their assembly requires that the slots are deliberately prised apart to enable their initial engagement. Indeed, under this prising effect the slot-width–dihedral-angle characteristic is now inverted with thinner slots unable to accommodate orthogonal slices without significant out-of-plane deflection of the slices, the maximum dihedral angle decreasing along with slot width until a zero-width slot (a slit) accepts only parallel slices without significant instability, even with very thin slices.

More generally, the intersections in a sliceform with flexible slices behave as a single degree-of-freedom hinge permitting the slices to rotate about their line of intersection with overall rigidity of the sliceform is then set by the spatial arrangement of slices as a mechanism so that lattice-style sliceforms are bi-directionally flat-foldable, as often utilised in the design of pop-up cards.

2.7 Automatic synthesis of a sliceform

Various approaches have been developed for the automated synthesis of a sliceform according to a prescribed volumetric geometry. Hildebrand et al. developed an automated approach to constructing cardboard structures from sliding planar slices based on the rectification of a three-dimensional axis-aligned grid of sample planes to form an assemble-able model[35]. The initial three-axis grid is geometrically infeasible as a slot-together system because the multiplicity of intersecting slices and intersection lines forms an array of closed cells in which some facets are non-insertable[3]. To resolve this the cross-sections are clipped so that they retain only their insertable portions[4]. Though straightforward to achieve, the final result is dependent on the order-of-assembly and a suitable sequence must be determined to ensure an effective visually impression is achieved. They propose two approaches: in the first, the slices are ordered by weighted score representing their area and proximity to the surface of the volume, which is effective for 'low-frequency' objects (*i.e.* with relatively smooth surface features), fig 2.8 (a); the second takes a more involved approach, with the slices ordered by a quality metric which measures the 'significance' of each slice to the overall result by

[3]The solutions from Fig. 2.5 allow a geometrically feasible set of intersections to be generated for a single closed cell (*c.f.* George Hart's slide together in section 2.9), but an array of such cells remains infeasible because it results in an unresolvable set of multi-interlinked slices containing internal holes.

[4]That each slice in the final design is no longer a complete cross-section raises a possible classification question as to whether these are true 'sliceforms'. It seems reasonable to consider that these structures in which the slices are originally derived as cross-sections as at least 'sliceform derived', though they are perhaps not as 'pure' as designs in which each cross-sectional slice is complete.

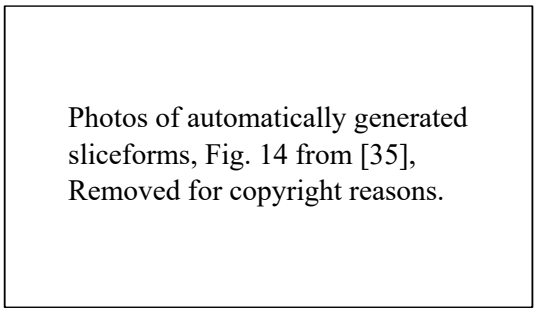

(a)

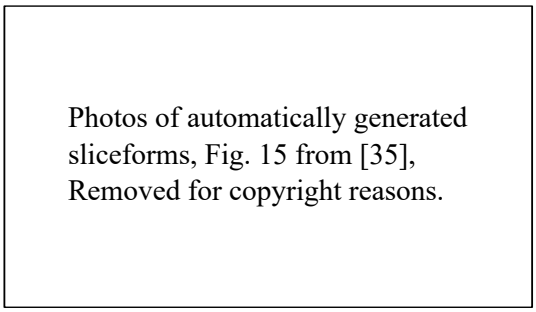

(b)

Fig. 2.8 Sliceforms automatically generated by Hildebrand et al.[35]. The layout of the initial three-axis grid of sample planes is clearly visible with slices clipped to remove non-insertable portions. For the gorilla in (a) and all examples in (b), additional user-oriented planes have been added in a second step to more effectively capture salient geometric features.

integrating the 'uniqueness' of each point on the cross-section versus neighbouring slices, the balance of volume's dimension above/below each point, and the alignment of the slice normal to the surface normal above/below each point, over the slice area, fig 2.8 (b). Both approaches generate effective results in many instances but are sensitive to the alignment of salient features to the axes of the original grid. They, therefore, include a faculty for manual addition of off-axis planes, with just one or two additional slices often significantly improving the visual impression of the final design.

Noting the limitations of using only a parallel (lattice-style) architecture, or 'semantic' variations (modified lattice-style), Schwartzburg & Pauly developed an approach for assisting the design of geometric structures with general, user-specified slice planes that can be constructed from thick slices[75]. Slice planes are specified sequentially with their algorithm automatically adjusting their orientations at each step to preserve the orthogonal-intersection constraint via an iterative method. They later extended their algorithm to allow some non-tight, non-orthogonal slots, pursuing rigidity of the final structure by ensuring that any such 'hinge edges' form part of a closed *cycle* of slices which will generally be rigid[76]. They also guarantee rigid-(dis)assemble-ability by optimising slices to avoid collisions during assembly. To aid tractability, their algorithm makes use of the observation that the characteristics of the slots (i.e. their orientation and dihedral angle) are dependent only on the spatial arrangement of slice planes and not the specific location or shape of the slice upon each. They observe that their dynamic, continuous optimisation approach (versus the purely sequential approach of Hildebrand, above) enables more complex structures can be designed, including non-trivial cycles which can only be assembled by merging separate sets of slices. As acknowledged by the authors, they do not consider the kinematics of the final assembly, in which a closed

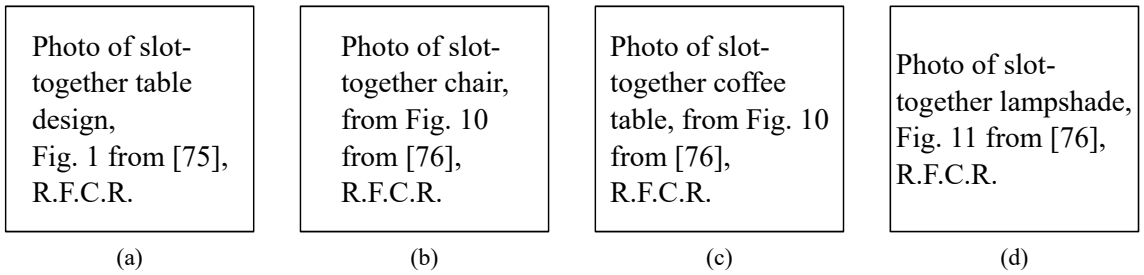

Fig. 2.9 Sliceform designs by Schwartzburg & Pauly: (a) Table with orthogonal slices; (b) & (c) 'strongly rigid' chair and table with non-orthogonal slices but tight slots[76]; (d) Lampshade with non-orthogonal slices and non-tight slots where rigidity is (weakly) ensured by formation of closed cycles of slices. Note that many of the slices are clipped and do not form full cross-sections. Figure (a) from [75], (b), (c) & (d) from [76]

cycle with non-tight intersections may in fact be mobile (*c.f.* a closed chain of four planes with parallel but non-tight intersections forming a parallelogram), instead pursuing rigidity by enforcing tight slots wherever possible. A selection of designs generated using their algorithm are shown in Fig. 2.9.

Le-Nguyen et al. developed an approach for automatically generating flat-foldable lattice-style sliceforms for pop-up cards[45]. Beginning with a global volume and a set alignment of the rectilinear grid, their approach seeks to automate the design of a visually-effective but sparse sliceform by determining an optimised, non-uniform spacing of the slice planes. To improve the appearance of the final result, they explicitly recondition the shape of the model in a two-step process, generating an abstracted 'generalised cylinder approximation' for each set of slices as follows, Fig. 2.10(a): starting with an initial set of densely spaced sample patches along one direction, small features are first absorbed onto their root slice, then sets of multiple adjacent patches are combined into projected silhouettes based on similarity and extruded to form the GCA. This is performed along both slicing directions independently and a slice generated for each extrusion. The stability of the model – *i.e.* that the slices are rigid except for the single-degree-of-freedom global shear mode – is ensured by discarding singly-connected slices and/or duplicating slices where necessary to form secondary connections. This approach is generally effective if important features are suitably well-aligned to the slice directions but the sliceforms, of which a set of examples are shown in Fig. 2.10(b) &(c), are more abstracted than those generated by Hildebrand et. al. They also explicitly anticipate the construction of the slices from paper or card and thus assume that bending may be accommodated during assembly, thereby permitting enclosed voids to be formed which can be assembled by interlocking concentric slices.

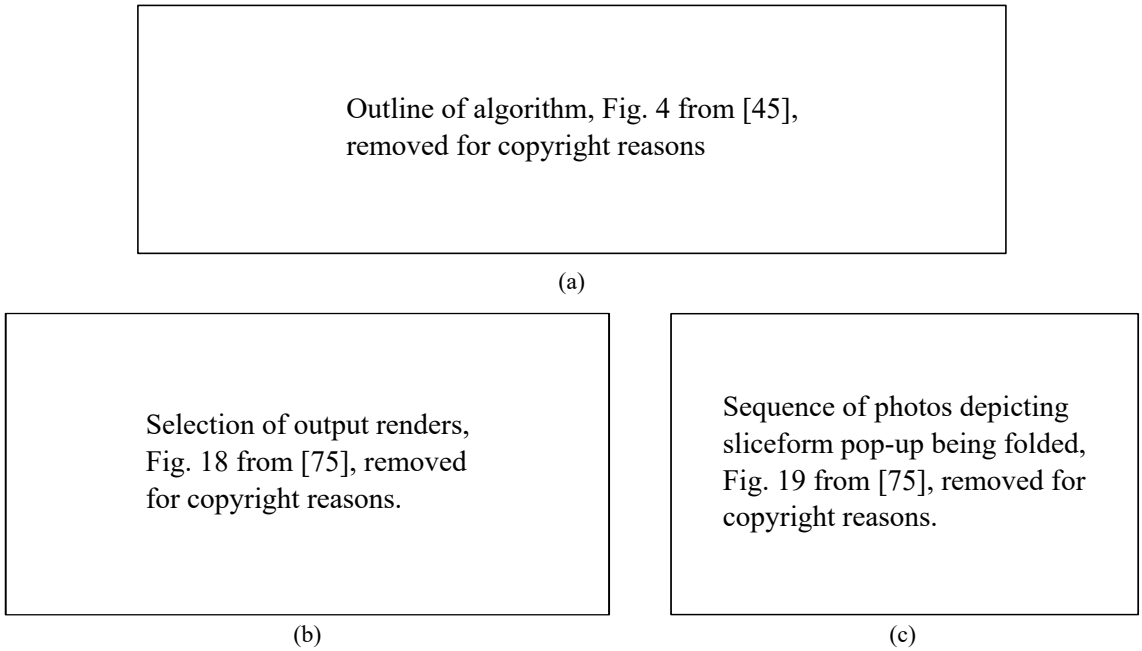

Fig. 2.10 Automatic generation of a flat-foldable lattice-style sliceform by Le-Nguyen et al. [45]. (a) Overview of method with slices generated via an intermediate 'generalised cylinder approximation' which collapses the silhouette of geometric features onto the slice planes. Also shown, a set of example sliceform designs to illustrate the robustness of this approach (b), and a demonstration of the generation of a flat-foldable pop-up card (c).

Though not sliceforms in the traditional sense, McRae et al. developed an interactive sketch-based system for designing abstract sculptures of interlocking slices[54, 53]. Their patented FlatFitFab software facilitates rapid generation of physical 3D models by enabling a user to place and draw the shape of each planar section directly before automatically generating appropriate slots for the pieces to be interlocked. This system is primary intended as a method for freehand sketching of 3D shapes[5], but does allow a user to import a 3D model from which a cross-section can be traced, Fig. 2.11(b), and also provides a feature in which a given model can be distorted by 'magnetic attraction' of the geometry toward the specified cross-section to collapse complex features onto a single silhouette, Fig. 2.11(c). Each slice is inherently semantic and aligned freely by the artist, but they ultimately require that the pieces are orthogonal at their intersections with the software indicating when they are not, and also indicate when a closed cycle cannot be assembled because the intersections are non-parallel. Because the slices and their arrangement are conceived directly by the user, with all errors resolved manually, this approach favours simple structures with the designs drawn by a test group based on a skeletal structural architecture (multiple singly-connected sections attached to a central 'spine'), Fig. 2.11(a).

All of these approaches treat sliceforms purely as a method for rendering physical copies of digitally modelled 3D forms. Though the results are somewhat abstracted, they can be cut from sheet material using only 2D manufacturing processes and assembled by hand. At the time, this was particularly attractive as a possible alternative to 3D printing which was relatively expensive, more specialist and less readily available than it has become over the last decade. Sliceforms nevertheless retain the advantage of being flat-packable when disassembled (or flat-folded in the case of an LS architecture), are often faster to manufacture than 3D printed, solid forms, are amenable to hand-crafting, applicable to a wider range of materials, and more readily scaled to larger objects such as the table and chair designed by Schwartzburg & Pauly (Fig. 2.9).

2.8 Kinematics of a sliceform

To date, the majority of research attention received by sliceforms has been directed at their geometric and aesthetic qualities. Relatively little formal attention has been paid to either the structural mechanics or kinematics of the resulting structures.

[5] A prior investigation sought to validate the accuracy of the shape communicated by a planar abstractions (*i.e.* model abstracted by cross-sectional slices)[52]

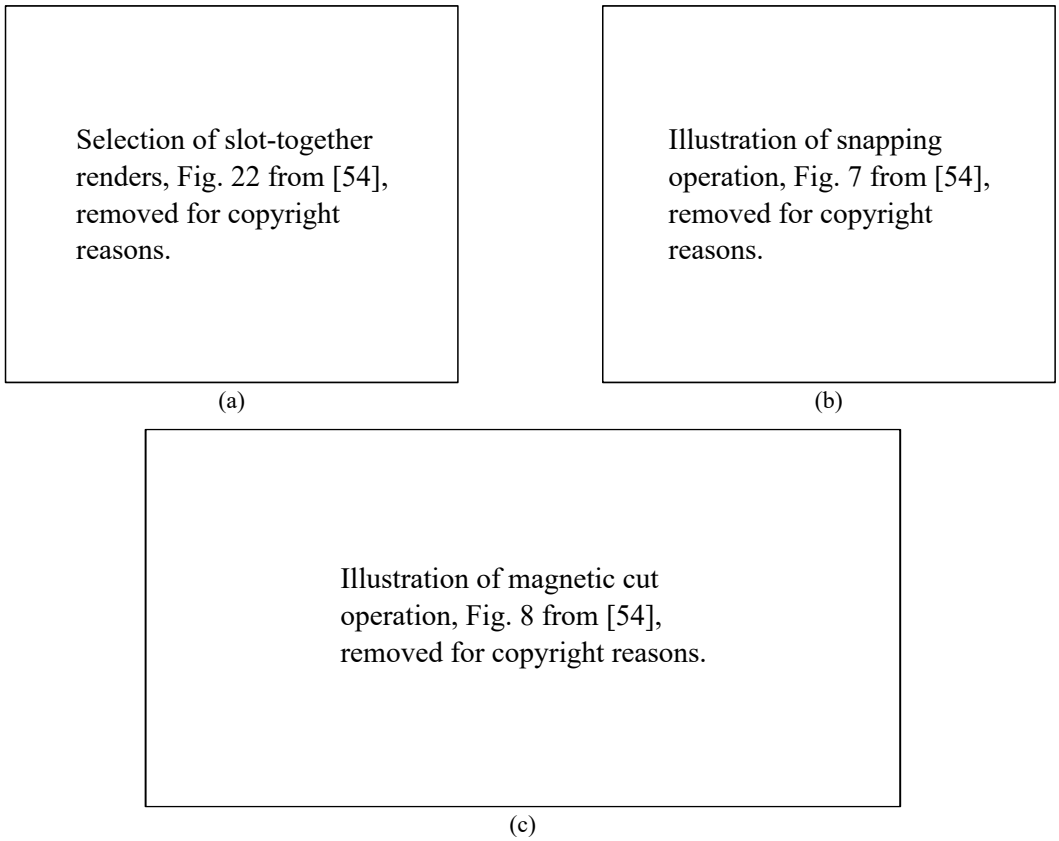

Fig. 2.11 Design of slot-together structures using the 'FitFlatFab' suite by McRae [54]. (a) A selection of models designed by a group of test participants. (b) Demonstration of the cross-section 'snapping' feature enabling a user to trace a true (or modified) cross-section from an imported 3D model. (c) Generation of an effective visual representation using 'magnetic cuts' to map the silhouette of each feature onto the local cross-section.

Mitani & Suzuki presented a brief overview of the use of the lattice architecture for the generation of "180-degree flat-foldable" pop-up cards exploiting the single-degree of freedom of an LS as a pin-jointed rectilinear grid[56]. They describe them as 180° flat-foldable because the single-folded mount (*i.e.* the cover of the card) is opened 180° from closed to laid flat on a surface to actuate the sliceform through a 90° shear from flat-folded to fully deployed.

However, designers are more usually concerned with ensuring the final arrangement of interlocked slices is 'stable'. Schwartzburg & Pauly include such a stability constraint at the optimisation stage in which they seek to ensure rigidity of the overall array. Using thick slices, this is pursued by ensuring intersections are orthogonal if possible, and that they form part of a closed cycle if not[76].

Le-Nguyen et al. consider the stability of the slices in their pop-up structures in an alternative sense. though the complete structure has a single degree of freedom (global shearing of the lattice) and is bi-directionally flat-foldable[45], they ensure that the grid of slices forms an array of closed cycles so that no slice is singly connected and thus free to rotate in isolation.

Both of these approaches are predicated on the fact that, with intersection mobility assured, global mobility (or rigidity) is dependent on the arrangement of the slices to form an array mechanism. The shape of the slices is largely unimportant (hence the ability to form pop-up structures conforming to any global shape using the lattice architecture) though it does influence their connectivity (along with the density of the structural architecture) with greater connectivity increasing the likelihood that the structure is rigid.

However, in pursuit of folding structures, and until the recent discovery of the foldability of the torus, only (very limited) variations on the lattice architecture have previously been found to be foldable. For example, a truncated pyramid sliceform built by John Sharp in which the slices are gently inclined, Fig. 2.12, and remains bi-directionally collapsible though there is some visible misalignment of pair of slots when flat-folded.

From a structural mechanics perspective, Hudert et al. investigated the structural performance of an interlocking particle structure (IPS) composed of six partially interlocking squares[39]. They used a finite element approach to evaluate the internal stresses generated under self-weight, finding that the peak stresses were located around the interlocking slots with the bending moment transfer causing the slot edges to clamp against the intermediate slice. This analysis was performed to check the design safety of a full-scale plywood prototype which was exhibited as a sculpture at the 2017 Aalto Festival in Espoo, Finland.

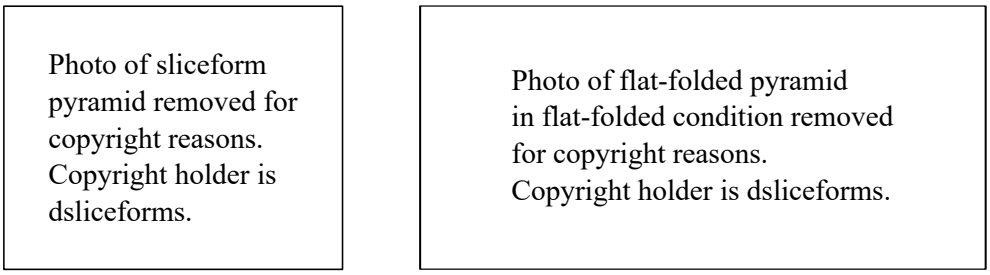

(a) (b)

Fig. 2.12 Truncated pyramid sliceform by John Sharp. The structural architecture is a modified form of the lattice architecture with slices inclined toward the peak of the pyramid and remains flat-foldable although pairs of interlocking slots become slightly misaligned.

Source: dsliceforms (2007) Sliceform Pyramid. *flickr.com*, https://www.flickr.com/photos/7265584@N04/414786597/

2.9 Related slot-together structures

A number of related slot-together structures are worth mentioning.

The mathematician George Hart notes that sliceforms are closely related to his *modular kirigami* – "symmetric assemblages [...] of multiple copies of cut paper shapes"[34] – which are themselves variants of his "Slide-Togethers"[33]. Some of these slide-togethers are effectively sliceforms of regular polyhedra with one slice plane per face oriented parallel to that face and just below its surface, Fig. 2.13(a). These designs do feature points where multiple intersections meet – which he terms "three-way corners" when three intersections meet at a vertex shared by three faces[6]. Though these violate the 'independent intersection' principle identified earlier, they are geometrically valid here (via use of the slot design in Fig. 2.5(b)) because only a single closed cell is formed and are nonetheless fiendishly tricky to assemble, requiring significant flexibility from the slices despite the proximity of the slots to the slice perimeter.

Kinked strips of paper can be interlocked to form visually striking geometric patterns which are inspired by Islamic and Arabic art, Fig. 2.13(b). Lu & Demaine developed a pattern tracing system to automate the design of the strips, describing these structures as an extension of traditional sliceforms[47]. However, the application of the term 'sliceform' to these structures seems somewhat of a misnomer as each strip is not primarily a cross-section.

[6]Note that for the design based on an icosahedron (right: 20 faces, 12 vertices of degree 5) the degree-5 vertices are truncated to prevent five-way corners needing to be assembled. The same is true for his design based on a rhombic triacontahedron (not shown: 30 rhombic faces, 32 vertices: 20 of degree 3, 12 of degree 5 which are truncated)

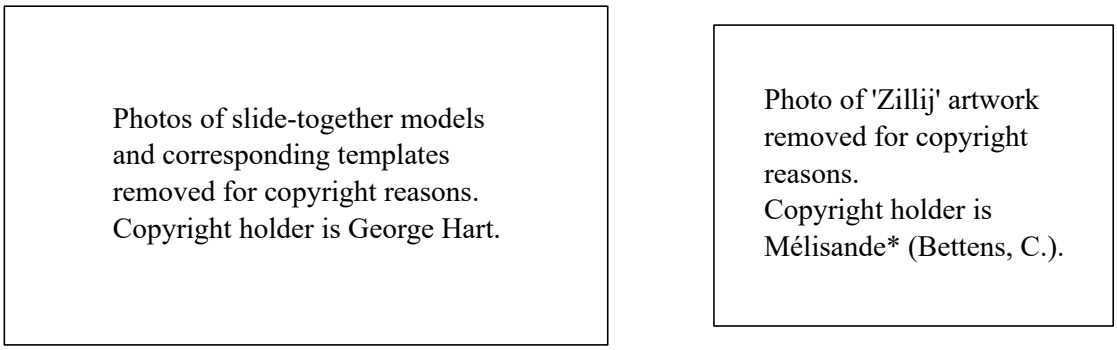

Fig. 2.13 Some examples of *modular kirigami*: (a) Slide-Togethers (and templates) by George Hart[33] (i) dodecahedron from pentagonal slices, (ii) dodecahedron from decagons (chamfered pentagons), (iii) icosahedron from hexagons (chamfered triangles)); (b) 'Zillij' by Christiane Bettens.

Source: (b) Mélisande* (Bettens, C.) (2009). Zillij: Sliceforms technique applied to patterns from arabic art. *flickr.com*, https://www.flickr.com/photos/melisande-origami/sets/72157613125224450

For sculptural models, the contours provided by the perimeter of each slice in a sliceform are limited by their planarity. Because each slice contour must form a complete loop around the surface of the inscribed volume, their alignment is necessarily a compromise from one side of the model to the other and the constraint on the structural architecture (that no pair of intersections may meet for full cross-sections to be realised) also limits their placement. An alternative approach to generating physical models from interlocking pieces has been developed by Cignoni et al.[7]. Named 'field-aligned mesh joinery', their structures are formed from an array of thin ribbon-like strips to form a hollow mesh-like grid, Fig. 2.14(a) & (b). The strips are short and no longer wrap fully around the model, allowing the orientation of the grid (derived from a smooth cross field) to vary across the surface for best alignment to its geometric features. Rigid assembly is assured by cutting some slots as 'wedges' to enable the simultaneous engagement of non-parallel intersections, Fig. 2.14(c). Orthogonality of the strips may be prescribed for local-stability, or not, with global rigidity achieved by the use of a sufficiently dense grid to ensure mutual interlocking of slices forming an array of rigid cycles. The results are visually impressive and significantly more material-efficient than conventional sliceforms.

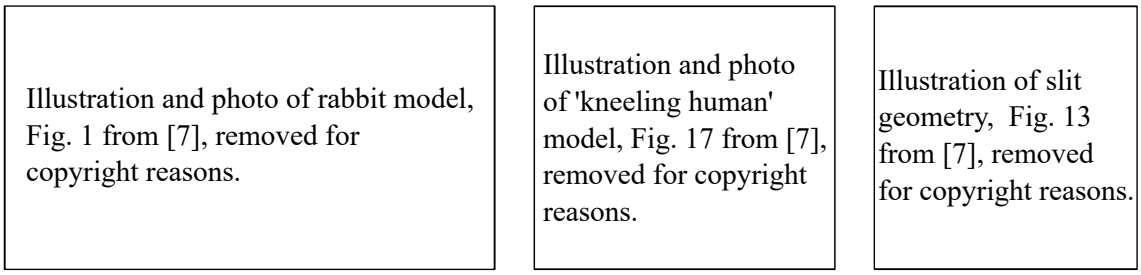

Fig. 2.14 Field aligned mesh joinery by Cignoni et al.[7]. (a) The Stanford bunny, (b) a kneeling figure, (automatically generated cross-field and final structure shown for both). (c) detail of slot design enabling non-orthogonal cycles to be completed via rigid-assembly – note the 'wedge' cut in place of a slot in the red piece so that it can interlock with the yellow piece whilst sliding along the direction of its intersection with the green piece.

2.10 Summary

The key principle for generation of a geometrically feasible sliceform has been identified: that no pair of intersection lines should themselves intersect within the global volume. Additionally, rigid slices require that a rigid assembly path can be designed, which necessitates that co-interlocking intersections (*i.e.* those that share a common slice and must be simultanously interlocked on addition of that slice to the assembly) are parallel. These conditions set relatively stringent limitations on the structural architecture, so most designs use a lattice-style structural architecture with two orthogonal sets of parallel slices, or a variant thereof in which at les. However, if the slices are flexible the design space is significantly increased as non-parallel intersections may be engaged simultaneously, though they must still remain relatively closely aligned.

With rigid slices, the range of rotation admitted by each pair of interlocking slots is dictated purely by their geometric fit, with tight slots accommodating only orthogonal intersections and non-tight slots allowing rotation of the slices through orthogonal until reaching an equal and opposite inclination. Using flexible slices, the intersections permit additional rotation about their axis under a prising action of each slice on each slot, and correspondingly allowing non-orthogonal intersections to be accommodated using material-width slots. Each intersection is then free to articulate as a simple hinge so that rigidity is dependent on the structural architecture as a spatial mechanism. A rigid-assemble-able lattice sliceform with parallel intersection lines is thus bi-directionally flat-foldable via a global shear action.

Several studies have been conducted into the development of methods for automated synthesis of a visually effective sliceform from a target volumetric geometry. In these previous investigations orthogonality of the slices is often prescribed so that the structure can be constructed from rigid slices, assuring global rigidity via the local rigidity of each intersecction, or global rigidity pursued by ensuring that each slice forms part of a closed cycle which will generally be rigid.

However, relatively little exploration has been done of the wider design space of non-rigid-assembleable sliceforms using flexible slices. The torus is one such example with its global mobility suggesting a clear opportunity to exploit this simple construction technique in the generation of new transformable or deployable structures. To date such structures have not been investigated and, unlike the simple shear-mode action of a lattice-sliceform, it is not immediately apparent how this new arrangement of slices leads to the unusual one-way deployability exhibited by the partially-assembled form. This thesis seeks to develop an understanding of how this unusual action arises and also to investigate whether this can be extended to the design of deployable sliceform structures of a more general form.

Chapter 3

Background concepts and related structures

3.1 Introduction

In the previous chapter the basic principles for the geometric design of a sliceform were identified. They have mostly been treated as sculptural forms with consideration of their structural mechanics limited to ensuring rigidity by use of tight intersections and thick slices, usually by prescribing orthogonality of each intersecting pair, or by forming an array of closed cycles. The sole exception is the design of 'pop-ups' based on a lattice-style architecture whose bi-directional flat-foldability follows from the array of parallel slices and parallel intersection lines.

The discovery that a sliceform torus is also foldable, albeit with an unusual one-directional flat-foldability, demonstrates that foldability is not limited to lattice sliceforms and suggests the possibility to design a wider range of deployable, volumetric sliceforms.

It is not immediately obvious how to approach their analysis because their structural form does not fit neatly within any other structural concept: a folding sliceform clearly functions as a linkage, but a linkage of plates rather than bars, and, unlike origami, each slice itself is not folded, mobility instead enabled by each pair of interlocking slots forming a rudimentary scissor-joint. Insights and inspiration into their treatment are therefore drawn from a range of disciplines; a broad overview is now provided.

3.1.1 Chapter outline

In this chapter, some basic principles and features of kinematic mechanisms are introduced, the design of folding scissor structures is explored in detail, and an overview of concepts and methods of analysis for origami structures is provided. In addition to specific kinematic principles, the techniques for analysis of these structural concepts serve to inform the investigation of sliceforms in the remainder of this thesis.

3.2 Kinematic mechanisms

The deployable motion of a sliceform is admitted by each slotted intersection functioning as a rudimentary hinge so that the array of interlocked slices thereby embeds a spatial mechanism. To lay the foundations for this investigation of sliceforms as deployable structures it is useful to first set out some principles and key results from mechanism engineering.

Fundamentally, most conventional mechanisms are an assembly of rigid *links* connected by kinematic joints, otherwise known as kinematic *pairs*[40]. The mobility, m, of a linkage with N links and j joints is given by the Grübler–Kutzbach mobility criterion[40]

$$m = \begin{cases} 3(N-j-1)+\sum_{i=1}^{j} f_i & \text{in two-dimensions,} \\ 6(N-j-1)+\sum_{i=1}^{j} f_i & \text{in three-dimensions} \end{cases} \tag{3.1}$$

where each f_i is the degrees-of-freedom afforded by the kinematic pair denoted as joint j_i.

This calculation sets the expected mobility of a general linkage based on its topology, with the true mobility of dependent on its specific geometry. Indeed, many of the most interesting linkages are *overconstrained*, meaning that they exhibit more degrees of mobility than this formula predicts. Such cases arise when the particular geometry of the linkage is such that one or more joints constrain the same degree of freedom and thus become *redundant*, or if subsets of the linkage are cognate and follow identical motion paths (often due to symmetry). Note that it is not possible for a linkage to exhibit fewer degrees of freedom than predicted by this formula, though a degree of freedom may be *idle*, meaning that it does not give rise to a change in linkage geometry, such as a doubly-ball jointed link rotating about its own axis[92]. The study of mechanisms is thus fundamentally a study of geometry.

3.2.1 Mobility of a bar structure

Of particular interest to structural engineers is the subset of mechanisms formed from a pin-jointed bar network, *i.e.* a pin-jointed truss. A similar mobility criterion can be derived for these systems by examining the equilibrium matrix relating the internal bar tensions to external nodal forces (or, equivalently, the compatibility matrix relating the nodal displacements to bar extensions, which is the transpose of the equilibrium matrix). From the dimension of the vector subspaces of these matrices, a simple counting rule for determining mobility was formulated by Maxwell in 1864[51], and generalised by Calladine in 1978[3]: for an unsupported bar framework with b bars and j joints,

$$m - s = \begin{cases} 2j - b - 3 & \text{in two-dimensions,} \\ 3j - b - 6 & \text{in three-dimensions} \end{cases} \tag{3.2}$$

where $m - s$ is the number of mechanisms (finite and infinitesimal) minus the number of states of self-stress.

Again, this topological calculation sets a rudimentary expectation of the mobility and determinacy of the structure, whose true behaviour is dependent on the specific geometry. It follows that two topologically equivalent bar networks with identical expected mobility can be rigid-determinate and mobile-indeterminate depending on their specific geometry.

Mobility of a repetitive bar structure

This rule is readily applied to a finite system of bars and joints, but must be adapted for infinite, repetitive structures. Examining the smallest repeating 'motif', the mobility of a periodic structure is[31]

$$m - s = \begin{cases} 2j - b + 1 & \text{in two-dimensions,} \\ 3j - b + 3 & \text{in three-dimensions} \end{cases} \tag{3.3}$$

where joints on the boundary are counted as '$\frac{1}{2}$'. Care must be taken when selecting an appropriate unit cell as only mechanisms that break symmetry but are consistent with the tessellation can be found.

Mobility of a mechanism with an embedded pin joint

The standard pin-jointed-bar model assumes that all bars carry only axial tension/compression and are free to rotate about each joint. An extended rule has been formulated by Seffen to accommodate frameworks with enclosed pins (*i.e.* scissor joints) by noting that each enclosed pin induces a shear force and bending moment profile in that bar and thus introduces two additional equilibrium terms[77]. His modified rule states that

$$m - s = 2j - b - 2j_e - 3 \quad \text{in two-dimensions} \tag{3.4}$$

j is the number of pin joints (including enclosed pins), and j_e is the number of enclosed pins.

An equivalent result is obtained by modifying the topology of the structure so that the standard counting rule can be applied by promoting each embedded pin out of the bar in which it is enclosed and joining it to that bars' ends by two additional bars, thus increasing b by two per embedded pin.

3.2.2 Range of motion of a finite mechanism

The mobility of a mechanism is a rudimentary measure of its (lack of) rigidity. However it does not say anything about the character of the motion admitted, which may be *finite* or *infinitesimal*. The former indicates that the system can deform continuously without the links themselves deforming; the latter that the system has an instantaneous mode of mobility that does not incur link deformations, but, upon motion, the deformed configuration is immediately rigid[89]. For deployable structures the former is often desirable so that the transformation between configurations can occur without damage, the latter is usually undesirable as it corresponds to a 'soft' mode in which the structure cannot carry load without first deforming to first order.

For a finite mechanism, the range of motion is dependent on the particular geometric design and may be limited by the collision of components, or joints reaching their maximum extension. However, the latter condition has a subtlety: via set theory, Connelly and Guest establish that "...if a finite mechanism is such that the motion seems to stop at some point, and must then retrace the same path used to arrive at that configuration, then it is not exactly a true finite mechanism", [9]: *i.e.* , save for limitations due to, for example, collisions between articulating members or contact with an external 'stop', a finite mechanism cannot have an endpoint. A finite mechanism may appear to have an endpoint if its motion exhibits a 'cusp' in which the motion of a joint reaches some limit then reverses, but is, in fact, tracing an

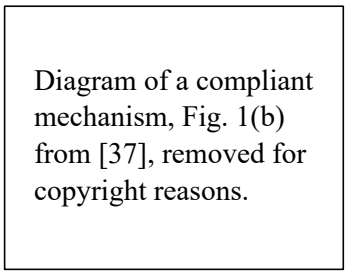

(a)

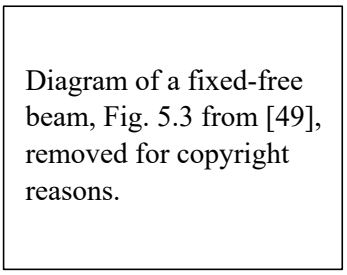

(b)

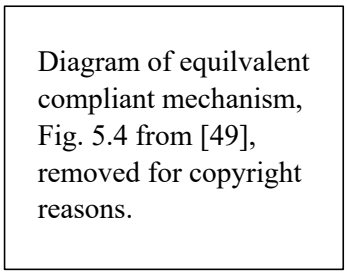

(c)

Fig. 3.1 (a) A compliant mechanism replicating a planar four-bar linkage. (b) Schematic of the deflection of a fixed-free beam with perpendicular end load, and pseudo-rigid-body model of the system using rigid links, pivot joints and torsional springs, (c). Figure (a) from [37], (b) & (c) from [49].

alternate path away from the cusp point and will eventually loop back around and retrace the original path.

3.2.3 Compliant mechanisms

Worth briefly mentioning are *compliant mechanisms*. As per the name, these are mechanisms which achieve motion via 'compliance' (*i.e.* elastic or plastic deformation – usually the former) of the components. Such designs commonly employ 'living-hinges' in which a contiguous beam is locally thinned so that its deformation is concentrated at that specific location which functions as a hinge, Fig. 3.1(a). These mechanisms can be manufactured from a single piece, with no moving parts, and without requiring assembly, making them simple to manufacture (*e.g.* by 3D printing) and useful for applications at small length scales and where reliability is critical. Design and analysis of these structures typically involves the formulation of an appropriate *pseudo-rigid-body* model (PSRB) – in which the compliant segments are replaced by pin-jointed rigid segments with appropriate torsional springs capture the elastic stiffness, Fig. 3.1(b)-(c) – so that its kinematics may be investigated via application of conventional techniques to this equivalent discrete mechanism[37, 38, 49].

3.3 Scissor structures

A class of mechanism of particular relevance to this investigation are *scissor structural mechanisms* (SSM) constructed from *scissor links*. A scissor-link (or *scissor-like element* (SLE), or *scissor-unit* (SU) is simply a pair of beams joined by an embedded rotational pivot. The two bars are free to rotate about this central pivot in neighbouring planes, and each unit

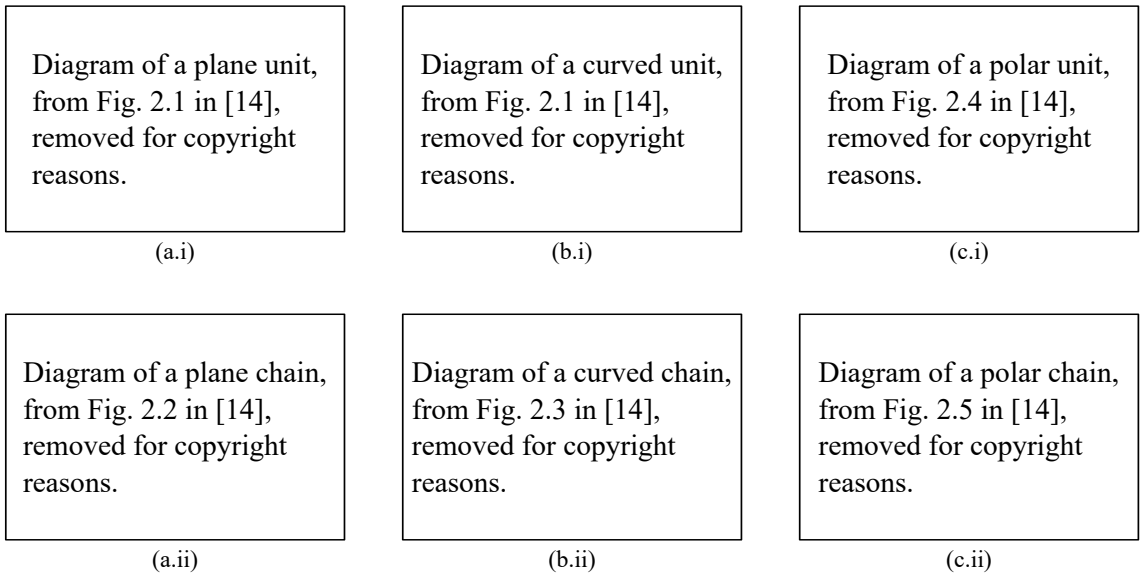

Fig. 3.2 Scissor unit topologies (top) and chains (bottom): (a) translational unit with equal length bars and midpoint pivots, (b) curved-translational unit with midpoint pivots and unequal length bars, (c) polar unit with off-centre pivot. Adapted from [14].

thus exhibits the same single-degree-of-freedom rotational mobility as a pair of interlocking slices. The potential of this kinematic scissor unit becomes apparent when arrayed to form two- or three-dimensional deployable structures. There has been much research into their design and analysis from which to appeal to for insight and inspiration toward the present study of deployable sliceforms.

3.3.1 Scissor mechanism

The motion of an SSM derives directly from the geometry of each SLE, of which there are several distinct generalised forms. Using straight bars the simplest unit is a symmetric *translational* unit which consists of a pair of equal-length bars spanning parallel interface lines with the pivot at their midpoint, Fig. 3.2(a). This unit generates rectilinear motion as it articulates with a chain of units deploying along a line. If the bars have unequal length, a *curved-translational* unit which generates rectilinear motion to an inclined path, and a chain may be constructed conforming to a curve, Fig. 3.2(b). Alternatively, moving the pin off-centre within each bar causes the unit to span a wedge with the angle subtended varying as the unit articulates, generating curvilinear motion about an arc, Fig. 3.2(c).

3.3.2 Foldable scissor structures

A single-degree-of-freedom chain is generated by combining scissor units in series so that each inherits its configuration from that preceding it. Such a structure is mobile between natural limits resulting from whichever unit first reaches its maximum deployment/contraction position as restricted by collision of the joints at the end of adjacent semi-lengths (*i.e.* from $0 \rightarrow \pi$).

For application in deployable structures, it is usually desirable that, upon folding, the units reach their maximum compactness simultaneously and so collapse to a bundle of *flat-folded*, (nominally) collinear bars. Examination of the series of quadrilaterals spanning each interface line, where the total length of the semi-bars on either side of the interface must be equal for this to occur, yields Escrig's *deployability condition*[16] (Fig. 3.3):

$$a + b = c + d$$

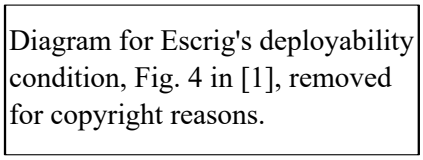

Fig. 3.3 Escrig's deployability condition for a flat-foldable chain of (straight) SLEs states that the total bar lengths either side of each closed cell must be equal: $a + b = c + d$ [16]. Figure from [1]

This deployability condition has an elegant geometric representation: a given pair of scissor links are flat-foldable when their pivots lie (anywhere) on the ellipse whose foci are the interface pins, Fig. 3.4. A flat-foldable chain of links thus embeds a tangential chain of similar ellipses and, inverting this relationship, a flat-foldable chain of scissor units conforming to an arbitrary planar curve can be designed by generating a series of tangential ellipses[72]. If the major axes of the ellipses are parallel, curved-translational units are generated; if the major units are inclined, a polar unit is generated between each pair.

A flat-foldable chain of curved-translational SLEs along an arbitrary curve is generated by arranging tangential ellipses with parallel major axes, Fig. 3.5. Using ellipses of constant size results in a linkage of constant thickness(*i.e.* span of unit endpoints along interface lines); a linkage of variable thickness is generated using similar ellipses of varying scale. The ellipses may also be centred on the curve, which then traces the midpoint of each interface, or arranged so that their tangents lie on the curve, which then runs through the unit pivots.

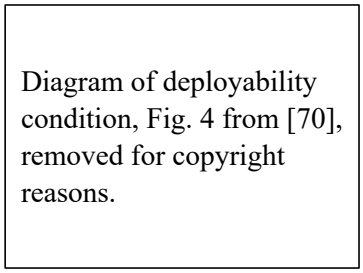

Fig. 3.4 Escrig's deployability condition has an elegant geometric representation. A pair of scissors are flat-foldable when their pivot points lie on an ellipse whose foci are the bar endpoints. Given the left-hand scissor unit, the pivot of the scissor unit on the right must lie on this ellipse for the pair to be flat-foldable: p, p' and p'' (and associated bars) are all possible solutions. This pair of units have thickness t in this deployed configuration. Adapted from [70].

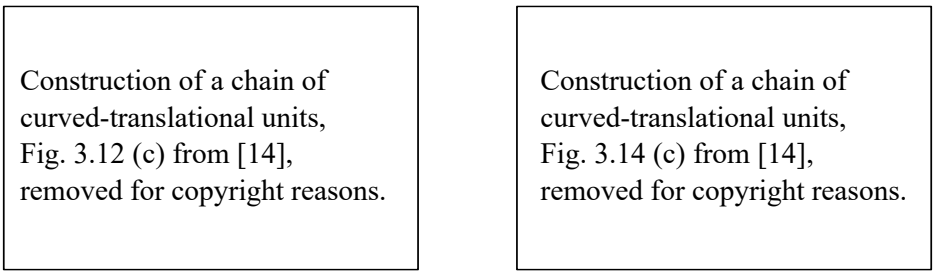

(a) (b)

Fig. 3.5 Geometric construction of a chain of curved-translational units confirming to a target curve. (a) A constant thickness chain is generated using identical ellipses with parallel major axes where double-size ellipses – as shown – are used to locate the centre-points of consecutive ellipses on the curve. (b) Using similar ellipses of various size generates a chain with varying thickness. Figures from [14].

For construction of a chain of polar units along a circular arc, the ellipse-fitting approach can be simplified by generating a series of tangential circles with their contact points along the base curve. The contact points locate the pivot of each unit and the interface lines radiate from the centre of curvature. Each cell is symmetric and the chain is flat-foldable[72]. This approach can also be applied to a curve comprising a series of conjoined circular arcs to generate a more general form[14].

3.3.3 Angulated elements

Scissor structures based on straight bars with the pivot at their cross-point generate either rectilinear or curvilinear motion as the chains expand and contract. An important development

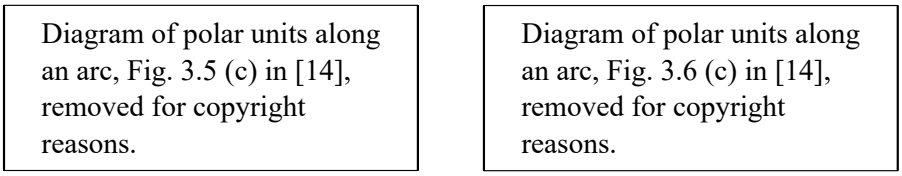

Fig. 3.6 Geometric construction of a chain of polar units confirming to a circular curve using tangential circles to locate each pivot point. (a) A constant thickness chain is generated using circles of constant radius. (b) A chain of varying thickness results from circles of non-constant radius. Figures from [14].

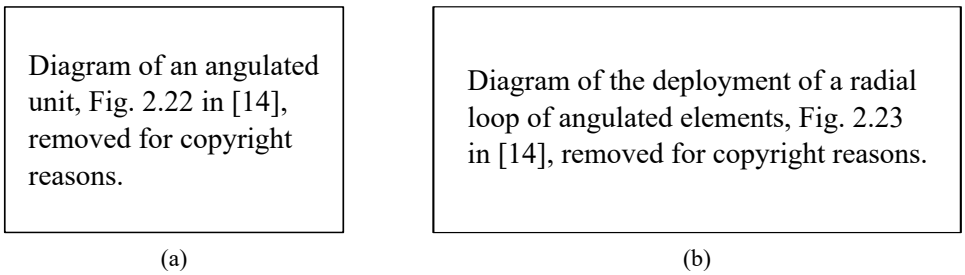

Fig. 3.7 Hoberman's angulated unit is formed from a pair of identical angulated rods joined at their vertexes, (a). This unit subtends a constant angle as it articulates and a circular loop expands and contracts like an iris, (b). Various 3D structures can be constructed from these elements which retain their shape as they expand and contract. Figures from [14]

was made by Hoberman who discovered the *angulated element* comprising a pair of identical angulated beams joined at their vertex to form a pair of similar isosceles triangles at their interface lines[36], Fig. 3.7(a). The angle subtended by this unit is invariant as the scissor articulates, producing a 'scaling' motion as it slides radially within the wedge it spans. A planar ring of elements can now open and close like an aperture while remaining a complete loop, Fig. 3.7(b).

These angulated units are no longer 'flat-foldable', instead reaching maximum compactness when the units reaches the apex of the wedge subtended and maximum expansion when the links are coincident. The maximum radius of the outer bar ends is achieved when the upper limbs become parallel, then slightly retract in the final phase of expansion as the inner bar ends move to meet them.

Generalised angulated elements

Much greater geometric flexibility to design rigid-foldable chains is afforded by *Generalised angulated elements* (GAE) whose semi-lengths may be equal – type I, forming a pair of

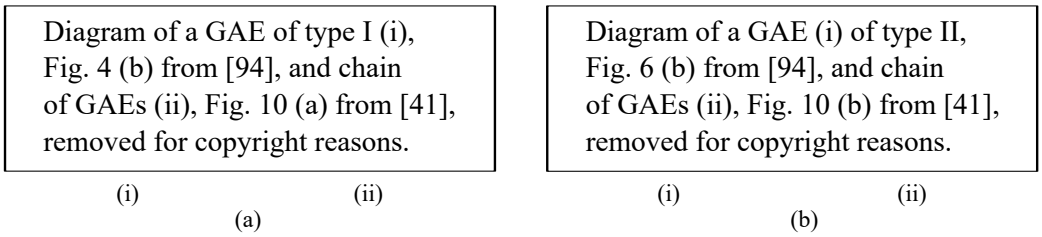

Fig. 3.8 Generalised angulated elements (GAE)[94], (i), and chains, (ii), of type I (equal semi-lengths, forming isosceles triangles), (a), and type II (proportional semi-lengths, forming similar triangles), (b). (i) from [94], (ii) from [41].

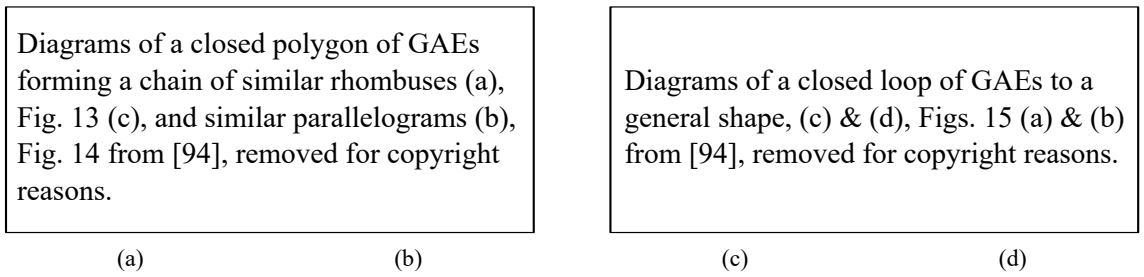

Fig. 3.9 Rigid-foldable, closed loops of GAEs can be generated form target polygon by constructing angulated units with their pivots at each vertex and semi-lengths along each edge: using symmetric GAEs generates a chain of similar rhombuses, (a); proportional GAEs form a chain of similar parallelograms, (b). These are foldable as each quadrilateral scales proportionally during actuation. For a general shape, a foldable bar structure can be generated from a chain of similar rhombuses, (c). If the shape is symmetric, any mirrored arrangement of GAEs of type I and II will be foldable, (d). Adapted from [94].

isosceles triangles – or proportional – type II, forming a pair of similar triangles[94]. A chain of GAEs consists of a series of articulating parallelograms.

Rigid-foldability of a general closed-chain of GAEs (*i.e.* non-circular) is not guaranteed because a mismatch in radial shift may arise about the loop during motion. Foldable loops corresponding to a given polygon are designed by geometric construction of the fully expanded configuration. Placing scissor units with their pivots at each vertex and semi-lengths proportional to each edge forms a series of similar parallelograms. These deform proportionally, thus ensuring that the radial shift sums to zero about the loop[94]. If the semi-lengths are equal to half of each side length, the GAEs are symmetric (Hoberman's) and the parallelograms are rhombuses[36]. Alternatively, if the target shape has one or more axes of symmetry, more general rigid-foldability designs can be generated with geometric compatibility invoked by simply mirroring the chain of GAEs across the axis so that the net radial shift must, again, sum to zero[94].

3.3.4 Scissor grids

A scissor unit articulates within its plane, and a chain of units form a two-dimensional linkage. By combining scissor units to form a grid, many two- and three-dimensional deployable structures can be constructed. Hanaor and Levy identified three main classifications: *linear* with multiple chains enclosing a prismatic section and deploying along its axis; *single-layer* (Single layer grid, SLG) with elements coplanar to the surface generated; and *double-layer* (Double layer grid, DLG) with elements perpendicular to the surface and spanning two layers of nodes[17, 32]. Linear structures are used for deployable booms, whilst SLGs and DLGs are used to generate shell-like structures which may be flat, singly- or doubly- curved.

Where an open chain of scissor elements is foldable because each single-degree-of-freedom simply matches the span of that preceding it, a grid forms an array of closed loops and so the principal challenge in designing a foldable three-dimensional scissor structure is to generate a set of scissor units which conform to the desired deployed shape and whose folding motion is geometrically compatible.

3.3.5 Single-layer grids/Multi-layer chains

Single-layer grids are formed from a two-dimensional grid of scissor units forming a surface and require curvature, preferably double curvature, to generate structural depth [67]. These lack the stiffness of double-layer grids (which orient the scissors perpendicular to the surface) so practical applications and associated research are limited; however, some basic principles are readily identified.

To form a planar single-layer grid, multiple chains of scissor elements must be be joined to form a two-dimensional array of cells. The challenge, then, is to find chains which can be laid side-by-side and whose nodes will coincide throughout motion.

The simplest case is if the scissors form a grid of aligned parallelograms with collinear bars: compatibility is assured by symmetry and successive bars may be joined to form a bi-directionally flat-foldable ‘trellis’, Fig. 3.10(a).

More interesting designs are possible though. Using straight bars, a pair of chains can be joined along their seam provided that the path through the lower nodes of the upper chain exactly matches the path through the upper nodes of the lower chain at all configurations This will not be true for a general pair of chains, even if they fit together in a single configuration. With translational units, a chain of equal, constant-thickness (so that upper and lower node paths are parallel) can be arrayed and joined along each seam, Fig. 3.10(b). Flat-foldability (in each sense) is governed by the usual deployability condition applied to each closed loop,

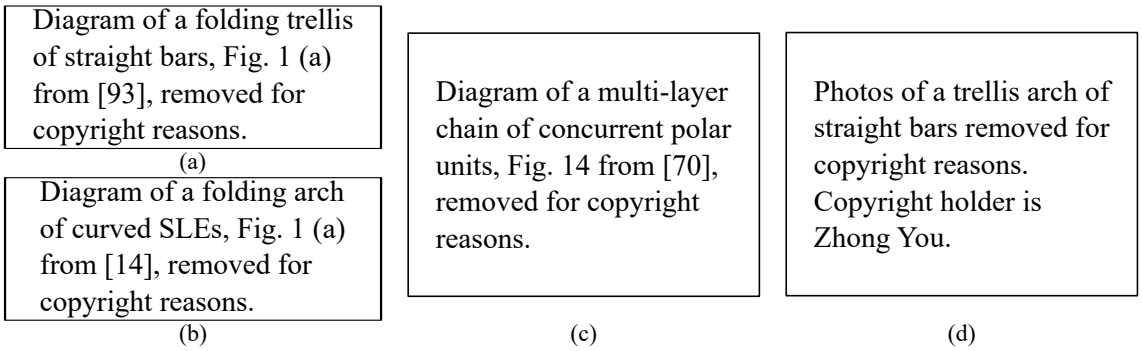

Fig. 3.10 Single-layer grids are formed from multiple adjacent chains of scissor links. (a) A trellis with a grid of aligned parallelograms is bi-directionally rigid-deployable by symmetry and the bars can be joined to continuous rods. (b) Multi-layer chains of curved-translational units with coincident interface lines mapping the same curve are rigid-foldable if each layer has constant thickness so that the upper and lower surfaces are parallel, (b adapted from . (c) The same applies to multi-layer chains of concurrent polar units in which each layer is appropriately scaled. Deployable but non-rigid-folding designs are also possible, such as the curved portion of this trellis arch, (d). (a) from [93], (b) from [14], (c) from [70]

Source: (d) Deployable trellis arch. *Deployable structures group, University of Oxford*, http://www2.eng.ox.ac.uk/deployable/research/toys.

and also each inset loop[17]. For flat chains (*i.e.* along a straight line), each layer may be of independent(though still constant)-thickness, with maximum extension limited by the thinnest layer, an effect employed by Zanardo in his design for a self-restraining deployable boom[96].

Using concurrent polar units, multiple chains with parallel upper and lower surfaces (note that this does not (necessarily) equate to constant thickness along each interface line) can be joined if successive chains are scaled to form a series of parallelograms along each seam[70], Fig. 3.10(c).

Deployable but non-rigid-foldable designs are also possible, such as the circular portion of the trellis arch in Fig. 3.10(d) where each cell is symmetric about the radius of the curve and thus flat-foldable.

More design options are afforded by using angulated elements. Concentric circular rings of symmetric angulated elements (which may be different from layer-to-layer) remain rigid-foldable. Using identical rings the maximum expansion and retraction of the system is limited by the inner and outer chains respectively, though, helpfully, the outer diameter remains relatively constant during folding, making such designs an ideal basis for retractable roofs[94]. Furthermore, with identical scissors in each layer the “contiguous angulated rods can be connected rigidly to one another, to form multi-angulated rods”[94]. A result that

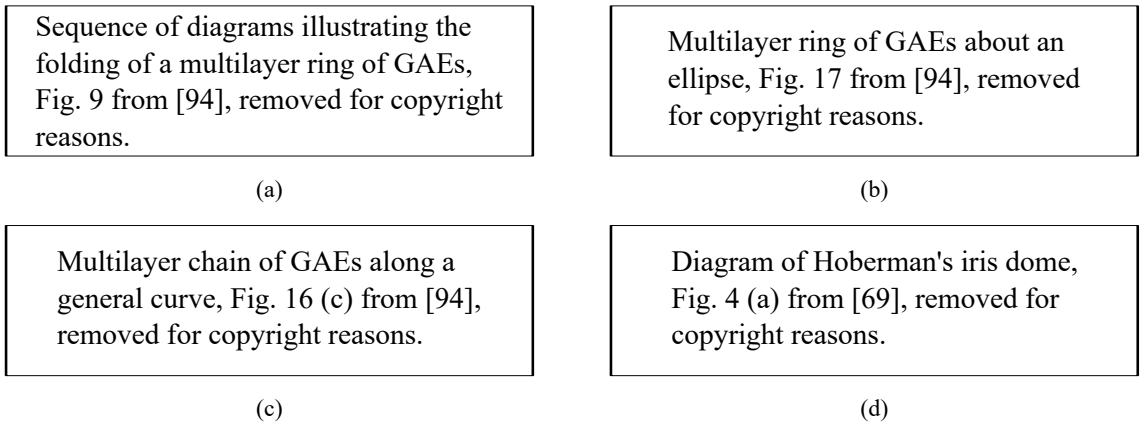

Fig. 3.11 Rigid-foldable single-layer grids of GAEs can be formed from concentric rings. For a planar ring with identical scissors in each layer, (a), "contiguous angulated rods" can be joined to form "multi-angulated rods" (*e.g.* $A_0 - A_1 - A_2 - A_3 - A_4$). This can be applied to general multi-layer linkages when each additional layer forms a series of parallelograms, *e.g.* an ellipse, (b), or general curve, (c). Hoberman's 'Iris dome', (d), uses concentric rings of angulated elements placed successively steeper conical surfaces to form a doubly-curved retractable roof. (a)-(c) from [94], (d) from [69].

is elegantly proved by demonstrating that the kink angle between the rods of successive layers is configuration-independent and thus constant throughout folding motion, Fig. 3.11(a). Additional layers of links can be augmented to chains of GAEs of general shape (closed or open), with multi-angulated rods viable when each additional layer forms a series of parallelograms, Fig. 3.11(b)&(c). Hoberman designed a doubly-curved, retractable 'iris dome' by placing rings of angulated elements on successively steeper conical surfaces[36], Fig. 3.11(d).

Conn & Rossiter designed a 'smart' radially foldable structure constructed from a ring of modified angulated elements[8]. By adjusting the kink-angle of each element in a rigid-folding ring (by a few degrees), the structure becomes geometrically compatible in only the retracted configuration. This geometric misfit is clearly visible if one joint is unlinked, the previously connected beams now separating as the ring is closed, Fig. 3.12(a). The monostable, fully connected ring can be forced to contract, but this requires the units to bend in opposition to the modification, storing strain energy in the system. When released, the structure automatically retracts driven by the release this strain energy, Fig. 3.12(b). Analysis of this structure is based on standard beam theory with the stored energy calculated from the elastic bending and compression required at each intermediate configuration, Fig. 3.12(c). The addition of an appropriate external spring enables bistable action so that the unit snaps between closed and retracted configurations.

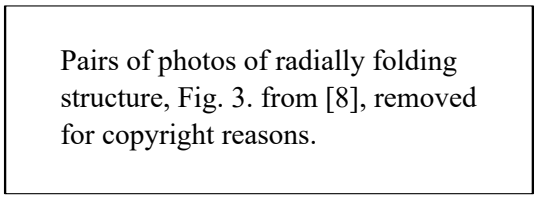

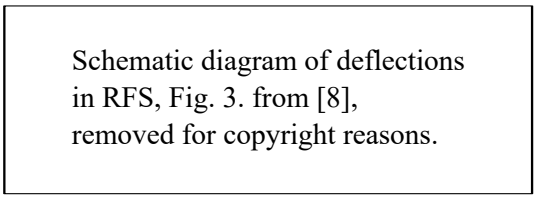

(a) (b) (c)

Fig. 3.12 A 'smart radially folding structure' by Conn & Rossiter. (a) It is constructed from a ring of modified GAEs in which each kink angle is misaligned so that the units fit together in the expanded, (ii), but not the contracted configuration, (i). (b) When this monostable structure is forcibly contracted. (i), the misfit is accommodated by elastic deformation of the beams, storing strain energy that drives the retraction of the loop when released, (ii). The strain energy stored in bending and compression of the elements at a given configuration is calculated via simple beam theory, (c). Figures from [8].

3.3.6 Double-layer grids

Foldable cells

Much greater research effort has been directed at the design and analysis of linear structures and double-layer grids. Both comprise an array of plane-faced-cells (linear and grid arrays, respectively), each a closed chain of scissor units. A single cell is a single-degree-of-freedom linkage when unwrapped, but compatibility of the two ends must be maintained for the closed-loop to be foldable, Fig. 3.13. The deployability constraint must be met about each edge for flat-foldability, in which case the scissor structure collapses to a compact bundle of bars. Langbecker constructed analytical expressions for the foldability conditions by setting the sum of 'foldability vectors' (*i.e.* the vector spanning each unit from interface midpoint to interface midpoint) equal to zero to complete a closed loop[44].

Quadrangular DLGs

Satisfaction of the non-trivial foldability condition for each loop is most straightforwardly achieved via symmetry: foldable doubly-curved DLGs can be generated by mutually translating a pair of chains of constant-thickness curved-translational units to form a quadrangular grid with parallel interface lines and symmetric cells[72], Fig. 3.14(a) & (b). A singly-curved design results when one of the chains is straight, in which case the curved chain may be formed from curved-translational or polar units (or a combination thereof), and may have non-constant thickness provided the straight chains are individually adjusted to match[67]. Multi-layer grids are also possible by adhering to the principles identified above[44], and

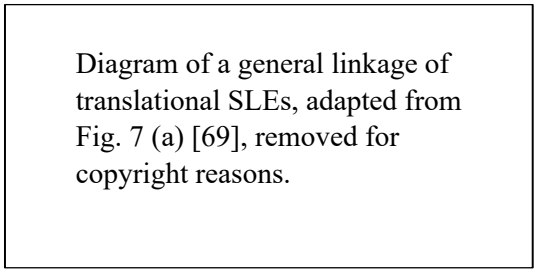

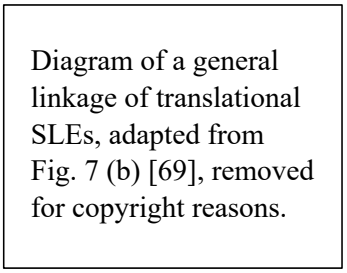

(a) (b)

Fig. 3.13 An open chain of scissor units has a single degree of freedom. The foldability of a unit formed by a closed chain of scissor units depends on the compatibility of the two ends of the unwrapped chain. The 'foldability vectors' across each cell must sum to zero to complete a closed loop. For a chain/cell of curved-translational units for which the component of each vectors parallel and perpendicular to the interface axes can be summed independently. Adapted from [69]

other tilings of symmetric, even-sided cells can be used to form more complex surface geometries[69], Fig. 3.14(c)-(e).

Using curved-translational units with parallel interface lines, it turns out that the loop closure conditions are independent of configuration, provided that the joints between units allow the enclosed angles to change – the projected shape varying due to the disproportionate variation in the span of each unit under articulation[69]. Thus, any such closed-loop of parallel-interface translational scissor units is rigid-foldable if it fits together in the design condition, *e.g.* example by construction on the surface of an n-sided prism, Fig. 3.15(a). A grid of these cells is rigid-foldable if the grid layout is able to accommodate the change of cell shape, *e.g.* a quadrangular grid with its in-plane shear mobility, Fig. 3.15(b). For flat-foldability, the layout must also be optimised so that each cell complies with the deployability condition[69].

This principle also applies to cells formed from concurrent polar scissor units, which can be formed by construction on the surface of an n-sided pyramid, Fig. 3.16(a). Spherical structures can be generated from quadrangular grids of polar units arranged in rhomboid and meridian patterns[18, 17], and non-spherical structures using the same layouts[68], Fig. 3.16(b)-(f). A grid with parallel upper and lower surfaces is achieved if the ratio of each bar's semi-lengths is constant, in which case foldable, multi-layer designs can be designed with each layer generated by scaling the previous by the same factor[70].

Note that even when each cell is rigid-foldable and the grid has an in-plane mobility, rigid-foldability of the overall structure is not guaranteed because the perimeter of each block

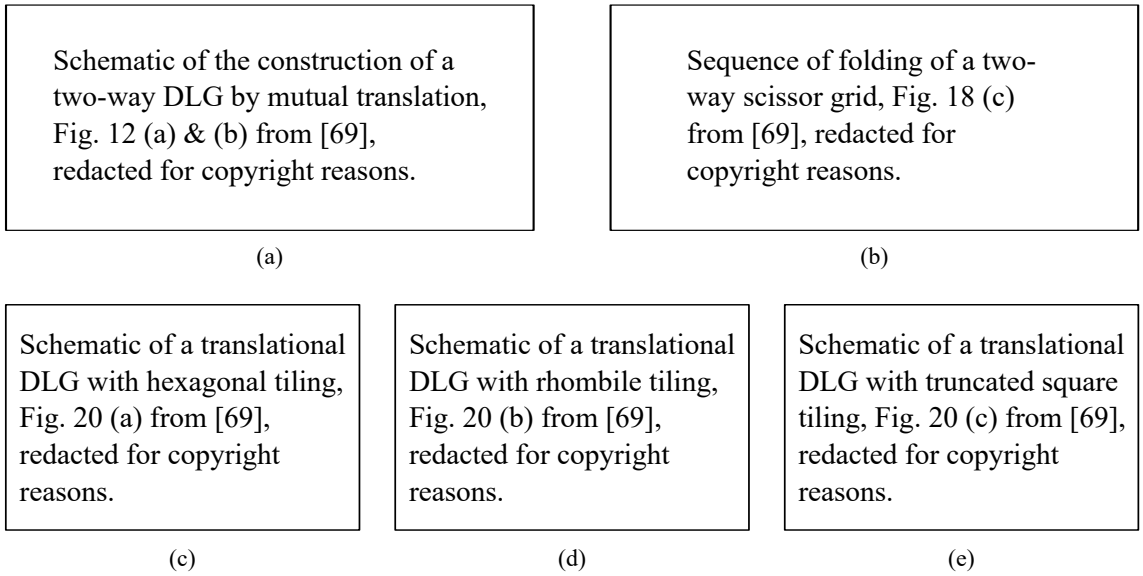

Fig. 3.14 A foldable DLG can be generated by mutual translation of a pair of rigid-folding chains of constant-thickness curved-translational scissor units, (a), to form an grid of symmetric, quadrangular cells describing a doubly-curved surface, (b). Rigid-foldability is assured by symmetry. This can be reproduced for other tilings of symmetric, even-sided cells to form complex folding surfaces, (c)-(e). Adapted from [69].

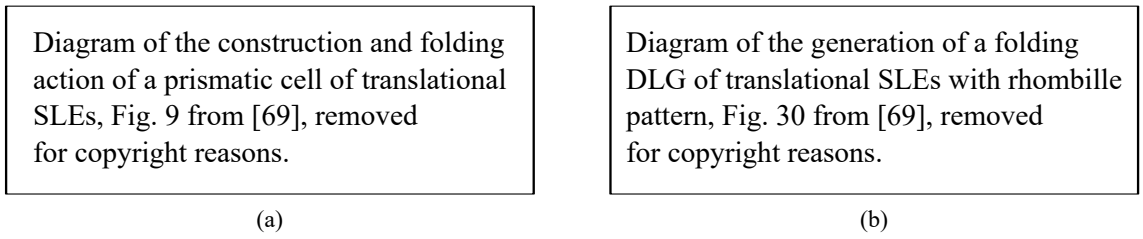

Fig. 3.15 A closed-loop of curved-translational scissor units with parallel interface lines is rigid-foldable if it fits together in a single condition, *e.g.* by construction on the faces of an n-sided prism, (a), though its projected shape will vary through articulation.A grid of prismatic cells is rigid-foldable provided it can accommodate this in-plane distortion, *e.g.* by using a grid of quadrangular cells. Therefore, a quadrangular DLG of curved-translational units mapping to surfaces of general curvature will usually be foldable, (b), with the layout of cells in this example also adjusted for deployability. Adapted from [69]

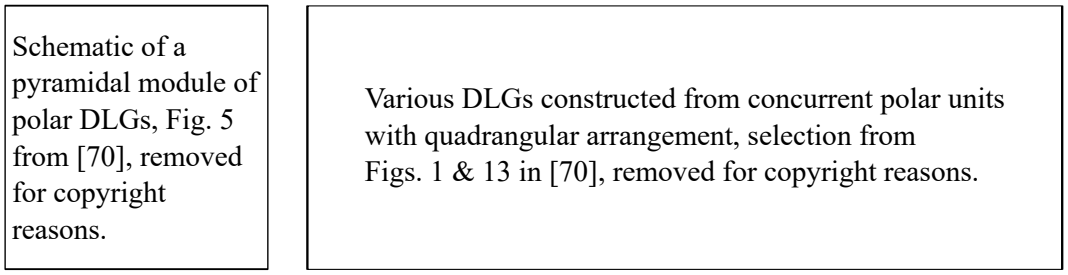

Fig. 3.16 A closed loop of polar scissor units is foldable if the interface lines are concurrent, though the shape of the cell may change during articulation. These cells can also articulate as a spherical linkage, (a), so a DLG generated from an array of concurrent polar units will generally be foldable provided the layout can admit this variation in cell shape. For example, (b) spherical grid of uniform rhomboids, (c) spherical grid of meridians, (d)-(f) non-spherical grids with uniform and lamellar rhomboid patterns. Adapted from [70]

of units must also accommodate the expansion of the internal grid. The array will be at-least bistable if flat-foldability conditions are otherwise met.

Quadrangular DLGs can also be constructed using angulated elements. Singly curved quadrangular grids are generated from a set of identical curved chains of GAEs bridged by a set of perpendicular chains of translational units to form symmetric cells, each of which slides within a wedge[44, 67]. Various closed volumes that expand and contract radially can be constructed as DLGs by placing chains of angulated elements along the edges of a polyhedron, or by forming networks of great arcs as in the eponymous and ubiquitous “Hoberman sphere”[36], Fig. 3.17(a). Axisymmetric surfaces can be modelled using meridians and parallels[42], *e.g.* Fig. 3.17(b), but more general shapes are possible – indeed, because the angle subtended by each unit is invariant, design of a foldable system of angulated elements is more straightforward than using scissors with straight bars. The key challenge in generating a DLG from a surface is to devise a suitable grid from the target surface. Roovers et al. suggest an approach in which the grid is devised from the networks of principal curvature so that adjacent gridpoint normals are coplanar. This grid can then be extruded perpendicular to the surface to generate a set of thin, developable strips: the *principal mesh*[66]. A well-conditioned mesh consists of an array of planar panels whose interface lines are normal to the surface which can then be populated with angulated scissor units, Fig. 3.17(c)-(e). Using multiple scissors along each panel provides more freedom for the designer to dimension the links: single scissors designs are generated via a circle-packing

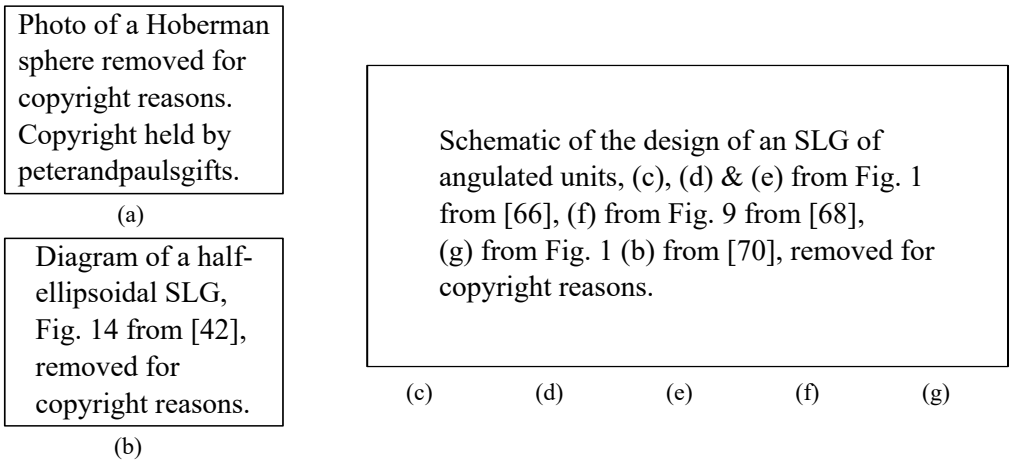

Fig. 3.17 The ubiquitous and eponymous 'Hoberman Sphere' comprises an array of great arcs formed by circular chains of symmetric angulated elements, (a). Axisymmetric surfaces can be modelled using a pattern of meridians and parallels (b), but more general 'scaling' grids can also be generated: either by devising a *principal mesh* with gridlines aligned to the directions of principal curvature, then populating each edge with a suitable chain of GAEs, (c)-(d)-(e); or, using single scissor units, via a circle packing method to locate each pivot, (c)-(f)-(g). (b) from [42], (c)-(e) from [66], (f) from [68], (g) from [70]

Source: (a) Hoberman Original - Transforming Sphere. *Peter & Paul's Gifts*, https://peterandpaulsgifts.com/products/hoberman-original-transforming-sphere

approach, the contact points locating the pivot points[68], Fig. 3.17(f)-(g). The best results are generated from ruled surfaces and surfaces of revolution.

Triangular DLGs

The in-plane mobility of the above designs, which is essential to enable their rigid-foldability, requires the addition of diagonal bracing elements to stabilise the cells in the deployed configuration (one per DOF), and so a foldable triangulated grid is desirable. A single triangulated cell with either parallel-interface curved-translational units or concurrent-interface polar units (a *tri-scissor*) is rigid-foldable, but because a curved triangulated grid is unable to accommodate changes in cell shape during articulation (a flat-foldable cell becoming equilateral when collapsed), compatibility of the cells can no longer be maintained at intermediate configurations[1]. As a result, only singly-curved triangular grids of curved-translational units

[1]Langbecker initially determined that a triangular loop of translational units could only be rigid-foldable if part of a planar grid, regardless of deployability, and proposed that pseudo-triangulated grids could be generated by forming one side of each cell from a double unit (*i.e.* forming a triangulated quadrilateral) and enabling rigid motion by sacrificing the in-plane rigidity originally sought[44]. However, his loop-closure analysis did not allow for the angles between scissor units to vary.

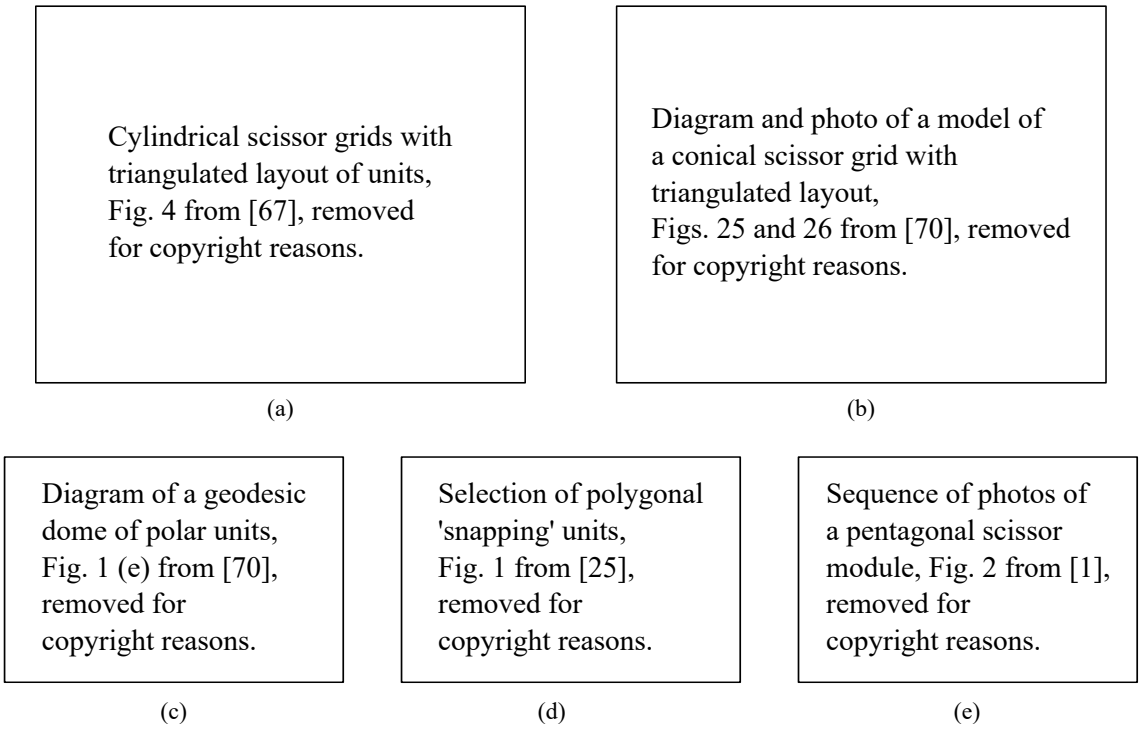

Fig. 3.18 A triangulated DLG may only be rigid-foldable if singly-curved with one row of units parallel or perpendicular to the ruled generators so that the cells are symmetric: *e.g.* cylindrical grids, (a), with polar units, (i), polar and plane-translational units, (ii), and plane- and curved-translational units, (iii); or conical with curved-translational units, (b). Doubly-curved triangulated DLGs may be flat-foldable but not rigid-foldable, in which case they are bistable, *e.g.* Zeigler's spherical geodesic dome using polar units, (c). Bistable DLGs can also be formed by triangulating a polyhedral grid to form an array of 'snapping' units, (d), with incompatible folding motion of a pentagonal cell shown in (e).
(a) from [67] , (b) & (c) from [70], (d) from [25], (e) from [1].

may be rigid-foldable. This is achieved when the grid consists of isosceles triangles oriented parallel or perpendicular to the ruled generator lines so that each cell may be symmetric[67][2], Fig. 3.18(a)-(b). A doubly curved DLG with a triangular grid of curved-translational or polar units may be flat-foldable but not rigid-foldable and are thus bistable, *e.g.* Escrig's geodesic dome[18, 70]. A spherical grid of angulated elements is non-flat-foldable but is rigid-foldable[68], Fig. 3.18(c).

A quadrangular grid of polar cells can be stabilised by addition of a pair of diagonal SLEs across each cell to form a triangulated 'snap-through' cell (or 'clicking' structure), an approach that can be reproduced for various even-sided polygonal tilings of a sphere to form

[2]Note that the conical DLG in Fig. 3.18(b) articulates much like the sliceform torus and the ring must be unlinked before it can be collapsed.

a variety of bistable triangulated spherical grids[97, 26], Fig. 3.18(d)-(e). These modules can also be placed in series to form a curved linear array, several of which may be repeated in parallel to form a singly-curved, bistable structure[25].

Rigid-folding and bistable DLGs

Rigid-foldability ensures that deployment of a scissor structure is smooth and strain-free. However, a rigid-foldable DLG will articulate freely between maximally contracted and expanded configurations, often allowing the structure to unfold beyond the target shape unless restrained by some sort of additional locking mechanism. This may be as simple as a set of wires that become tensioned once sufficiently deployed[93] or the membrane which the system is originally designed to support[70].

By contrast, bistable designs are 'self-stabilising' in the deployed configuration and can carry loads without needing external restraint. These structures are easier to generate initially (only needing to satisfy the deployability condition) but have more complex, dynamic motion between states. This requires careful design and testing to ensure that the structure will not become damaged during transition, usually trading-off stiffness in the deployed configuration against the stresses which must be accommodated during deployment without causing damage[26, 1].

Designing deployable DLGs

Foldable DLG's can be designed by ensuring the deployability condition is met about each interface line so that the resulting structure is, at least, bistable. This can be pursued by formulating the deployability constraint for a general unit and solving for the required semi-lengths, either analytically for simple geometries [69], or numerically for more complex cases [25]. Alternatively, a geometric approach can be used, as now described. A 3D linkage meets the deployability condition when, for each gridpoint, the pivot points of the scissor units lie on the surface of a prolate-spheroid (ellipsoid) aligned to the interface line, Fig. 3.19(a). Again, this geometric interpretation can be inverted to facilitate the design of flat-foldable DLGs, now by tangential ellipsoid fitting with the pivots of each scissor unit lying at their contact points. On a planar or spherical surface, this enables the design of a flat-foldable DLG (using translational and polar units, respectively) by solving a circle-packing problem to locate each interface axis and pivot point[68], Fig. 3.19(b).

On a general surface, the ellipsoid fitting method enables design of foldable structures using either curved-translational units with parallel interface lines, or polar units with concur-

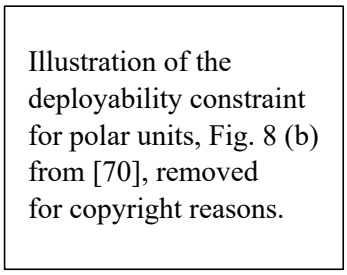

(a)

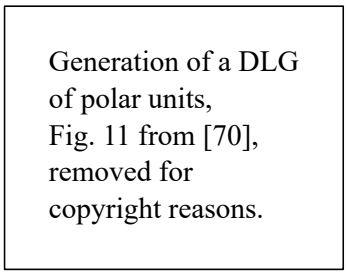

(b)

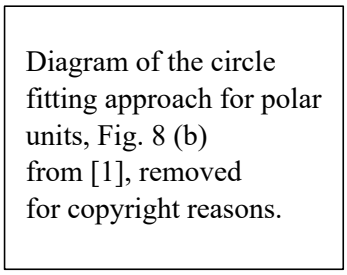

(c)

Fig. 3.19 A closed cell of scissor units is deployable when the pivots of each adjacent pair of scissors must lie on the surface of an ellipsoid centred on their interface line, (a). Therefore, deployable DLGs can be generated by fitting an array of tangential, similar ellipsoids. For general grids a bistable grid can be designed by fitting an array of tangential ellipsoids, as for the 'blob' structure using concurrent polar units in (b); for planar grids of translational units and spherical grids of polar units this can be simplified to a circle-fitting problem, (c); (a) & (b) from [70], (c) from [1]

rent interface lines to form non-spherical 'blobs'[70], Fig. 3.19(c). As usual, quadrangular designs are more readily rigid-foldable thanks to the in-plane mobility of the grid, whilst triangulated designs are usually bistable.

Where the design of a deployable chain of scissor units by generation of a set of tangential ellipses along a curve is relatively straightforward, each ellipse simply generated in sequence; the geometric conditions for a grid-structure are more complex because the scissor units meeting at each gridpoint must satisfy the deployability condition with all surrounding gridpoints simultaneously. During geometric construction, this usually requires the generation of a pair of flat-foldable scissor links that span the open ends of a pair of existing units, simultaneously satisfying two deployability conditions (*i.e.* addition of two edges to complete a quadrilateral cell in a grid). The challenge is to generate the ellipsoid that is tangential to the ellipsoids of both existing interfaces and lies on the surface to be synthesised. García-Mora & Sánchez-Sánchez have recently developed an approach to finding suitable solutions by generating the 'convergence surface' for a given pair of ellipsoids. This contains all points at which an ellipsoid can be centred and – when correctly oriented (coplanar to both existing interfaces) – will be tangential to both initial ellipsoids[27]. Generation of this surface is numerically expensive (though an approximate solution is more readily achieved[28]) but contains all possible flat-foldable solutions, from which the designer can select the point which is aligned to the existing grid and lies on the reference surface. Conventionally the DLG is centred on the surface at the midpoint of each interface, but this approach also enables

generation a DLG whose bar ends lie on the reference surface instead (useful for suspending an internal membrane, for example).

Design details

For design and analysis purposes, the joints between scissors in a DLG are treated as points, but consideration must be given to their practical design. Ball joints would allow the bar axes to remain coincident at each connection whilst rotating about the pivot and interface axes, thereby avoid altering the kinematics of the structure; however, these are complex and expensive. A simpler joint hub can be used if the scissor units are offset from the interface lines to add space between the bar ends (represented schematically by bar lines). For translational units the kinematics are unaffected if the bar lines are parallel or perpendicular to the interface lines[69], Fig. 3.20 (a)-(c), for polar units the bar lines must be perpendicular to the interface lines and scaled so that the now split interface lines remain coincident[70], Fig. 3.20 (d). Translational structures can thus be built with hubs of constant radius, while polar structures require a bespoke set of hubs. Bistable polar structures (*e.g.* a geodesic layout of concurrent polar units) are already incompatible at intermediate configurations so simpler, constant-radius hubs, Fig. 3.20 (e), can be used without altering the characteristic behaviour of the structure[70].

A common secondary objective is the minimisation of component diversity (*i.e.* number of different bar and joint geometries) for simplified manufacture and assembly, for which symmetrical or regular geometries are favoured[67].

3.4 Origami engineering

Conventional bar mechanisms are based on two- and three-dimensional assemblies of one-dimensional bar elements with nominally zero-dimensional joints. By contrast, papercraft structures comprise arrays of two-dimensional facets (which may be planar or singly-curved) with the folds, seams or slotted intersections forming one-dimensional hinges. Therefore, though a sliceform is formed from interlocking slices rather than folded plates, its basic geometric form is common to papercraft and principles and methods that might be applicable in this work can be sought in the study of these other forms. In particular, much attention has been directed at Origami (from *ori* meaning “folding” and *kami* meaning “paper”) which has been extensively studied by artists, mathematicians, engineers and scientists of all disciplines.

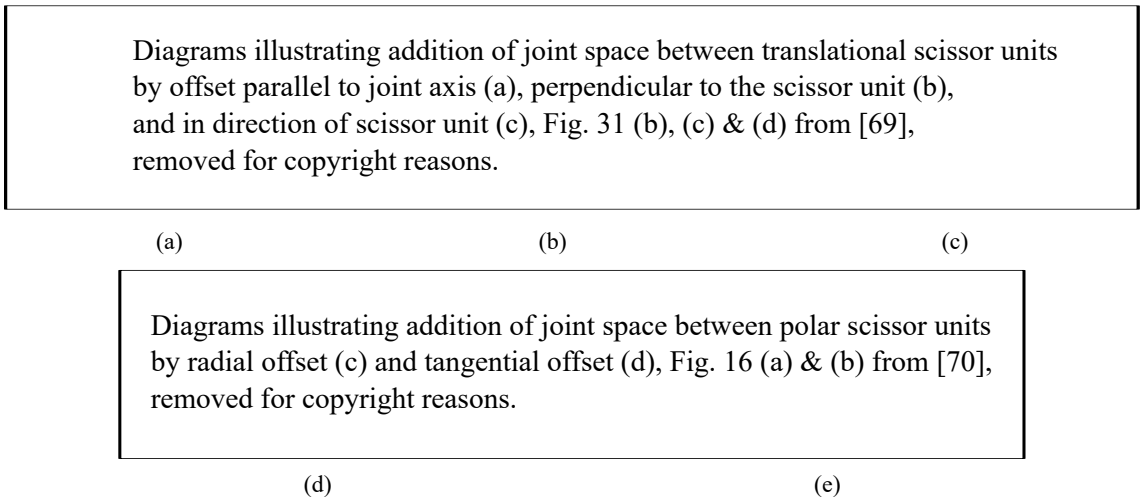

Fig. 3.20 Joint design for a DLG is simplified by adding space between each scissor unit, the joint represented schematically by *joint lines*. For translational units, the kinematics are unaffected if the joint lines are parallel to the interface lines, (a), perpendicular to the scissor unit, (b), or perpendicular to the interface lines and coplanar to the scissor unit, (c). Using polar units, the joints lines must be perpendicular to the interface lines and scaled so that concurrency is maintained to preserve rigid-foldability, (d); if the joint lines are constant length, (e), the deployability of the array is unaffected but a rigid-folding structure will become bistable. (a)-(c) from [69], (d) & (e) from [70].

The generation of three-dimensional structures from continuous two-dimensional sheets poses an interesting technical challenge which is encapsulated by Gauss' *Theorema Egregium* (Latin for "*Remarkable Theorem*") stating that the Gaussian curvature of a sheet, which is the product of its principal curvatures, is an intrinsic property and can only be changed by in-plane strain stretching (or compression) of the material[4]. Thus, under bending, an initially flat sheet can only become singly curved, with such surfaces described as being *developable*. For geometric design, only singly curved surfaces can be generated by developable transformations (bending, creasing, cutting, gluing) of an initially planar sheet. Non-developable, doubly-curved surfaces can only be approximated, either by a pattern which allows the mid-surface of a pleated sheet to map the surface of interest, *e.g.* [15, 5], or by a pattern which approximates the surface with an array of singly-curved facets and panels[85].

From a structural mechanics perspective, bending a sheet embeds it with a non-zero curvature meaning that it cannot now be bent or folded about any other axis without stretching, crumpling (thin sheets will crumple, *i.e.* buckle before compression becomes significant) or first flattening the material. The cross-section perpendicular to this axis now has structural depth, increasing the second moment of area and corresponding bending stiffness (this is the

principle behind corrugated sheets). Folding a sheet out-of-plane (*i.e.* not 180°) has the same effect along a line with the crease now acting as a rigid edge.

Origami engineering refers to any engineered structure manufactured or inspired by folding of a sheet. For a comprehensive survey of engineering applications for origami structures the reader is directed to Peraza-Hernandez et al.[64], Turner et al.[91], and Tachi[86], but several key classifications are relevant:

Kirigami (*kiri* = "cut" and *kami* = "paper") is a related form of papercraft in which sheets are cut before folding. The cutting pattern may feature straightforward 'slits' in which no material is removed, may remove external material to shape the planform of a sheet, or may even form internal holes. Fundamentally, the cutting operation enables surface discontinuities to be formed, permitting a wider range of geometric shapes to be folded.

Origami engineering refers to any engineered structure manufactured or inspired by folding of a sheet. Origami structures may be *active*, in which the folds act as hinges allowing motion of the structure, or *static*, with the folds generated by permanent deformation to form rigid creases and a rigid structure in which the pattern enables formation of a three-dimensional geometry or modification of the structural properties of the folded sheet versus its original planar form.

Rigid origami pertains to those origami patterns in which the facets are rigid, remaining planar and inextensible during folding, and thus joined by a network of straight creases along which the deformations of the sheet are concentrated. Alternatively, *curved origami* concerns patterns comprising an array of developable, singly-curved panels joined by curved folds. It is worth noting that many of the more complex artistic origami models are 'wet folded' in which the paper is initially dampened to enable it to be moulded to gentle curved shapes (often non-developable, though based on an underlying rigid origami pattern) which are retained when dried.

Modular origami structures are assembled from multiple (often very many) folded components, sometimes an array of identical 'motifs'.

Kirigami (*kiri* = "cut" and *kami* = "paper") is a related form of papercraft in which sheets are cut before folding. The cutting pattern may feature straightforward 'slits' in which no material is removed, may remove external material to shape the planform of a sheet even form internal holes. Fundamentally, the cutting operation enables surface discontinuities to be formed, permitting a wider range of geometric shapes to be folded.

3.4.1 Rigid origami

Most engineering research has attended to rigid origami whose patterns are composed of straight fold lines meshing an array of vertices as it is readily replicated at a large scale from robust engineering materials with rigid panels joined by precision hinges. From an examination of each vertex, Maekawa and Kawasaki's theorems provide conditions for flat-foldability: that the number of valley and mountain folds must differ by exactly two, and that the alternating sum of angles equals zero[19]. Some non-developable patterns are still rigid- and flat-foldable, such as the eggbox pattern which is manufactured from multiple creased strips by bonding them together along their seams.

The *configuration* of a given pattern is described by the set of crease *fold angles* (the signed dihedral, zero when flat) which locates a point in the configuration space of the pattern. When all are zero, the sheet is in its degenerate, planar condition; a pattern is foldable if at least one non-degenerate solution exists in which the facets are planar and geometrically compatible, and rigid-foldable if a continuous path can be traced between these points. Of course these fold-angles are not usually independent and the folds about each interior vertex form a *spherical parallel link mechanism*[86]. The configuration space is a subset of the fold-angle space with dimensions equal to the degrees-of-freedom of the pattern[84]. Modifying the Grübler–Kutzbach mobility criterion (Eqn 3.1) determines that each non-boundary vertex with N facets and crease lines has $N-3$ degrees of freedom ($N-2$ for vertices along the boundary)[95], so that a degree-four vertex has a single degree of freedom. Of course, when tessellated to form a crease pattern, the degrees of freedom at each vertex are not independent and mobility is only maintained if intrinsic symmetry conditions are met so that the array of vertices form an overconstrained linkage, as in the case of the Miura-ori pattern. Determination of the degrees of freedom of such a pattern is more involved and requires examination of the interaction between adjacent vertices[95].

To model the mechanical motion of an origami pattern a number of approaches may be followed. For simple or highly symmetric fold patterns a bespoke analytical model of the folding motion can be formulated by geometric construction. For a repetitive pattern, it is often sufficient to examine a single cell with compatibility between adjacent cells satisfied by symmetry, *e.g.* the folding of a Miura-ori sheet[74].

Taking a more general approach, Tachi has developed a numerical rigid origami simulator which acts on the fold-angle description[84]. The relationship between fold angles about each vertex is captured by formulation of the corresponding constraint function describing the transformation across each fold and facet (which must form a closed loop). At any condition, the rigid-folding trajectory is equivalent to projecting into the constraint space along the

normal direction to this function so the rigid-folding action of a pattern can be tracked by iteratively displacing the pattern in this manner, correcting for numerical error at each step.

3.4.2 Non-rigid origami

A surprising discovery from the investigation of the kinematics of origami is that many traditional origami patterns are not, in-fact, rigid-foldable, with the facets required to bend, twist or stretch during motion even if the folded state is ultimately strain-free. If permitted, even small violations of the rigid-folding conditions (*i.e.* bending and/or stretching) significantly increase the design space of origami structures, enabling many complex folded geometries to be formed, and significantly alter the structural response[30].

A further distinction is made between patterns which remain developable during motion, *i.e.* in which the facets bend at intermediate configurations, and patterns which are non-developable, *i.e.* in which the facets must stretch or twist and/or creases may move through the sheet at intermediate configurations, *e.g.* the conventional paper shopping bag pattern[2]. Patterns that remain developable during motion can be accommodated in the fold-angle based, numerical rigid-origami simulation by the addition of supplementary creases to model the developable deformation of each facet[84]. This approach is akin to the pseudo-rigid-body models formulated for compliant mechanisms and simple examples can be explicitly formulated as such[65].

For more complex patterns, a key insight is that their crease lines remain straight once folded so they behave as a stiff bar connecting the vertices at either end. A triangulated pattern (whether originally triangulated or by addition of crease lines across each quadrilateral facet to approximate developable bending) can thus be modelled by the equivalent pin-jointed framework. Such an approach was pioneered by Schenk and Guest to investigate the structural mechanics of a pair of representative folded shell structures: a Miura-ori and eggbox sheet, both consisting of a tessellation of identical parallelogram facets with the former developable and thus folded from a single sheet, the latter non-developable and assembled from multiple folded strips which are glued together[73]. Both exhibit rigid-folding in-plane modes and can be flat-folded in two directions (both also adopting negative curvature when a sheet is twisted), but their most intriguing property, and the motivation for his study, is their out-of-plane behaviour under bending: the Miura-ori sheet with a negative stretching Poisson ratio adopting negative Gaussian curvature (as is more commonly associated with a positive Poisson ratio), and *vice-versa*. Geometric analysis of a single cell is sufficient to capture the rigid-folding, in-plane motion and stretching Poisson ratio of each pattern, but not the

non-rigid-folding, out-of-plane deformations. These are modelled by including an additional fold line across the (minor) diagonal of each facet, enabling it to bend out-of-plane and thus capture the compliant motion of the facet. The supplementary hinge lines are oriented to match physical observations (this is irrelevant to a first-order but important when examining large displacements). Folding of this equivalent pin-jointed bar mechanism is assessed by examining the nullspace of the compatibility matrix (relating nodal displacements to bar extensions, itself the transpose of the equilibrium matrix relating bar tensions to nodal forces), which contains the set of displacements that can occur with no bar extensions (both finite and infinitesimal, and including the developable non-rigid modes which are of interest).

The purely geometric construction described above is sufficient to capture the basic characteristics of the folded sheets, with the rigid-folding in-plane behaviour recovered by including a constraint to the bending of each facet. The large-displacement behaviour of the sheets is tracked by iteratively incrementing the infinitesimal mechanism (and correcting at each step), just as in Tachi's fold-angle formulation. Investigation of the out-of-plane behaviour of the folded sheets requires an extended stiffness approach in which relative stiffnesses are specified for the fold and facet bending lines. The many modes of 'soft' deformation are each an eigenmode of the extended stiffness matrix whose relative stiffness is given by the associated eigenvalue. Selecting a mode, the large-displacement, developable out-of-plane deformation can then be simulated for a set of cells (this cannot be extrapolated from a single unit cell in isolation as only the in-plane modes tessellate).

Bar-and-hinge models are appealing as computational tools for the investigation of origami behaviour due the the reduced computational expense versus finite element simulations (FE) and scalability to complex geometries. Provided appropriate values for the fold and panel stiffnesses are specified, realistic large-displacement and bending-active deformations can be simulated and stiffness characteristics can be investigated via eigenvalue analyses[20]. An important caveat is that they do not accurately capture the local behaviour of each facet.

3.4.3 Origami architectured materials

Origami architectured materials (OAM) are a form of modular origami assembled from tessellations of multiple separate sheets to form three-dimensional cellular compositions. The resulting structures are a form of mechanical metamaterial in which the global structural behaviour is influenced by the local geometric design, offering the possibility to engineer deployable or morphing metamaterials with distinctly anisotropic (and potentially tailored) mechanical characteristics.

The global mobility of an OAM is dependent on both the mobility of the sheets/cells themselves and the compatibility of the modules during deployment. The structure may have a single or multiple degrees of freedom, the former usually a flat-foldable system that can act as a load-bearing structure when deployed, the latter a reconfigurable system whose structural characteristics vary from state-to-state. By consequence of the Bellows theorem[10] – which states that a closed polyhedron with finite number of creases cannot change its volume via rigid-folding – the final assembly must form an array of open cells if it is to be foldable.

Filipov & Tachi have pioneered tube-cellular materials generated from assemblies of 'zig-zag' tubes based on the Miura-Ori pattern, Fig. 3.21(a). When multiple kinematically matched tubes are concatenated in a 'zipper' formation, Fig. 3.21(b), their motion is coupled. These systems can be designed for increased stiffness throughout motion, increased peak stiffness once deployed, or to constrain the motion for increased buckling resistance and/or so that the system becomes locked when expanded to the desired shape[83, 23, 22]. These tubes may be straight or curved and can be generated according to a target surface, with various examples shown in Fig. 3.21(c). The structural mechanics of these constructions have been analysed via a bar-and-hinge approach, demonstrating, in particular, that coupled systems can exhibit a large eigenvalue *band gap*, indicating that they are easy-to-deploy whilst retaining high stiffness to unintended deformations[24].

Each tube in these structures is a zig-zag extrusion of a planar polygon, and foldable tubes with more general (filled or hollow and reconfigurable) cross-sections can also be generated by designing polygons in which each edge is matched by an identical opposing edge so that foldability is assured by symmetry[88, 21]. The extrusion can also be mapped to a singly-curved surface to generate curved-fold structures[87, 22].

Overvelde et al. have pioneered a 'snapology' inspired approach to generating reconfigurable metamaterials by prismatic extrusion of tessellated polyhedra[62, 63], an example of which is shown in Fig. 3.22. The structures are assembled from individual cells, which are folded from their net, and exhibit a wide range of mobilities with their stiffness under loading depending on their configuration.

One challenge to the usage of origami-derived structures for practical applications, either as load-bearing systems or impact absorption, is the apparently contradictory requirements for mobility during deployment and stiffness and rigidity once deployed. Rigid-foldable designs are favoured because they have a predictable and well-controlled deployment sequence, retain their transformability when manufactured from robust engineering materials, and actuate freely between the natural limits imposed by maximum hinge rotations or self-contact. For use in some intermediate configuration, the structure must be externally restrained or

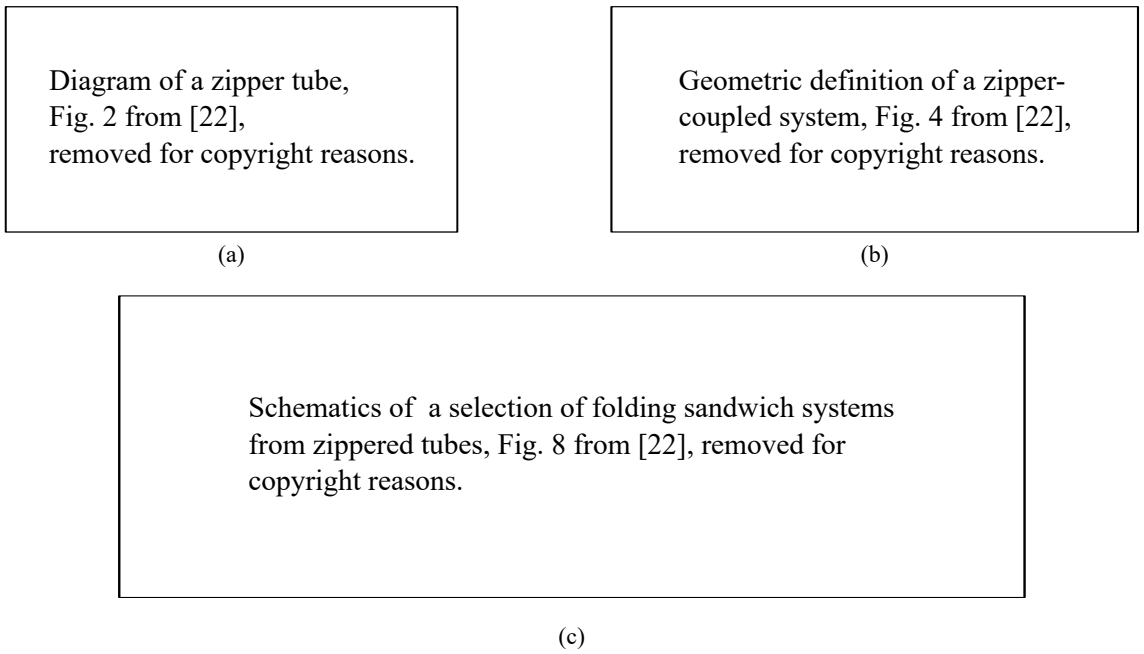

Fig. 3.21 (a) Foldable Miura-ori inspired tubes are generated by zig-zag extrusion of a rectangle. (b) Multiple tubes can be concatenated in a zipper pattern, their kinematics coupled for increased transverse stiffness while retaining rigid-foldability. (c) These coupled tubes can also be designed to form deployable structures conforming to a variety of shapes. Figures from [22].

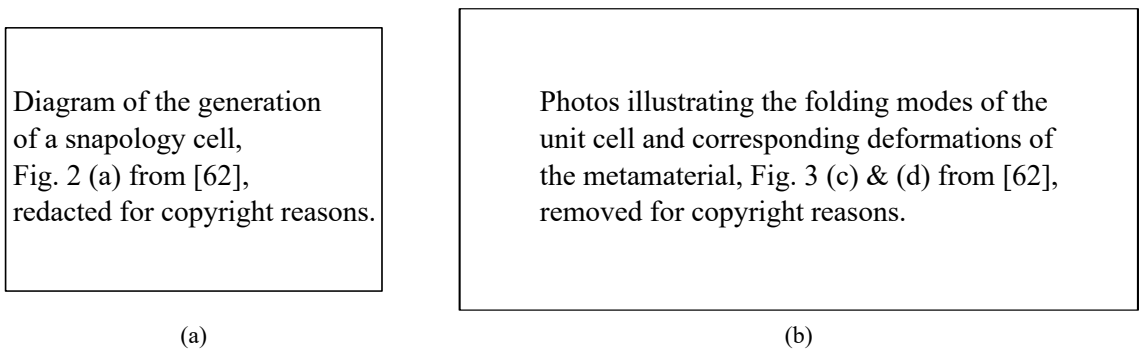

Fig. 3.22 “Snapology” inspired cellular origami structure by Overvelde et al.[62]. The unit cell is generated by prismatic extrusion of a polyhedron, (a). This example has three degrees of freedom and can transform continuously between configurations with several notable states illustrated in (b). The stiffness of the structure depends on its configuration.

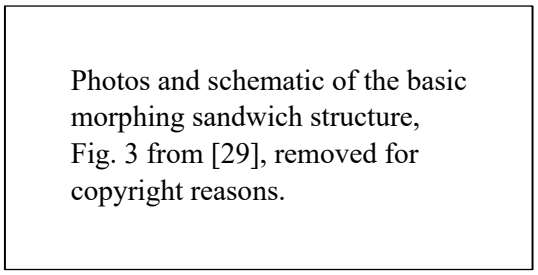

(a)

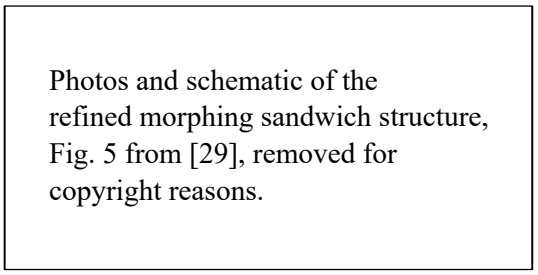

(b)

Fig. 3.23 Geometric design of a self-locking morphing sandwich structure from Miura-Ori sheets[29]. In (a) the upper and lower face sheets become fully extended before the core sheet, restraining it from extending further, though an infinitesimal mechanism remains via deflection of the coplanar facets of the now triangulated quadrangular cells. This is resolved in an improved design by changing the ratio of crease spacing on the face and core sheets so that the cells in the deployed configuration are truly triangular, (b).

augmented with a restraint system. This adds complexity so designs in which the interaction between the units acts to mutually constrain their motion once the design configuration is reached are actively sought. In these designs, the combined structure may fold and deploy freely in one direction while self-stabilising and rigidifying against loading in another. Such rigid-foldable, self-stabilising structures can be generated by employing a geometric design in which some panels become coplanar and lock-out at the desired deployed configuration, sometimes in conjunction with a triangulation effect produced by internal contacts. For example, Gattas and You have designed multi-layer Miura-ori sandwich structures from sheets with compatible rigid-foldability, in which the face sheets are designed to restrain the core layers to produce a self-stabilising effect once deployed[29], Fig. 3.23.

Origami tessellations also inspire the design of non-mechanical structures. Cheung et al. have developed an origami-inspired ‘tube interleaved cellular material’ whose 3D printed form is based on a tessellation of a foldable ‘flip-flop’ module to form an eggbox-like mesh[6], Fig. 3.24. Though rigid in kinematic terms, the stiffness of the material is highly anisotropic, corresponding to the differential mobility of the original cell along each axis.

3.5 Summary

Kinematic mechanisms

The expected mobility of a mechanism can be determined by a topological calculation – which have been formulated for linkages and pin-jointed bar mechanisms – which determine the overall determinacy of the structure. However, the true performance of a linkage is dependent

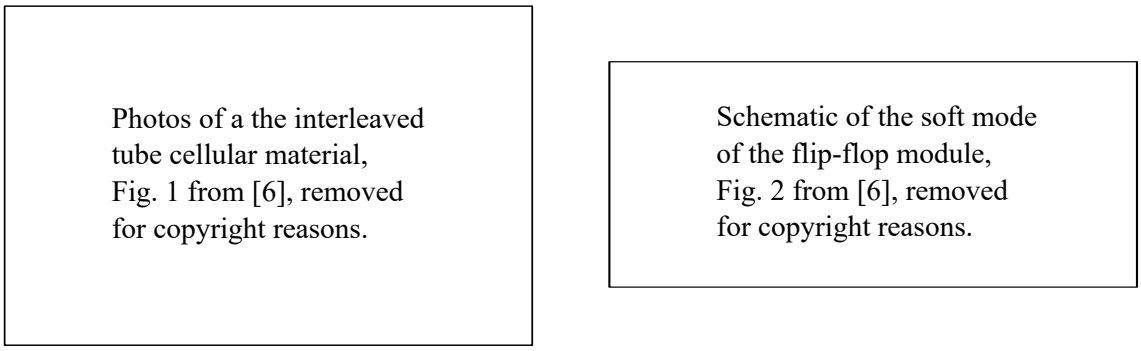

Fig. 3.24 Origami-derived, interleaved tube cellular material [6], (a). The foldable motion of the tessellated flip-flop module, (b), imbues the 3D-printed bulk material with a soft mode whilst remaining relatively stiff along the perpendicular axis.

on its specific geometry, and, in particular, a structure may have unexpected mobility if multiple joints constrain the same degree of freedom – an overconstrained mechanism. Rigid mechanisms exhibit smooth actuation across the full range of motion permitted by joint articulation (or until self-contact).

Scissor structures

When the slices are thin, each slotted intersection actuates as a rudimentary hinge allowing each pair of interlocking slices to articulate as scissor link. Sliceforms, therefore, share much in common with scissor structural mechanisms which take a rich variety of forms.

The motion of a scissor unit depends on its geometry and may be translational (curved-translational unit), curvilinear (polar unit) or scaling (angulated unit). Chains of scissor units can be generated along an arbitrary curve. A chain composed of straight bars is flat-foldable (*i.e.* the units reach maximum compactness simultaneously and thus collapse to a bundle of collinear bars) if the deployability condition is met across each interface. This condition places the pivots of adjacent units on an ellipse whose foci are the intermediate joints, a representation that can be inverted to design flat-foldable chains along a target curve by construction of a set of tangential similar-ellipses. Foldable closed-loops of angulated elements are generated by constructing units to form a chain of similar rhombuses that scale proportionally, ensuring compatibility about the ring.

Scissor grids can be constructed by arraying scissor units to form linear, single-layer or double-layer grids. Single-layer grids are formed by arraying scissor units in two directions and can be generated by joining adjacent, compatible chains along their seams. Using straight bars, foldable grids can be generated by arraying identical chains of curved-translational

units with parallel interface lines or scaled chains of concurrent polar units where the upper and lower surfaces are parallel in both. The usual deployability condition applies for flat-foldability in both directions. Using angulated elements, foldable grids are formed from concentric rings. When successive layers form rows of parallelograms, the angle between contiguous rods is invariant and multi-angulated rods can be used.

Linear- and double-layer grids are formed from arrays of plane-faced cells, each face a scissor unit. The challenge is to satisfy geometric compatibility about each cell and block of cells. Solutions can be generated by symmetry with singly- and doubly-curved grids generated by mutual translation of chains of constant thickness curved-translational units. Examining a single cell, both a prismatic cell of parallel-axis, curved-translational units and a pyramidal cell of concurrent polar units are rigid-foldable provided the shape of the cell may change. Quadrangular grids can usually accommodate these variations in cell shape and single- and doubly-curved grids are possible; triangulated grids usually cannot, though some singly-curved designs are foldable by symmetry. A grid is flat-foldable if the deployability condition is met by all units meeting at each node, and, in particular, non-rigid-foldable grids can still be deployable, and such bistable grids can be generated by tangential placement of similar-ellipsoids. Though bistable scissor structures must overcome an intermediate geometric compatibility during deployment, they are self-stable in their design configuration without need for external restraint. This is unlike rigid-folding structures which must be restrained once deployed.

Origami engineering

The fundamental geometric form of a sliceform – of planar facets joined along straight lines – is reminiscent of folded structures, *i.e.* origami. Origami engineering thus provides many relevant insights and inspiration to this study.

Rigid origami concerns patterns with planar facets and straight creases whose configuration is captured by the set of fold angles. The folds meeting at each vertex form a spherical linkage, and the corresponding fold angles must form a closed loop. For simple patterns, the folding motion can be simulated by bespoke geometric construction. The articulation of more complex patterns can be simulated numerically by formulating the corresponding constraint functions and then iteratively displacing the pattern whilst preserving these geometric constraints to track its folding motion.

It has been found that many rigid origami patterns are not, in fact, rigid-foldable and require the facets to deform during folding. This can be modelled by the addition of

supplementary crease lines to the nominal geometry and/or allowing existing crease lines to migrate at intermediate configurations.

Crease lines remain rigid so a triangulated crease pattern is kinematically equivalent to the corresponding pin-jointed bar network, which is its dual. Rigid-folding modes can be sought by examining the nullspace of the compatibility matrix (corresponding to nodal displacements that do not cause bar extensions) and the folding motion can be simulated by iteratively tracing these displacements. This approach can be extended to quadrangular patterns by the addition of diagonal edges across each facet with the planarity of the facets enforced explicitly. Alternatively, the 'soft' (*i.e.* non-rigid) folding motion of a quadrangular pattern can be simulated by allowing folding across these 'creases', mimicking developable bending of the facets. The stiffness characteristics of the pattern can be investigated by specifying stiffnesses for the fold and facet creases and then constructing the stiffness matrix and examining its eigenmodes.

Origami architectural materials are constructed from multiple sheets folded and bonded together in layers, tubes or cells to form a volumetric structure. Because the characteristics of the bulk structure are derived from the characteristics of the independent components and their interaction, highly anisotropic characteristics can be engineered. For such structures to be rigid-foldable, they must have an open cellular form; several concepts deliberately combine cells so that their motion is mutually constrained and the final structure is foldable in one direction but stable once deployed.

Insights and inspiration

All of these fields provide insight and inspiration to the investigation of deployable sliceforms. For rigid-folding, the sliceform must embed a rigid-mechanism for which topological calculations can set an expected mobility. The revolute action of each slotted intersection embeds a scissor joint, and it is clear that it is their kinematic compatibility across the array that is essential for enabling global motion. A sliceform is perhaps most closely related to a single-layer scissor grid with the array of slices directly corresponding to the array of bars. The literature surveyed here demonstrates the successful analysis of their deployable and kinematic characteristics via geometric treatment – for which the deployability condition can clearly be adapted to a spatial embodiment – and also demonstrates that this can then directly inform the design of new deployable examples. The treatment of double-layer scissor grids is based on an analysis of each cell and their local interaction, rather than needing to consider the global articulation in entirety. Similarly, the torus is highly symmetric and so a bespoke model is likely to be sufficient to model its folding motion by examination of the simplest

repeating unit, rather than pursuing a numerical model of the complete structure that captures the folding action but does not provide the same insight. Similarly, the analysis of a non-rigid-folding action by a simplified model of the compliant action (both for mechanisms and origami) allows the application of conventional rigid-folding methods, preserving tractability of analytical approaches for the development of insights whilst capturing the realistic action of the structure.

Part I

Rotational Sliceforms

Introduction to Part I: Rotational sliceforms

Rotational sliceforms, such as the torus in Fig. 1.3, are synthesised with two sets of inclined slice planes which form a closed ring. Unlike an LS, the intersection lines are not parallel, so rigid-assembly is no longer viable and assembly is dependent on the inherent flexibility of the thin slices to permit non-parallel intersections to be engaged simultaneously. The final structure is (kinematically) rigid with each slice securely fixed in place. The array of slices form an array of closed loops, and the intersection lines are non-parallel (unlike an RS) so global rigidity is expected. However, at mid-assembly, a partial RS exhibits a surprising deployable characteristic in which the incomplete sliceform is one-way flat-foldable, but abruptly 'locks out' on expansion to the design configuration

The discovery that this design is flat-foldable suggests an obvious opportunity for the design of new flat-folding, volumetric structures that retain load-bearing or impact-absorption capabilities when deployed. Overall the deployable action of an incomplete RS resembles the articulation of a chain of scissor links except that it occurs about an out-of-plane loop and proceeds smoothly but only over a finite range of motion and without any apparent cause for the expansion limit. The underlying motivation is investigate and model the kinematic action of these structures and, in particular, to determine the source of the restriction to their range of motion where the smoothness of initial articulation and rigidity set contradictory expectations of rigid-folding.

Specific objectives

The primary objective of this part is to characterise the general form of an RS, and to construct a model of the folding action of an incomplete ring to resolve the conflict between folding and locking-out. This work is set in the context of an RS as a scale-independent form of overconstrained spatial linkage.

It is desired to use an analytical approach where possible and to construct simple models in order to understand and develop insights into the behaviour of these structures which might inform the design of more general formulations.

Outline of part

Part I comprises two chapters. In Chapter 4, the design, synthesis and structural geometry of a complete RS as a static structure are formalised, the limitations of this formulation explored and the synthesis of a set of representative designs demonstrated. Then, Chapter 5, concerns

the investigation of their deployable action, dealing exclusively with the incomplete, open form. A set of simple examinations are performed to assess the nature of the folding action, informing construction of a kinematic model to capture and explain the characteristic features of their smooth-but-finite articulation.

Chapter 4

Synthesis, structural architecture and geometry of a rotational sliceform

4.1 Introduction

As identified in Section 2.4, the basic requirement for a geometrically feasible sliceform is a *structural architecture* in which no pair of intersection lines themselves intersect within the *global volume*, ensuring that a set of slots can be generated without splitting any slice in two. It follows that a *lattice-style* architecture, with two sets of parallel slices and a parallel array of intersection lines, is the default for bulk sliceforms. However, for any given *global volume*, an almost infinite arrangement of bespoke structural architectures can be generated in which the intersection lines are not parallel but simply intersect outside the global volume, though consideration must also be given to the assurance of assemble-ability, *i.e.* that the individual slices can be slotted together once manufactured. Assemble-ability requires that the slots in each slice are suitably aligned as to be engaged simultaneously. With rigid slices, those intersections lines must be parallel; with flexible slices, the intersection lines must still be relatively closely arranged but non-parallel slot pairs can be engaged by careful distortion of the array as they are interlocked.

Consequently, structural architectures with two sets of slices in which the slice planes similarly oriented within each set are inherently favourable because adjacent intersections will be relatively closely aligned. Using two sets of slices also aids in satisfaction of the compatibility requirement with slots generated uniformly across the sets of slices. A particularly elegant example of this is the sliceform torus.

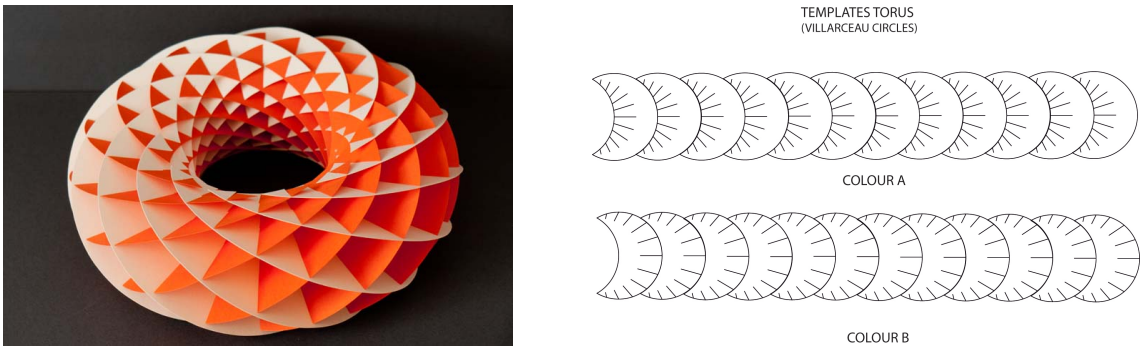

(a) (b)

Fig. 4.1 The sliceform torus built from Villarceau circles (Repeated from Fig. 1.3). The assembled sliceform, (a), and crescent-shaped slice templates, (b), each bounded by the pair of overlapping Villarceau circles found on a torus' double-tangent plane, (b).

Source: María García Monera (2012). Torus. *flickr.com*, https://www.flickr.com/photos/mgmonera/albums/72157632885563751

4.1.1 'The Torus'

The sliceform torus illustrated in Figure 4.1 was devised independently by Yoshinobu Miyamoto[1] and María García Monera, and formalised by the latter[60]. It is constructed from two sets of slices whose planforms are generated by slicing along the torus' double-tangent plane (which is tangential to the torus at two points on opposing insides of the hole) with each set of slices defined by the pair of overlapping 'Villarceau' circles.

The assembled torus is visually striking, but the most intriguing feature of this design is only revealed during construction: though the complete ring is rigid, at mid-assembly, a partial ring of slices is found to expand and contract smoothly about the axis of the torus, collapsing to a flat-folded compact stack of interlocked slices. This articulation aids the manual assembly of the sliceform with each additional slice worked into place until the complete complement of slices have been interlocked, whereupon the stack is expanded until the outer slices meet and are incrementally meshed together, completing the sliceform and locking the array into place.

4.1.2 Chapter outline

The torus is an example of a *rotational sliceform*, or *RS*, a class of sliceform formed with a rotational array of slice planes. In this chapter the complete, rigid form of an RS is explored.

[1] Miyamoto. Y ('Prof. YM') (2010). Torus. *flickr.com*, https://www.flickr.com/photos/yoshinobu_miyamoto/albums/72157633506287093/with/4400657560/

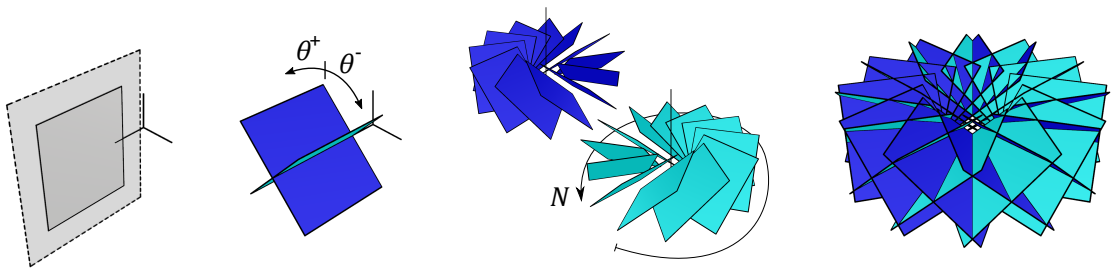

Fig. 4.2 Generation of the rotationally symmetric structural architecture: A vertical reference plane, (a) with rectangular patch inset, is rotated in opposite senses about horizontal axis to produce two base planes, (b). These base planes are propagated at regular intervals about a central axis of symmetry to produce two sets of slice planes, (c), and superimposed to form the RS architecture, (d). The RS architecture is parameterised by the number of slices in each set, N, and their opposing inclinations from vertical, θ^+ and θ^-.

Firstly by formalising the RS structural architecture, followed by an examination of their *structural geometry* – that is the geometric arrangement of slices and intersections, independent of overall form – and finally through synthesis of a set of examples to demonstrate the range of possible geometries and their potential for practical application, and to explore the limits of this formulation.

4.2 RS structural architecture

The RS architecture is formed from two sets of uniformly inclined slices arranged at regular intervals about a central axis of rotational symmetry. Formally, the array of slice planes is generated by a pair of consecutive rotations, Fig. 4.2: a vertical reference plane is first rotated about a horizontal axis by $\pm\theta^{\pm}$ to form two base planes; then each of these is then recursively generated at regular intervals about the vertical central axis to generate two sets of slice planes. This is parametrised as (N, θ^+, θ^-), where θ^+ and θ^- describe the inclination from vertical of each plane of the "positive" and "negative" set, and N is the number of slices in each. Typically the slices of each set are equally inclined with $\theta^+ = \theta^- (= \theta)$ so that the array is also mirror-symmetric, a *symmetric RS*, with reduced parametrisation (N, θ).

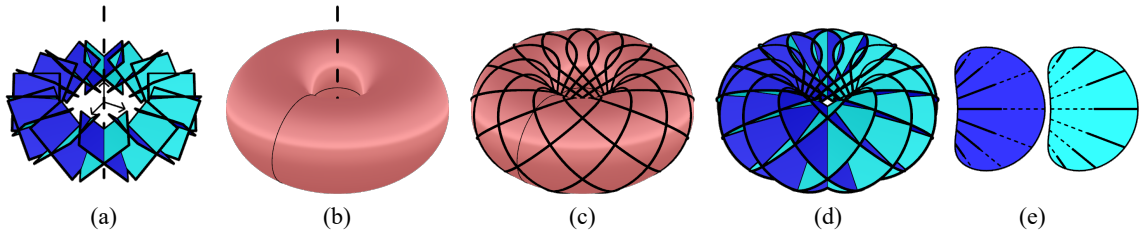

Fig. 4.3 Synthesis of an RS torus. A rotational sliceform is synthesised by combining the rotationally symmetric array of slice planes, (a) with $(N = 12, \theta^{+} = 45°, \theta^{-} = 45°)$ here, with a gloabl volume, (b) here a torus, and excising cross-sectional slices corresponding to each slice plane, (c)-(d). The slice templates are completed by furnishing pairs of interlocking slots along each intersection, inside-out for one set, and *vice versa*, (e).

4.2.1 Basic synthesis of an RS

Using this RS architecture, synthesis of a sliceform proceeds as usual, with cross-sectional slices excised from a suitable global volume and pairs of slots placed along each intersection line, now oriented 'inside-out' for one set of slices and 'outside-in' for the other, Fig. 4.3.

These slices are then cut from a sheet of stock material and manual assembly proceeds by addition of consecutive pairs. With non-parallel slices, assembly is more complex than for an LS because each adjacent pair of intersections span a wedge and there is no longer a rigid assembly path. With some flexibility of the thin slices, each new slice is delicately twisted and squeezed into place. Though this requires significant compliance from the slices themselves, setting their thickness to be small, the assembled structure is robust, with each slice held securely in place. As identified, the incomplete assembly can be collapsed and expanded by simply pulling the outermost slice pairs away from each other, this mobility aiding the addition of each successive slice. Once all slices are interlocked to form an open chain, the assembly is expanded about the central axis until the outer slices meet and can be incrementally meshed together, completing the sliceform and locking the array into place. In reverse, removal or disengagement of a few slices opens the ring which can then be collapsed to a flat-folded compact stack.

Though material-thickness slots are sufficient because the slices are already flexible by requirement of the structural architecture, setting the slot width to be slightly greater than the material thickness greatly reduces the challenge in engaging the intersections between pairs of non-orthogonal slices. From trials, a slot width of $1.3\times$ material thickness provides a good balance between ease of assembly and robustness of the assembled form with friction along the length of each intersection providing sufficient restraint from disengagement of the slices.

4.3 Structural geometry of an RS

The deployability of an RS is a property of its structural architecture and independent of the global volume. Just as the cross-sectional planforms fill only a portion of each slice plane, the slotted intersection lines span only a portion of each line of intersection. All rotational sliceforms share this same underlying arrangement of slice planes and intersections and have a common *structural geometry*.

Examining the slices of a typical RS, it is apparent that their in-plane geometry comprises two distinct components: a cross-sectional planform; and an overlaid fan of intersections along which each slot is generated, usually to the midpoint. With each slice plane generated by rotations of the base plane about axes through a common point (the origin in Fig. 4.2(a)), it follows that all of these intersection lines also extrapolate back to this point, the *focus* of the sliceform. Across the RS, these intersection lines form a spherical array, and upon each slice they form two sets of congruent fans, Fig. 4.4(b). Each fan is described by the set of in-plane elevations of each intersection line from horizontal, $\beta_i^{\pm}$, Fig. 4.4(d). To capture this geometry two approaches are presented below.

4.3.1 Structural geometry via vectors

The spherical array of intersections has a convenient vector description which is now outlined. This approach is similar to that used by Monterde & Monera in formulating a description of the geometry of the Villarceau torus [60], but here the generality of the final expressions in terms of the architectural parameters is preserved.

In a Cartesian coordinate system, a natural description of the $i^{\pm}$-th slice plane is the set of points, p_i, which must satisfy

$$(p_i - p_0) \cdot \hat{\mathbf{n}}_i^{\pm} = 0 \tag{4.1}$$

where p_0 is a point on the plane and $\hat{\mathbf{n}}_i^{\pm}$ is normal unit vector. Setting the origin as the common point, $p_0 = (0,0,0)^T$, each slice plane is uniquely captured by its normal vector. Given the unit normal to the reference plane, $\mathbf{n}_{\text{ref}}$, each $\hat{\mathbf{n}}_i^{\pm}$ is generated by reproducing the consecutive rotations detailed in Fig. 4.2 so that

$$\hat{\mathbf{n}}_i^{\pm} = \mathbf{R}_{i\phi}^{z} \mathbf{R}_{\pm\theta^{\pm}}^{x} \hat{\mathbf{n}}_{\text{ref}} \tag{4.2}$$

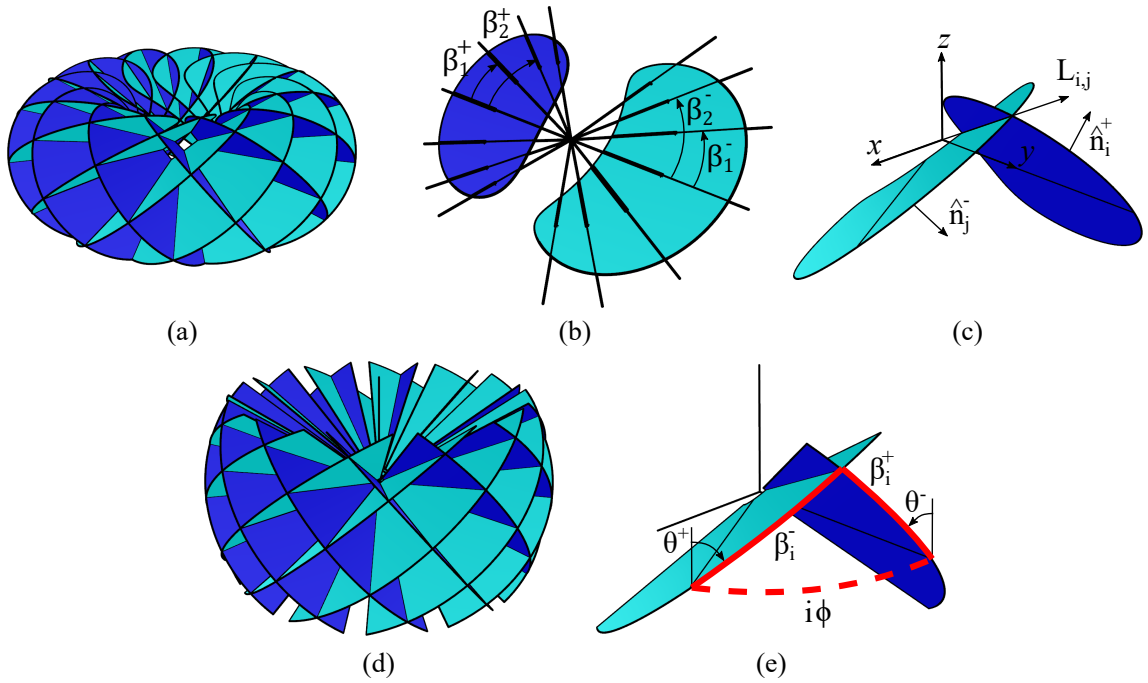

Fig. 4.4 Each slice of an RS – *e.g.* a torus, (a), here with $(N = 12, \theta^+ = 40°, \theta^- = 50°)$ – comprises a cross-sectional planform furnished with slots along the planar fan of intersection lines, (b). Across the sliceform, these intersection lines are concurrent, intersecting at a single common point; upon each slice plane, the intersection lines are located by their in-plane elevation angle from horizontal, β_i. A vector aligned to the intersection between the ith plane of the $+$ve set and the jth plane of the $-$ve set, L_{ij}, is generated by the vector product of the normals to each slice plane, $\hat{\mathbf{n}}_i^+$ and $\hat{\mathbf{n}}_j^-$ respectively, (c). Alternatively, starting with an RS inscribing a sphere of unit radius, (d), the in-plane elevation of each intersection may be found from the spherical triangle formed by tracing an azimuthal arc about the equator, (e), where each arch length is equal to the angle subtended.

where $\mathbf{R}^x_\theta$ and $\mathbf{R}^z_\phi$ are the transformation matrices for rotations of θ and ϕ radians about the $x-$ and $z-$ axes respectively

$$\mathbf{R}^x_\theta = \begin{bmatrix} 1 & 0 & 0 \\ 0 & \cos\theta & -\sin\theta \\ 0 & \sin\theta & \cos\theta \end{bmatrix}, \quad \mathbf{R}^z_\phi = \begin{bmatrix} \cos\phi & -\sin\phi & 0 \\ \sin\phi & \cos\phi & 0 \\ 0 & 0 & 1 \end{bmatrix} \tag{4.3}$$

Furthermore, with the reference plane aligned to the xz-axes, $\hat{\mathbf{n}}_{\text{ref}}$ is simply the unit $\mathbf{y}$-vector $\left([0,1,0]^T\right)$, and the set of unit normal vectors are

$$\hat{\mathbf{n}}_{i^\pm} = \begin{bmatrix} -\cos\theta^\pm \sin i\phi \\ \cos\theta^\pm \cos i\phi \\ \pm\sin\theta^\pm \end{bmatrix} \quad \text{for} \quad 0 \le i < N \quad \text{and} \quad \phi = \frac{2\pi}{N} \tag{4.4}$$

The plus-sign applies for θ^+ and *vice-versa*, throughout.

This description is convenient because a vector aligned to each intersection line can now be generated from the vector product of the normal vectors to each intersecting plane

$$\mathbf{L}_{i,j} = \hat{\mathbf{n}}^-_j \times \hat{\mathbf{n}}^+_i \tag{4.5}$$

where $\mathbf{L}_{i,j}$ is an outward-pointing vector parallel to the intersection between the i-th plane of the positive set and j-th plane of the negative set, Fig. 4.4(c). Substituting for the above expressions, the set of aligned vectors, $\mathbf{L}_{i,j}$, are obtained

$$\mathbf{L}_{i,j} = \begin{bmatrix} \cos\theta^+ \sin\theta^- \cos i\phi + \sin\theta^+ \cos\theta^- \cos j\phi \\ \cos\theta^+ \sin\theta^- \sin i\phi + \sin\theta^+ \cos\theta^- \sin j\phi \\ \cos\theta^+ \cos\theta^- \sin(i-j)\,\phi \end{bmatrix} \quad \text{where} \quad 0 \le i, j < N \tag{4.6}$$

Within each set of slices, the in-plane elevation of each intersection can now be found via the scalar product. By symmetry, each set of fans are congruent so, to simplify the resulting expressions, it is sufficient to consider the layout of intersections in the base (zeroeth) plane of each set, where the reference horizontal is simply the unit x-vector. *i.e.* , for the ith intersection in each fan,

$$\mathbf{L}_{0,i} \cdot \begin{bmatrix} 1 & 0 & 0 \end{bmatrix}^T = |\mathbf{L}_{0,i}| \cos\beta^+_i$$
$$\mathbf{L}_{i,0} \cdot \begin{bmatrix} 1 & 0 & 0 \end{bmatrix}^T = |\mathbf{L}_{i,0}| \cos\beta^-_i$$

Substituting Eqn. 4.6 and rearranging in terms of each cosine term explicitly, this is re-written

$$\cos\beta_i^{\pm} = \frac{\cos\theta^{\pm}\sin\theta^{\mp} + \cos i\phi\,\sin\theta^{\pm}\cos\theta^{\mp}}{\sqrt{\begin{array}{l}\left(\cos\theta^{\pm}\sin\theta^{\mp} + \cos i\phi\,\sin\theta^{\pm}\cos\theta^{\mp}\right)^2 \\ +\left(\sin i\phi\,\cos\theta^{+}\cos\theta^{-}\right)^2 + \left(\sin i\phi\,\sin\theta^{\pm}\cos\theta^{\mp}\right)^2\end{array}}} \tag{4.7}$$

For a symmetric RS in which $\theta^{+} = \theta^{-}\,(=\theta)$, the positive and negative fans of intersections are also congruent and the expressions for each $\beta_i^{\pm}\,(=\beta_i)$ reduce to

$$\cos\beta_i = \frac{\sin\theta\sqrt{\cos i\phi + 1}}{\sqrt{2 - \cos i\phi\cos^2\theta - \cos^2\theta}} \tag{4.8}$$

4.3.2 Structural geometry via spherical trigonometry

The spherical array of intersection lines can also be computed directly via spherical trigonometry. The structural geometry of an RS is best expressed by an RS with a spherical global volume, Fig. 4.4(d), where each slice is a segment of a circle whose outer edges form a grid of great arcs. Isolating a pair of intersecting slices, the image of their intersection is located at the apex of a spherical triangle formed by the slice edges and completed by tracing an arc about the equator, Fig. 4.4(e). If a unit radius is set, the elevation of this intersection upon each slice plane is simply the arc-length of the corresponding edge, found by application of the cotangent rule for spherical triangles [90]

$$\cot\beta_i^{\pm} = \cot i\phi\,\sin\theta^{\pm} + \csc i\phi\,\cos\theta^{\pm}\tan\theta^{\mp} \qquad \text{where} \qquad \phi = \frac{2\pi}{N} \tag{4.9}$$

4.4 Synthesis of alternate geometries

The RS architecture can be employed in the synthesis of a range of distinctive deployable sliceforms. The following examples are selected to demonstrate something of the scope and limitations of this formulation. The physical models presented in this section are laser-cut from mountboard using templates cultivated within Rhino via the Grasshopper plug-in for algorithmic modelling [55, 71].

4.4.1 'Sliceforming' using digital design tools

The synthesis of an RS is readily achieved using digital design tools to generate each cross-sectional planform and locate the lines of intersection along which to place slots. This

can be implemented in a wide variety of digital design suites; in this work the Rhinoceros 3D modelling suite is used in conjunction with the 'Grasshopper' plugin for algorithmic modelling. Grasshopper provides a visual scripting interface in which the algorithm for generating a particular object can be built from a library of native operations (components), *for example* defining a point by x-,y-,z-coordinates, drawing a line between two points, or 'lofting' a surface through a set of curves. Within the interface, these components are arranged with the output of one (which may be a numerical value, coordinates of a point in space, a curve, a surface *etc.*) provided as the input of another by drawing a 'wire' to connect them so that the overall algorithm resembles a flow diagram.

This algorithmic approach provides the ability to generate designs in which any input parameter (*e.g.* a side length, angle subtended between two lines, or angle of rotation) can be altered, with the algorithm then recomputing all downstream operations to re-generate the adjusted output geometry (this is completed 'live' with the geometric adjustments visualised in real time).

Crucially, the Rhino/Grasshopper suite has a comprehensive set of functions for evaluating the properties of geometric objects that have been generated. The outputs of these geometric evaluations are returned as data values and geometric objects, which can then be utilised-in and operated-on in subsequent steps so that an algorithm may be responsive to the particular geometry generated. In this way, the algorithm for generation of the templates for the slices of an RS from a prescribed global geometry can be written for a basic example (the torus) and then used to generate appropriate slices for an alternate global geometry simply by replacing that input to the algorithm.

Usefully, the Grasshopper suite also has powerful native functionality for handling 'lists' and 'lists-of-lists' (or 'trees') of data or repetitive geometric features, with each item or 'branch' operated on in parallel by each subsequent component. This provides an efficient approach to generating these repetitive structures with each geometric operation only needing to be defined once (though it must be robust to the various geometric cases which can occur).

Briefly, the algorithm for generating each sliceform and its templates operates on the set of parameters defining the rotational structural architecture and a general global geometry defined as a boundary surface. The tools for finding the intersection between geometric objects form the basis of the generation of each cross-sectional planform and their lines of intersection, with the post-processing steps necessary to convert each of these cross-sections to a slice template (conditioning of the 'raw' cross-sections and generation of slots) also fully automated through carefully written routines. A more complete description of the algorithm is provided in Appendix A.

4.4.2 Volumetric sliceforms

Though not as generalisable as the LS architecture, for reasons explained below, the spherical layout of intersection lines also satisfy the conditions for geometric compatibility by virtue of sharing a single (common) concurrency point, the focus. Therefore, the slices can be propagated indefinitely in a radial direction without any pair of intersection lines re-converging, and an RS can be shaped to fill almost any singular global geometry. Typically, this architecture is best suited to shapes that echo the rotational symmetry, such as the torus and sphere presented in figures so far. When the axes of symmetry for the rotational structural architecture and the global volume are aligned, the slices will form two congruent slices; if the global geometry is M-fold rotationally symmetric, each slice will repeat M/N-times in each set. For a general, free-form volume, each slice will usually be unique.

4.4.3 Limitations of the RS formulation

There are two subtleties to the RS architecture which are worthy of discussion.

Semi-infinite slice planes

The first is that each slice is not, in fact, a complete cross-section. Consider the sliceform torus in Figure 4.1 where each slice plane spans the hole in the torus – each cross-sectional planform actually consists of two complimentary crescents. Because the structural architecture is symmetric with an even number of slice planes, each crescent is duplicated by the opposite slice plane of the opposing set so it is straightforward to split these cross-sectional components between them.

In a more general formulation with an odd number of slice planes, or unequal slice inclinations, each cross-section will be unique and more robust strategy must be established. The solution is to 'clip' each cross-sectional planform along its line of intersection with the adjacent slices of the same set so that each is reduced to a semi-infinite plane bounded by a pair of dovetailing straight edges, Fig. 4.5(a) & (b). Repeating across the array of slices, this ensures that the slices of each set do not 'self-intersect', thus preserving the independence of each intersection line and the geometric feasibility of the array.

These self-intersections, which define the limits for each cross-section, also converge to the focus, defining a symmetric sector for each slice, Fig. 4.5(b). The elevation of these edges, $\beta^{\pm}_{\mathrm{Lim}}$, are located by finding the line of self-intersection just as in section 4.3: either

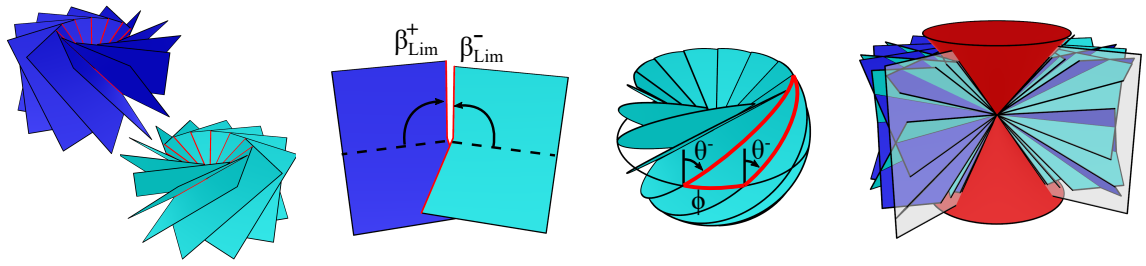

(a) (b) (c) (d)

Fig. 4.5 To prevent self-intersection between slices of the same set, each slice plane of an RS is strictly semi-infinite, limited by its intersection with the preceding and following slices, (a). These limiting intersections are located at an in-plane elevation of $\beta^{\pm}_{\text{Lim}}$, (b), found by considering the spherical triangle formed by adjacent slices of the same set, (c). Each set of slice planes in the RS architecture also exhibit an inherently 'un-fillable' zone consisting of a double-cone aligned to the axis of symmetry with semi-angle equal to the rotation of each slice from vertical, $\theta^{\pm}$, (d).

by generating a vector aligned to each edge via the vector product of adjacent slice normals,

$$\begin{aligned} \mathbf{L}^{\pm}_{i^{-}} &= \hat{\mathbf{n}}_{i^{\pm}} \times \hat{\mathbf{n}}_{(i-1)^{\pm}} \\ \mathbf{L}^{\pm}_{i^{+}} &= \hat{\mathbf{n}}_{(i+1)^{\pm}} \times \hat{\mathbf{n}}_{i^{\pm}} \end{aligned} \tag{4.10}$$

(where $\mathbf{L}^{-}_{i^{+}}$ is the vector aligned to the 'forward' limit of the ith slice of the negative set, with the elevation of each limit, $\beta^{\pm}_{\text{Lim}}$, determined by scalar product as before); or by determining $\beta^{\pm}_{\text{Lim}}$ directly by consideration of the spherical triangle pertaining to a pair of adjacent slices of the same set in a unit spherical RS, Fig. 4.5(c),

$$\cot\beta^{\pm}_{\text{Lim}} = \sin\theta^{\pm}\left(\cot\phi - \csc\phi\right) \qquad \text{where } \phi = \frac{2\pi}{N} \tag{4.11}$$

Formally clipping the slices in this way is justified by acknowledging that each 'half-section' of an even-sliced RS is complemented by a corresponding half-section belonging to the opposing set, though they are not coplanar if the sets are unequally inclined. For an odd-sliced RS, each cross-section is partial but uniformly so. In either case, by adjustment of the number of slices or by rotation of the architecture about the axis of symmetry, any radial cross-section can be captured.

For a symmetric RS with even number of slices, opposing pairs of half-sections will still overlap slightly and each must actually be clipped along a 'vertical' line (perpendicular to the horizontal intersection line about which they are rotated) which traverses the focus.

'Un-fillable' double-cone

The second subtlety is that whilst the layout of slices can be adjusted to map any feature about the equator, each set of slices exhibits an inherently 'un-fillable' zone consisting of a double-cone aligned to the axis of rotational symmetry[2], Fig. 4.5(d). The semi-angle of the un-fillable zone for each set is equal to the rotation of the slices from vertical, *i.e.* $\theta^{\pm}$.

4.4.4 Design principles for rotational sliceforms

When designing an RS, the architectural parameterisation must be chosen carefully to ensure that the resulting slices are 'well-conditioned'. The total number of slices, N, defines the 'resolution' of the final sliceform, with a higher value producing more detail at the expense of geometric compactness of the folded form and ease of assembly. The connectivity of the final sliceform is directly influenced by the number of slices in each set and their rotation away from vertical, increasing with higher values of each. The inclination of each set of slice planes, (θ^{+}, θ^{-}), also defines the un-fillable cone so that a tall global volume is better captured by parameterisations with lower values, otherwise an evenly distributed set of contours from the global volume are usually formed by maintaining complementary inclinations of the sets (so that each pair is perpendicular). The axis and focus of the sliceform can also be re-oriented and re-located to best capture the global volume and minimise the impact of the un-fillable cone.

In addition, the in-plane geometry of each slice must be monitored to prevent fragile connections forming where the slots along an intersection line lie too close the outline of a slice. This is relatively straightforward for axially symmetric geometries, where the slices are congruent, but a more careful process of trial-and-improvement is required to find the best case layout for more general shapes.

4.4.5 Shell-like RS

A particularly intriguing set of deployable structures are generated by slicing a thin shell-like surface to excise a set of curved planar strips. The resulting sliceform is a deployable, gridshell-like structure in which the structural depth of each strip is oriented close to the through-thickness direction of the surface. The short length of each intersection dramatically simplifies assembly of the sliceform versus a volumetric design, in particular simplifying

[2]Strictly this is an N-sided double-pyramid which is the result of superimposing the wedges above and below each pair of slices, tending to a smooth double-cone as N is increased and vanishing only if one of the sets of slices remains vertical.

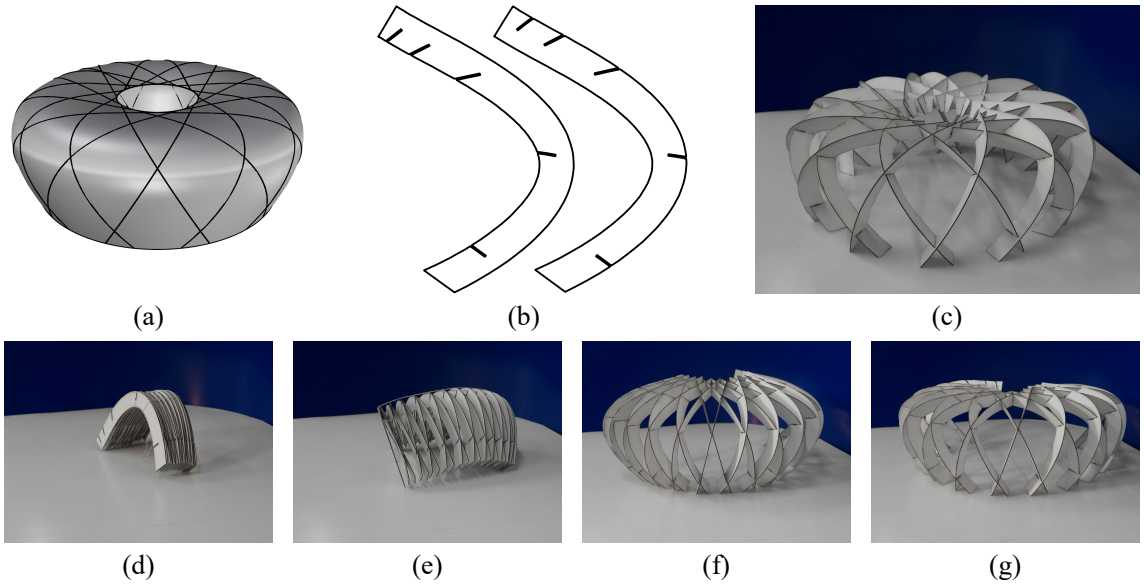

Fig. 4.6 A shell-like RS is generated from a thin 'shell-of-revolution', (a). The slices are curved strips, (b), and the final sliceform resembles the 'Birds nest' stadium in Beijing, (c). With a few intersections disengaged, the structure is flat-foldable and deployable, (d)-(g).

the (dis-)engagement of the outermost slices when completing and rigidify the completed sliceform, or releasing it for collapse.

From a surface of revolution resembling a stadium roof a 'birds nest' sliceform is generated (so named after its visual similarity to the Olympic stadium in Beijing), Fig. 4.6. Each set of strips are congruent and there is obvious practical potential for use as a framework for a rapidly-deployable shelter or dome.

Using a more general global geometry, a sliceform 'skew cube' is synthesised from a cube whose axis of symmetry is inclined relative to the rotational axis of the structural architecture, Fig. 4.7. The resulting slices form a series of unique and apparently random multi-angulated strips from which it is particularly pleasing to observe the regular surface of the cube emerge on deployment.

The un-fillable cone is conspicuous in both of these examples as the 'hole' in the sliceform surfaces along the axis of rotational symmetry.

4.4.6 Tube-like RS

Combining volumetric and shell-like approaches, a tube-like sliceform is synthesised by slicing a torus shell to generate a set of closed loops. Reorienting the slots "inside-out" and "outside-in" relative to the topological hole in each set of slices – as in Fig. 2.6 – the sliceform

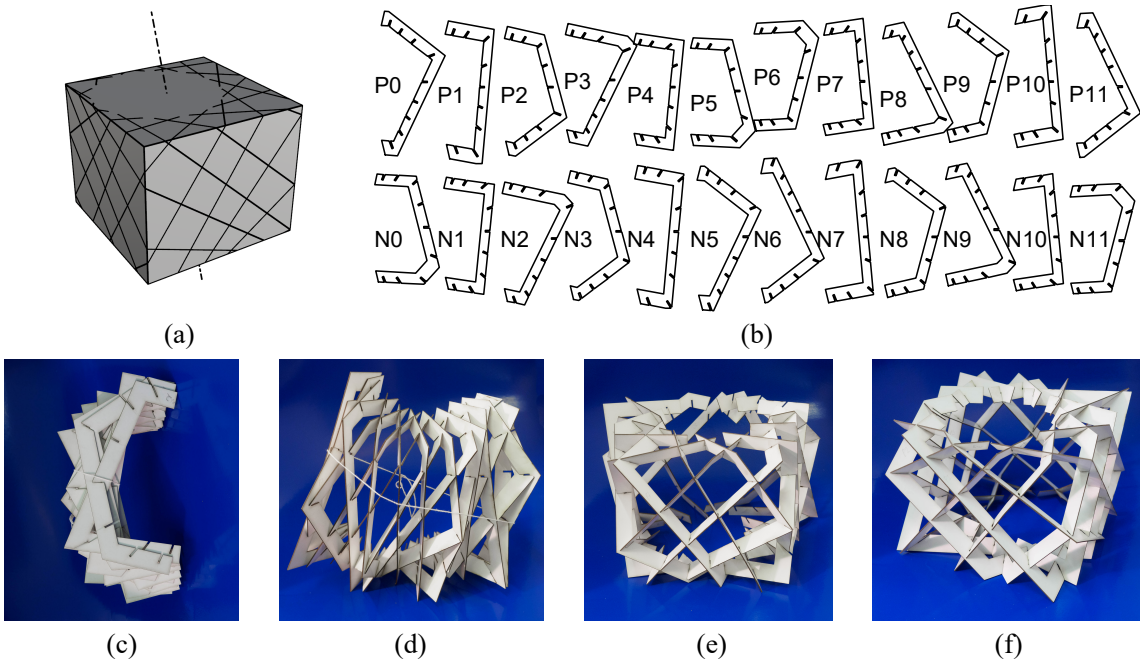

Fig. 4.7 A shell-like RS cube generated by slicing a thin-walled cube to excise a series of angulated strips, (a)-(b). The axis of revolution is inclined to the z-axis of the cube so that global symmetry is broken and each slice is unique. The assembled but incomplete sliceform is flat-foldable with the regular form of the cube emerging from the apparently random arrangement of interlocked strips as it is deployed, (c)-(f).

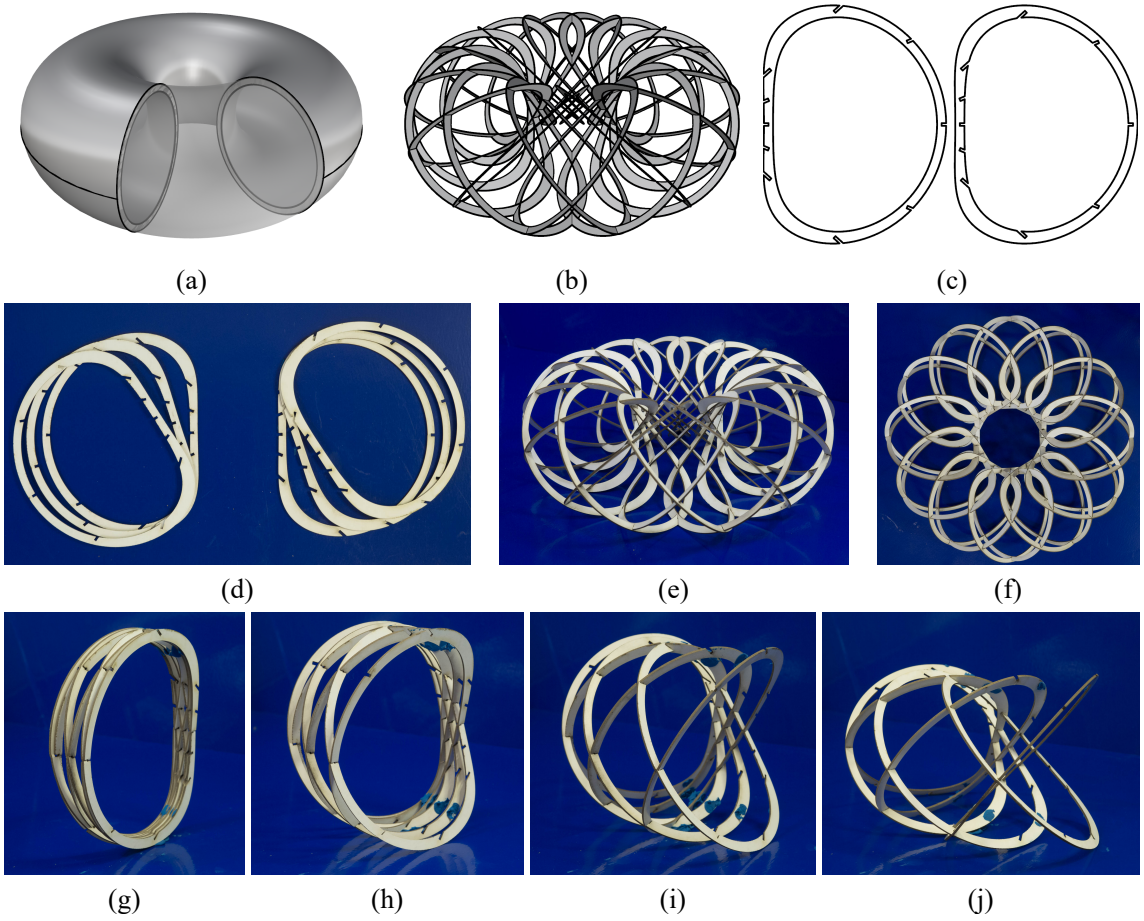

Fig. 4.8 A hollow sliceform is synthesised from a thin-walled toroidal tube (a)-(b). The cross-sectional slices are a set of rings, (c), with the sliceform assembled by fitting one set of slices within the other, (d)-(e), with top view, (f). The incomplete sliceform is flat-foldable and deployable as usual, (g)-(j).

is assembled according to the usual piece-wise manner with one set of slices now enclosed by the other. The resulting sliceform contains an internal void; the incomplete ring deploys about a circular path, as usual, Fig. 4.8.

4.4.7 Practical considerations for RS derived deployable structures

For practical application, a significant limitation of the RS architecture is the necessity to engage the subset of intersections in the outermost slices to close the chain and rigidify the ring at the final stage of deployment, and *vice versa* for collapse. This final step is often non-trivial, requiring an incremental process in which the connectivity of the outer slices is gradually increased until all intersections are engaged. In practice, a deployable RS structure

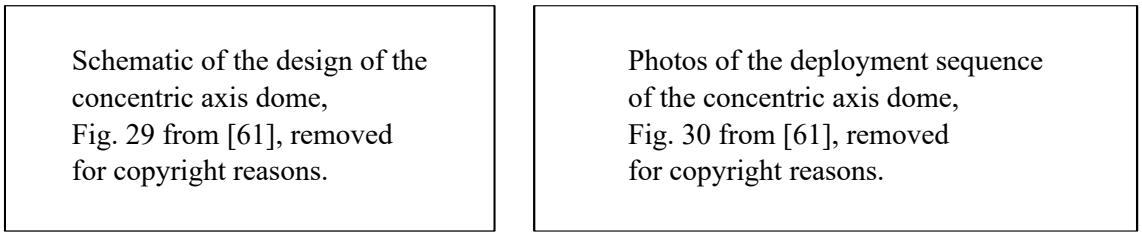

Fig. 4.9 Deployable 'concentric axis dome' by by Muñoz-Vidal et al.[61]. The geometric construction of the dome matches the rotational sliceform architecture, (a). The final structure is constructed from scissor-jointed circular bars with radial pins, retaining the deployable characteristic of an RS, (b).

might be modified to incorporate a set of *seam* elements – perhaps by splitting one set of slices between an adjacent pair of the other – with a latching mechanism to enable the closed loop to be rapidly completed when deployed, or disengaged for collapse, on demand.

Similarly, functional load-bearing structures are more likely to be constructed as *pin-jointed frameworks* where a framework matching the structural architecture of an RS would retain an identical deployable capability. Such a design can be imagined if the through-thickness depth of the shell-like sliceforms is reduced to zero so that each strip collapses to a curved line. Applying this idea, a deployable, hemispherical dome has recently been designed and manufactured by Muñoz-Vidal et al.[61], Fig. 4.9. Their 'concentric axis dome' uses two sets of curved bars – which are simply the great arcs on the surface of a hemispherical RS – one with a slightly smaller radius than the other, which are scissor-jointed by inserting bolts along concurrent axes aligned to the intersection lines of an RS. Their dome is flat-foldable when some bolts are removed, and these joints are readily engaged when the dome has been expanded to its design configuration to lock the structure into place.

4.5 Summary

Rotational sliceforms are constructed from two sets of inclined slices arranged at regular intervals about an axis of rotational symmetry. Their structural architecture is parameterised by the number of slices in each set, N, and their rotation from vertical, θ^+ and θ^-; in a symmetric RS the sets have equal inclination, $\theta^+ = \theta^- (= \theta)$.

The structural architecture of an RS embeds a spherical array of intersection lines which are concurrent at the focus of the sliceform and form a polar fan upon each set of slices. Using a vector formulation, this structural geometry is captured in general form by generation

of a vector aligned to each intersection line via the vector product of the normal vectors to the interlocking slices. Upon each set of slice planes, the in-plane elevation of each intersection line from horizontal is determined from the scalar-product to each intersection vector and the horizontal reference vector. Alternately, the in-plane elevation of each intersection line can be determined directly from the spherical array of slice planes by application of spherical trigonometry to a spherical triangle pertaining to the image of the array on a spherical surface where each slice traces a great arc.

The articulation of an RS is a function of the structural architecture and independent of the global volume. This formulation can therefore be employed to generate a range of deployable sliceform structures, with this potential demonstrated by the synthesis of a selection of deployable volumetric, shell-like, and tube-like sliceforms, all of which are flat-foldable. Some practical considerations and associated design principles have been identified.

Chapter 5

Deployable motion of a rotational sliceform

5.1 Introduction

Rotational sliceforms exhibit a surprising deployable characteristic. With a few of the intersections disconnected to open the ring, and with the slotted intersection lines functioning as simple revolute joints, the chain of slices can be smoothly expanded and contracted about the central axis of rotational symmetry, Fig. 5.1. This motion aids assembly of the sliceform and also provides the opportunity to design a range of deployable structures, such as the examples presented in the previous chapter.

This deployable motion is highly intriguing. With only a partial complement of slices, a segment of a complete RS articulates smoothly in the collapsing direction, a symmetric

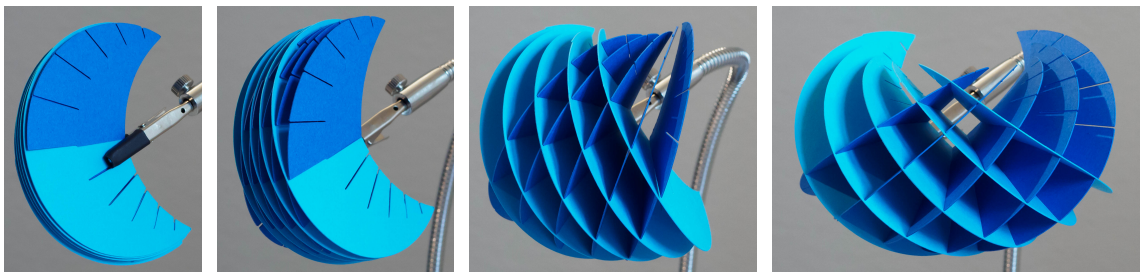

(a) (b) (c) (d)

Fig. 5.1 Sequence of deployment of the partially assembled sliceform torus. (Repeated from Fig. 1.4). From flat-folded, (a), the sliceform deploys smoothly and without resistance until the design configuration is reached, (d) – as if excised from the complete ring, whereupon it abruptly 'locks-out' and cannot be over-expanded without deformation of the slices.

RS collapsing to a flat-folded stack of coplanar slices in the limit of zero thickness. On deployment, the incomplete RS initially expands smoothly until abruptly 'locking out' once the slices have reached their design inclination – as if perfectly excised from a complete ring. The sudden ceasing of mobility is not warranted by any apparent interference between the slices, nor any intersection reaching the limit of its range of motion.

This unusual behaviour is somewhat paradoxical. The smoothness of initial articulation suggests rigid-folding but this conflicts with the finite range of motion because a rigid-mechanism has a continuous motion path[9]. Such natural and sudden limits on otherwise mechanistic folding poses an attractive opportunity for the design of self-arresting deployable structures in which the need for a secondary system to prevent over-expansion is removed.

5.1.1 Chapter outline

The principal objective this chapter is to determine the nature of this unusual articulation to resolve the conflict between folding and locking out, and its relationship, or otherwise, to the presumed rigid-folding capability. The analysis throughout this chapter pertains to an incomplete RS; a complete RS is rigidified by the closure of the loop.

Informal experiments of small-scale models are first conducted to investigate the effect of the parameterisation of the structural architecture on the foldability of the incomplete sliceform. The topological mobility of an RS is then determined and an *intrinsic* view of the sliceform as an array of cells proposed. Conditions for flat-folding are established by examination of each cell, and rigid-folding is assessed by consideration of the *extrinsic* motion of the slices. A simple model of the folding action is then constructed to determine the source of the 'locking-out' characteristic.

5.2 Deployable motion of an RS

The deployable motion of an RS becomes apparent during assembly of the sliceform with an incomplete chain of slices readily collapsing or expanding about the axis of rotational symmetry. To emphasise that this is a function of the structural architecture and independent of the shape of its slices and overall global geometry, Fig. 5.2 illustrates the synthesis of a simplified RS with rectangular slices (rather than excised from a prescribed global volume) which, with a few slices removed, is readily collapsed and expanded as usual.

On comparing the motion of partial sliceforms with a range of parameterisations, informal experiments demonstrate that the range of motion becomes progressively more restricted

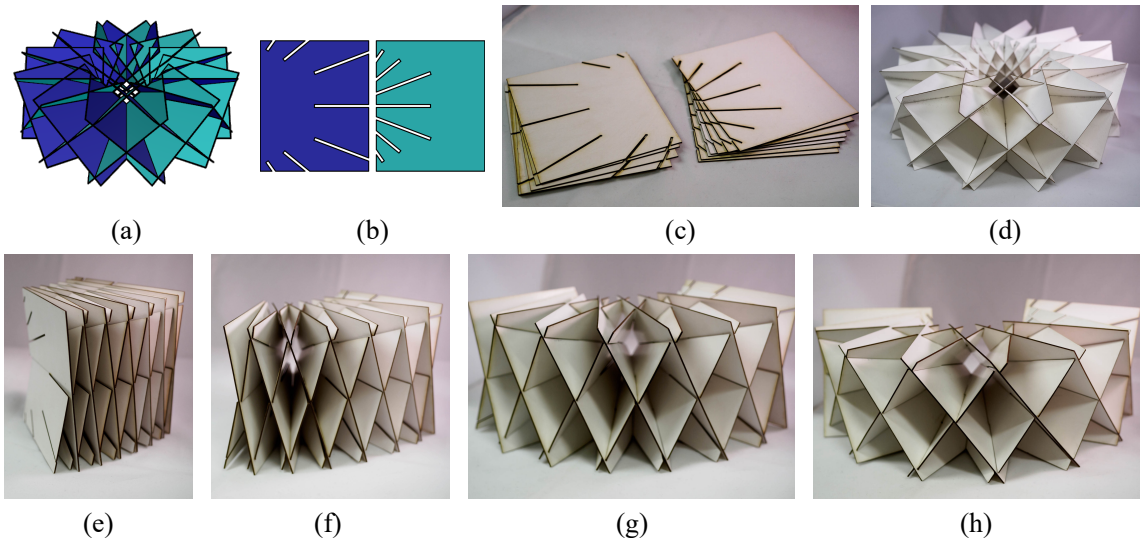

Fig. 5.2 Synthesis of simplified RS with rectangular slices and $(N = 12, \theta^+ = 45°, \theta^- = 45°)$, (a)-(d). The complete sliceform (d) is rigid, but with several slices removed, the incomplete RS collapses and expands about its vertical axis of symmetry, (e)-(h) (fully flat-folded condition not shown). When deployed to the design configuration, (h), the sliceform has reached its maximum expansion and 'locks out'.

with increasing asymmetry of the slice inclinations, Fig. 5.3. Only the symmetric design is flat-foldable, though in all cases the maximum expansion ostensibly coincides with the design configuration – measurements reveal this to be a slight overshoot with increasing asymmetry resulting in a more abrupt maximum expansion.

It is worth highlighting that this behaviour is distinct from the deployable motion of a decorative 'tissue paper ball'. Though sharing a visually similar honeycomb-like structure, these are assembled from a series of pleated semicircles glued along alternating horizontal lines so that they fold to a zig-zag pattern as the ball is deployed.

5.3 Mobility of an RS

Before examining the kinematic motion of an RS in detail, their expected mobility can be assessed by examining their topology. As identified in the preceding chapter, the polar arrays of slice planes form a spherical array of intersection lines, Fig. 5.4(a)-(b). With each slotted intersection performing as a revolute joint, this embeds a spherical single-layer scissor grid, which remains topologically identical to an RS (a planar single-layer scissor grid), Fig. 5.4(c).

From section 3.2.1, the expected mobility (or inversely determinacy) of a two-dimensional linkage is given by Calladine's modified version of the Maxwell rule (from Section 3.2,

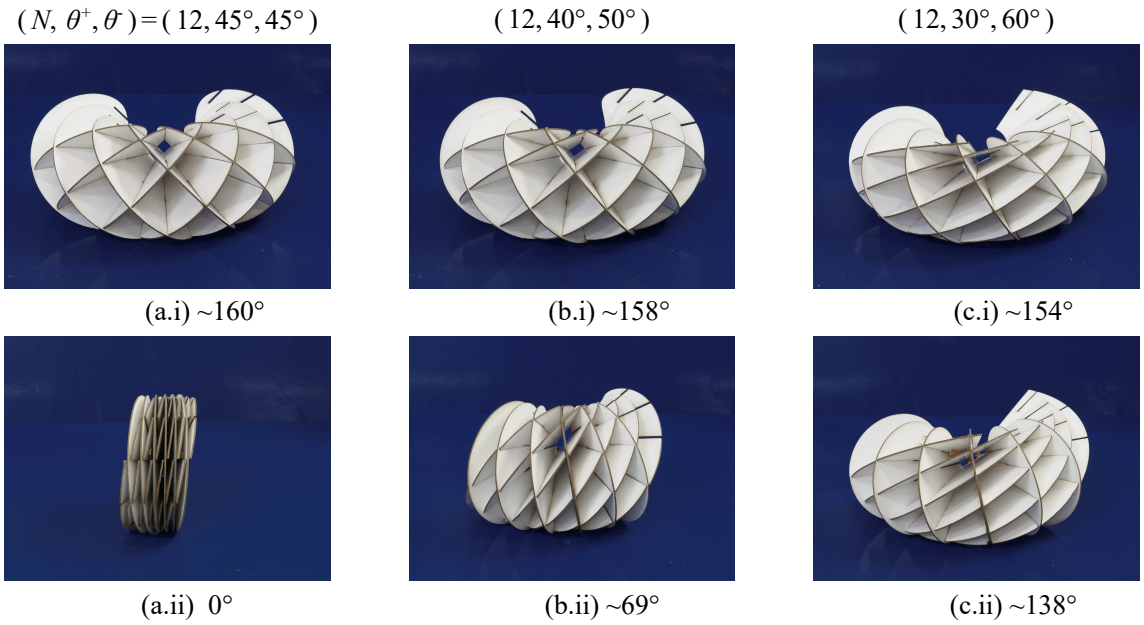

Fig. 5.3 The range of motion exhibited by an incomplete RS is dependent on the initial parameterisation of its structural architecture. Informal experiments are conducted on a set of tabletop scale models. Each has $N = 12$ slices in each set with their inclination from vertical is varied between each model (indicated above – these three architectural parameterisations are used as a standard sample throughout this chapter). In the design configuration, top, all incomplete sliceforms subtend 150° between the outermost intersection lines and expand only slightly when stretched, returning to the design condition when released. On compaction, bottom, the symmetric RS is flat-foldable, (a); an asymmetric RS is not, (b) and (c), with the range of admissible motion decreasing with increased asymmetry.

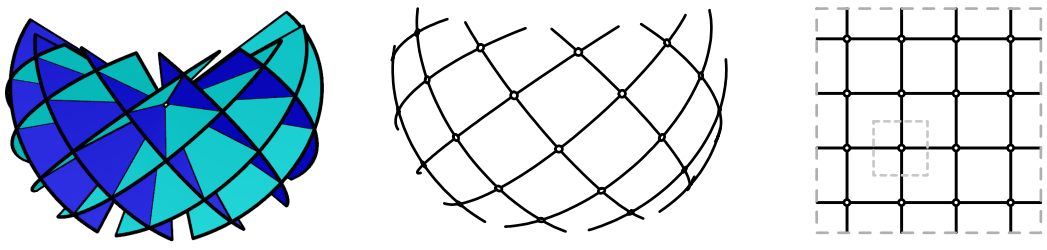

Fig. 5.4 An RS, (a), embeds a spherical scissor grid, (b), with concurrent axes of revolution. This 2D linkage is topologically identical to the planar scissor grid embedded by a lattice sliceform, (c). The topological mobility of a grid of quadrilateral units is determined by examination of a single motif, indicated on (c), with counting rules determining it to be overconstrained by degree 3 per cell. Note that in (b) and (c) the pins are embedded in each bar.

Eqn. 3.2)

$$m - s = 2j - b - 3$$

This applies to a finite framework of links, whereas a sliceform is periodic. Guest and Fowler's modified rule for a two-dimensional periodic framework is (from Eqn. 3.3)

$$m - s = 2j - b + 1$$

This modified rule is still not straightforwardly applied to the image of a sliceform because each slice is continuous across each slotted intersection line. This can be accommodated by adding Seffen's modification for a framework with j joints (total) and j_e embedded pins, which is (from Eqn. 3.4)

$$m - s = 2j - b - 2j_e - 3$$

to yield a counting rule for a periodic framework with embedded pins

$$m - s = 2j - b - 2j_e + 1 \tag{5.1}$$

This combined rule applies to the minimal repeating motif, which, for an LS or RS, is simply a pair of intersecting slices (indicated in Fig. 5.4(c)), *i.e.* a pair of crossed bars with mutually embedded pins. Thus

$$m - s = 2(1) - 2 - 2(2) + 1 = -3$$

and the system is overconstrained by degree three per motif.

For a lattice structure, this result can be interrogated by simply examining the geometric conditions. With parallel sets of bars, each row of segments are identical by symmetry. An independent state of self-stress can therefore be induced by adjusting the length of any one bar and each motif thus has $s = 4$ degrees of self-stress, $m = 1$ mechanism and is an overconstrained linkage. For the spherical linkage embedded by an RS, such symmetry conditions are not so readily evaluated by inspection – in particular, no pair of bars can be parallel – but this calculation nonetheless determines that it is overconstrained.

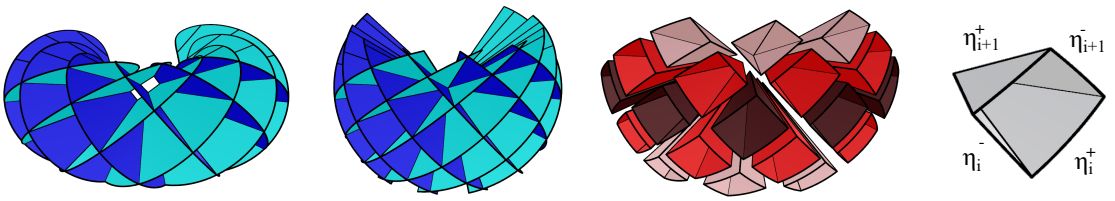

(a) (b) (c) (d)

Fig. 5.5 The structural architecture of an RS embeds a spherical array of intersection lines, (a). Across the array, the slices form a series of open-faced pyramidal cells, best visualised for a spherical RS, (b). The cells of each horizontal row are identical, as indicated by colouring accordingly in an exploded view, (c). Each individual cell has concurrent edges with facets spanning adjacent intersection lines, embedding a spherical 4R linkage whose range of motion is dependent on the ratio of its facet angles, η_i.

5.4 Structural geometry of an RS as an array of pyramidal cells

An RS comprises an array of interlocking planar slices but, to assess the folding motion, it is insightful to re-conceptualise this structural geometry as an array of open-faced, four-sided cells. The sliceform overall comprises rows of identical cells, with each offset from those above/below by half a cell, Fig. 5.5(c). The complete array is globally anti-symmetric in a horizontal plane. The intersection lines are concurrent so each cell is pyramidal and, with freely hinged facets, thus embeds a spherical 4R linkage [4]. From this perspective, the articulation of an RS is more intuitively understood as the synchronous, symmetrical expansion and contraction of the array of single-degree-of-freedom cells, apparently as an overconstrained linkage.

Each pyramidal cell has facets subtending the in-plane angle between successive intersections. Each cell of the ith row above the midplane has facet angles, $\eta_i^{\pm}$, as illustrated, Fig. 5.5(d). These facet angles follow directly from the structural geometry derived previously

$$\eta_i^{\pm} = \beta_i^{\pm} - \beta_{i-1}^{\pm} \tag{5.2}$$

where expression for $\beta_{i-1}^{\pm}$ is found by replacing i with $i-1$ in Eqn. 4.7 or 4.9.

5.5 Flat-foldability of an RS

Using the *intrinsic* viewpoint introduced in the previous section, something of the range of motion of an RS can be immediately deduced by examination of each pyramidal cell. In isolation, the range of motion of each pyramidal cell is governed by the ratio of its facet angles. From an intermediate position, each is mobile in two senses, corresponding to the collapse and expansion of the sliceform. The cell is instantaneously triangulated when the shorter pair of adjacent facets become parallel and are coplanar. Though motion of the isolated cell may continue, with the parallel facets inverting until obstructed by internal contact, the slices of a sliceform cannot not rotate beyond coplanar. Therefore, the triangulated condition sets an upper bound on the range of motion of the parent sliceform.

It follows that local flat-foldability of each cell is a requirement for the global flat-foldability of an RS. In each folding sense, this requires that opposing pairs of facets subtend the same angle so that they become coplanar simultaneously, an analogous condition to Escrig's 'deployability condition' for a pair of scissor-links, see Section 3.3.2. The row of midplane cells about the equator are (at least) anti-symmetric in the midplane and thus flat-foldable in both collapsed and expanded senses. This is true for any choice of architectural parametrisation.

For each cell of the i-th row above/below the midplane - with facet angles η_i^+, η_i^-, η_{i+1}^+, and η_{i+1}^- - no symmetry is guaranteed and flat-foldability must be determined explicitly.

Considering first the expanded sense, flat-foldability requires that upper and lower pairs of facets subtend the same total angle,

$$\eta_i^+ + \eta_i^- = \eta_{i+1}^+ + \eta_{i+1}^- \tag{5.3}$$

It is usually not possible to express η_i in closed form but by substitution of numerical values η_i is observed to decrease outwards from the midplane. For any given cell above the midplane, $\eta_{i+1}^{\pm}$ is smaller than $\eta_i^{\pm}$ so that

$$\eta_i^+ + \eta_i^- > \eta_{i+1}^+ + \eta_{i+1}^-$$

and *vice-versa* for cells below the midplane. Therefore, the condition in Eqn. 5.3 can never be satisfied, and, on expansion, the outermost facets, with angles $\eta_{i+1}^{\pm}$, will become parallel before the innermost facets, $\eta_i^{\pm}$, triangulating the cell in a horizontal sense. Thus, an RS cannot be flat-foldable in the expanding sense. Note also that this condition always occurs first for the outermost rows of cells about the midplane.

In the collapsing sense, flat-foldability requires that left- and right-most pairs of facets subtend the same total angle,

$$\eta_i^+ + \eta_{i+1}^- = \eta_i^- + \eta_{i+1}^+ \tag{5.4}$$

This condition can be determined by substituting either Eqn. 4.7 or 4.9 into Eqn. 5.2. However, as each facet angle is a non-linear function of the architectural parameters, a closed-form solution is not readily attained. Instead, progress is made by proceeding graphically and plotting surfaces of total angle subtended by the left- and right- facet pairs for each cell at a range of parameterisations, locating flat-foldable parametrisations wherever they intersect.

Surfaces of combined facet angles for a cell of each of the first four rows of an RS across a range of slice inclinations and $N = 12$ slices in each set are plotted in Figure 5.6 (characteristically identical results are obtained for all realistic values of N). These plots are generated by using MATLAB [50]. The midplane cells are confirmed to be always flat-foldable whilst cells of each subsequent row are flat-foldable when $\theta^+ = \theta^-$. Thus, all cells of a symmetric RS are flat-foldable in a collapsing sense, but each non-midplane cell of an asymmetric RS is not and will become triangulated. Therefore, parametric symmetry is a necessary condition for an RS to be flat-foldable.

Furthermore, for collapse of a non-flat-foldable RS or expansion of any RS, an upper bound on the range of motion is set by whichever row of cells is triangulated first. However, except for the flat-folding symmetric RS, the articulation exhibited by the small scale physical models is much reduced than this analysis predicts, Fig. 5.3. The implication is that the limiting constraint must emerge from the kinematic interaction between the cells rather than the cells themselves.

5.6 Modelling the deployable motion

The intrinsic cell-based model of an RS elucidates the conditions for flat-folding but does not capture anything of the constrained motion. In the context of an overconstrained mechanism, a full kinematic model must reproduce the motion of the array of slices and cells together and so describe the *extrinsic* geometry of the array of planes and intersection lines at any intermediate configuration.

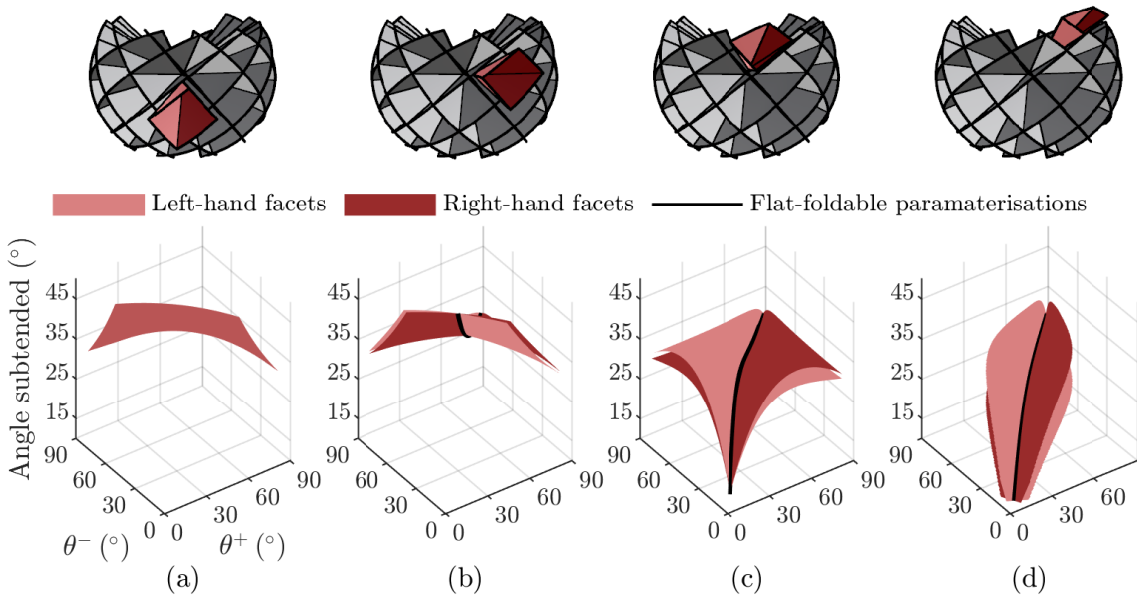

Fig. 5.6 Each cell of an RS is flat-foldable in a collapsing sense when left- (pale) and right-most (dark) facet pairs subtend the same total angle. To assess the influence of the initial parameterisation on flat-folding, the angle subtended by each half of a cell from each row is plotted throughout the (θ^+, θ^-) space for a constant value of $N = 12$. Flat-foldable parameterisations are located wherever these surfaces intersect. Apart from the midplane cells, which are always flat-foldable, (a), the cells are only foldable when the architecture is symmetric with $\theta^+ = \theta^-$, (b)-(d). Qualitatively identical results are obtained for all other realistic values of N.

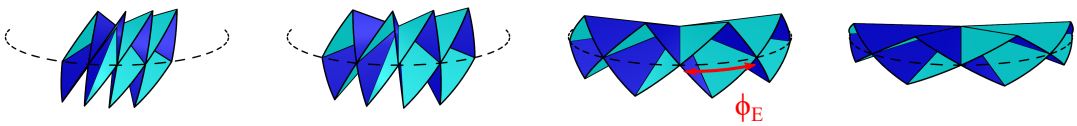

Fig. 5.7 The *extrinsic* kinematics of an RS, *i.e.* the rotation of each slice plane, are captured by the commensurate expansion of the midplane cells about the equator as a chain of spherical scissor links. This articulation is parameterised by the azimuthal angle subtended by each cell, ϕ_E, between flat-folded conditions in both senses (not shown).

5.6.1 Articulation of the chain of midplane cells

The array of interlocking slices of an RS embed a spherical pantograph with each row of cells embedding a chain of spherical scissor elements. Inspired by the treatment of single-layer scissor grids, the prospective kinematics of the array can be modelled by first considering the commensurate expansion of the midplane row.

The expansion and contraction of this row of cells about the equator is characterised by the azimuthal expansion angle, ϕ_E, subtended by each Fig. 5.7(a-d). Between flat-folded configurations of these cells, the maximum range of motion is

$$|\eta_1^+ - \eta_1^-| \leq \phi_E \leq \eta_1^+ + \eta_1^- \tag{5.5}$$

5.6.2 Assessment of rigid-folding

At a given midplane expansion, the rotation of each set of facets, $\theta_E^{\pm}$, is found by considering the spherical triangle formed by the upper half of each midplane cell and the equator, where the cosine rule for sides gives

$$\sin\theta_E^{\pm} = \csc\phi_E \csc\eta_i^{\pm} \cos\eta_i^{\mp} - \cot\phi_E \cot\eta_i^{\pm} \tag{5.6}$$

Under speculated rigid-folding, the remainder of the RS can then be reconstructed by extension of each facet within its plane to form each subsequent cell, Fig. 5.8. Projecting circular arcs across each slice-plane forms a spherical sliceform.

Rigid-folding is viable if the facet angles do not change throughout motion. With slice planes aligned to each facet of the midplane cells, the intersection lines are located by

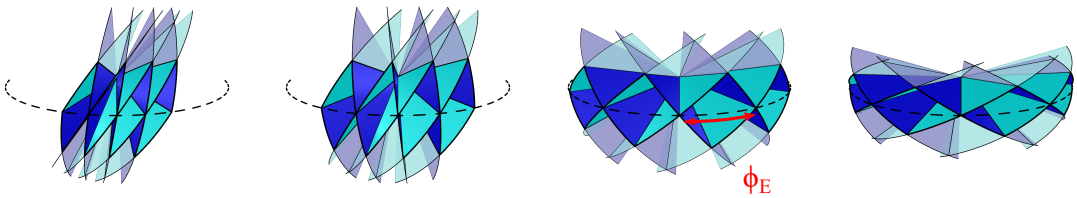

Fig. 5.8 A model of the speculated rigid-folding of an RS: The articulation of the midplane cells, Fig. 5.7, captures the *extrinsic* kinematics of the slice planes. The remainder of the sliceform follows by extrapolating their facets in-plane to reconstruct the array of cells. Rigid-folding is viable if the *intrinsic* geometry of each cell is invariant through motion. For clarity only the first row of additional cells are reconstructed here.

substituting the expanded configuration, ϕ_E & $\theta_E^{\pm}$, back into Eqn. 4.7 or 4.9 to determine their in-plane elevation in this prospective reconstruction, $\beta_{i,E}^{\pm}$. The sector angle of each facet, or 'facet angle', $\eta_{i,E}^{\pm}$, follows via Eqn. 5.2. The outcome above and below the midplane is, of course, symmetrical.

For parameterisations matching the physical models in Fig. 5.3, the variation of the first three facet angles throughout motion are calculated using MATLAB[50] and plotted in Figure 5.9. The vertical dashed lines from left to right illustrate the minimum- (flat-folded), design- ($\phi_E = 30°$), and maximum- (flat-folded) expansions of the midplane cells. Only the midplane facet angles, upon which this model is constructed, remain constant, and it is immediately clear that the articulation of an RS is incompatible with rigid-folding. Each non-midplane facet angle takes its design value at only the design expansion, varying appreciably throughout articulation with the outer facet angles increasing by upwards of 10° from collapsed to expanded.

5.6.3 Modelling compliant-folding

With the structural geometry of an RS incompatible with rigid-folding, it follows that their deployable motion must be wrought by some additional mobilities. The variation of each facet-angle in the speculated rigid-folding model also does not provide any insight into this motion or the difference in range of motion between a symmetric and asymmetric RS. Whilst some angle variation could be enacted by in-plane elastic compression/stretching or out-of-plane buckling of each slice, or by some movement arising from loose-fitting slots, the magnitude of deformation required is not observed in physical sliceforms which cannot realistically accommodate such significant in-plane distortions.

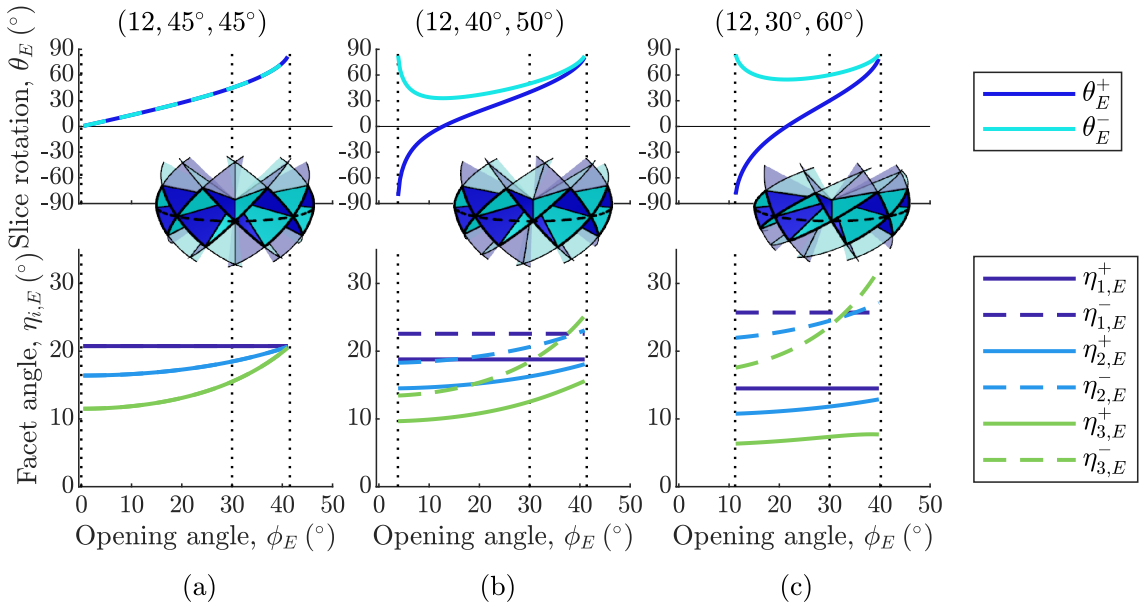

Fig. 5.9 Assessment of the rigid-folding of an RS using the speculated rigid-folding reconstruction illustrated in Fig. 5.8. Figure 5.8, where rigid-folding is viable if the intrinsic geometry of each slice is invariant (*i.e.* when each facet angle is constant). The rotation of each set of slice planes, top, and the variation in their facet angles, bottom, are plotted for sliceforms with design parameterisations (indicated above) matching the set of physical models in Figure 5.3. From left to right, the vertical dotted lines upon each plot denote the minimum, design and maximum expansions of the midplane row cells. Only the midplane facets, upon which this model is based, subtend a constant angle. Therefore an RS is not rigid-foldable.

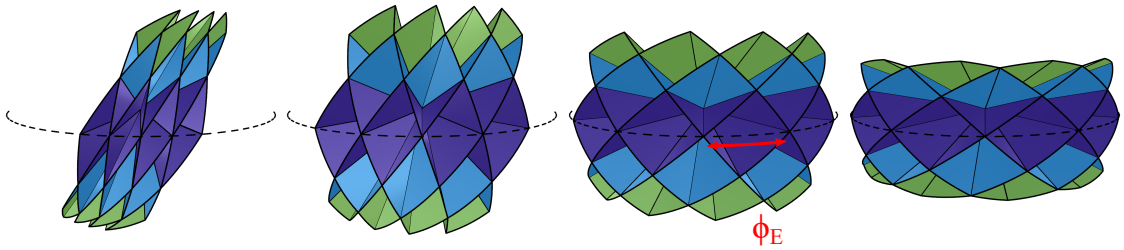

Fig. 5.10 A model of the compliant folding of an RS via out-of-plane 'kinking' of each slice. Based on the symmetric articulation of the midplane cells, Fig. 5.7, each successive row of facets are oriented to form each row of closed cells. This preserves the intrinsic geometry of each cell, but coplanarity of contiguous facets is no longer guaranteed.

Much more likely is that the slices bend out-of-plane. Inspired by Pellegrino and You's investigation of foldable bar structures with multi-angulated rods[94], a model is now constructed in which the facets retain their intrinsic geometry during articulation but successive facets on a given slice plane are no longer required to remain coplanar. Removal of the planarity constraint across each intersection allows consecutive facets to bend out-of-plane, in effect allowing each slice to 'kink'. This kinking model emulates a simplified transverse bending of the slices, a mode which is visible on over-expansion of a partial RS.

Removal of the planarity constraint across each intersection line introduces two additional degrees of freedom at each intersection; preservation of the symmetric expansion of the midplane cells about the equator reduces this to a single global degree of freedom, again captured by the azimuthal expansion of each midplane cell, ϕ_E. Each successive row of facets is then positioned to exactly span the peaks of the previous, and so forth, Fig. 5.10, with the magnitude of the kinks across each intersection, or *planar defects*, providing a measure of the extrinsic geometrical incompatibility throughout motion.

Geometric motion of the compliant array

To capture this motion geometrically, construction begins with a set of cells from a spherical RS whose facet edges trace segments of great arcs on the surface of an inscribed unit sphere. Tracing 'horizontal' great arcs across each pyramidal cell divides the array of edges into a series of horizontal 'layers', each comprising a sequence of alternately oriented spherical triangles, Fig. 5.11(a).

With corresponding geometrical parameters defined as illustrated in Fig. 5.11(b) – noting in particular ϕ_i as the angular span of the ith layer of triangles, where ϕ_1 is set equal to ϕ_E – the rotation of each set of facets is calculated moving through successive storeys as follows.

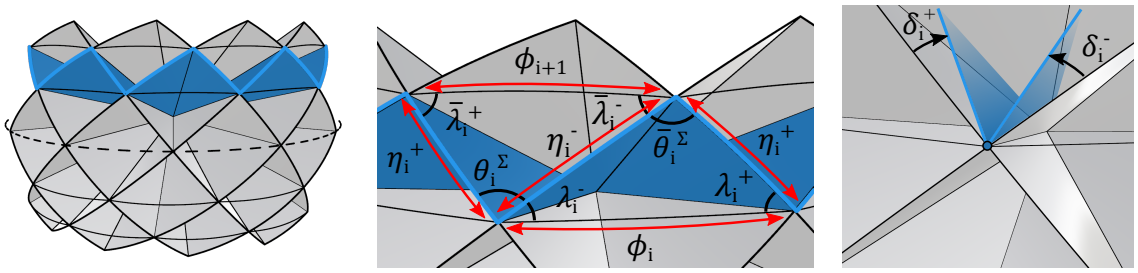

(a) (b) (c)

Fig. 5.11 Geometric construction of the compliant 'slice-kinking' model of an RS. Tracing a segment of a great arc across each cell divides the array into a series of horizontal 'layers', (a), with the second layer above the midplane highlighted. Each layer imprints a series of alternating spherical triangles on the surface of a unit sphere, with angles defined as shown, (b). The distortion of the array is captured by measuring the pair of planar defects, $\delta_i^\pm$ – calculated as the upward kink of contiguous facets – across each intersection, (c).

Given the span of each cell in that row, and the set of facet angles of the base sliceform, the elevation of each facet edge from horizontal, $\lambda_i^\pm$, is found via the cosine rule for sides

$$\cos\lambda_i^\pm = \frac{\cos\eta_i^\mp - \cos\phi_i\cos\eta_i^\pm}{\sin\phi_i\sin\eta_i^\pm} \tag{5.7}$$

The dihedral angle between facet edge pairs, denoted θ_i^Σ, is found by summing angles about each lower intersection, noting that the arcs spanning each cell are tangential about the equator only and where the corresponding inclinations of each facet edge at their upper end are denoted by an overbar

$$\begin{aligned}\theta_i^\Sigma &= \theta_i^+ + \theta_i^- \\ &= \pi - \left(\lambda_1^+ + \lambda_1^-\right) && \text{for } i = 1 \\ &= 2\pi - \left(\bar{\theta}_{i-1}^\Sigma + \bar{\lambda}_{i-1}^+ + \bar{\lambda}_{i-1}^- + \lambda_i^+ + \lambda_i^-\right) && \text{for } i > 1\end{aligned} \tag{5.8}$$

From the upward triangle, the cosine rule for sides gives the upper dihedral,

$$\cos\bar{\theta}_i^\Sigma = \frac{\cos\phi_i - \cos\eta_i^+\cos\eta_i^-}{\sin\eta_i^+\sin\eta_i^-} \tag{5.9}$$

and the cotangent rule gives the rotation from 'vertical' at the upper intersection,

$$\cot\bar{\lambda}_i^\pm = \cos\eta_i^\pm\cot\theta_i^\Sigma - \cot\eta_i^\mp\csc\theta_i^\Sigma\sin\eta_i^\pm \tag{5.10}$$

The upper edge span of each inverted triangle, ϕ_{i+1}, then follows from the cosine rule for sides

$$\cos\phi_{i+1} = \cos\eta_i^+ \cos\eta_i^- + \cos\theta_i^\Sigma \sin\eta_i^+ \sin\eta_i^- \tag{5.11}$$

giving the span of each cell in the next row.

Assessment of geometric compatibility through articulation

At any intermediate expansion, each pair of planar defects, $\delta_i^\pm$ – determined as the relative 'upward' rotation of consecutive facets, Fig. 5.11(c) – is found by summing angles about each intersection,

$$\pi + \delta_i^\pm = \lambda_i^\pm + \bar{\lambda}_{i-1}^\mp + \bar{\theta}_i^\Sigma \tag{5.12}$$

Geometrical compatible configurations of the sliceform are located at any expansion where the planar defects are simultaneously zero.

The variation in each planar defect throughout the range of motion of the midplane cells are calculated using MATLAB [50] and plotted in Figure 5.12 for a set of sliceforms with design architectures matching the physical models in Fig. 5.3.

For the symmetric RS, Fig. 5.12(a), the planar defects are simultaneously zero at the design configuration and the fully-collapsed, flat-folded state, indicating that both are strain-free. Between these conditions there is a shallow variation in each planar defect, suggesting a *bistable* transition from flat-folded to deployed, which this model suggests can be accommodated by a small amount of transverse bending of each slice. This bistability is not observed in practice, likely because the maximum defect of around 6° (across the third-level intersection line) is sufficiently slight as to be accommodated via other modes of compliance, discussed below. Upon over-expansion, each planar defect reverses in sign and increases rapidly. This correlates well with observations of physical models and the deflections certainly exceed what can be admitted by the slices without damage. It is this effect that yields the observed 'seizing-up' and stiffening of the sliceform (which must actually occur just slightly beyond the design expansion).

By contrast, an asymmetric RS is geometrically compatible at only its design configuration, Figs. 5.12(b) and (c). The intermediate physical model does admit some articulation in the collapsing sense, which, again, correlates well with the relatively shallower variation in incompatibility in this direction, (b), until the defects increase rapidly toward the end of collapse, producing a locking out effect in both senses of motion.

The indicated limits for each planar defect denote the configurations at which each pair of facets become coplanar, triangulating the row of contained cells, always occurring first

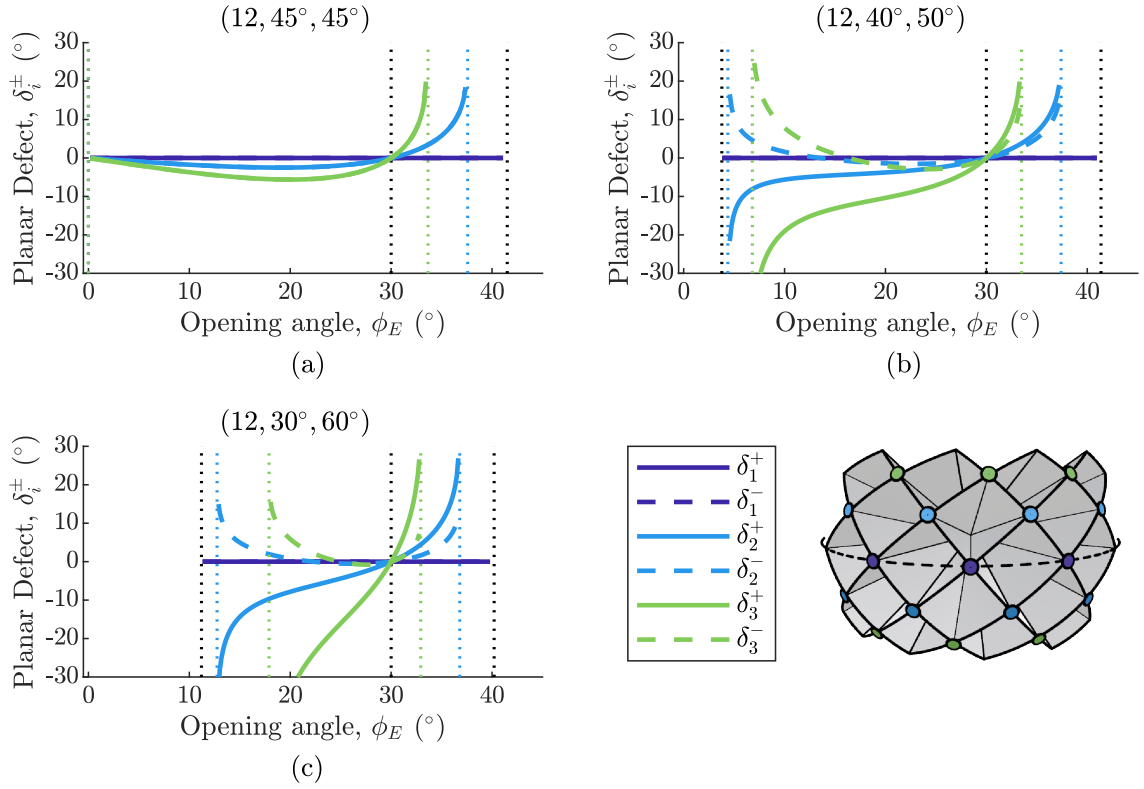

Fig. 5.12 Assessment of the compliant-folding of an RS using the slice-kinking model illustrated in Figure 5.10. The variation in the planar defect across each intersection line is plotted for sliceforms with design parameterisations matching the set of physical models in Figure 5.3 (indicated above each plot). The row of intersection lines that each planar defect belongs to is indicated by its colour, corresponding to those indicated on the schematic illustration in the bottom right. Geometrically compatible configurations of each sliceform are located wherever its planar defects are simultaneously zero: a symmetric RS is geometrically compatible at the fully collapsed (flat-folded) and design states, (a); the asymmetric RSs are compatible at the design expansion only, (b) and (c). The vertical lines denote the expansion at which each row of cells are triangulated, each setting an upper bound on the range of motion of the compliant model.

at the outermost row. The first-triangulated configurations represent the ultimate limit for expansion and contraction as permitted by this kinking mode but are not reached in practice.

Comments on modes of compliance

It is important to emphasise that the planar defects incorporated in this compliant kinematic model are strictly only a measure of the geometric incompatibility which must be accommodated via the proposed kinking mode. The slices are initially planar and thin so bending is a realistic and low-stiffness mode by which some incompatibility can be accommodated and, indeed, is evident on over-expansion. Of course, the true bending profile is more uniformly distributed than this simplified kinking mode assumed here, but the curvature will still be concentrated on each intersection line, where the bending moment is maximised and the in-plane depth of each slice is halved by the presence of a slot. The difference in geometry of the true deformation will have little effect on the qualitative behaviour of the sliceform.

The contribution of other sources of compliance to the accommodation of the geometrical incompatibility are more likely sources of any differential performance between a physical sliceform and this model. In particular, this analysis assumes that each intersection behaves as a perfect revolute joint but, with each slot cut slightly wider than the material thickness, some inherent 'play' is inevitable. Such additional compliances reduce that which must be accommodated via elastic modes and, with such a slight overall incompatibility at intermediate configurations, such inelastic compliances may be sufficient to accommodate the intermediate incompatibilities entirely. It may be this which ultimately undermines the predicted bistability in the physical models, allowing the smooth articulation exhibited by them in practice.

5.7 Equivalent deployable bar structure

The 'concentric axis dome' constructed by Muñoz-Vidal et al.[61], and introduced in the previous chapter, Fig. 4.9, has an identical structural geometry to an RS and is therefore identically bistable. Due to the increased precision of the joints (versus interlocking slots) this bistability ought to be more prominent, though is clearly still insufficiently to cause their example to 'snap' to a stable state if released at an intermediate configuration.

The replacement of slices with bars may, however, affect the mode of deformation. The out-of-plane kinking mode identified for an RS remains sufficient to enable the transition from flat-folded to deployed, but the bars themselves lack the structural depth of a slice

so in-plane bending or axial torsion, which will have comparable stiffness, may make a significant contribution to the accommodation of the intermediate geometric incompatibility. Similarly because the stiffness of the bar will be limited by the compliance required to enable this transition, this may limit the stiffness that can be achieved by the overall structure. Adding multiple concentric layers of bars with common joints, *i.e.* nesting multiple (scaled) versions of this dome, would increase the relative stiffness of the in-plane bending and axial twisting modes relative to the out-of-plane bending mode, enabling the overall load bearing capacity of the dome to be increased without disabling the compliant mobility.

The requirement for the hinge lines to be concurrent for the system to embed a spherical mechanism has practical implications for the design of bar structures with alternative shapes, *c.f.* a RS bar structure with curved bars approximating the 'birds nest' from section 4.4.5. Such a design would require careful detailing to ensure that the joint axes remain radial rather than simply perpendicular to the bars which would no longer be circumferential which may add significant complexity to manufacture of the structure.

5.8 Summary

In this chapter the deployable motion of an incomplete RS has been investigated. The RS architecture contains a spherical array of concurrent intersection lines and so the sliceform embeds a spherical scissor grid. This 2D linkage is topologically identical to that embedded by an LS for which a simple counting rule sets the expected mobility to be overconstrained by order 3 per motif, from which an overconstrained rigid-folding mechanism is initially speculated.

The structural geometry of an RS can be re-conceptualised as an array of open-faced four-sided cells arranged in rows of identical cells. With concurrent intersection lines, each cell is pyramidal, embedding a spherical 4R linkage which is rigid-foldable in isolation. For flat-foldability of a cell in isolation, opposing halves must span the same total facet angle. Therefore, the anti-symmetric midplane cells are bi-directionally flat-foldable but the cells of each subsequent row cannot be flat-foldable in the expanding sense and only the cells of a symmetric RS are flat-foldable in the collapsing sense: a symmetric RS may be flat-foldable, an asymmetric RS cannot. The triangulation of each cell sets an upper bound on the range of motion of the parent sliceform, however this is much greater than the range of motion exhibited in practice with physical sliceforms 'locking out' prior to any cell becoming triangulated.

From an extrinsic perspective, the interlocking slices of an RS embed a spherical scissor-grid with each row of cells forming a chain of scissor links. The general form of the expansion and contraction of the array follows the symmetric expansion and contraction of the midplane cells. Rigid-folding of an RS is assessed by propagating each facet of the midplane cells to reconstruct the array, from which it is determined that the slotted slices are geometrically compatible in only the design condition and an RS is incompatible with rigid-folding. The variation in each facet angle is much greater than can be accommodated by elastic deformation of the slices or by imperfect slot fitting so in-plane actions are not responsible for the apparent mobility.

Preserving the intrinsic geometry of each cell, a compliant-folding mode is modelled by removing the coplanarity constraint between contiguous facets, allowing the slices to kink out-of-plane. Realistic motion corresponds to the single-degree-of-freedom, symmetrical expansion and contraction of the array about the axis of rotation. Reconstructing the geometry of this modified array, the pair of 'kink angles' or 'planar defects' across each intersection line provide a measure of the geometric incompatibility of the original sliceform. For a symmetric RS the planar defects are simultaneously zero at the flat-folded and design configurations but undergo a slight variation (of a few degrees) between them: a symmetric RS is bistable. For an asymmetric RS the planar defects are simultaneously zero at only the design configuration: an asymmetric RS is monostable. On over-expansion, the planar defects increase rapidly, inducing the locking-out characteristic observed in physical models. The variation in planar defects of an asymmetric RS on contraction is dependent on the asymmetry, less asymmetry results in a shallower variation in defect, corresponding well with the variation in range of motion of the physical models.

In practice, other inelastic compliances, particularly imperfect articulation of the slots – which are wider than the material thickness – contribute to the accommodation of the intermediate incompatibility without inducing notable elastic deformations. Hence the smooth and not evidently bistable articulation of an RS in the collapsing sense. Importantly this compliant kinematic model reproduces the characteristic deployment features of an incomplete RS and provides insight into the unexpected locking-out motion.

Part II

Curve Sliceforms

Introduction to Part II: Curve Sliceforms

The rotational sliceforms studied in Part I exhibit a surprising bistable foldability. Though kinematically 'rigid', an incomplete ring can be flat-folded and deployed over a finite range of motion. The symmetry of the design geometry is sufficient to enable overall flat-foldability but not rigid-folding, with the cells developing a frustration as they articulate. The deployable motion has been demonstrated to result from a compliant transition between bistable states – flat-folded and deployed – with the transition enabled by a small amount of out-of-plane bending of the slices. The RS formulation can be applied to the design of a range of deployable structures-from-slices, and the underlying structural geometry can be translated to the design of deployable structures with more conventional structural forms, *i.e.* a bar linkage.

An RS is cognate to a single-layer, spherical scissor grid. Though not rigid-foldable, the structure is flat-foldable with the midplane cells of an incomplete sliceform articulating about a circular arc. That rigid-folding is not a pre-requisite for viable deployable action, immediately suggests that a range of more general compliant-deployable sliceform structures might be generated in which the structural geometry is suitably 'close to mechanistic' that a large global transformation is enabled by a small degree of local elastic deformation as compliant-deployable structures. In Part II a range of sliceform structures synthesised from a smooth spatial 'basis' curve, which may be closed or open – so-called *curve sliceforms*, or *CS* – are introduced. Despite the lack of overall symmetry, a CS has a similar layout of slices to an RS and retains the characteristic flat-foldability.

Specific objectives

The overall objective in this part is to formalise and develop the technique for designing curve sliceforms, and to investigate the scope of this approach for the design of generalised deployable structures. Unlike an RS, a CS lacks any overall symmetry, so it is expected that a model of the folding action will need to be based on the intrinsic, local geometry of the array of slices along the curve, but does provide significantly increased scope for geometric design. It is still desired to preserve the generality of the models and solutions where possible so that the underlying principles and insights gained might be translated to the design of generalised deployable structures with more conventional structural forms.

Outline of part

This investigation of curve sliceforms is presented in three phases. In Chapter 6 the structural architecture and parametric synthesis of a CS is formalised and explored via design and construction of a set of novel sliceforms, demonstrating the flexibility and robustness of this technique for the design of geometrically-feasible, deployable structures. The structural geometry of a CS is explored in Chapter 7; though lacking the *extrinsic* symmetry of an RS, their *intrinsic* geometry is captured in general form and directly informs an investigation of their performance as kinematic structures in Chapter 8. The articulation of a CS involves significant additional compliances versus an RS, in particular relating to the articulation of the slices about each intersection line, so a complete model of the global articulation of a CS is not forthcoming, but a simple modified linkage model of a single cell is developed, providing insight into the nature and characteristics of the overall deployable motion.

Chapter 6

Structural architecture and synthesis of a curve sliceform

6.1 Introduction to Curve Sliceforms

The deployable characteristic of a rotational sliceform (RS) was discovered when assembling a sliceform torus originally designed to illustrate the Villarceau circles on an oblique cross-section aligned to the double tangent plane. In Part I this intriguing mobility as demonstrated to arise from the spatial arrangement of interlocking slice planes, independent of the inscribed global geometry, enabling synthesis of a range of generalised deployable structures using this underlying structural architecture.

An open, symmetric RS (*i.e.* with the ring disconnected) is foldable despite the rigidity of the nominal architecture, which forms a spherical scissor-grid. The deployable action has been determined to be a bistable transition between strain-free expanded and flat-folded configurations, in which a small degree of local elastic deformation – out-of-plane kinking of the slices – permits a large range of global articulation. This discovery suggests that other compliant-deployable structures-from-slices with more general structural architectures may be possible. Noting that an RS generates deployable motion about a circular arc, we are inspired to generate sliceforms according to a variety of general input curves – a *curve sliceform*, *CS* – and find that they retain the deployable characteristic of an RS.

A basic overview of the synthesis of a CS is illustrated in Figure 6.1 for a sliceform synthesised along a portion of a helix. To generate the generalised structural architecture of a CS, perpendicular *base planes* are first placed at regular intervals along the curve, (b), and then 'cleaved' apart by opposite sense rotation to form two sets of inclined slice planes, (c). A swept tube is employed as a suitable neutral global geometry, and two sets of cross-sectional

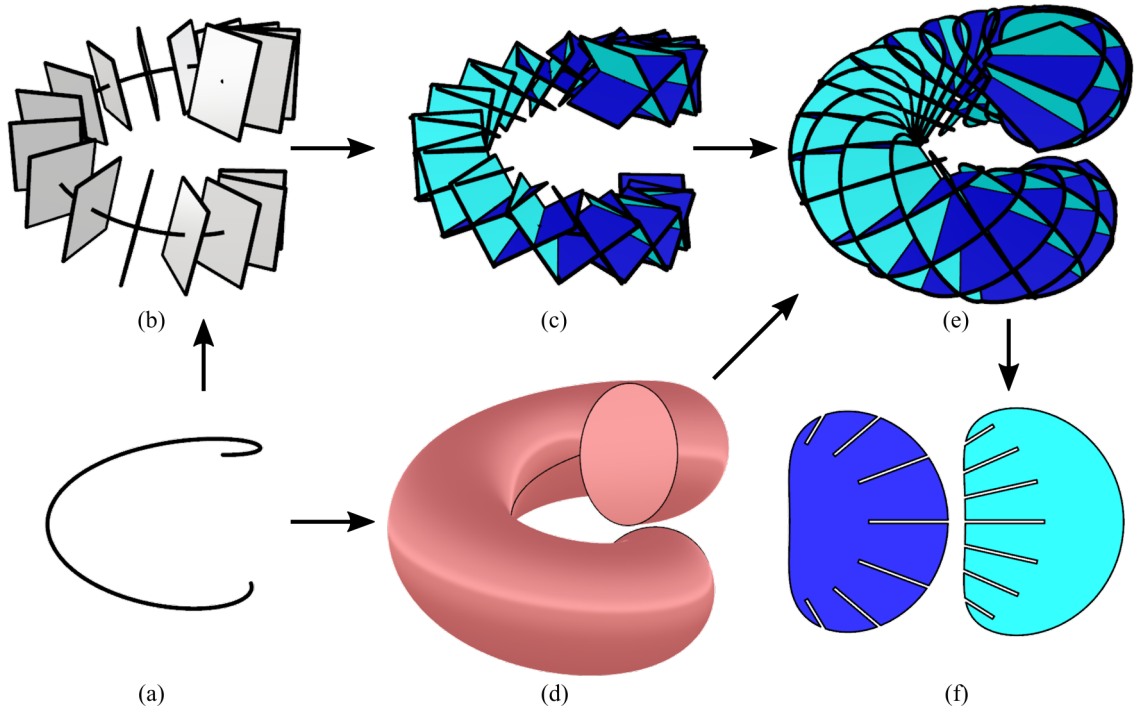

Fig. 6.1 The basic synthesis of a *curve sliceform* (CS) from a basis curve, illustrated for a CS generated along a portion of a helix. Beginning with a prescribed basis curve, (a), a series of perpendicular base planes are placed at regular intervals, (b), and two sets of slice planes are generated by opposite-sense rotation, (c), so forming the CS structural architecture. A neutral global geometry is generated by sweeping a circular cross-section along the basis curve to form a tube, (d), from which the sliceform is generated by excising a cross-sectional planform according to each slice plane, (e). The slice templates, (f), are completed by placing complementary pairs of slots along and to the midpoint of each intersection line.

planforms are excised. The slices are completed by and furnishing complementary pairs of slots along and to the midpoint of each intersection line which interlock when the structure is assembled. Note, in particular, that this approach can be applied to closed or open curves equivalently – indeed an RS is simply a CS synthesised about a circle.

To demonstrate the viability of this approach, the helical CS is manufactured from a thin sheet of stock material with slices cut according to the templates and assembled in successive pairs to complete the CS, Fig. 6.2(a). Just as for an RS, the misalignment of adjacent intersection lines precludes rigid-assembly of the sliceform, but the slots in each slice remain relatively closely aligned so assembly is once again possible by careful manipulation of the slices to enable the simultaneous engagement of non-parallel intersections. Once assembled, the sliceform is robust and strain-free, with the converging slots holding each slice securely in place. This design retains the deployable characteristic of an RS and is readily collapsed

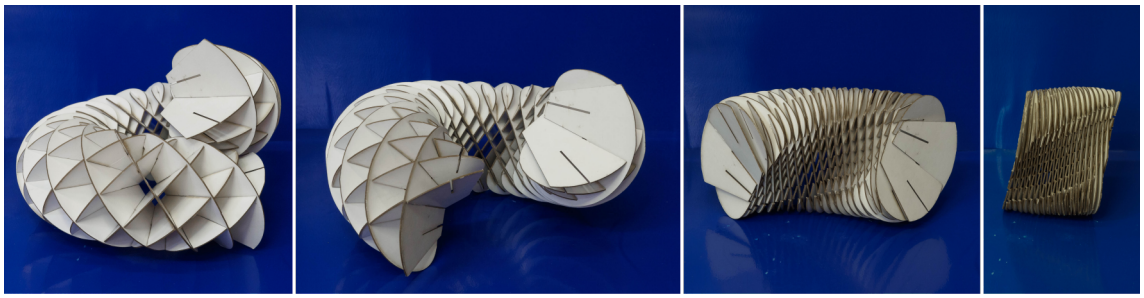

(a) (b) (c) (d)

Fig. 6.2 Deployment of a tabletop-scale model of the helical sliceform synthesised in Fig. 6.1. Shown in the design configuration, (a), and successive stages of collapse until flat-folded, (b) - (d). Like an RS, the CS articulates smoothly but cannot be expanded beyond the design configuration.

to a 'flat-folded' stack of parallel slices, (a)-(d). Upon expansion, the sliceform extends smoothly along the helical path until once-again 'locking-out' when the design configuration is reached.

6.1.1 Chapter outline

In this chapter an approach to the synthesis of deployable curve sliceforms from a range of spatial basis curves is introduced and developed. The basic technique is first formalised and demonstrated for two simple examples: a helix and an ellipse. The scope of this technique is then extended by development of a dynamic approach to the synthesis of well-conditioned sliceforms along more complex curves, including a planar spiral, conical spiral and an 'S-curve'. Finally, the robustness and generality of this approach is demonstrated by synthesising a set of technically challenging examples.

6.2 Basic synthesis of a CS

The generalisation of an RS to a CS is intuitive but requires careful formal definition. That the synthesis of a sliceform can be considered in terms of its hierarchical architecture, first defining the global geometry, then generating a suitable structural architecture and finally excising the set of cross-sectional slice planforms was highlighted in Part I. This remains true for a CS except that, for reasons discussed in section 6.2.2, their global volume must more directly echo the structural architecture, and so the basis curve is now set as the common geometry from which both the global volume and structural architecture are derived in parallel.

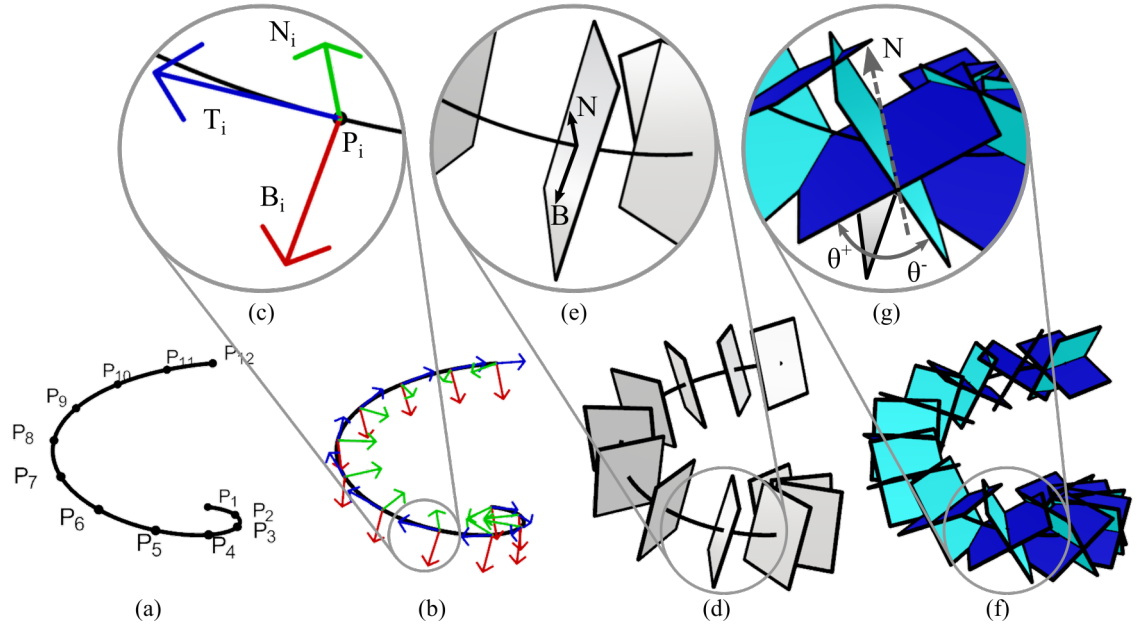

Fig. 6.3 Formalisation of the structural architecture of a CS. A set of curve points, P_i, are placed at regular intervals along the basis curve, (a), and the local Frenet-Serret curve frame is determined at each, (b) - inset detail in (c). The perpendicular base planes span each pair of N-B axes, (d) - inset detail in (e), and the two sets of slice planes are generated by opposite sense rotation of each base plane about the local normal, (f) - inset detail in (g). As for an RS, the CS structural architecture is parameterised by the number of slices in each set, N, and the inclination of each set of slices from perpendicular, θ^+ & θ^-.

6.2.1 Structural architecture: Slice planes from Frenet-Serret curve frames

The structural architecture of a CS - the spatial arrangement of slice planes - consists of N pairs of inclined slice planes generated at regular intervals along the basis curve. These pairs of slice planes are located at the set of evenly spaced *curve points* and generated by opposite sense rotation of a perpendicular plane about the local radius of curvature. The complete process is illustrated in Figure 6.3, with each plane indicated by a small rectangular patch.

Starting with the basis curve, a set of N curve points, P_i, are generated at regular intervals, (a). A set of local basis frames are given by the set of Frenet-Serret frames at each point, (b), each spanned by the local tangent, $\mathbf{T}_i$, normal, $\mathbf{N}_i$, and binormal, $\mathbf{B}_i$, vectors, (c).

Formally, where $\mathbf{r}(t)$ is a spatial curve with arc length $s(t)$, the Frenet-Serret vectors are defined as[11]

$$\begin{aligned} \mathbf{T} &= \frac{d\mathbf{r}}{ds} \\ \mathbf{N} &= \frac{\frac{d\mathbf{T}}{ds}}{||\frac{d\mathbf{T}}{ds}||} \\ \mathbf{B} &= \mathbf{T} \times \mathbf{N} \end{aligned} \tag{6.1}$$

and satisfy the Frenet-Serret formulas

$$\begin{aligned} \frac{d\mathbf{T}}{ds} &= \kappa\mathbf{N} \\ \frac{d\mathbf{N}}{ds} &= -\kappa\mathbf{T} + \tau\mathbf{B} \\ \frac{d\mathbf{B}}{ds} &= -\tau\mathbf{N} \end{aligned} \tag{6.2}$$

where $\kappa = ||\frac{d\mathbf{T}}{ds}||$ is the local (scalar) curvature (the speed of rotation of the tangent vector), and $\tau = -\mathbf{N} \cdot \frac{d\mathbf{b}}{ds}$ is the local (scalar) torsion (the speed of rotation of the binormal vector).

From these local curve frames, the series of perpendicular *base planes*, (d), are readily defined by the normal, **N**, and binormal, **B**, vectors, (e). Each pair of inclined slice planes follows by opposite sense rotation of each base plane about the local normal axis, (g), by θ^+ and θ^- in the positive and negative senses respectively. Combined, these slice planes form the structural architecture of the CS, with each set denoted as 'positive' and 'negative' according to the sense of the rotation. Note that these rotation senses are the opposite as defined for an RS in which the rotation vector points outward from the focus rather than inward toward the centre of curvature.

6.2.2 Neutral global geometry of a CS: Swept-section tube

With each slice plane indicated by a small patch, the form of a CS is already apparent. However, unlike an RS where the toroidal RS in section 4.2 is constructed directly from the structural architecture by placing a series of rectangular patches, a CS cannot be constructed in the same manner because adjacent pairs of slice planes are misaligned and the intersection lines between such patches will not fully span the slices. Instead, a suitable global geometry must first be specified from which to generate a set of cross-sectional slices inscribing a continuous outer surface, with a suitable result generated by sweeping a circular section along the basis curve to form a tube, Fig. 6.4. Formally, the orientation of the cross-section is fixed relative to the local curvature, and does not follow its spatial twist.

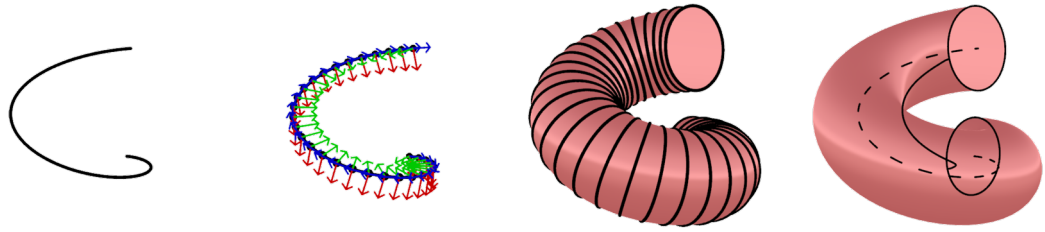

(a) (b) (c) (d)

Fig. 6.4 Generation of a neutral global geometry, (d), from the basis curve, (a), by sweeping a smooth surface through a series of circular cross-sections, (c), each aligned to the N-B plane of a Frenet-Serret frame, (b).

From this swept tube a cross-sectional planform is excised for each slice, so generating a volumetric sliceform directly from the basis curve, Fig. 6.5(a)-(f). The slice templates are completed by locating the lines of intersection upon each cross-section, (g), and apportioning pairs of complementary slots along and to the midpoint of each intersection line, (h). Just as for an RS, these must be consistent within each set of slices and are arranged so that they face "inward" in one set and "outward" in the other. The choice of slot orientation is free, but the final sliceform is more readily assembled if 'inward' slots are placed on the slice whose intersection lines are closest to parallel, if this distinction exists.

The choice of shape for the *swept section* is arbitrary, but a circular section generates an elegant sliceform with pleasingly smooth cross-sectional planforms that are advantageous when assembling each model.

6.2.3 'Localised' geometry of a CS

Before proceeding to discuss the treatment of each cross-sectional planform, it is interesting at this point to return to the structural architecture of a CS and consider it in more general terms. Recall that a key principle for generating a geometrically feasible sliceform is that no pair of intersections may themselves intersect within the inscribed volume. For a bulk sliceform this restricts the design space to a lattice whose intersections are mutually parallel with the RS architecture a special case in which the intersection lines form a spherical array of radial lines converging at a single point. The location and orientation of each slice plane in a CS is derived from the basis curve which, in principle, places slice planes, and their intersection lines, arbitrarily in space. Therefore, a CS cannot be geometrically feasible in general. However, given a smooth curve and a sufficient density of slices, adjacent slice planes within each set of slices will be similarly oriented and 'self-intersect' far from the basis curve. Since the opposing set of slices are generated by rotation about the curve normal,

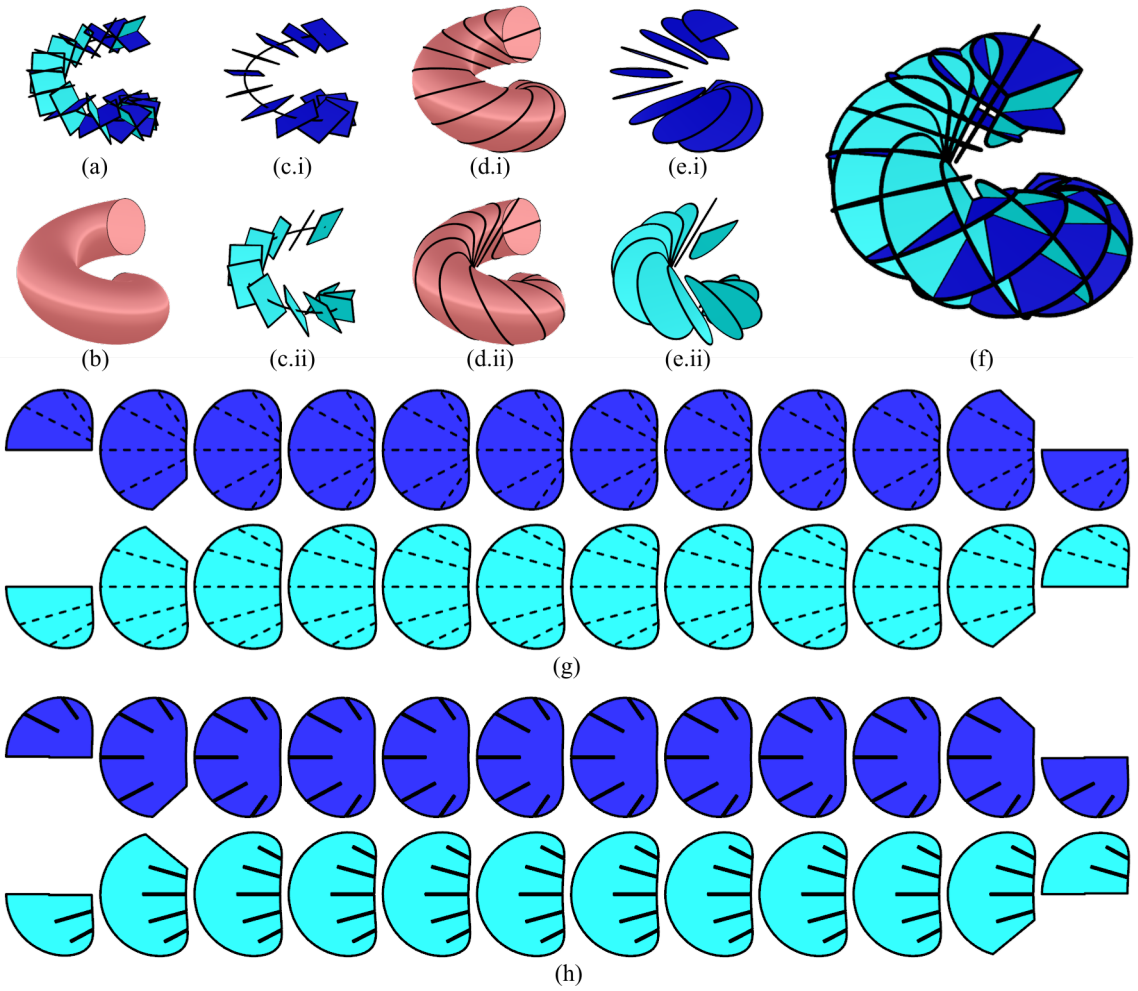

Fig. 6.5 Full synthesis of curve sliceform, (f), from the structural architecture generated in Fig. 6.3, (a), and swept global volume generated in Fig. 6.4, (b). For each set of slices, (c.i & ii), a series of cross-sections inscribing the swept volume are excised, (d.i & ii), two sets of cross-sectional planforms generated, (e.i & ii), to form the sliceform, (f). The slice templates are completed by placing slots along and to the midpoint of each intersection line, (g)-(h), outside-in for one set and inside-out for the other.

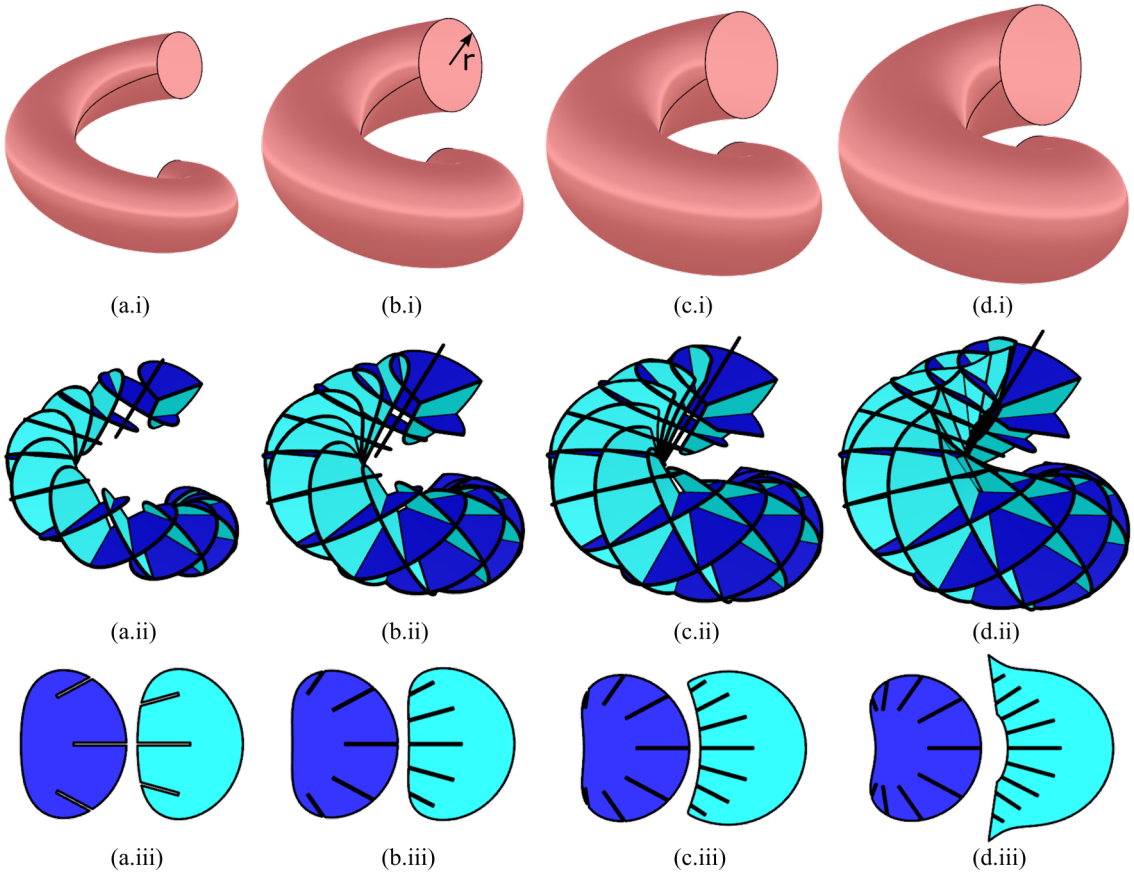

Fig. 6.6 For a given basis curve and structural architecture parameterisation, the swept-section radius, r, determines the connectivity of the resulting sliceform. As the swept-section radius increases, top row, so too does the connectivity of the resulting curve sliceform, middle row, increasing the number of slots on each slice, bottom row (not shown at equal scale). In (d) the slices of the light blue set have been 'clipped' to prevent self intersection.

and any pair of closely spaced curve normals will be broadly aligned. The intersection line between slices separated by a short segment will also be broadly aligned to these normals, forming a broadly parallel array of intersection lines in the vicinity of the curve (adjacent intersections meet at the same-set intersection lines which are far from the curve). Thus, the slice planes of a CS are locally well-behaved, and a geometrically feasible sliceform can be constructed within this local volume.

For this reason, a tube swept along the basis curve is a good choice for the global volume. The dimension (radius) of the swept section is a secondary parameter, specifying the slenderness of the tube and thus the connectivity of the sliceform: a thicker tube permits each slice to intersect with a a greater number of neighbouring slices of the opposing set, and *vice-versa*, Fig. 6.6. A larger swept section will generate a more robust sliceform, but if the

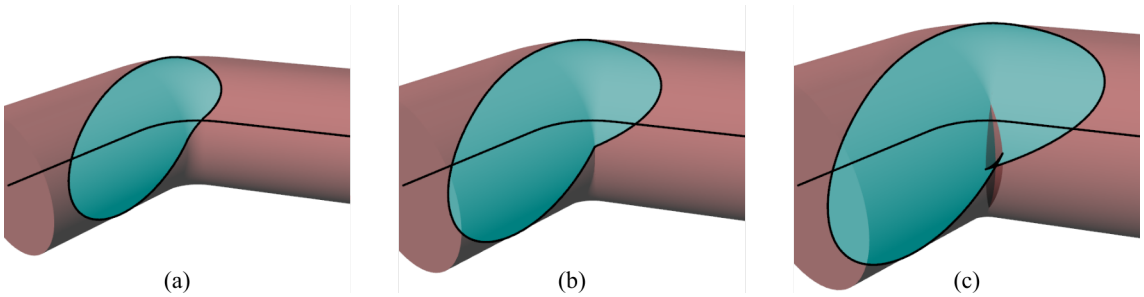

Fig. 6.7 The swept section radius, r, must be less than or equal to the the minimum radius of curvature of the basis curve, as shown in (a) and (b), respectively. Setting r to be greater than the minimum radius of curvature causes the swept global geometry to be ill-formed, containing an closed pocket across which the perimeter of each cross-sectional planform forms a cusp, (c). The condition in (b) sets an upper limit on the swept-section radius for a given curve.

swept section radius, r, exceeds the local zone of geometric compatibility, adjacent slices of the same set may intersect before fully spanning the cross-section, as in Fig. 6.6(d). When this occurs additional treatment of the cross-sectional planforms is required (addressed in the following subsection) to ensure a geometrically compatible set of slices result.

The swept section radius must also be smaller than the minimum radius of curvature of the basis curve, otherwise the swept surface will pivot about an internal point, self-intersecting to form a closed pocket and producing a loop on the boundary of each slice planform, Fig. 6.7. Though this pocket could be removed so that the tube and cross-sections have a cusp, this is inconvenient and it is generally more straightforward to ensure that the surface is initially well-conditioned. Also evident is that the cross-sectional radius must be smaller than half the distance of the closest approach between any two segments of the curve to avoid overlap, *e.g.* the swept section radius of the helix must be lesser than half the pitch between successive loops.

6.2.4 Treatment of cross-sectional planforms

Once the structural architecture and global geometry have been defined, a cross-sectional planform can be excised for each slice plane. However, as for an RS where the sections were strictly semi-infinite, it is often necessary to apply a series of post-processing steps to ensure that the subsequent sliceform is geometrically feasible.

This is best explained by way of example with the synthesis of an elliptical CS illustrated in Figure. 6.8. From the basis curve, (a), the structural architecture, (b), is generated according to the number of slices in each set and their rotation from perpendicular, and the swept section,

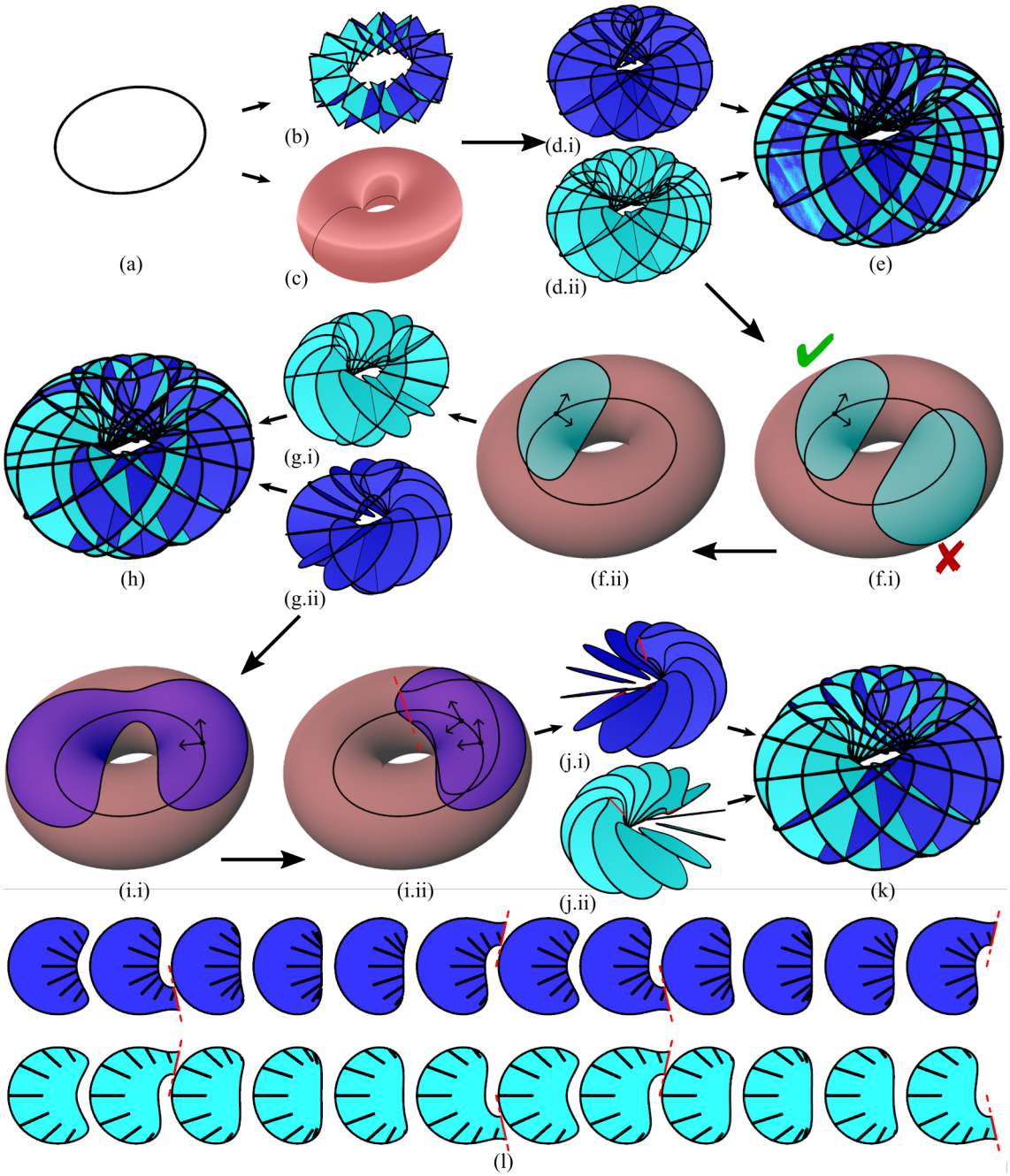

Fig. 6.8 Overview of the basic treatment of the cross-sectional platforms to ensure geometric feasibility. Starting from the basis curve, (a), the structural architecture, (b), and swept volume, (c), are generated as described above. The 'raw' cross-sectional planforms excised for each set, (d.i) &(d.ii), are ill-conditioned forming an infeasible sliceform, (e). This is resolved in two steps: firstly, any cross-sections containing multiple parts are consolidated by removing the extraneous parts, (f)-(g); then the slices are 'clipped' along their lines of self-intersection with their same-set neighbours, (i)-(j). The result is a geometrically feasible sliceform, (k), and set of slice templates, (l).

(c), is defined by the swept section radius. However, the raw cross-sectional planforms appear somewhat chaotic, (d.i & .ii), and are geometrically infeasible as a sliceform, (e), with both sets of slices self-intersecting. To resolve this, the planforms must first be *consolidated* by discarding extraneous portions wherever a cross-section contains multiple parts due to the slice plane re-intersecting the swept volume, (f.i - .ii). The resulting sets of planforms are much improved, (g.i, .ii & h), but some self-intersections within each set remain. These typically occur at regions of high curvature if a slice plane is inclined so that it remains internal as the curve bends away, producing a planform formed by multiple concavely conjoined sections, (i.i). To remove these self-intersections, the offending slices must be *clipped* along their line of intersection with their adjacent neighbour, (i.ii), resulting in two sets of well-behaved planforms, (j.i & .ii), and a well-formed, feasible sliceform, (k).

This secondary clipping action requires particular care in determination of the 'sense' in which the slices should be clipped. Consider that both slices in (i.ii) could be clipped along their line of intersection but it is sufficient to clip only the slice which 'lies onto' its neighbour (when viewed so that the slices rotate away from the viewer). Note that this will occur in opposite senses above and below the basis curve, where the *clip boundaries* - are illustrated in red on the layout of slices, (l). In some instances this may occur for a series of successive slices so that the clipping operation occurs in a staggered fashion with the slices meeting sequentially, as for the example in Figure 6.6(d). Note that where a slice is clipped in both directions, the clip edges are often non-coincident at the midline of the slice and must be joined by a short segment along this midline to complete the perimeter of the slice.

These modifications to each cross-sectional planform (which are fully automated in the Rhino/Grasshopper implementation) are necessary to ensure feasibility of the sliceform but do perhaps detract from the 'purity' of a true sliceform in which each slice represents a full cross-section. Unlike an RS, each clipped planform is not usually completed by the complementary slice of the opposing set. Though retaining the core principle of a sliceform as a three-dimensional structure constructed from an array of interlocking slices, a CS is therefore perhaps more accurately described as a *sliceform derived structure*.

6.2.5 Illustrative examples

Following the steps described in this section, a geometrically feasible CS, and corresponding set of slice templates, can be synthesised from a prescribed basis curve. The *sliceforming* process is completed by the manufacture of the slices from a sheet of thin stock material and assembly in sequential pairs to yield the final physical sliceform.

As discussed in the introduction, assembly of a curve sliceform is non-trivial due to the converging or diverging array of intersection lines upon each slice. However, provided the slices are themselves slightly flexible, the sliceform can be assembled in a sequential manner with the existing assembly of slices carefully manipulated to temporarily prise apart the slices and enable each additional slice to be slotted into place, whereupon the slices return to their unstrained planar condition. Usually it is straightforward to start at one end of the basis curve and add consecutive pairs of slices until the sliceform is complete. If synthesised along a closed curve the open ends are then interlocked to complete the loop.

The complete sliceforming process for a helical and elliptical CS is illustrated in Figures 6.9 & 6.10, with small-scale scale physical models cut from standard 300gsm card using a tabletop, computer-controlled 'Cricut' cutting plotter. Both examples are flat-foldable though some slices of the ellipse must first be disengaged to 'open' the loop. This mobility once again aids construction of the sliceform.

6.3 Parametric design of a CS along complex curves

The methodology for the synthesis of a CS introduced in the preceding section is well-suited to sliceforms along simple basis curves, such as the helix and ellipse presented above. The parametric design space of these structures is spanned by the number of slices in each set, N, the rotation of each set of slices from the perpendicular base planes, $\theta^{\pm}$, and the radius of the swept volume, r; each of which can be independently varied between practical limits to yield a design with well-formed slices and intersections.

However, while the parameters in this basic formulation are sufficient for the helix and ellipse with (relatively) constant curvature, they are usually insufficient for the generation of a well-conditioned design along a curve with large variations in curvature due to competing constraints on each parameter.

To demonstrate this, Figures 6.11 & 6.12 depict the synthesis of a CS along a portion of a logarithmic planar spiral and, its 3-D equivalent, a logarithmic conical spiral, using the basic scheme. In both instances, the regular spacing of the curve points results in dramatically different angular intervals between consecutive slice pairs from one end of the curve to the other, and, as a result, it is not possible to reach sufficient 'resolution' at the inner end without also yielding a highly dense result at the outer end, and vice-versa. Similarly, the swept section radius is necessarily limited by the curvature at the inner end, limiting the connectivity of the sliceform and generating a swept volume that becomes increasingly slender as the curve unwinds.

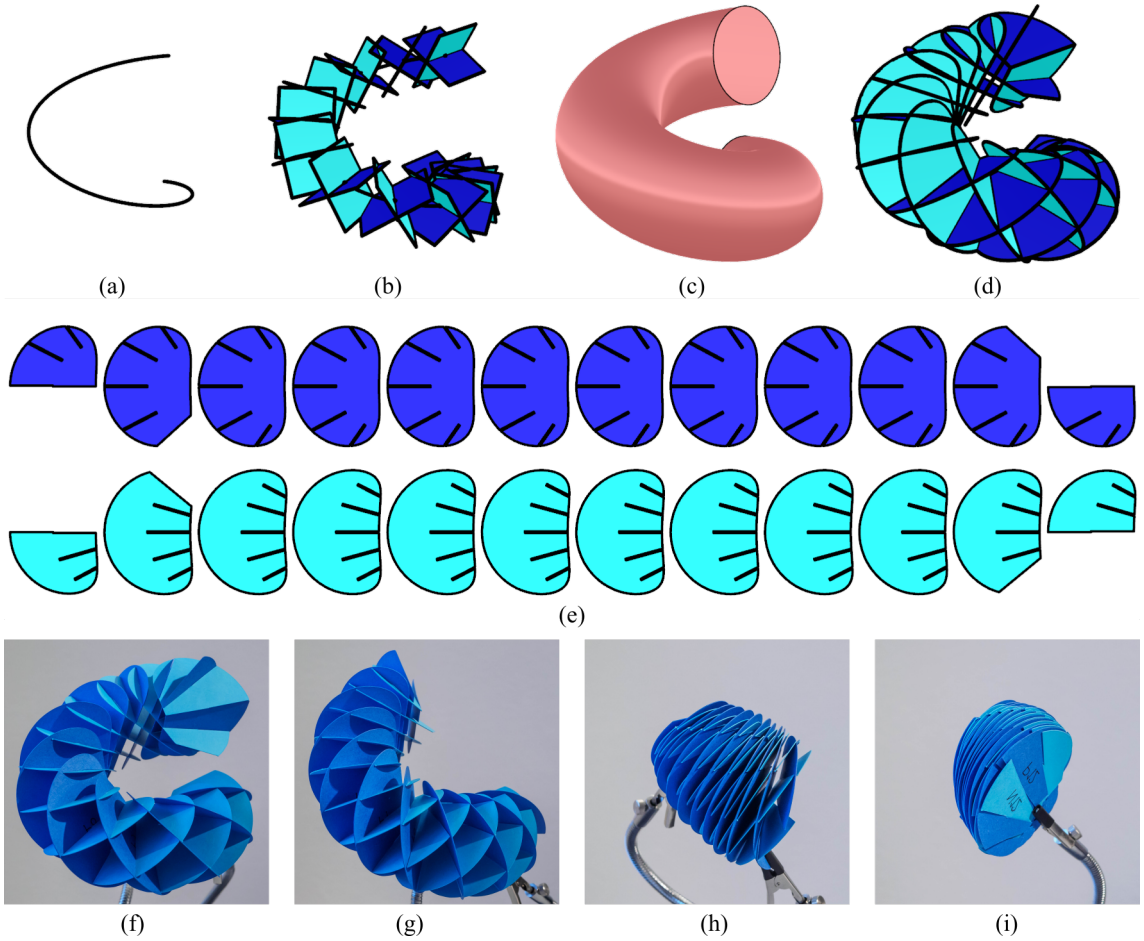

Fig. 6.9 Synthesis of a CS along a helix, (a)-(d), slice templates, (e), and small-scale, one-way-deployable model constructed from card, (f).

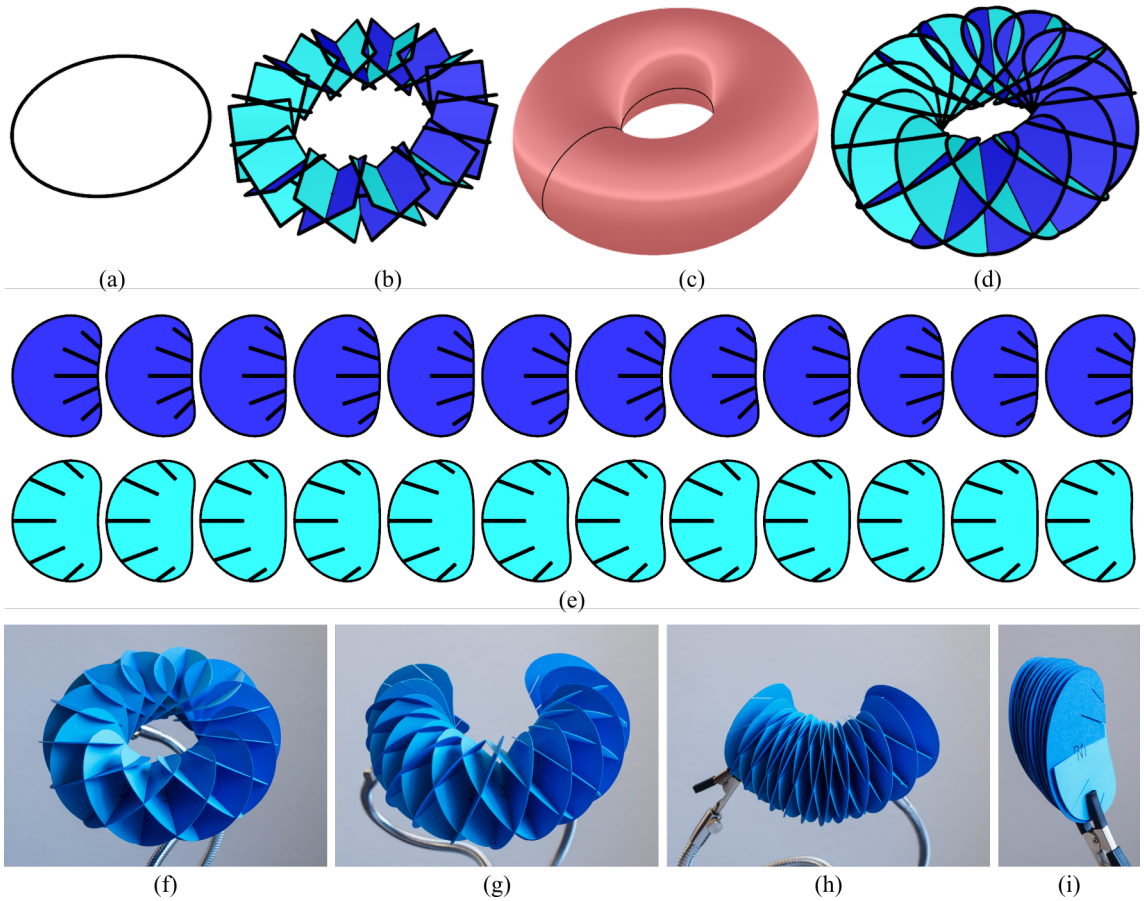

Fig. 6.10 Synthesis of a CS about an ellipse, (a)-(d), slice templates, (e), and small-scale, one-way-deployable model constructed from card, (f).

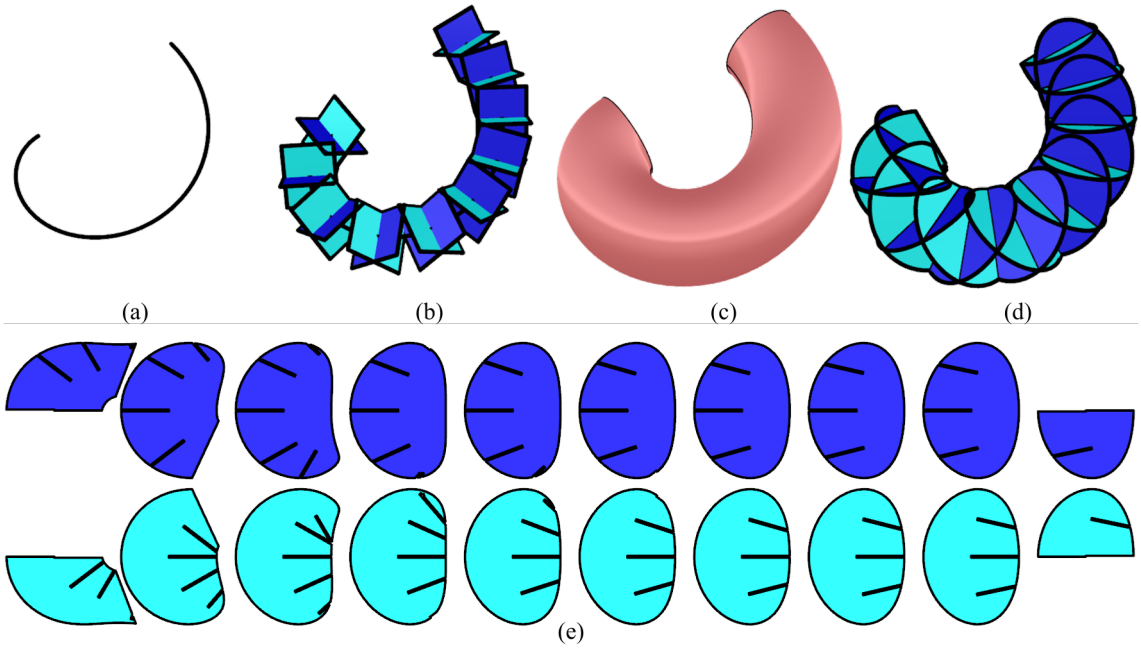

Fig. 6.11 Synthesis of a CS along a portion of a logarithmic spiral using the basic scheme to demonstrate that an ill-conditioned sliceform results. The swept-section radius is limited by the curvature at the inner point on the spiral, which results in low connectivity at the outer end of the curve.

Some modifications to the basic scheme to improve the efficacy of this formulation when synthesising a CS along more complex basis curves are now introduced. Each modification introduces an additional design parameter, adding an extra dimension to the parametric design space but, counter-intuitively, enabling a more responsive generation of the sliceform from the geometry of the basis curve.

6.3.1 Designing for compliant-deployability

Recalling that the ultimate intention is to develop a generalised approach for synthesis of a deployable structure from a basis curve, and anticipating that the mobility of a CS is likely to involve a rigid-compliant mode similar to that exhibited by an RS, modifications to the basic scheme can be informed by the insights from Part I.

In particular, the flat-foldability of an RS is dependent on a symmetric parameterisation, with the range of motion permitted by an asymmetric RS for a given degree of compliant bending of the slices decreasing with increasing parametric asymmetry. It follows that a ‘more symmetric’ CS ought to require less compliance to achieve a given range of motion. However, in the absence of global symmetry, definition of a symmetric parameterisation

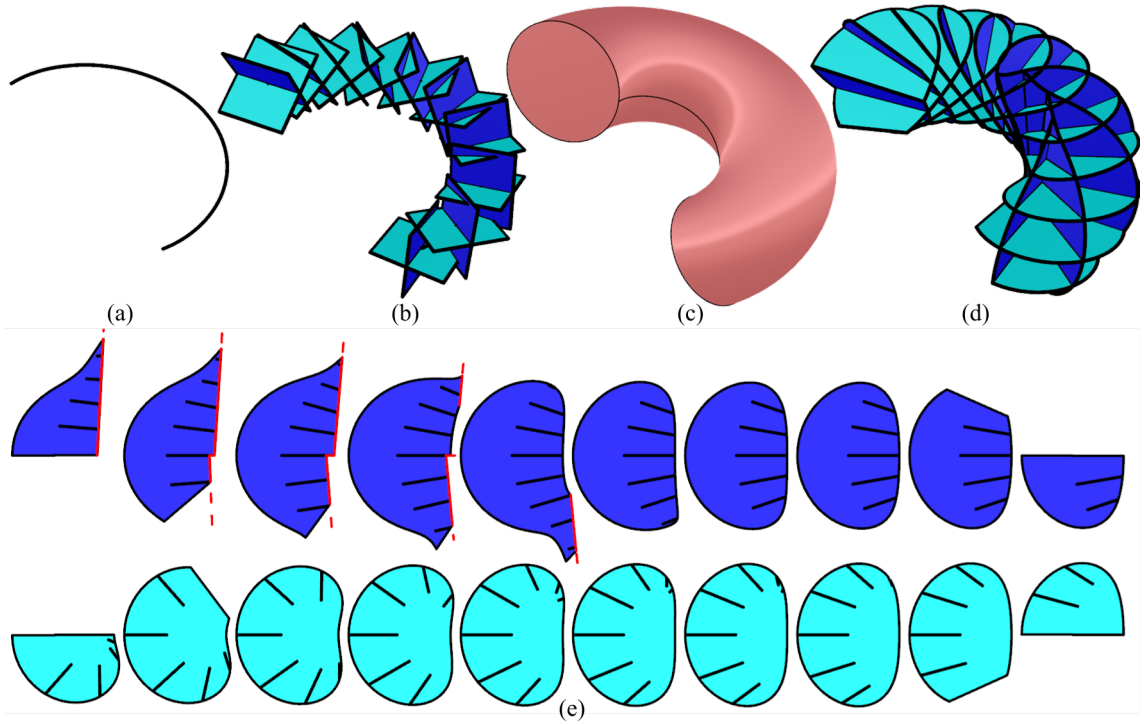

Fig. 6.12 Synthesis of a CS along a portion of a logarithmic conical spiral using the basic scheme to demonstrate that an ill-conditioned sliceform results. The swept-section radius is limited by the curvature at the inner end of the curve, though this is less restrictive than for the planar spiral in Figure 6.11 and the outer section remains well-connected. However, the large angle subtended by adjacent slice planes at the start of the curve results in a series of badly clipped slices.

for a general CS is not forthcoming. Instead,a design in which the structural architecture is *self-similar* along the length of the curve can be pursued. Failing that, a design in which the sliceform is generally 'consistent' along its length (in terms of the geometric arrangement of intersections) is likely to more uniformly distribute any incompatibility during compliant motion and perhaps more readily admit flat-foldability. The modifications introduced in this section are designed with this objective in mind.

6.3.2 Dynamic spacing of curve points

Perhaps the most apparent design parameter to address is the spacing of the curve points and resulting slice planes along the basis curve. For simple curves of constant curvature the constant arc-length resolution produces a regular spatial structure, but for more complex curves this will always be an awkward compromise between what is too dense along straighter segments, and what is too coarse along sections of higher curvature. Instead, it is desirable to vary the spacing of the curve points inversely to the radius of curvature so that the angle subtended by adjacent slice pairs is more uniform. Specifying curve points so that the rotation between successive Frenet-Serret frames is constant is not usually practical for a spatial curve as this requires some approach to balancing rotation and twist between frames and is not well suited to large ranges in curvature. This is improved by implementing a dynamic spacing approach in which curve points are 'attracted' toward tightly curved sections and 'repelled' from straighter segments produces a smooth transition between regions of high and low curvature.

Adjustment of the curve points in accordance with the curvature of the basis curve is realised by numerically integrating the curvature along its length, and plotting a curve of 'total curvature' versus arc-length. Points placed at regular arc-length intervals along this secondary curve are then used to define the location of each curve point along the original basis curve[1]. Where the basis curve has higher curvature, the gradient of the secondary curve is increased and the evenly spaced sample points along this secondary curve have reduced spacing along the arc-length axis and that the spacing between each curve point on the basis curve is correspondingly decreased, and *vice versa*. The result can be tuned by first raising the initial curvature to an *attraction exponent* and then scaling the total result by an *attraction factor*. A range of dynamic curve point spacings are illustrated across the grid of results presented in Figure 6.13.

[1]This method is based on an approach devised by grasshopper forum user Evan Chakroff, https://www.grasshopper3d.com/forum/topics/divide-curve-by-curvature

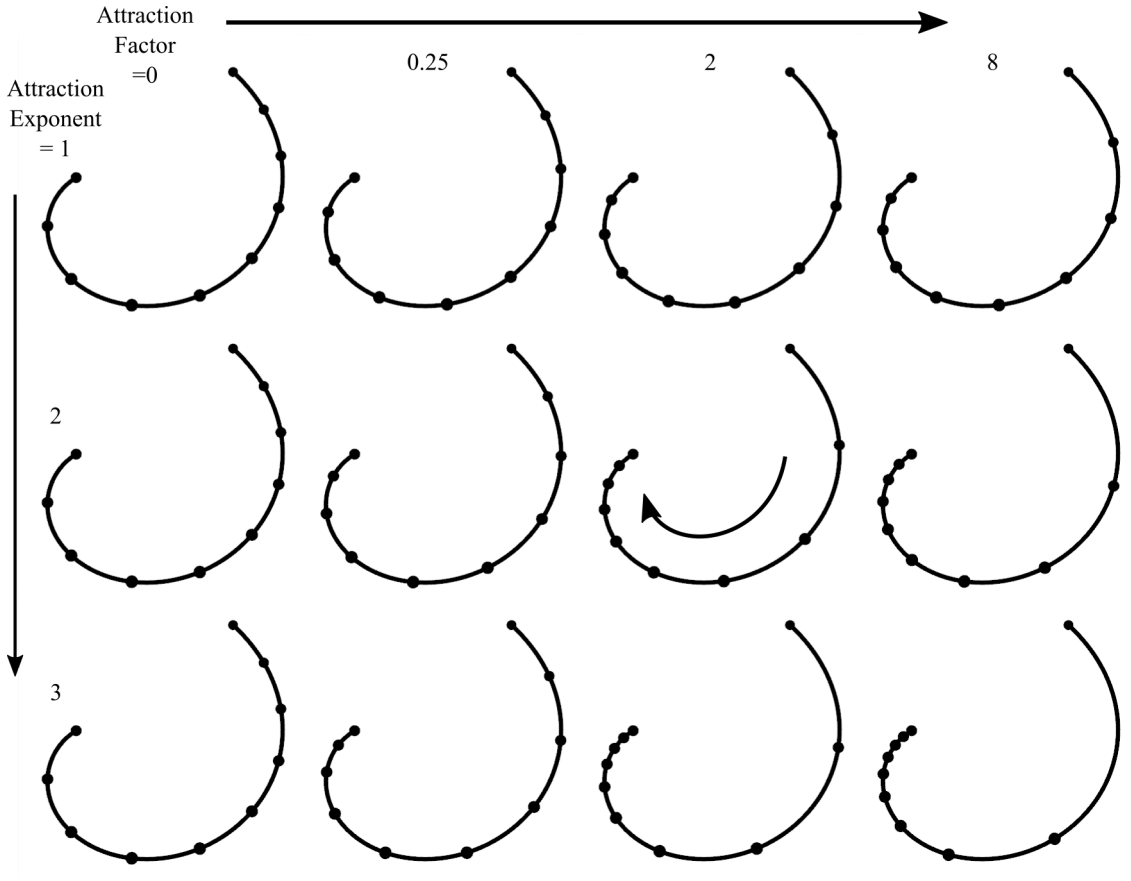

Fig. 6.13 Grid of two-parameter dynamic spacing of curve points along the logarithmic spiral by ‘attraction’ toward regions of higher curvature to provide a more uniform ‘curvature-resolution’. The examples at bottom-right are too extreme to generate a viable sliceform but provide a clear illustration of the effect of each parameter in enabling the designer to specify both the difference in slice spacing between regions of high- and low- curvature and the ‘skew’ of the intermediate transition.

Though somewhat involved, this approach provides a means by which to balance angular and arc-length spacings, ensuring, for example, that straight segments of a polycurve are not simply skipped, and is thus well-suited to a wide variety of basis curves. Selection of an appropriate parameterisation is assisted by plotting the variation in arc length between curve points, the angle subtended between successive base planes, and the variation in angle between successive base planes along the length of the curve, providing the designer with direct visual feedback as to how well balanced the current design is.

6.3.3 Dynamic swept section radius

The second parameter to modify is the radius of the swept-section, r. Typically it is desired to set this radius to ensure sufficiently high connectivity – *i.e.* the number of adjacent slices of the opposing set each slice interlocks with – that the CS forms a robust honeycomb-like array and maintains relatively constant connectivity along the curve. In the basic formulation, a constant radius results in large variations in connectivity, which naturally tends to increase at the regions of higher curvature where the longitudinal dimension of each cross-sectional planform (perpendicular to the normal axis of the curve) is stretched. This is exacerbated by the dynamic spacing of curve points introduced above, which increases the resolution (and connectivity) of slices along tightly curved sections while reducing the resolution (and connectivity) along straighter segments. Furthermore, whilst a larger radius is desirable as it decreases the resolution required to achieve a given connectivity or at-least prevent the tube from becoming disconnected along straighter segments, this is limited by the smallest radius of curvature of the basis curve.

An improved approach is to specify a dynamic swept section radius, r' which varies in concordance with the radius of curvature of the basis curve, $R = \frac{1}{\kappa}$, decreasing where the basis curve is more tightly curved and increasing when it straightens out. In this implementation, an exponential relationship in which $r' \propto R^{\alpha}$ – where the exponent, α, sets the variation in section radius, and the constant of proportionality is calculated so that the average swept section radius per curve length is equal to some target value, r – has been found to provide a suitably flexible and intuitive approach. As illustrated by the examples in Figure 6.14, this enables a significantly more satisfactory design to be generated whilst remaining a direct derivation from the basis curve.

Again, direct feedback is provided by plotting the cross-section radius as a proportion of the radius of curvature along the length of the curve to immediately indicate whether the cross-section radius exceeds the radius of curvature (which is not permitted), and the

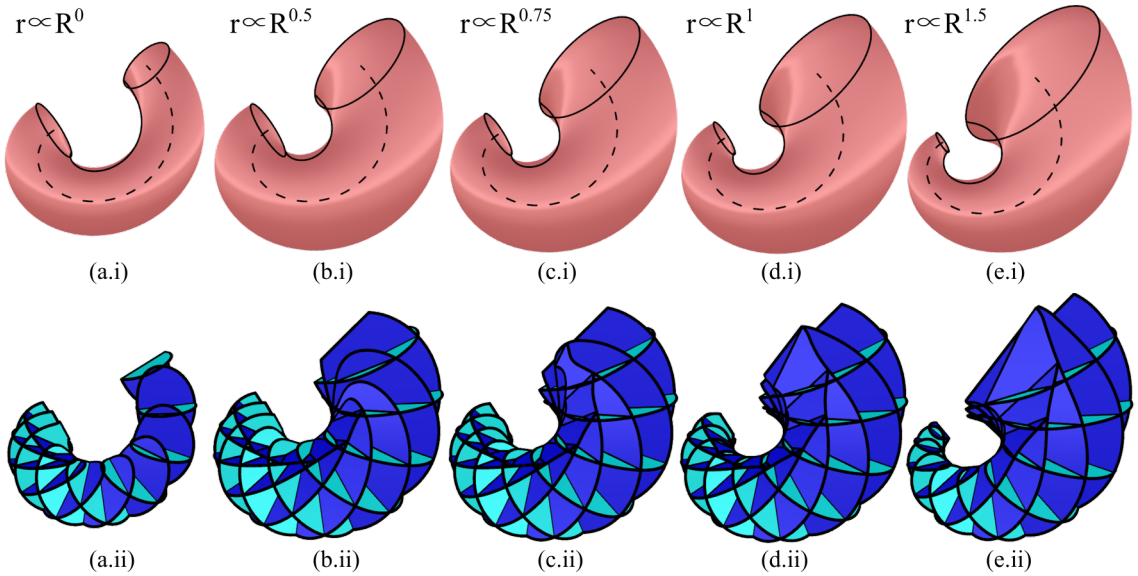

Fig. 6.14 A set of spiral curve sliceforms synthesised with various dynamic variations in swept-section radius set by specifying an exponential relationship between the the dynamic swept-section radius, r', and the radius of curvature, R, as $r' \propto R^{\alpha}$. In (a) the swept-section radius is constant, and thus limited by the minimum radius of curvature. In (b)-(e) an increasing exponent is specified with the constant of proportionality determined such that the average cross-sectional radius, r, is equal across these examples.

variation in its rate of change (difference between successive, evenly spaced sample points) which assists in determining whether the parametrisation is achieving a balanced design.

This modification is well suited to curves whose curvature varies continuously (G^2 continuous) but is not appropriate for piecewise curves which are continuous in tangent but have step-changes in radius of curvature (G^1 continuous). In this latter case a constant swept section radius tends to be satisfactory. Some examples are provided in the following sections.

Furthermore, the choice of a swept-section shape is somewhat arbitrary, with the circular section introduced as merely the simplest neutral shape from which to generate a global volume which echoes the localised structural architecture of a CS and remains within its well-behaved domain – indeed, a CS can be generated by sweeping any polygon along the basis curve, though a concave polygon may cause the planforms to connect in multiple separate places along a single intersection line. However, as the radius of the circle is increased, the limiting condition is met on the inside of the curve when it reaches the radius of curvature. This limits the connectivity that can be achieved. In addition, the lines of self-intersection along which each planform is clipped against its neighbour to ensure geometric compatibility of the slices tend to be broadly perpendicular to the curve – see the slices of the conical

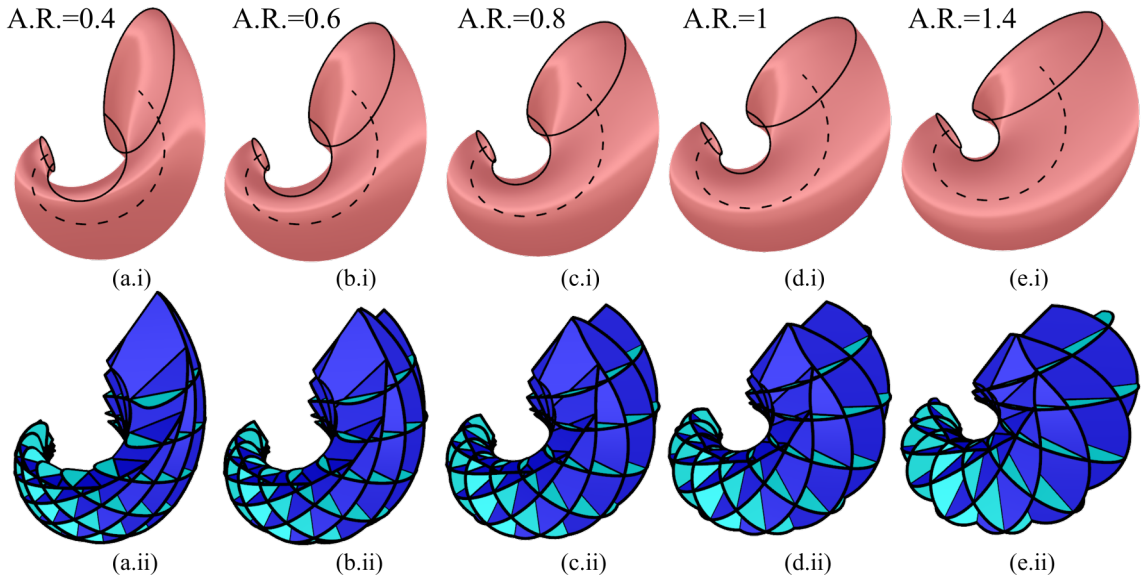

Fig. 6.15 A set of spiral curve sliceforms synthesised with elliptical swept-sections of varying aspect ratio. The total area of each section is equal with the radius of the equivalent circular section varying as $r' \propto R^1$. The array of intersection lines are broadly perpendicular to the curve so a 'taller' cross-section will generally produce a more well-conditioned result, achieving greater connectivity before the slices reach their self-intersection limits.

spiral in Fig. 6.12(d). An open-cellular form is generally desirable, and it follows that the connectivity of the sliceform can be increased without exceeding that limit by stretching the swept section perpendicular to the (broadly parallel) array of intersection lines – *i.e.* in the direction of the local binormal vector – so that it forms an ellipse whose aspect ratio becomes an additional parameter. This preserves the smooth surface of the global volume, and corresponding cross-sectional planforms. A set of examples with various aspect ratios are illustrated for the planar spiral in Figure 6.15.

6.3.4 Connectivity limit: Slice trimming

Anticipating that the mobility of a CS is likely to echo that of an RS with the incompatibility at a given expansion increasing across each additional row of intersections, the compliance required to enable motion is expected to be directly dependent on the connectivity of the sliceform. In some instances it is useful to prescribe a maximum connectivity of the slices, either to guarantee a constant connectivity along the curve in the interest of self-similarity (which is expected to result in a more uniform compliance requirement along the length of the basis curve) even when it is not possible to find a suitable parameterisation to achieve that intrinsically, or to improve the manufacture- and assemble-ability of the resulting sliceform

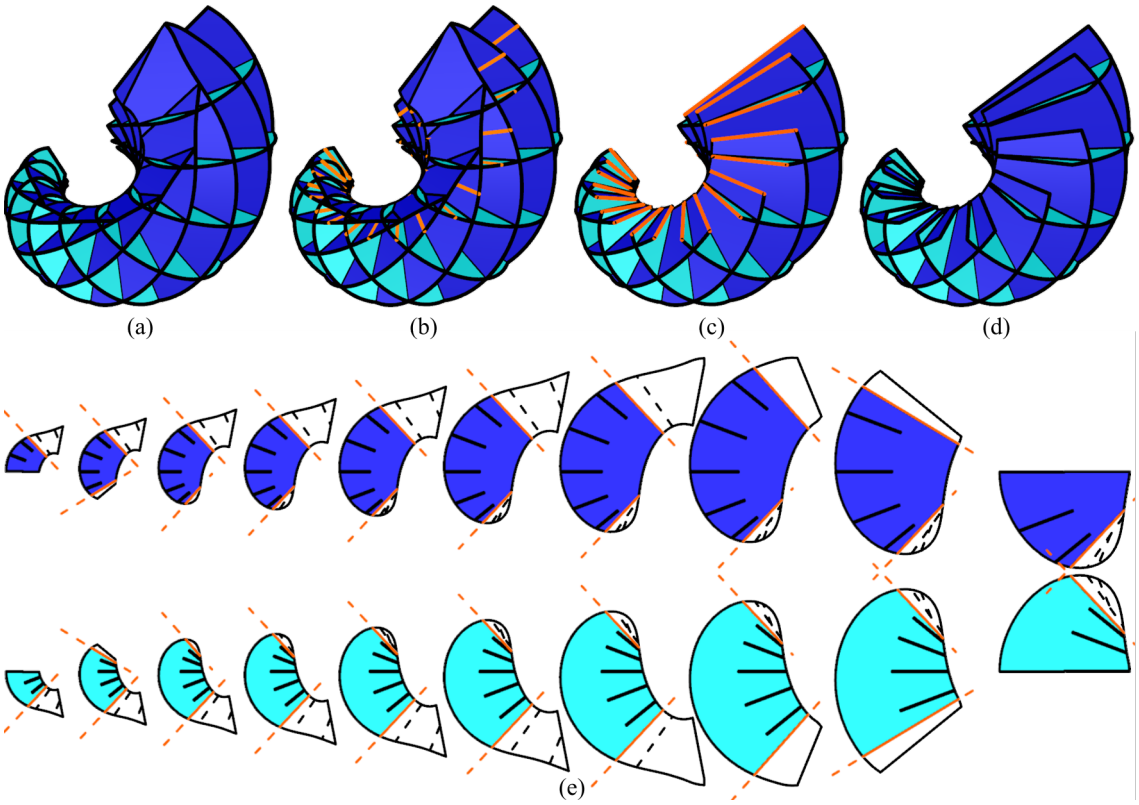

Fig. 6.16 To ensure a constant connectivity and reduce geometric complexity of a given design for improved manufacture- and assemble-ability of the resulting sliceform, but without dramatically decreasing the swept section radius, each slice can be *trimmed* to remove unwanted outer segments. Each *trim line*, shown in orange, bisects the facet outside of the maximum specified intersection line. For consistency, the end slices are trimmed outside of their outermost intersection line to remove the excess overhangs.

by reducing the connectivity without altering the structural architecture or dramatically decreasing the cross-sectional area.

A simple solution is to *trim* each slice outside of the specified intersection, with each *trim line* a secant bisecting the facet outside of the outermost intersection to be kept, Fig. 6.16. Across the CS the effect is akin to having initially swept a truncated circle with upper and lower segments removed.

For slices at the ends of the curve in which the 'next' intersection lines do not exist, the trim lines are generated by rotating the outermost intersection lines 'outward' by a consistent portion of the preceding facet angle – typically half. This removes the excess overhanging surface area.

6.3.5 Interactive design of a CS and aesthetic proxy

In combination, these additional parameters enable a designer to adjust the structural architecture and global geometry and generate a 'balanced' CS from a given basis curve. This multi-parameter design process allows careful fine-tuning of each CS so that the final sliceform is well-conditioned with suitably consistent connectivity along the length of the basis curve and a refined set of consistent cross-sectional slice planforms. In practice, this tends to be relatively intuitive and simply requires that a designer iterate through a few cycles of trial-and-improvement to hone in on a satisfactory parameterisation.

Figures. 6.17 & 6.18 illustrate the synthesis of well-conditioned sliceforms from the logarithmic planar and conical spirals introduced at the start of this section. Small-scale cardstock models are manufactured and assembled for each. These models are readily collapsed-to and deployed-from a flat-folded stack of slices, expanding and contracting smoothly across this range of motion. The 'lock-out' point is not so readily pronounced, and the models can be expanded past the design configuration if force is applied, though they do not flat-fold in an expanded sense.

As described in section 6.3.1, these modifications are introduced with the objective of generating deployable curve sliceforms. The relationships between each of these additional parameters and the mobility of the final structure are yet to be established, so, in the absence of a more objective metric for designing for deployability, the 'aesthetic' approach described here serves as a useful proxy for navigating this design space in this first instance. In particular these modifications enable sensible designs to be generated from a much wider set of basis curves than the basic approach permits, with the examples presented in this thesis representing a first attempt to generate deployable structures of this type. Each of the modifications is completely automated within the Rhino/Grasshopper implementation developed alongside this investigation, which is also sufficiently robust to generate a design even if an ill-conditioned set of parameters are initially selected, thereby enabling the designer to generate a start point from which to interactively adjust the parameterisation until a suitably well-conditioned design is found.

6.4 Algorithmic design of a CS: Details and implementation

The previous sections introduced the basic principle of a CS as a generalisation of an RS and developed an approach to generating well-conditioned sliceform from a set of sample basis

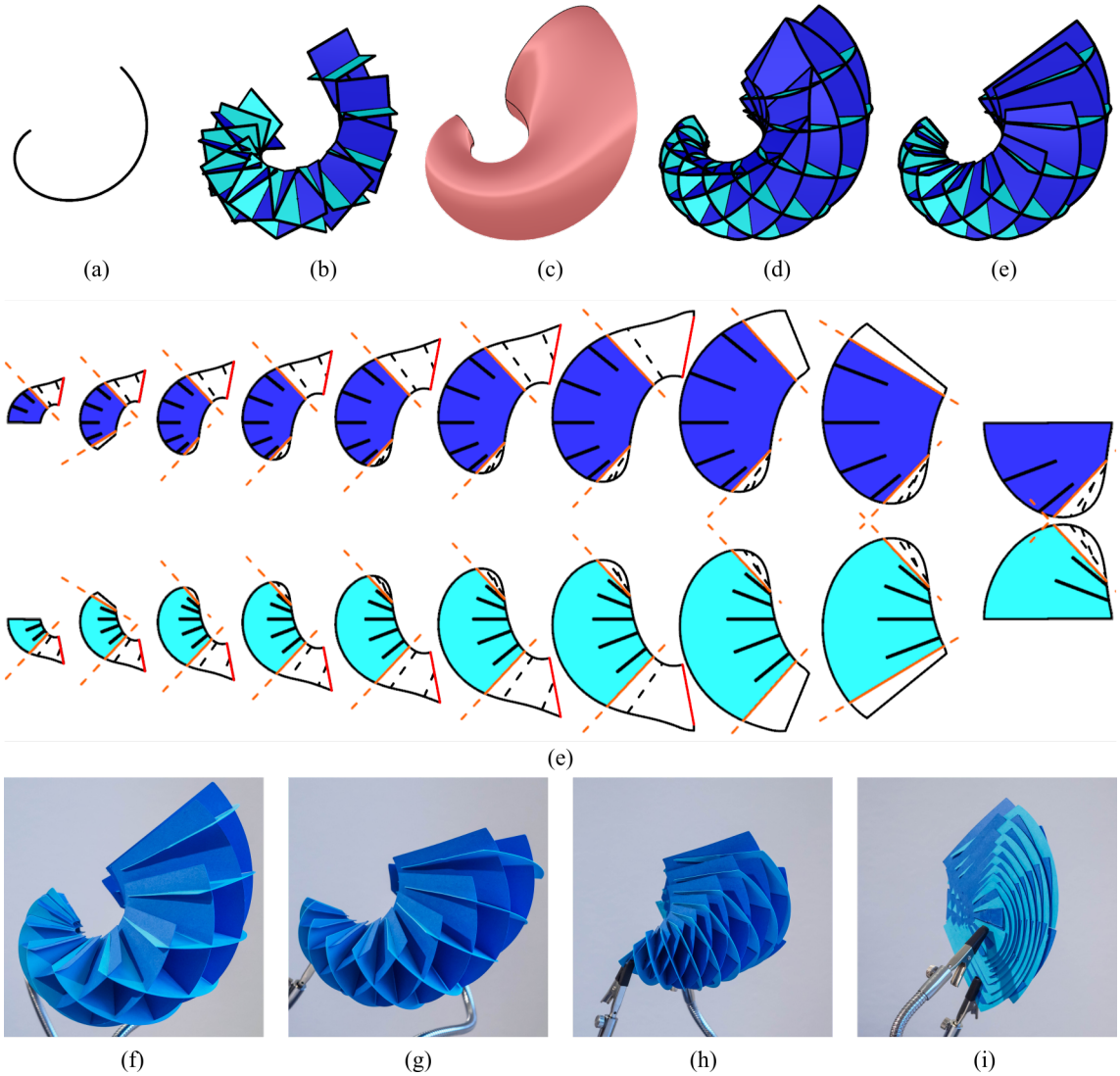

Fig. 6.17 Synthesis of a CS along a spiral with a 'balanced' design, and articulation of the assembled sliceform which is flat-foldable.

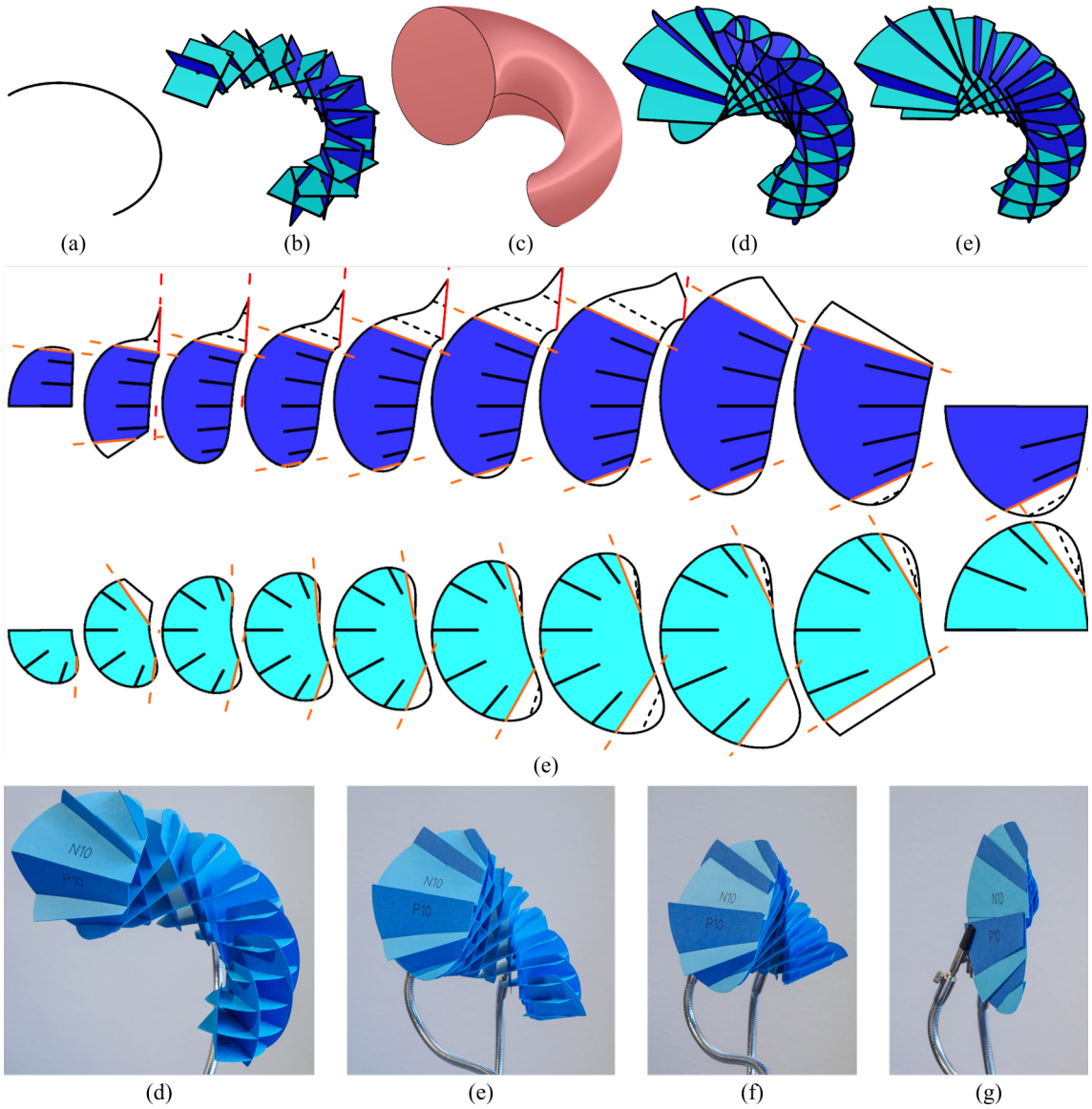

Fig. 6.18 Synthesis of a CS along a conical spiral with a 'balanced' design, and articulation of the assembled sliceform which is flat-foldable.

curves. Though this methodology is intuitive and generally robust, there are several technical design details and challenges that must be addressed in practice. These are now discussed.

6.4.1 Implementation of CS design

The inherently parametric synthesis of a CS is well-suited to implementation in the Grasshopper parametric design environment for the Rhinoceros 3D modelling suite [55, 71]. In this software, the design process is constructed as a live algorithm acting on the supplied basis curve so that each design can be interactively optimised by adjusting the design parameters.

A more detailed description of the algorithm for generating a CS is provided in Appendix B but the four main stages are now outlined briefly.

Stage 1: Construction of the fundamental geometry

This first stage concerns the definition of the basis curve (by the designer) and then the generation of the parameterised structural architecture and swept volume in parallel, thus forming the *fundamental geometry* of the CS.

Stage 2: Generation of the basic sliceform

Once the fundamental geometry of the SA has been generated, the basic sliceform is constructed by first excising each 'raw' cross-sectional planform, consolidating each slice by discarding unwanted secondary sections and clipping those that remain along any same-set–intersections (self-intersections).

Stage 3: Slice trimming

The third stage concerns the conditioning of the sliceform through the trimming of each slice (if prescribed). This requires careful definition of the geometry of each intersection line.

Stage 4: Preparation for manufacture

Once the final planforms have been generated, they are converted to slice templates by generating a set of geometrically compatible slots along each intersection line, then tiled or nested onto a sheet for manufacture.

6.4.2 Ensuring robustness: Degenerate and special Cases

The synthesis of a CS from each basis curve is dependent on the formulation of the set of Frenet-Serret frames, both for construction of the structural architecture and generation of the swept global geometry. Given a well-behaved curve, this is generally robust and readily implemented within Grasshopper. In this context, a well-behaved curve is one that does not self-intersect and is $\mathbf{G}^2$ continuous (*i.e.* the curvature varies continuously) or a $\mathbf{G}^1$ continuous (*i.e.* the tangent vector varies continuously, curvature is discontinuous) piecewise curve constructed from $\mathbf{G}^2$ continuous segments which are co-planar at their joins.

However, there are four cases of curves that do not meet the latter criteria and whose Frenet-Serret frames are ill-defined, but for which the CS nonetheless follows intuitively and can be synthesised as special cases by careful generation of a set of appropriate *pseudo-frames*, with pseudo normal vector $\mathbf{N}^*$ and pseudo binormal vector $\mathbf{B}^*$. Note that a complete set of curve frames is required for the generation of both the swept surface and the slice planes.

Degenerate case of a CS along a line: an LS

Perhaps the most obvious special case is a CS generated along a straight line. In this instance the lack of curvature means that the Frenet-Serret frames are ill-defined with only the local normal vectors well-defined. This is trivial to resolve by selection of an arbitrary perpendicular direction to which the normal axes can be aligned and a set of consistent N-B frames generated, Fig. 6.19.

The structural architecture of this design consists of two sets of parallel planes: a CS along a line collapses to an LS. Alternatively, this can be considered to be the degenerate case of a CS generated about a circle (an RS) of infinite radius.

Transition from straight to curved segments: 'Kink'

A similar issue occurs when generating a sliceform along a 'kink' consisting of two mis-aligned, straight segments joined by a rounded corner of arbitrary curvature, Fig. 6.20. The Frenet-Serret frames are, again, ill-defined along the straight legs but in this case they must be consistent with the well-defined frames along the central curve. synthesis proceeds by extrapolating the alignment of those at either end of the curved central segment.

That this example is collapsible is significant because it implies that a collapsible CS could be generated according to any planar polyline with rounded corners.

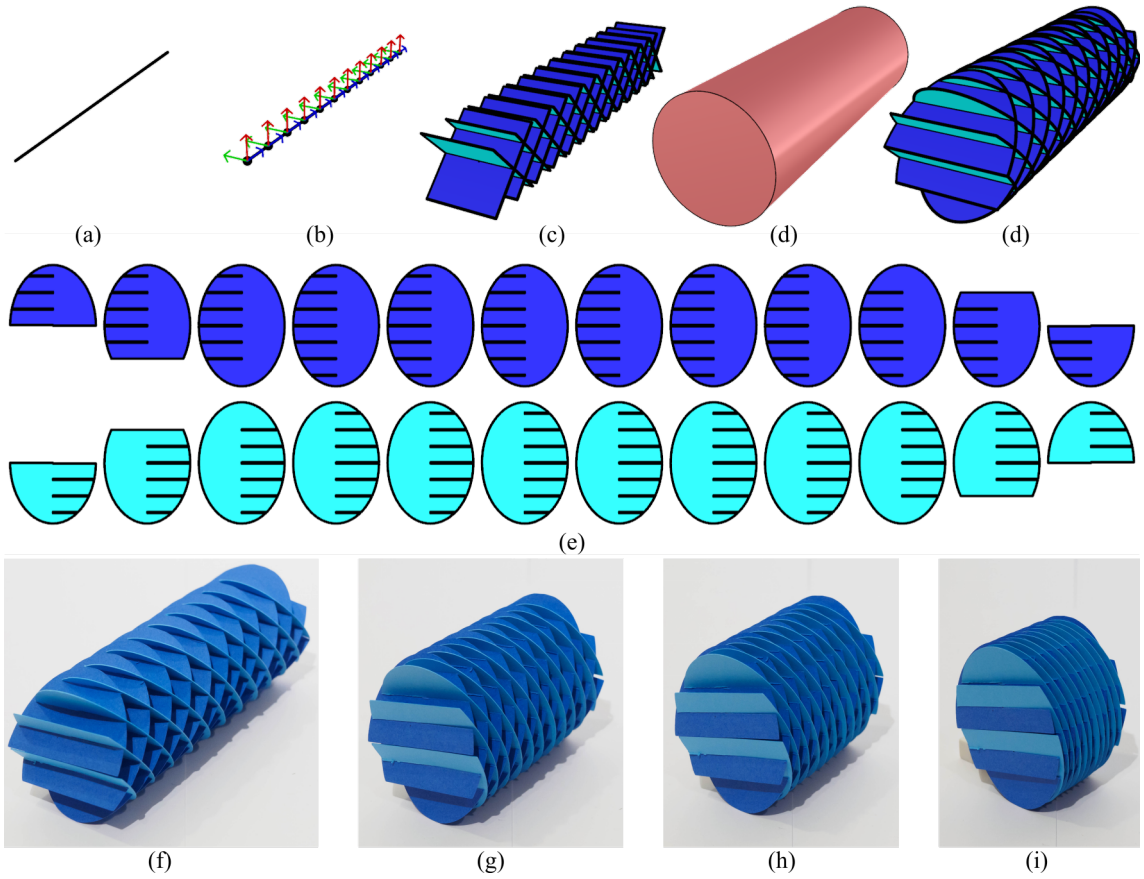

Fig. 6.19 Synthesis of a CS along a line. The curvature is zero at each curve point and the Frenet-Serret frames are not defined. This is resolved by specifying an arbitrary perpendicular direction to which each 'normal' vector is aligned with each 'binormal' vector generated by vector product to generate a set of consistently oriented *pseudo*-frames, enabling generation of the structural architecture and swept global volume as usual. The final result is an LS which is bi-directionally flat-foldable.

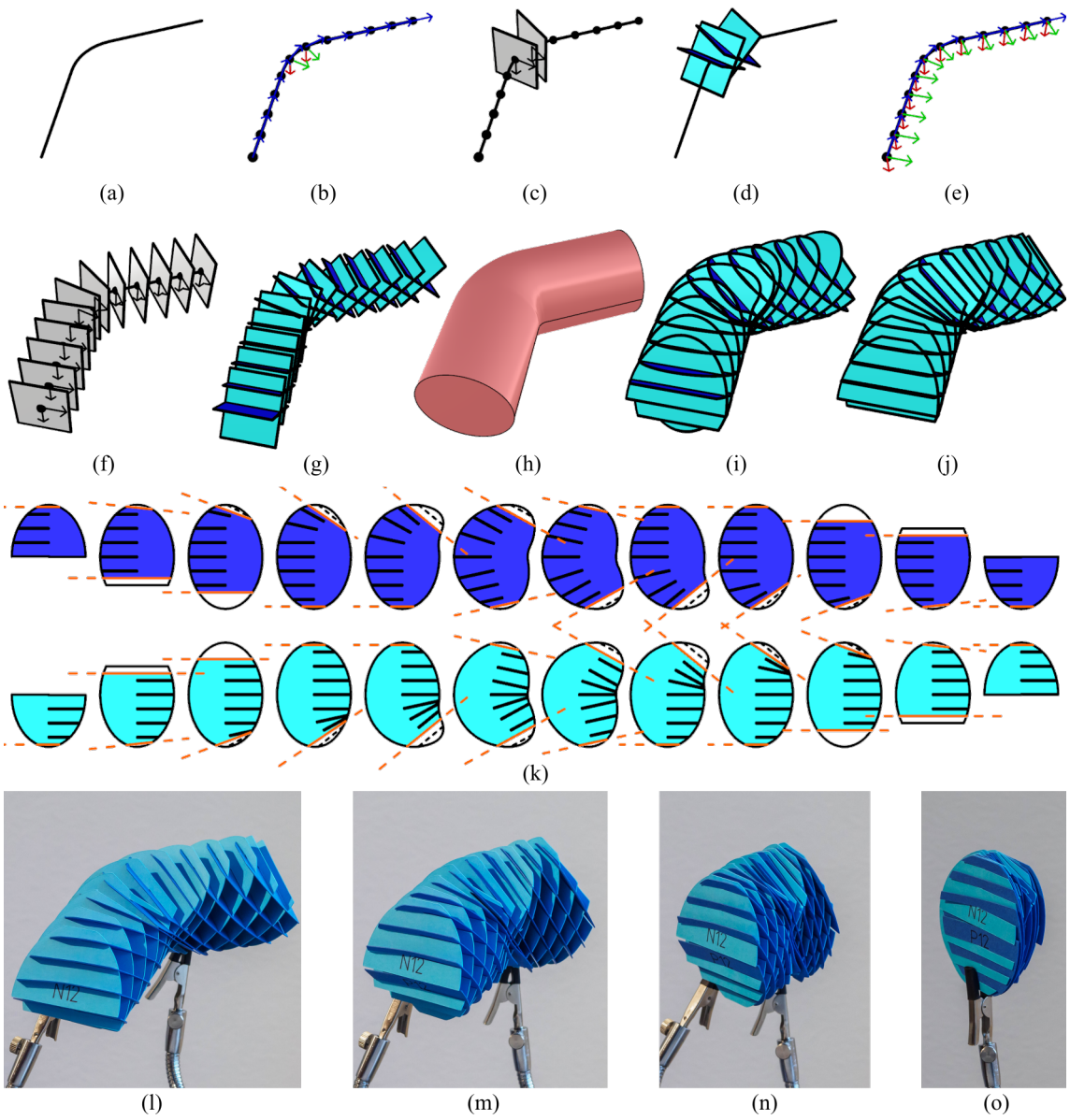

Fig. 6.20 Synthesis of a CS along a planar 'kink' comprising two straight legs joined by a circular arc. The Frenet-Serret frames are not defined along the straight legs but a well-formed result is achieved by generating a set of pseudo-frames whose normal vectors are coplanar to the curvature of the central curved portion.

Planar curvature reversal: 'S-curve'

A more subtle difficulty arises when synthesising a CS along a planar curve which reverses in sense, such as an 'S'-curve, Fig. 6.21. The Frenet-Serret frame is well defined at along the two arcs, (b), but a problem arises due to the instantaneous inversion of the curvature at the point of inflection. Though it initially appears that perpendicular base planes can be generated as usual, (d), when rotated about each local normal to generate the two sets of slice planes their inclination is inconsistent, as if the two sets are switched at the midpoint, (e). This occurs due to the instantaneous reversal of the curvature vector, and corresponding rotation vector, and is resolved by inverting the Frenet-Serret frames along the second arc before proceeding to generate the swept surface, base planes and slice planes as usual, (f)-(h). These modified curve frames are considered to be *sided* as the pseudo-normal vectors now point to a consistent 'side' of the curve.

This resolution can be generalised for a planar curve, including the line and kink presented above, with the sided frames oriented so that the pseudo-binormal vectors are aligned to the 'upward' normal of the global plane.

Straight line with intrinsic twist

A complementary scenario to the kinked curve is obtained when two non-coplanar curved segments are joined by a straight line, Fig. 6.22. In this instance the curve planes are well defined along both of the curved segments but not along the central line. Since the frames at either end of the line are misaligned each intermediate frame must be oriented by interpolation to produce a smooth transition.

Whilst the frames of a CS follow the spatial twist of the basis curve as a rule, in this scenario the CS has no spatial twist, but pure intrinsic twist. Note also that the incomplete set of sided frames should first be generated from the incomplete set of well-defined frames, before interpolating the intermediate frames to minimise the interpolated twist, which can always be less than 90°.

6.4.3 Manufacture of slices and assembly of sliceform

Once the final slice templates have been generated, slices can be manufactured from stock material and assembled to construct the sliceform.

Each slice of a CS is usually unique and they often vary significantly in dimension, so a simple grid layout is not usually an efficient use of material. A more efficient approach is to

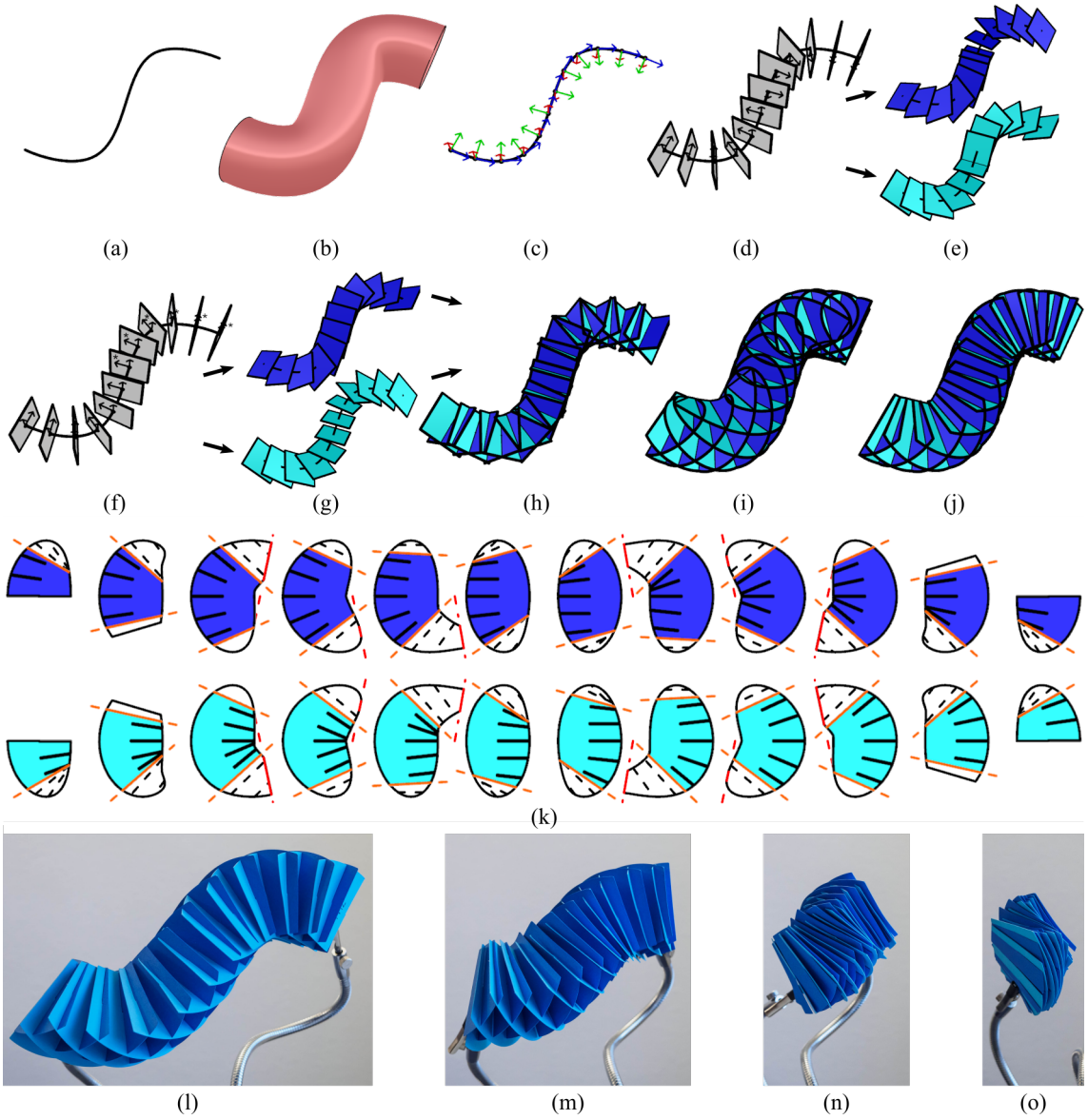

Fig. 6.21 Synthesis of a CS along an 'S'-curve, (a). Though the swept surface, (b), Frenet-Serret curve frames, (c), and base planes, (c), are well-defined, the reversal of curvature-sense causes problems when each set of slices is generated by rotation about the local normal axis, (e). This is resolved by first re-orienting the base planes following the inflection point to form a consistent set of 'sided' planes, (f), from which two sets of slices, (g). Using this rectified structural architecture, (h), the cross-sectional slice planforms are excised as usual, (i), and and trimmed for a uniform connectivity along the curve, (j). The slice templates for this design are shown in (k). The assembled sliceform is flat-foldable, (l)-(o), demonstrating that a reversal in curvature does not impede deployability.

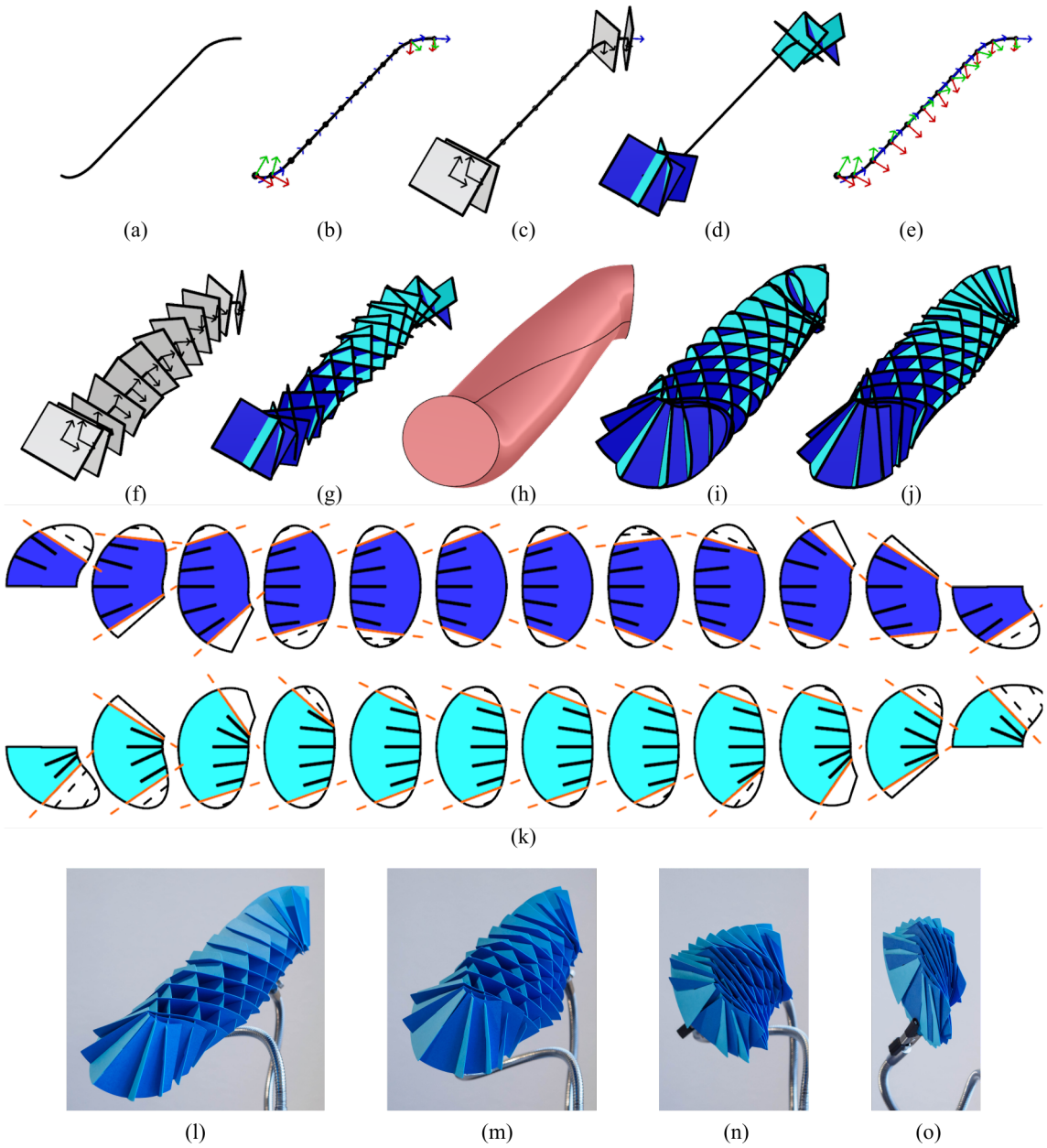

Fig. 6.22 Synthesis of a CS along a 'twisted line' comprising a straight line joining a pair of non-coplanar curved segments, (a). The Frenet-Serret frames and base planes are well-defined at each curved end but un-defined along the straight section, (b). Generating the perpendicular base planes, (c), and subsequent slice planes, (d), along the curved ends, it is intuitively apparent that the intermediate frames can be interpolated to form a smooth transition between the two ends and thus form a segment with intrinsic twist, (f)-(h). Slices are excised as usual, (i), and trimmed to set their maximum connectivity, (j) & (k). Note that the slices of each set are identical in the twisted portion. The assembled sliceform is flat-foldable, (l)-(o), demonstrating that an intrinsic twist does not impede deployability.

employ a 'nesting' software – such as the OpenNest plug-in for Grasshopper[2] – to generate suitable layouts.

Once a suitable layout of slices has been prepared, they are cut from stock material and assembled in successive pairs until the CS is completed. The foldability of each design once-again aids assembly.

It is worth noting that each set of slices can be assembled in two mirror-image configurations and care must be taken to ensure that the first few slices are assembled in the desired orientation, if this is of importance.

6.5 Summary

In this chapter curve sliceforms (CS) has been introduced as a generalisation of the deployable rotational sliceforms investigated in Part I. The definition of their structural architecture has been formalised and a robust methodology for the synthesis of a neutral CS inscribing a swept global volume generated directly from the prescribed basis curve has been developed.

This basic formulation is well-suited to simple curves of (relatively) constant curvature but often produces an ill-conditioned result when a more complex basis curves with greater variation in curvature is supplied. The basic approach has been extended by development of several additional parameterisations, enabling responsive generation of a balanced design in which the sliceform is self-similar along the length of the curve.

This method can be applied to generate a deployable sliceform from any basis curve which is $\mathbf{G}^2$ continuous and also any piecewise curve consisting of $\mathbf{G}^2$ continuous segments which are $\mathbf{G}^1$ continuous and coplanar at their join. The structural architecture of a CS is ill-defined when the basis curve is straight or contains a reversal of curvature, though this is readily rectified by interpolating or inverting curve frames where necessary.

All of the curve sliceforms generated in this chapter exhibit a similar deployable characteristic to an RS and can be collapsed to a flat-folded stack of parallel slices.

[2] Vestartas, P. (2019). Opennest v1.2. *food4rhino.com*, https://www.food4rhino.com/app/opennest

Chapter 7

Structural geometry of a curve sliceform

7.1 Introduction

The curve sliceforms introduced in Chapter 6 are a novel class of deployable structure synthesised by generating a sliceform along a prescribed basis curve. Developed as a generalisation of the rotational sliceforms introduced in part I, a CS exhibits a characteristically similar deployable motion with the interlocking slices rotating about each intersection to enable expansion and contraction via a global shearing motion. Before investigations of this kinematic action can proceed, the *structural geometry* of a CS in the static design configuration must first be described.

The *structural geometry* captures the spatial arrangement of the intersection lines and the facets spanned between each adjacent pair, independent of the particular global volume of the CS, which informs the shape of each cross-sectional planform, though both are inherently localised. Thus a pair of CSs along identical basis curves with identical structural architectures but different swept section radii embed the same structural geometry though the resulting sets of slice templates will be different.

Like an RS, the pantograph-like array of interlocking planar slices of a CS form a honeycomb-like array of open-faced cells; unlike an RS the spatial arrangement of slices of a general CS possesses no global symmetry. The geometric arrangement of slices and intersections must therefore be captured in a generalised form.

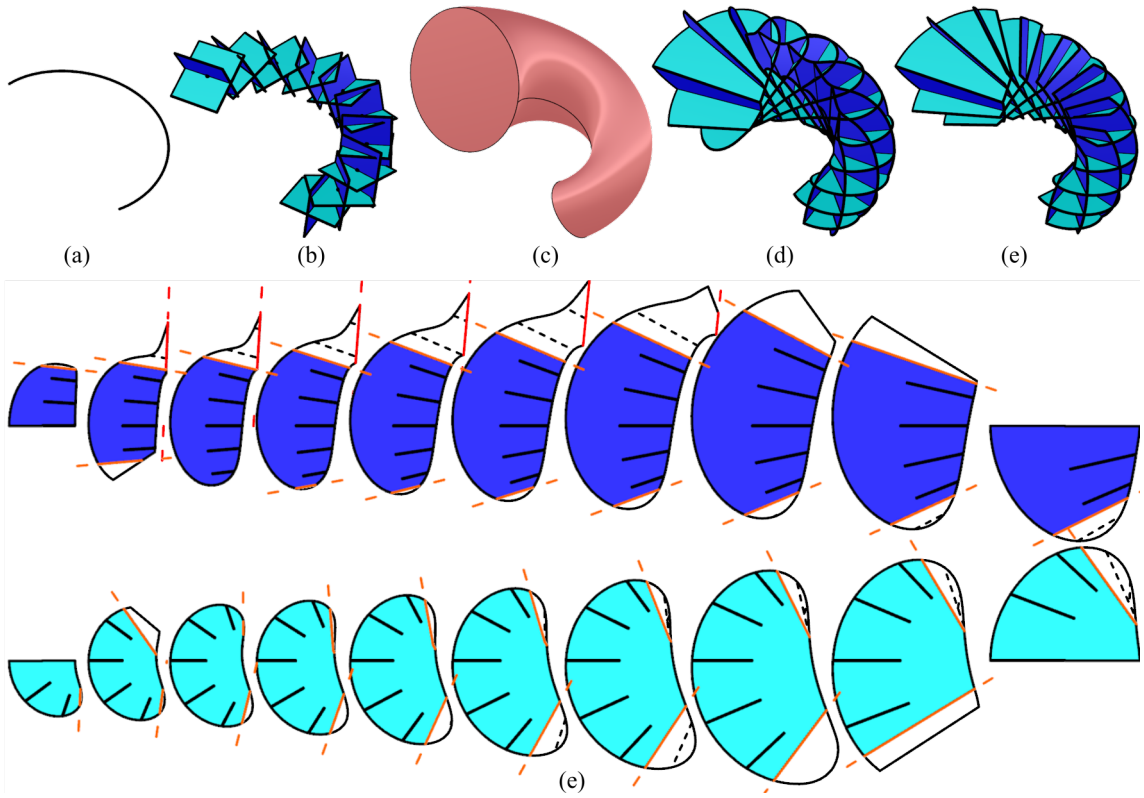

Fig. 7.1 Synthesis of a CS along a conical spiral with a 'balanced' design. Repeated from Fig. 6.18. This sliceform is the basic example used to illustrate the various descriptions of the structural geometry of a CS formulated in this chapter.

7.1.1 Chapter outline

In this chapter the structural geometry of a CS in the expanded *design configuration* is examined, establishing several approaches to describing and generating their geometry to inform our investigation of the kinematic properties of these structures in the next chapter.

Unless otherwise stated, each approach is illustrated by examining the structural geometry of the 'balanced' conical spiral CS synthesised in the previous chapter – reproduced here in Fig. 7.1 – whose basis curve has out-of-plane, continuously variable curvature.

7.2 Structural geometry of a CS as an array of intersecting planes

The *generative* structural architecture of a CS – as opposed to the *deterministic* architecture of an RS – precludes the formulation of a description of the structural geometry directly from

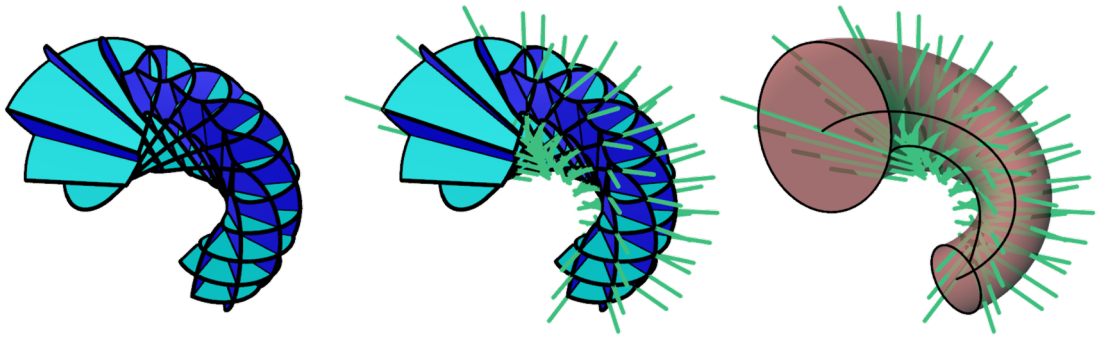

(a) (b) (c)

Fig. 7.2 Locally, a CS comprises a two-dimensional array of slices, (a), forming a two-dimensional grid of intersection lines, (b). Adjacent intersection lines are similarly oriented, their intersection points lying on the inside of the curve from which they diverge forming a local volume within which to construct a geometrically feasible sliceform, as is achieved by the swept volume designs generated in the previous chapter, (c).

the parametrisation. Instead, a general approach that can be applied to any given basis curve geometry must be formulated.

By prescription of an appropriate basis curve, the slice planes (and their lines of intersection) can be oriented freely in space, apparently violating the basic principle for geometric feasibility of a sliceform in which adjacent intersection lines must not themselves intersect. However, because successive slices of each set are similarly oriented, adjacent intersection lines are likewise similarly aligned, and the array is broadly aligned to the local radius of curvature. The CS is thus locally geometric compatible. Furthermore, self-intersections between slices of the same set are explicitly prevented by the clipping of any planforms that would otherwise meet within the localised global volume, ensuring that a two-dimensional array of intersection lines is formed, Fig.7.2.

7.2.1 A vector description of the structural geometry

Perhaps the most straightforward description of this structural geometry is attained from the vector description of the structural architecture.

For a general basis curve, the structural architecture can be described by an array of points and normal vectors corresponding to each slice plane. Addressing each curve point as P_i, where $0 < i \leq N$, the local Frenet-Serret frame is spanned by (unit) vectors $\hat{\mathbf{T}}_i$, $\hat{\mathbf{N}}_i$ and $\hat{\mathbf{B}}_i$, generated as outlined in section 6.2, Fig. 7.3(a).

From these *curve frames*, the set of 'sided' *slice frames* are generated by inverting the the normal and binormal vectors where necessary (across any inversions in curvature) and

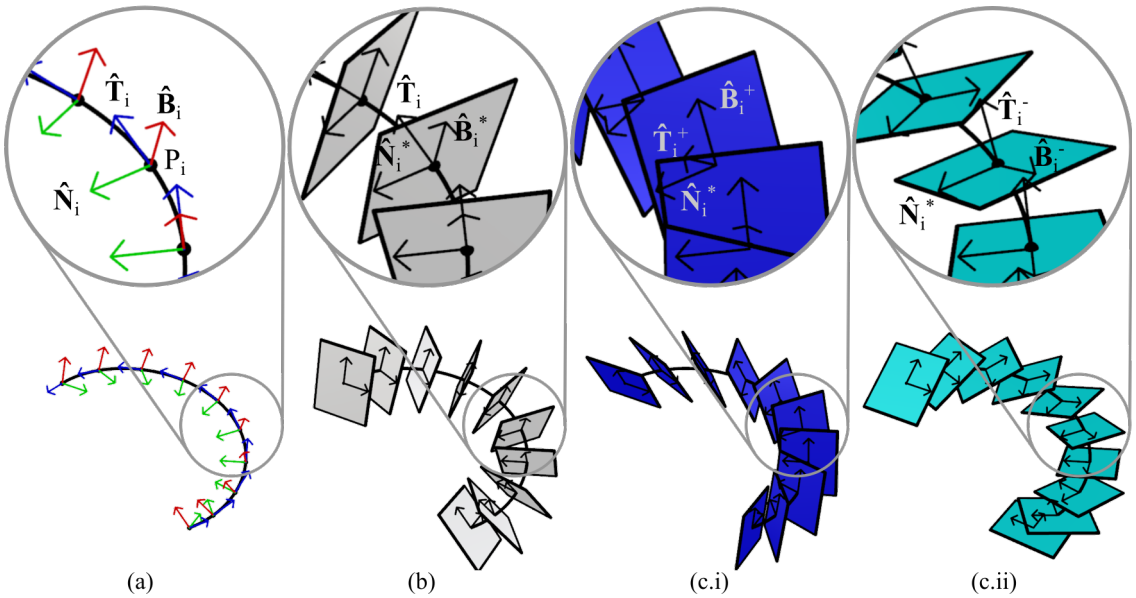

Fig. 7.3 The RS structural architecture is generated as in Figure. 6.3. The Frenet-Serret *curve frame* ($\hat{\mathbf{N}}_i$-$\hat{\mathbf{B}}_i$-$\hat{\mathbf{T}}_i$) generated at each curve point, P_i, (a). These are the basis for the set of 'sided' *slice frames*, ($\hat{\mathbf{N}}_i^*$-$\hat{\mathbf{B}}_i^*$-$\hat{\mathbf{T}}_i$) – where the * denotes that they have been reversed where necessary to accommodate inversions of curvature – and corresponding set of perpendicular *base planes* ($\hat{\mathbf{N}}_i^* - \hat{\mathbf{B}}_i^*$), (b). The two sets of rotated slice planes are spanned by vectors $\hat{\mathbf{N}}_i^* - \hat{\mathbf{B}}_i'$, with unit normals, $\hat{\mathbf{T}}_i^{\pm}$, (c).

interpolating suitable pseudo-frames where the Frenet-Serret frame is ill-defined (when the basis curve is straight). The set of base planes, Fig. 7.3(b), span the refined normal and binormal vectors, denoted by an asterisk, $\hat{\mathbf{N}}_i^* - \hat{\mathbf{B}}_i^*$, where $\mathbf{N}^* = \mathbf{N}$ when the frame is unchanged and $\mathbf{N}^* = -\mathbf{N}$) when inverted. The normal to each base plane is simply the curve tangent, $\hat{\mathbf{T}}_i$, which is unmodified by these adjustments.

Each pair of slice planes, $S_i^{\pm}$, are spanned by vectors $\hat{\mathbf{N}}_i^* - \hat{\mathbf{B}}_i'$ where $\hat{\mathbf{B}}_i'$ is the curve frame binormal rotated about the local normal axis in the appropriate sense ($\hat{\mathbf{B}}_i^{*+}$ or $\hat{\mathbf{B}}_i^{*-}$), Fig. 7.3(c.i)&(c.ii). Likewise, the slice normal, $\hat{\mathbf{T}}_i' = \hat{\mathbf{T}}_i^{\pm}$, is generated by the same rotation of the curve tangent. Note, again, that the sense of each set of slices is opposite to that used in describing an RS.

This schematic description is provided for completeness and further detail regarding the formulation of these vectors for a particular CS is not provided in this dissertation, though the application of successive rotations could be achieved via, *for example*, quaternions.

7.2.2 Vector description of the array of intersections

The two sets of slices form a two-dimensional array of intersection lines where $I_{i,j}$ ($0 < i, j \leq N$) is the intersection between the i-th slice of the positive set, S_i^+, and the j-th slice of the negative set, S_j^-.

In the vector formulation, each line of intersection is oriented by an *aligned vector*, $\hat{\mathbf{I}}_{i,j}$, and located by a suitable *intersection point*, $\mathbf{p}_{i,j}$, lying at an arbitrary position on the line of intersection, Fig. 7.4(a). Note that these indices will be cyclical for closed curves.

Each intersection vector is readily generated from the set of *curve-point–normal-vector* pairs describing the array of slice planes – $S_i^{\pm}\left(P_i, \hat{\mathbf{T}}_i'^{\pm}\right)$ as introduced above – by taking the vector-product of the normals to the intersecting planes,

$$\hat{\mathbf{I}}_{i,j} = \hat{\mathbf{T}}_i^+ \times \hat{\mathbf{T}}_j^- \tag{7.1}$$

as illustrated in Fig. 7.4(b). The order of this operation is opposite to the equivalent expression for an RS as the sense of rotation of each set of slices is inverted.

This formulation generates a set of 'sided' intersection vectors which are aligned consistently along the length of the curve, as is required for orientation of the slots along each intersection. If the slice planes are not corrected for consistency across any inversions of the basis curve, the intersection vectors generated will point 'outward' with respect to the radius of curvature rather than from one side of the curve to the other.

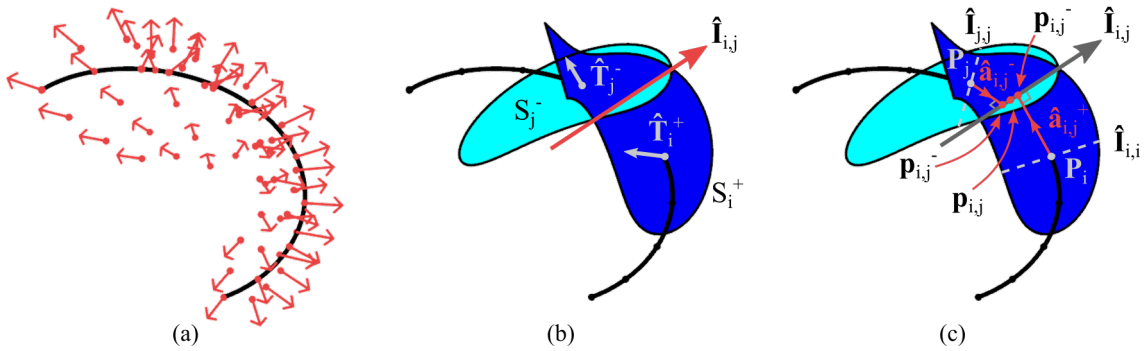

Fig. 7.4 The 2D array of intersection lines is described by a set of aligned vectors, $\hat{\mathbf{I}}_{i,j}$, and intersection points, $\mathbf{p}_{i,j}$, (a). Each aligned vector is generated by the vector product of the normals to the slice planes spanned, $\hat{\mathbf{I}}_{i,j} = \hat{\mathbf{T}}_i^+ \times \hat{\mathbf{T}}_j^-$, (b). Each intersection point may lie anywhere along the line of intersection but a consistent approach is to use the midpoint of the pair of points located by constructing the line perpendicular to the intersection and through the curve points of the spanned slice planes, (c).

Generation of a suitable intersection point is more involved, but one robust approach is to locate a pair of points along each intersection line by constructing the pair of lines perpendicular-to the intersection and passing through each curve point, $\mathbf{p}_{i,j}^{\pm}$, then taking their midpoint, $\mathbf{p}_{i,j}$, Fig. 7.4(c).

Formally, the two lines spanning from each curve point to (and orthogonal to) the intersection line are aligned to unit vectors $\hat{\mathbf{a}}_{i,j}^{\pm}$, given by the vector product of the slice plane normals to the intersection line

$$\begin{aligned} \hat{\mathbf{a}}_{i,j}^{+} &= \hat{\mathbf{I}}_{i,j} \times \hat{\mathbf{T}}_j^{+} \\ \hat{\mathbf{a}}_{i,j}^{-} &= \hat{\mathbf{T}}_j^{-} \times \hat{\mathbf{I}}_{i,j} \end{aligned} \tag{7.2}$$

and span a distance $\lambda_{i,j}^{\pm}$ across each slice (as yet unknown). Thus

$$\begin{aligned} \mathbf{p}_{i,j}^{+} &= \mathbf{P}_i + \lambda_{i,j}^{+} \hat{\mathbf{a}}_{i,j}^{+} \\ \mathbf{p}_{i,j}^{-} &= \mathbf{P}_j + \lambda_{i,j}^{-} \hat{\mathbf{a}}_{i,j}^{-} \end{aligned} \tag{7.3}$$

Since these construction lines are each perpendicular to the intersection line, they too are orthogonal and skew. The segment of the intersection line joining points $\mathbf{p}_{i,j}^{\pm}$ spans their closest approach, a distance $C_{i,j}$ along the unit intersection vector $\hat{\mathbf{I}}_{i,j}$ from $\mathbf{p}_{i,j}^{+}$ to $\mathbf{p}_{i,j}^{-}$ so that

$$\mathbf{p}_{i,j}^{-} = \mathbf{p}_{i,j}^{+} + C_{i,j} \hat{\mathbf{I}}_{i,j} \tag{7.4}$$

Substituting from Eqn. 7.3

$$\mathbf{P}_j + \lambda^-_{i,j}\hat{\mathbf{a}}^-_{i,j} = \mathbf{P}_i + \lambda^+_{i,j}\hat{\mathbf{a}}^+_{i,j} + C_{i,j}\hat{\mathbf{I}}_{i,j} \tag{7.5}$$

To determine each $\lambda^{\pm}_{i,j}$ and thereby locate each $\mathbf{p}^{\pm}_{i,j}$, taking the scalar product of each side with each of $\left(\hat{\mathbf{a}}^{\pm}_{i,j} \times \hat{\mathbf{I}}_{i,j}\right)$ gives

$$\begin{aligned}\mathbf{P}_j \cdot \left(\hat{\mathbf{a}}^+_{i,j} \times \hat{\mathbf{I}}_{i,j}\right) + \lambda^-_{i,j}\hat{\mathbf{a}}^-_{i,j} \cdot \left(\hat{\mathbf{a}}^+_{i,j} \times \hat{\mathbf{I}}_{i,j}\right) &= \mathbf{P}_i \cdot \left(\hat{\mathbf{a}}^+_{i,j} \times \hat{\mathbf{I}}_{i,j}\right) \\ \mathbf{P}_j \cdot \left(\hat{\mathbf{a}}^-_{i,j} \times \hat{\mathbf{I}}_{i,j}\right) &= \mathbf{P}_i \cdot \left(\hat{\mathbf{a}}^-_{i,j} \times \hat{\mathbf{I}}_{i,j}\right) + \lambda^+_{i,j}\hat{\mathbf{a}}^+_{i,j} \cdot \left(\hat{\mathbf{a}}^-_{i,j} \times \hat{\mathbf{I}}_{i,j}\right)\end{aligned}$$

which can be rearranged to yield

$$\begin{aligned}\lambda^-_{i,j} &= \frac{\left(\mathbf{P}_i - \mathbf{P}_j\right) \cdot \left(\hat{\mathbf{a}}^+_{i,j} \times \hat{\mathbf{I}}_{i,j}\right)}{\hat{\mathbf{a}}^-_{i,j} \cdot \left(\hat{\mathbf{a}}^+_{i,j} \times \hat{\mathbf{I}}_{i,j}\right)} \\ \lambda^+_{i,j} &= \frac{\left(\mathbf{P}_j - \mathbf{P}_i\right) \cdot \left(\hat{\mathbf{a}}^-_{i,j} \times \hat{\mathbf{I}}_{i,j}\right)}{\hat{\mathbf{a}}^+_{i,j} \cdot \left(\hat{\mathbf{a}}^-_{i,j} \times \hat{\mathbf{I}}_{i,j}\right)}\end{aligned} \tag{7.6}$$

These are substituted back into to Eqn. 7.3 to find each perpendicular point and, finally, the intersection point, $\mathbf{p}_{i,j}$, is set to their midpoint

$$\mathbf{p}_{i,j} = \frac{\mathbf{p}^+_{i,j} + \mathbf{p}^-_{i,j}}{2} \tag{7.7}$$

7.2.3 In-plane array of intersections

The vector approach outlined above is a generalised description of the structural geometry of a CS from a global perspective. However, unlike for an RS, the lack of global symmetry precludes the distillation of any meaningful insights from this description. A more useful, localised description of the structural geometry is obtained by examining the layout of intersection lines upon each slice plane.

The specific layout of intersection lines upon the slices of a given sliceform is dependent on both the form of the basis curve and the parameterisation of the structural architecture, and is generally unique to each slice (unless the curve has constant curvature, in which case the slices are identical within each set). Nevertheless, successive intersection lines are generally closely oriented so they still form a fan-like array on each slice, Fig. 7.5. In this perspective,

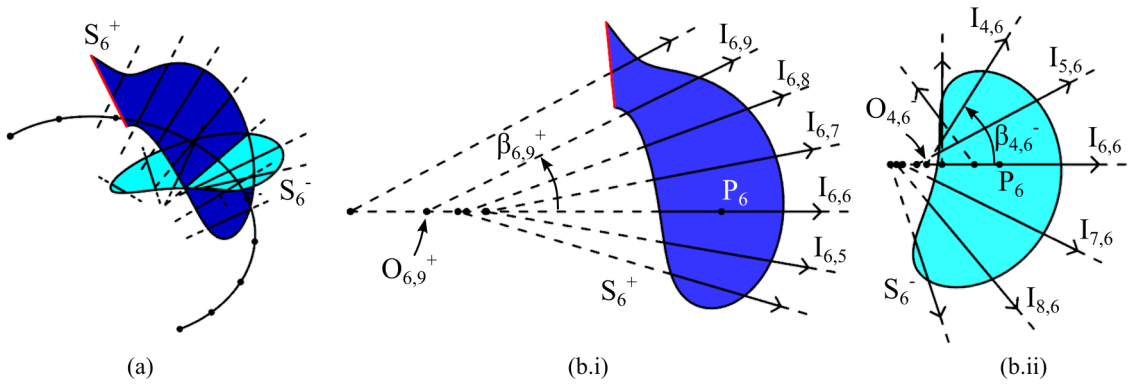

Fig. 7.5 The intersection lines of a CS form a unique fan upon each slice plane. Each intersection line, $I_{i,j}$, is located in-plane by an origin point on the midline, $O^{\pm}_{i,j}$, and its elevation from horizontal, $\beta^{\pm}_{i,j}$.

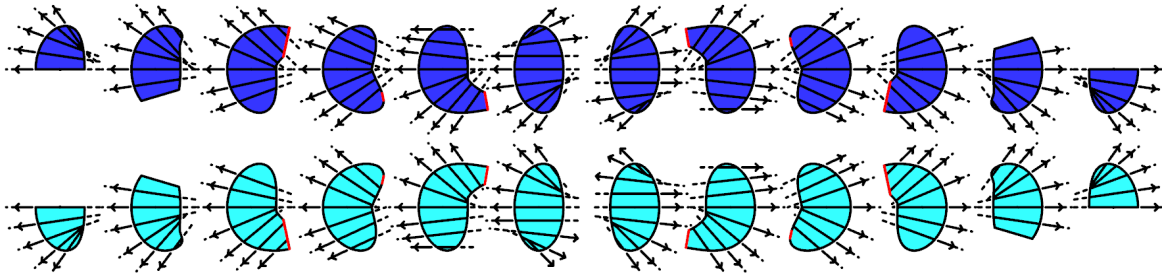

Fig. 7.6 The intersection lines are re-oriented to point 'outward' from the midline within each slice, illustrated for the slices of the S-curve synthesised in Fig. 6.21. Note that these directions are relevant to the layout of intersections upon each slice and are not consistent between each set of slices.

each intersection line is located by an *origin point*, $O^{\pm}_{i,j}$ – where the superscript denotes whether the positive (S^{+}_{i}) or negative (S^{-}_{i}) slice plane is being viewed – and an *elevation angle*, $\beta^{\pm}_{i,j}$, from the nominally horizontal *primary* intersection in that slice, $I_{i,i}$.

Thus intersection line $I_{i,j}$ *originates* at point $O^{+}_{i,j}$ on slice plane S^{+}_{i} at its intersection with the line $I_{i,i}$, and point $O^{-}_{i,j}$ on slice plane S^{-}_{j} at its intersection with the line $I_{j,j}$.

Within each plane, the intersection vectors can now be re-oriented '*outward*' with respect to their in-plane rotation from the midline. As illustrated in Fig. 7.6, this is not always the same as the 'sided' sense (which is used to generate the slots) and may not be consistent between the two sets of slices.

Upon each slice, successive pairs of intersection lines subtend a series of facets, Fig. 7.7(a). Across the CS these facets form a 2D array and are indexed as $F^{\pm}_{i,j}$ which denotes the intersection at the leading edge, $I_{i,j}$, and the set of slices it forms part of. Thus, facet $F^{+}_{i,j}$ lies

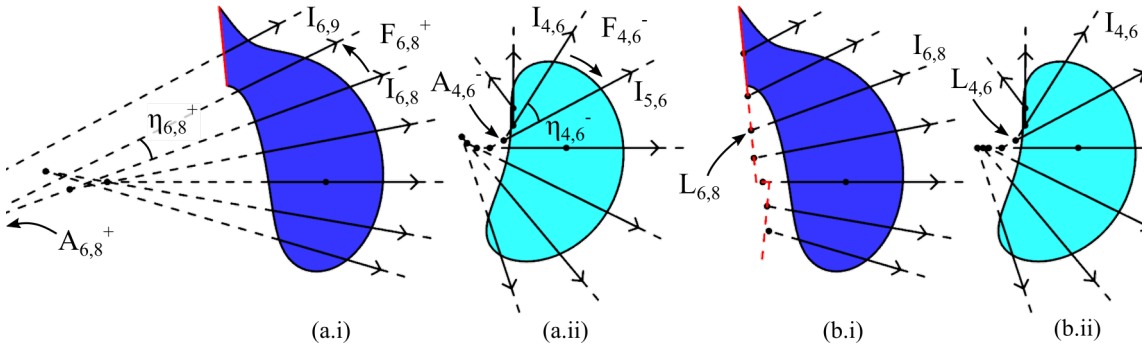

Fig. 7.7 Successive intersections divide each slice into a series of facets, $F^{\pm}_{i,j}$, indexed by the intersection at their leading edge and the set to which the slice belongs, (a). The apex of each facet, $A^{\pm}_{i,j}$, lies at the point of intersection of the intersection lines it spans, subtending a facet angle, $\eta^{\pm}_{i,j}$. In general, the intersection point between any pair of coplanar intersection lines is their vertex, $V_{i,(j,k)}$ between intersections $I_{i,j}$ & $I_{i,k}$, (not illustrated). The outward-most vertex along each intersection line is its limit, $L_{i,j}$, (b), and these intersection limits are consistent between the slices, usually lying at the apex of the enclosed facet on one slice, (ii), and upon the clip line of the other, (i).

on slice S^{+}_{i} and spans intersections $I_{i,j}$ and $I_{i,j+1}$, whilst facet $F^{-}_{i,j}$ lies on slice S^{-}_{j} and spans intersections $I_{i,j}$ and $I_{i+1,j}$. The apex of each facet, $A^{\pm}_{i,j}$, lies at the point of intersection of the intersection lines spanned, and each subtends facet angle, $\eta^{\pm}_{i,j}$. For a well-conditioned sliceform the intersections spanning each facet are sufficiently well-aligned that the apex lies outside the planform.

It is apparent from this perspective that the area of each slice is composed of a series of facets constructed outward from the midline where each successive facet contains all area not yet enclosed by the preceding intersection lines. Each intersection line is, itself, clipped against all intersections it encloses (toward the midline).

For completeness, the point of intersection between any pair of intersection lines is their *vertex*, $V_{i,(j,k)}$, where the subscript indices denote that this refers to the intersection of the j- and k-th intersection lines upon the i-th slice plane of the positive set. Similarly, $V_{(i,k),j}$ is the vertex of intersection lines $I_{i,j}$ and $I_{k,j}$ (which are coplanar to the j-th slice plane of the negative set). It follows that $V_{i,(i,k)}$ is the origin of intersection $I_{i,k}$ on slice S^{+}_{i} (*i.e.* $O^{+}_{i,j}$).

The outward-most vertex between each intersection line and those preceding it, upon either slice plane, is the *limit* of that intersection, $L_{i,j}$, Fig. 7.7(b). This will usually correspond to the apex of the enclosed facet on one of the two intersecting slices and lie on the clip line of the other.

Furthermore, the elevation of successive intersections will not necessarily increase in magnitude outward from the midline, and may be constant between successive intersections –

when the opposing slices are parallel so that the facet enclosed is rectangular – or decrease such that the apex of the enclosed facet lies on the opposite (outward) side of the slice. This latter case typically occurs when the intersection is between slices spanning a reversal in curvature of the basis curve. To resolve construction issues, the intersection vectors can be (re-)oriented *facet-wise* with respect to the elevation of each intersection line from that directly preceding it. Rarely, an intersection line may also be clipped at its outer point by a preceding intersection of a higher elevation, in which instances the the enclosed facet fills a 'valley'.

This localised, slice-view description is more insightful. Satisfyingly, the in-plane layout of intersections upon each set of slices echoes the treatment of the complementary slices during synthesis: whenever the limit of an intersection lies within the planform of a slice (whether at the apex of a facet or not) this is simply the imprint of the clipping of the corresponding slices of the opposing set against its neighbour[1].

7.3 Structural geometry of a CS as an array of skew cells

The interlocking slices of a CS form a honeycomb-like array of plane-faced cells which shear synchronously during articulation of the sliceform. The structural geometry of CS is now examined from a cell-based perspective.

7.3.1 CS as a array of truncated wedges

The structural architecture of a CS can be re-conceptualised as an array of open-faced four-sided cells which are stacked in familiar rows along the basis curve, illustrated in Fig. 7.8(a)-(b) for the conical spiral sliceform. For a well-conditioned CS, each cell is bounded by four facets and open faced at both ends.

In accordance with the locally-well-behaved array of slice planes, opposing facets are closely aligned, converging on the 'inside' of the basis curve. Extending the facets to form the 'roof' of the cell, opposing pairs of facets do not (usually) converge coincidentally and form a wedge, Fig. 7.8(c). Viewed from the outside of the curve, each cell appears as if looking up into a (truncated) steep-faced 'hip roof' whose *spine* joins a pair of degree-3

[1]This reveals a slight fragility the clipping method as defined because each slice should actually be clipped against all following slices in the sense of the rotation, not just the immediate neighbour, just as each intersection line is clipped against all inward intersections from an in-plane perspective. In practice, the simpler neighbour-slice clipping method is sufficient in almost all realistic examples.

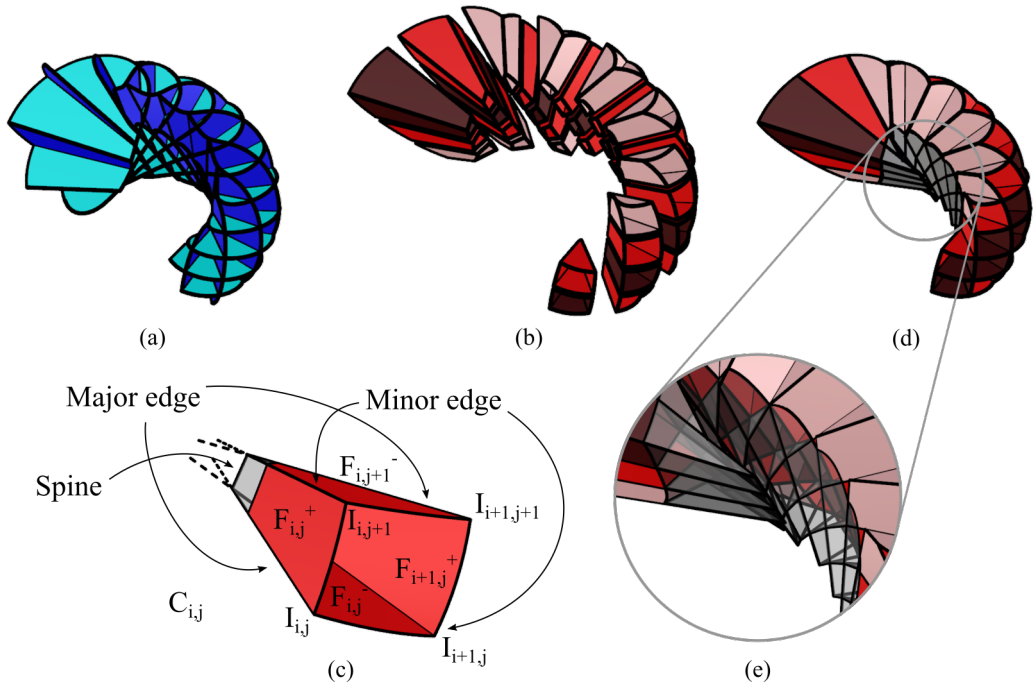

Fig. 7.8 A curve sliceform, (a), can be re-conceptualised as an array of open-faced, four-sided cells, (b) (visualised exploded for clarity). These cells are arranged in rows stacked along the basis curve with the primary cells (dark) lying on the curve itself, secondary cells (medium) in the valleys between their peaks, and so forth. Each cell, $C_{i,j}$ (indexed by the intersection at its leading edge), inscribes the volume between four adjacent facets, themselves subtending the four adjacent intersection lines along the edges of the cell. (c). The major edges span the cell in the lengthwise sense of the basis curve, the minor edges span the cell transverse to the basis curve. Opposing pairs of facets converge independently to form a wedge capped by a spine. The roofs of adjacent cells are offset along one diagonal and aligned to the clip lines of the slices along the other, (d) & inset (e). In this instance the 'positive' slices self-intersect first and so the spine is the intersection of the 'positive' facets, but the reverse may also be true depending on the geometry of the basis curve.

vertices along a portion of the line of self-intersection between opposing facets belonging to adjacent slices of the same set.

Following directly from the 2-D array of slices, each cell in this 2-D array is indexed by the intersection at the leading edge. Thus, cell $C_{i,j}$ is the cell whose leading edge is $I_{i,j}$, inscribing intersections $I_{i,j} - I_{i,j+1} - I_{i+1,j+1} - I_{i+1,j}$ with facets $F^{+}_{i,j} - F^{-}_{i,j+1} - F^{+}_{i+1,j} - F^{-}_{i,j}$. For each cell in isolation, the edges (intersection lines) form a *major* pair, spanning the cell in the lengthwise sense of the curve, and a *minor* pair, spanning the cell transverse to the curve.

The cells of each successive row outward from the curve (primary, secondary, tertiary,...) fill the valleys between the peaks of the cells of the preceding row, sharing intermediate facets. Across the array, each diagonal row of cells fill the wedge spanned by a pair of adjacent slice planes with the apex points of the transverse, intermediate facets lying on their line of self-intersection. Thus, which pair of facets meet along the spine of each cell depends on which pair of slice converge first, with the spine itself simply a segment of their self-intersection. The spines of adjacent cells are simply successive segments of each clip line, Fig. 7.8(c) & (d). Along the transverse diagonal, the cell roofs are staggered with each cell extending slightly further than the previous, and each intermediate facet extending beyond the first spine until reaching the second.

7.3.2 Skew geometry of each cell

Unless the basis curve has constant curvature (in which case each row of cells has an identical repeating unit), each cell of a CS is has a unique geometry and a more general formulation is required.

Consider a primary cell lying along the basis curve and inscribing consecutive pairs of slice planes, Fig. 7.9(a). The major edges of this cell are the primary intersection lines of each slice, which are aligned to the normal vector of the corresponding Frenet-Serret curve frames. For a general out-of-plane basis curve, these edges are skew and so such cells are termed *skew cells*. The same is true for each cell of the secondary row, whose major edges are the minor edges of the primary cells, and so forth: a CS is an array of skew cells.

Returning to the original primary cell, $C_{i,i}$ – which spans consecutive curve points P_i and P_j – its 'skewness' is captured by its *skew frame*, (b). This skew frame is constructed by generating the *skew axis* which is mutually perpendicular to the primary intersections and joins them at their closest points, the *skew points*, $s^i_{i,i}$ & $s^j_{i,i}$, with aligned unit vector $\hat{\mathbf{s}}_{i,i}$. The primary intersections span a *skew angle*, $\phi_{i,i}$, about this skew axis and are offset by the *skew distance*, $d_{i,i}$. Note that the subscripts index the cell that the skew frame belongs to and not the particular intersection lines.

Though the major edges of this primary cell are skew, each minor edge intersects with both at its origin within each slice plane, which cannot be coincident, (c). Each of the minor intersection lines has an origin point on each major intersection line, and these four points are the apexes of each facet of the cell. The spine of the cell simply connects whichever pair of opposing facet apexes is reached first, truncating the tips of the other pair of facets.

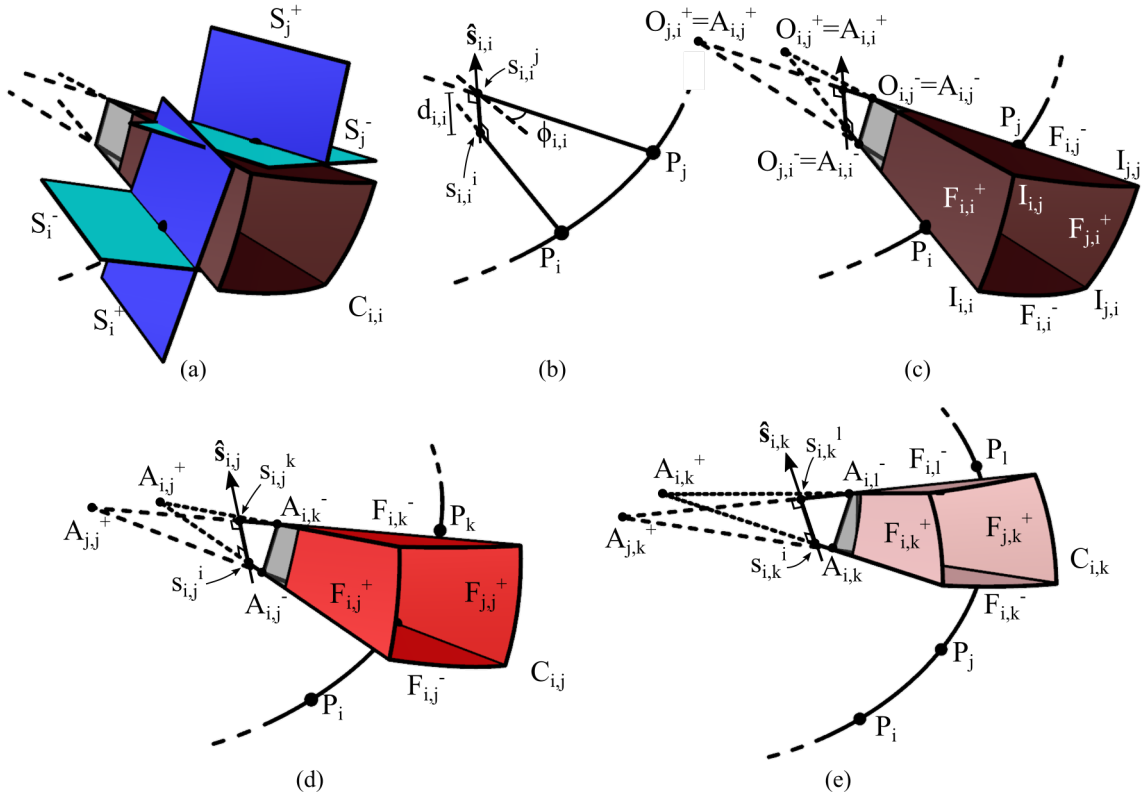

Fig. 7.9 Examining a primary cell inscribing adjacent pairs of slice planes, (a), it is apparent that the major edges, aligned the normal vector of each curve frame, will generally be skew. For each primary cell the local *skew frame* is constructed by drawing the mutually perpendicular *skew axis* which joins the major edges at their closest points, (b). Each minor intersection intersects with each major intersection at its origin within each slice plane, and these points are the origin of each facet of the skew cell, (c). The major edges of each cell of the second row are the minor edges of the primary cells, which are also skew, (d), and so forth, (e). A CS is thus an array of *skew cells*.

This construction an now be repeated for cells of the secondary, (d), and tertiary, (e), rows, generating their skew frames and locating the apex of each facet along their (skew) major intersection lines. For these non-primary cells, the four intersection points now locate solely the apex of each facet on its leading edge.

If the basis curve is planar, the major edges of the primary cells are coplanar to the curve and intersect within this plane (or can be considered to have a 'skewness' of zero) – the four apexes converge and the cell is pyramidal. However, unless the basis curve also has constant curvature (*i.e.* a circular arc) the apexes of successive primary cells will not be coincident, and the secondary cells remain skew, and so forth.

7.3.3 Tetrahedral geometry of each cell

To extend the localised formulation of the structural geometry of a CS as an array of skew cells and connect the geometry of each cell to the parametrisation of the structural architecture – *i.e.* in the interest of constructing their geometry directly – it is insightful to examine the intrinsic geometry of each skew cell itself.

Construction of the skew geometry for a cell locates a pair of points lying along each intersection line – the apexes of the adjacent facets. Joining these points with segments of each intersection line and connecting the apexes of opposing facet pairs (where the spine of the skew cell connects the first pair) forms a tetrahedron, Fig. 7.10(a). This tetrahedron, $T_{i,j}$ for cell $C_{i,j}$, which inscribes the volume swept between the tips of the truncated facets, is the geometric dual of the skew cell. Each tetrahedral facet, $F'^{\pm}_{i,j}$, subtends the same pair of intersection lines as the corresponding facet of the parent skew cell, sharing both apex point and facet angle, (b).

The tetrahedron can be constructed for each cell of the CS, shown for a series of (separated) cells in (c); indeed, the array of skew cells is fundamentally an extension of this array of tetrahedra with each cell projected outward from its spine (d). This array of tetrahedra captures the structural geometry of a CS in a generalised fashion, via which the geometry of each skew cell can be determined directly from the skew frame.

That the primary skew cells of a planar curve are pyramidal has already been mentioned, a few other special cases which may arise are now considered.

If the basis curve reverses in sense then the skew cells either side of the inversion converge on opposite sides of the basis curve and the tetrahedral cells must also switch sides. In the transition region – where the intersections span slice planes at points with opposing curvature

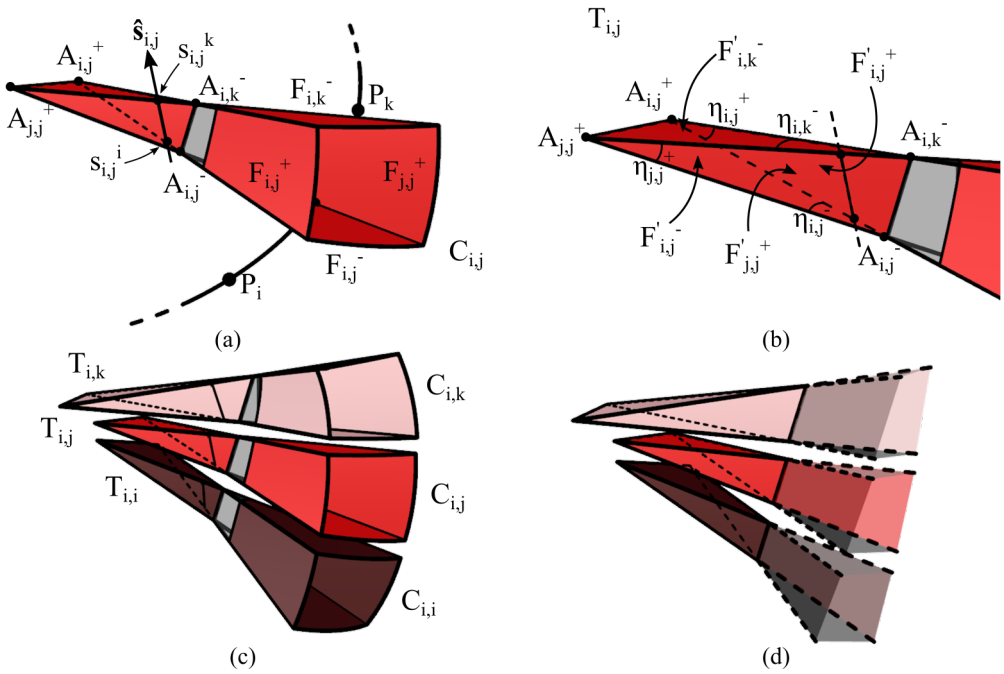

Fig. 7.10 The apexes of each facet of a skew cell are unique, locating a pair of points along each major edge and inscribing a tetrahedron that lies just beyond the roof of the cell, (a). Each tetrahedron, $T_{(i,j)}$, is the geometric dual of its parent cell, with its facets, $F'^{\pm}_{(i,j)}$, echoing the geometry of the corresponding facet of the CS, (b). A tetrahedron can be constructed for each cell of a CS, (c); indeed, the structural geometry of a CS is simply a projection of this array of tetrahedra, (d).

– the cells of the sliceform actually inscribe a (doubly-truncated) portion of the tetrahedron itself rather than a skew cell extended from one end.

Similarly, if the basis curve is a line with intrinsic twist, the skew axis between successive frames is coincident with the basis curve joining those points. Opposing facets of each slice converge on opposite sides of the curve and the cells, again, inscribe a central portion of the tetrahedron. Upon each planform, the fans of intersections are inverted between the two sets and the slots will appear outside-in, or *vice-versa*, on both.

If the curve is circular, the primary cells are pyramidal and their apexes are coincident. Their minor intersections also intersect at the same point and the secondary cells are pyramidal with coincident apexes, and so forth to form the spherical architecture as an RS. This can occur along a portion of a curve, *e.g.* an 'S'-curve with two conjoined semicircles, along which the structural architecture is a spherical array.

If the curve frames spanned by an intersection line are parallel, the 'skew lines' are also parallel and the skew frame and tetrahedron cannot be constructed. The cell spanning these curve points is a prism and the intersection lines at the upper and lower minor edges are parallel to the midline in each slice plane. This is the case for every intersection and cell of a CS along a line, forming an LS.

7.3.4 Skew geometry of each intersection line

Just as an RS is a spherical array of pyramidal cells, a CS is a curve-wise array of skew cells, each a projection of the tetrahedron lying just beyond its roof. Where the global symmetry of an RS enabled calculation of the orientation of each intersection line directly from the parameterisation of the structural architecture; the construction of each skew cell from its skew frame and tetrahedron can be used to compute a localised description of the array of intersections (as opposed to their globalised description via an array of aligned vectors as described above).

To determine the local orientation of intersection $I_{i,k}$ (where $k = i+2$) within slices S_i^+ & S_k^- – which is the upper minor edge of cell $C_{i,j}$ (where $j = i+1$) which lies in the second row of cells – requires construction of the 2×2 block of cells spanning from P_i to P_k and centred on the basis curve with $C_{i,j}$ at its peak, Fig. 7.11(a). The primary cells locate each intermediate intersections within each plane, the secondary cells locate intersection $I_{i,k}$ relative to these predecessors. This can be replicated for every intersection in the array, each time generating the skew frame and tetrahedra for each 'sub'-cell within the block to successively reconstruct each slice plane as a series of facets.

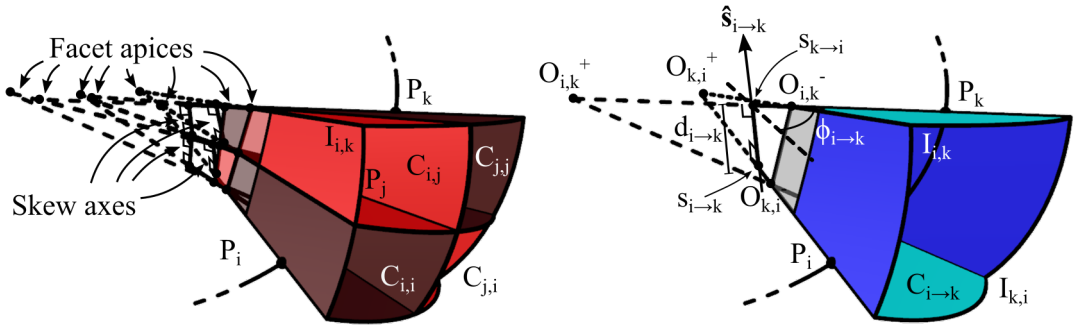

Fig. 7.11 The local orientation of each intersection line within each slice plane can be determined by constructing the the appropriate block of cells, illustated in (a) for intersection $I_{i,k}$. The skew geometry of each 'sub'-cell locates is minor edges relative to its major edges, which are the minor edges of the previous cells, and so forth. Alternatively, each intersection line forms the minor edge of the 'super'-cell, $C_{i\to k}$, inscribing the pairs of slice planes at the curve points it spans, (b), which directly locates that intersection within each slice.

However, a more direct description can be obtained by examining the geometry of the 'super'-cell inscribing the outermost slice planes, Fig. 7.11(b). The major edges of this super-cell are aligned to the local normal vectors at adjacent-but-one curve points P_i & P_k, which are skew, and so the super-cell is also a skew cell. Constructing the skew frame for this cell locates the origin of the minor edge intersections upon the midline of each slice plane, with the facet angles now providing their in-plane elevation. Again, the geometry of this cell is characterised by the geometry of its dual tetrahedron.

The notation for this super-cell is derived from the usual notation for a skew cell, the subscript now indicating the curve points spanned as follows. The cell illustrated here is $C_{i\to k}$, the skew frame has skew axis vector $S_{i\to k}$ and spans skew points $S_{i\to k}$ & $S_{i\to k}$ upon the major intersections which are the primary intersections upon each slice plane. The skew angle, $\phi_{i\to k}$, and skew distance, $d_{i\to k}$, follow as expected. The apex of each facet is simply the origin of the minor intersection on the slice plane for which the usual notation ($O^{\pm}_{i,k}$ for the upper intersection points) is used and the angle subtended is its in-plane elevation, $\beta^{\pm}_{i,k}$ for the upper facets[2].

Before proceeding with this construction, it is worth explicitly noting the distinction between between the outer surface of the block of nested sub-cells, and the super-cell

[2]This notation is a reduced version of the full notation for a general super-cell, $C_{(i,j)\to(r,s)}$, which spans from from $I_{(i,j)}$ at its leading edge to $I_{r,s}$ at its trailing edge and may be non-square. The full skew frame notation follows this standard subscript notation, and the vertices of the tetrahedron are the various intersection points (intersection vertices) between the intersections spanned ($I_{(i,j)} - I_{(i,s)} - I_{(r,s)} - I_{(r,j)}$).

inscribing the same outer slice planes. The former is a portion of the physical CS, the latter is simply a geometric construction. Though it may be visualised with facets inscribing the same global volume as the CS, neither the roof nor the tetrahedron of this super-cell embody any physical feature of the original sliceform. More specifically, the apexes of successive facets on each slice plane are not coincident and each slice comprises a series of staggered facets, whereas the facets of the super-cell do not take account of this internal geometry. Likewise, the roofs of the sub-cells are staggered where each slice plane is successively clipped by the next and do not simply coalesce to form the roof of the super-cell. Unlike an RS where each block of concurrent pyramidal cells forms a larger pyramidal cell, a block of skew cells do not coalesce to form a larger skew cell, though the exterior geometry inscribed (*i.e.* the spatial arrangement of the outermost edges) is also skew – as modelled here.

Geometry of a skew cell via its tetrahedron

The local structural geometry of the CS is captured by construction of the skew frame and tetrahedron belonging to the appropriate skew super-cell for each line of intersection. Attention is not turned to computing the location of the tetrahedron vertices along each major edge, *i.e.* the origin of the minor intersection lines, and the angle subtended by each facet, *i.e.* their in-plane elevation.

The starting point for this analysis is the local structural geometry of the CS which derives from the basis curve and parameterisation of the structural architecture and is captured in standard form by the local skew frame, Fig. 7.12(a).

To rectify the relative positions of the skew frame and the local basis frames, the inclination of the skew axis to the binormal vector of each frame is defined as the *skew offset*, $\alpha_{i\to k}$ & $\alpha_{k\to i}$, about each normal axis. For consistency this offset is measured in the positive sense from the local binormal to the skew axis – both $\alpha_{i\to k}$ & $\alpha_{k\to i}$ are positive in the illustrated example. The skew points are a skew distance, $s_{i\to k}$ & $s_{k\to i}$ (using the same notation as to label the points themselves), from the respective curve points, P_i & P_k.

The location of each vertex of the tetrahedron is most readily approached by calculating their offsets from the skew point on the corresponding major edge, $R_i^{\pm}$ & $R_j^{\pm}$, Fig. 7.12(b).

Translating each major edge along the skew axis to form a pair of reference 'rails', each vertex is located by constructing a system of right triangles as follows (illustrated in Fig. 7.12(c) for vertex $O_{i,k}^{+}$ which corresponds to the origin of edge $I_{i,k}$ on slice plane S_i^{+}).

The first right triangle is formed by drawing three lines: from the chosen vertex to the opposing major edge, meeting it at a right angle; from the chosen vertex to the translated

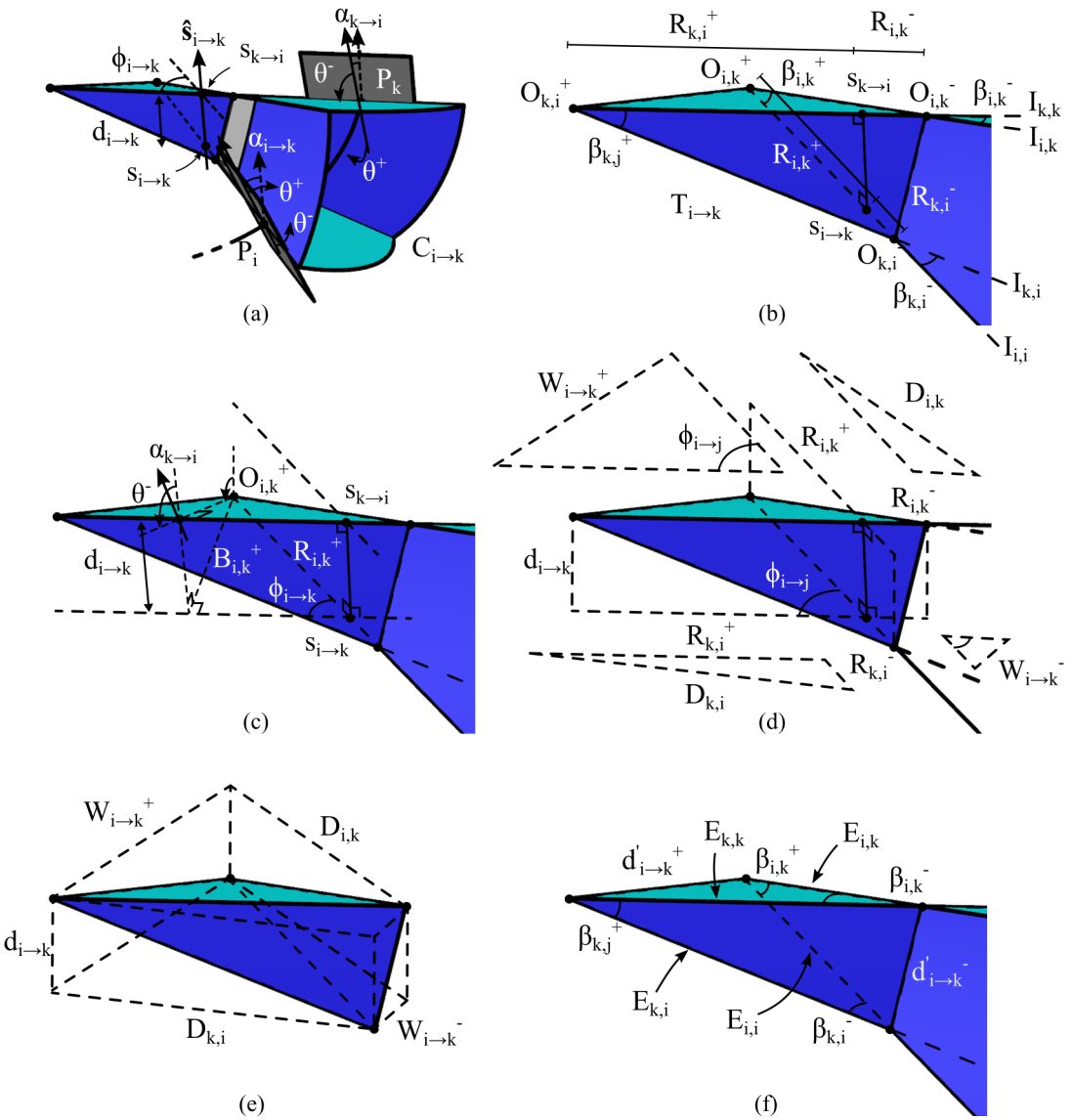

Fig. 7.12 The local, *i.e.* in-plane, geometry of each intersection line can be determined directly from the skew geometry of the curve points it spans by geometric construction of the tetrahedron of the appropriate skew cell, where the same cell is used for complementary intersection lines $I_{i,k}$ and $I_{k,i}$. This cell and tetrahedron are fully defined by the local skew frame spanning the curve points and the rotation of each set of slices relative to that frame, (a). The origin of the intersection lines upon each slice plane are simply the vertices of the tetrahedron, (b), which are offset from the skew points along each major edge by distances $R_i^{\pm}$ & $R_j^{\pm}$. These offsets are found by constructing a system of right triangles, (c). The in-plane elevations of each intersection line are simply the facet angles of the tetrahedron. To determine these, the prism enclosing the tetrahedron and aligned to the skew axis is first constructed, (d)-(e), where the edge lengths of interest are the diagonals of the rectangular faces, found via the Pythagorean theorem. With all edge lengths ($E_{i,k}$ for the segment along intersection $I_{i,k}$) known, the facet angles are calculated via the law of cosines applied to each facet of the tetrahedron, (f).

image of the opposing major edge, also meeting it at a right angle and perpendicular to the skew axis; and the line joining the ends of the first two which is parallel to the skew axis.

The second right triangle is formed by: the major edge upon which the chosen vertex lies, the translated image of the opposing edge, and the second line of the first.

This system can be solved by noting that the hypotenuse of the first triangle lies upon the tetrahedral facet corresponding to the skew cell facet with which the original facet shares a minor edge, and is perpendicular to the opposing major edge. It is about this edge which the slice plane was rotated so its inclination to the skew axis is simply the rotation of that set of slices plus or minus the skew offset of the skew axis from the binormal axis. Its height is the skew distance. The length of the common edge, $B^{+}_{i,k}$, follows by simple trigonometry

$$B^{+}_{i,k} = d_{i\to k}\tan(\theta^{-} + \alpha_{k\to i}) \tag{7.8}$$

The second right-triangle subtends the skew-angle of the cell. The offset of the chosen vertex along its major edge, $R^{+}_{i,k}$, is its hypotenuse, again following by simple trigonometry

$$R^{+}_{i,k} = \frac{B^{+}_{i,k}}{\sin(\phi_{i\to k})} = d_{i\to k}\frac{\tan(\theta^{-} + \alpha_{k\to i})}{\sin(\phi_{i\to k})} \tag{7.9}$$

This is repeated for each vertex to determine the offset of each apex. Care must be taken when determining the inclination of each facet from the skew axis by addition or subtraction the skew offset as appropriate.

$$\begin{aligned}
R^{+}_{i,k} &= \frac{B^{+}_{i,k}}{\sin(\phi_{i\to k})} &&= d_{i\to k}\frac{\tan(\theta^{-} + \alpha_{k\to i})}{\sin(\phi_{i\to k})} \\
R^{-}_{i,k} &= \frac{B^{-}_{i,k}}{\sin(\phi_{i\to k})} &&= d_{i\to k}\frac{\tan(\theta^{+} - \alpha_{k\to i})}{\sin(\phi_{i\to k})} \\
R^{+}_{k,i} &= \frac{B^{+}_{k,i}}{\sin(\phi_{i\to k})} &&= d_{i\to k}\frac{\tan(\theta^{-} + \alpha_{i\to k})}{\sin(\phi_{i\to k})} \\
R^{-}_{k,i} &= \frac{B^{-}_{k,i}}{\sin(\phi_{i\to k})} &&= d_{i\to k}\frac{\tan(\theta^{+} - \alpha_{i\to k})}{\sin(\phi_{i\to k})}
\end{aligned} \tag{7.10}$$

Combined with the skew distances, these values locate the origin of the minor edge intersections within each slice plane.

To determine the apex angles of each facet, the length of each edge of the tetrahedron is first required. The major edges are simply the sum of the offsets of each apex from the skew

point, but the minor edges and end lines corresponding to the intersection of opposing slices which requires further treatment.

Viewed along the skew axis, the tetrahedron appears as a pair of crossed skew edges joining the vertices of adjacent facets along each major edge, a pair of longitudinal edges joining the apexes of facets along each minor edge, and the end 'caps' joining the apexes of one pair of opposing facets along the intersection line of the other pair, Fig. 7.12(c). Projected along the skew axis, the perimeter edges form a prism framing the tetrahedron, (d), where the unknown edges are now a diagonal of a rectangular facet. This is computed as follows.

The lengths of the longitudinal faces (indexed in accordance with the edge along their diagonal) and the width of the end caps (indexed in accordance with the sign of the apexes at their vertices) are found by applying the cosine rule to each segment of the tetrahedron in plan view

$$\begin{aligned} W^{+}_{i\to k} &= \sqrt{(R^{+}_{i,k})^2 + (R^{+}_{k,i})^2 - 2R^{+}_{i,k}R^{+}_{k,i}\cos\phi_{i\to k}} \\ D_{i,k} &= \sqrt{(R^{+}_{i,k})^2 + (R^{-}_{i,k})^2 + 2R^{+}_{i,k}R^{-}_{i,k}\cos\phi_{i\to k}} \\ D_{k,i} &= \sqrt{(R^{+}_{k,i})^2 + (R^{-}_{k,i})^2 + 2R^{+}_{k,i}R^{-}_{k,i}\cos\phi_{i\to k}} \\ W^{-}_{i\to k} &= \sqrt{(R^{-}_{i,k})^2 + (R^{-}_{k,i})^2 - 2R^{-}_{i,k}R^{-}_{k,i}\cos\phi_{i\to k}} \end{aligned} \tag{7.11}$$

The unknown tetrahedron edge lengths follow via the Pythagorean theorem

$$\begin{aligned} E_{i,i} &= R^{+}_{i,k} + R^{-}_{k,i} \\ E_{i,k} &= \sqrt{D^2_{i,k} + d^2_{i\to k}} \\ &= \sqrt{(R^{+}_{i,k})^2 + (R^{-}_{i,k})^2 + 2R^{+}_{i,k}R^{-}_{i,k}\cos\phi_{i\to k} + d^2_{i\to k}} \\ E_{k,i} &= \sqrt{D^2_{k,i} + d^2_{i\to k}} \\ &= \sqrt{(R^{+}_{k,i})^2 + (R^{-}_{k,i})^2 + 2R^{+}_{k,i}R^{-}_{k,i}\cos\phi_{i\to k} + d^2_{i\to k}} \\ E_{k,k} &= R^{-}_{i,k} + R^{+}_{k,i} \\ d'^{+}_{i\to k} &= \sqrt{(W^{+}_{i\to k})^2 + d^2_{i\to k}} \\ &= \sqrt{(R^{+}_{i,k})^2 + (R^{+}_{k,i})^2 - 2R^{+}_{i,k}R^{+}_{k,i}\cos\phi_{i\to k} + d^2_{i\to k}} \\ d'^{-}_{i\to k} &= \sqrt{(W^{-}_{i\to k})^2 + d^2_{i\to k}} \\ &= \sqrt{(R^{-}_{i,k})^2 + (R^{-}_{k,i})^2 - 2R^{-}_{i,k}R^{-}_{k,i}\cos\phi_{i\to k} + d^2_{i\to k}} \end{aligned} \tag{7.12}$$

Finally, the apex angle of each facet can be calculated via the cosine rule, yielding the elevation of the minor intersections in each slice plane

$$\begin{aligned}
\cos\beta^{+}_{i,k} &= \frac{E^2_{i,k} + E^2_{i,i} - (d'^{-}_{i\to k})^2}{2E_{i,k}E_{i,i}} \\
\cos\beta^{-}_{i,k} &= \frac{E^2_{i,k} + E^2_{k,k} - (d'^{+}_{i\to k})^2}{2E_{i,k}E_{k,k}} \\
\cos\beta^{+}_{k,i} &= \frac{E^2_{k,i} + E^2_{k,k} - (d'^{-}_{i\to k})^2}{2E_{k,i}E_{k,k}} \\
\cos\beta^{-}_{k,i} &= \frac{E^2_{k,i} + E^2_{i,i} - (d'^{+}_{i\to k})^2}{2E_{k,i}E_{i,i}}
\end{aligned} \tag{7.13}$$

The final expressions for each angle in terms of the skew dimensions and structural architecture, obtained by substituting the expressions in Eqn. 7.10 into Eqn. 7.12 and again into Eqn. 7.13, are somewhat cumbersome and not reproduced here.

Using the approach outlined above, the in-plane geometry of any intersection is found by constructing the tetrahedron for the appropriate super-cell containing that intersection as its minor edge. This generalised method can be applied to each intersection of a CS generated along any basis curve to determine the local structural geometry.

7.4 Intrinsic geometry of a CS

Having identified that the structural geometry of a CS is an array of skew cells, it is interesting to consider the intrinsic form of their volumetric geometry. This is perhaps best explained by way of comparison to an LS and an RS. As identified in Chapter. 2, an LS is a planar array of prismatic cells which can be generated by an extrusion of a 2D grid of straight lines – its intrinsic volumetric geometry is a 2D 'slab'. An RS has a rotational symmetry and its intersections form a spherical array – its intrinsic volumetric geometry is a sphere (with un-fillable double cone removed). The equivalent geometry for a CS is now pursued

7.4.1 Direct synthesis of a CS from the structural geometry

It has already been identified that the structural geometry of a CS is an array of skew cells projected from an array of tetrahedra, Fig. 7.10. For a well-behaved cell (*i.e.* not lying in the transition region of a reversing curve or along a twisted line where the cells form a portion of

the tetrahedron itself) the intersections diverge from the roof and the facets can be extended infinitely, or at least until colliding with another portion of the sliceform.

The curve sliceforms synthesised in the preceding chapter required the generation of a swept global geometry to generate a viable shape for each slice. A CS could now be generated directly from the structural architecture by projecting the facets outward from the array of tetrahedra.In fact, it is apparent that the geometrically feasible domain of the sliceform is the complete volume lying outward of the cell roofs. Of course a semi-infinite sliceform cannot be constructed in practice and some finite distance to which to extend the cells is sought. Whilst inscription of a sphere centred on the focus was the obvious choice for an RS, resulting in a sliceform whose intersection lines have a constant length, such a simple approach cannot be applied to a CS because each intersection line has two distinct in-plane geometries with distinct origin points on the midplane of each slice and each bordering four facets with four distinct apex points.

Instead, generation of a consistent set of 'outer' points along each intersection line is approached from an in-plane perspective where a natural reference point within each slice plane is the curve point along each primary intersection. From this reference point various arrangements of points along each intersection line can be constructed.

Firstly, the construction from section 7.2.1 can be re-used to generate a 'perpendicular' point on each intersection, Fig. 7.13(a). Tracing a polyline or spline through these points on each slice plane produces a set of slice templates whose outer edge 'wraps around' the basis curve, a 'curved edge' solution, Fig. 7.13(d.i/ii/iii).

Alternatively, a similar construction locates the points one each intersection which lie on a line coincident with the curve point and perpendicular to the midline of the slice. Again, this produces two points on each intersection, one from each slice plane. Taking the midpoint of each pair generates a set of 'straight edge' points. A polyline or spline through these points is typically slightly concave in one set and convex in the other, Fig. 7.13(e.i/ii/iii). However, the span of the pair of points along each intersection line increases rapidly with each successive row of intersections, tending to generate a less uniform result.

Combining these approaches, a well-formed sliceform whose outer surface is broadly perpendicular to the array of intersections is generated by taking the midpoint of the 'straight' and 'curved' points on each intersection line, Fig. 7.13(f.i/ii/iii).

In any case the slice templates and resulting skeleton CS are generated directly from the basis curve. The form of the resulting sliceform has no physical significance but this approach provides a robust method for synthesising an intrinsic sliceform which embodies the pure structural geometry of the CS, with each cell closed at its roof and open at its base,

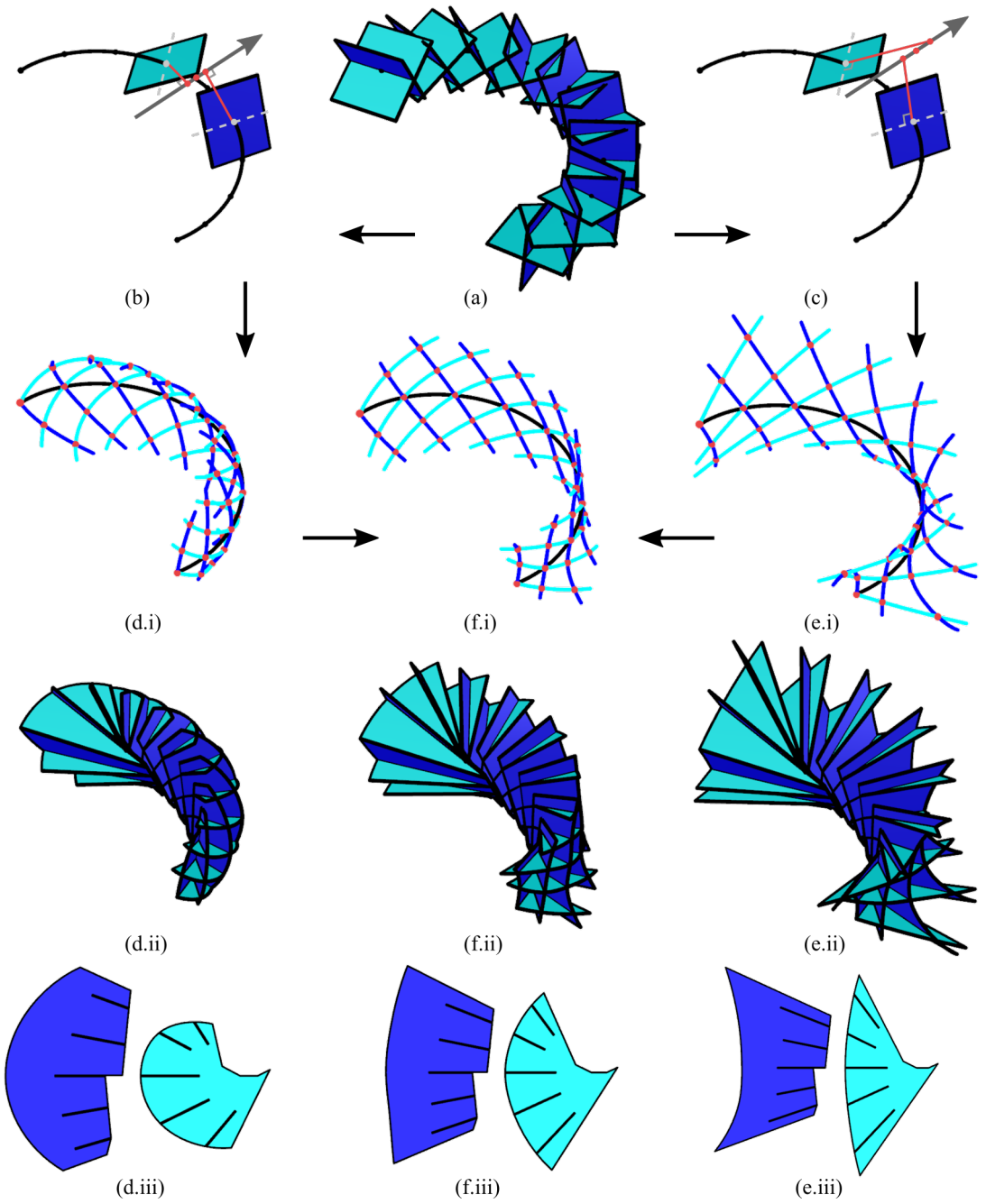

Fig. 7.13 Each cell of a CS is a projection from its tetrahedron. Therefore, a CS can be generated directly from the structural architecture by defining a set of *projection points* for each intersection line. A consistent set of points are generated from the in-plane geometry by taking the midpoint of the points located by perpendicular projection from each intersection line to each curve point, (b), or perpendicular projection from each midline to each intersection line, (c). Drawing a series of curves through either set of points generates a set of 'curved' and 'straight' edges on each slice plane, respectively,(d/e.i), or an intermediate design uses the midpoint of the two solutions, (f.i). The projected sliceform is constructed by projection of each cell from its roof to these edges, (d/e/f.ii), with representative slices of each design shown in (d/e/f.iii).

and could be extended freely from the outer surface (until colliding with another portion of the sliceform).

In these examples the connectivity of the slices must be prescribed which sets the number of facets to form in each slice and the number of cells to form in the array. The slots are generated along and to the midpoint of the fully-formed portion of each intersection, as usual, with the slices extended slightly beyond the outermost intersection by extrapolation of the edge curve to form a portion of the next facet to enable the outermost slots to be fully formed and those intersections interlocked. Each skew cell is closed at its roof with successive 'spines' forming the clip lines for each slice.

Note that this approach is valid only for basis curves which have a singular curvature sense, *e.g.* the helix, planar spiral or conical spiral. If the curvature reverses, the intersection points are still valid but the facets must switch sides of the curve at some intermediate point and a coherent slice is not formed.

7.4.2 Ribbon geometry of a CS

An alternative approach to generating an intrinsic geometry for a CS is to consider the surface it embeds directly from the curve, rather than from the array of intersections. Consider the analogous cases of an LS, which is an extrusion of a planar lattice of straight lines, and an RS, which is a spherical extrusion of a lattice of great arcs on a sphere. The dimension of the sliceform in the direction of the intersections, the radius of the sphere and the depth of the slab, is 'redundant' and both collapse to a two-dimensional scissor-grid (planar and spherical, respectively) when the thickness along this direction is reduced to zero.

For an RS this spherical surface can be constructed at any radius and is centred on the origin, for an LS the planar basis surface and can be taken at any 'height'. In both cases, the surface is perpendicular to each intersection in the array.

For a curve sliceform, a perpendicular surface is not so readily generated, but a consistent solution is the ribbon generated by sweeping a line aligned to the binormal axis of the Frenet-Serret frame along the curve itself. This ribbon is perpendicular to the radius of curvature along the length of the curve and provides a surface upon which to generate a set of planar curves corresponding to each slice plane. It could be considered that a CS thus embeds a 'ribbon scissor-grid', but this is not quite consistent with the equivalent models of an LS as a planar lattice and an RS as a spherical scissor mechanism because the rotation axes of a CS are not perpendicular to the ribbon's surface.

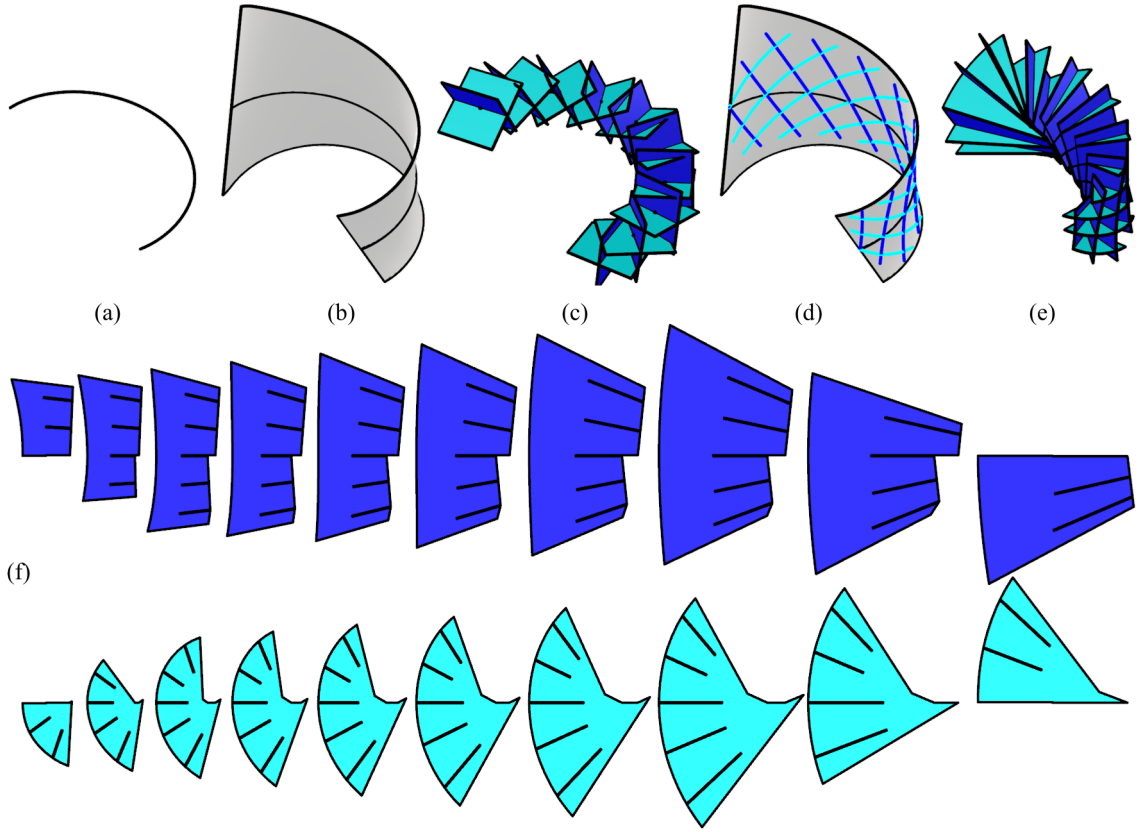

Fig. 7.14 A ribbon CS is synthesised by sweeping a line perpendicular to the radius of curvature along the basis curve to form a ribbon surface, (a)-(b). On this surface, a set of planar ribbon curves are generated corresponding to each slice plane, (c)-(d), defining a set of edge curves for a ribbon sliceform, (e), with slice templates, (f).

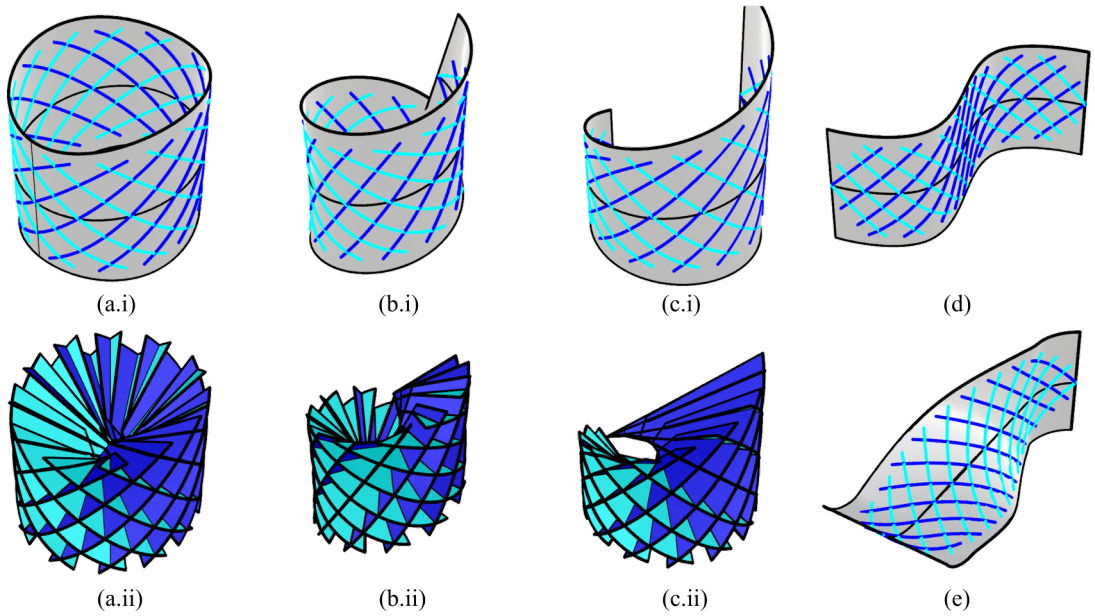

Fig. 7.15 Generation of the ribbon geometry for sliceforms along a set of basis curves – an ellipse (a.i); a spiral, (b.i); a helix, (c.i); an S-curve, (d); and a line with intrinsic twist, (e) – and ribbon sliceforms for those whose tetrahedra lie on a consistent side of the curve, (a.ii,b.ii,c.ii).

This ribbon geometry can be generated for a CS along any basis curve with a set of examples illustrated in Fig. 7.15. For curves whose structural geometry is well-behaved and the cells are projections of a set of tetrahedra who lie on a consistent side of the curve – *e.g.* the ellipse, (a); helix, (b); and spiral, (c) – the ribbon sliceform can be synthesised by projecting each slice from the roof of each cell to this surface (though note the interference between of cells from opposing sides of the ellipse whose roofs overlap). Otherwise, only the ribbon geometry can be generated – as for the S-curve, (d), and line with an intrinsic twist, (e).

In these examples, the width of the ribbon strip is proportional to the width of the swept section designed in the previous chapter. It turns out that generation of the ribbon geometry is a useful tool to aid selection of an appropriate dynamic parameterisation of the CS, in particular for matching the variation in the cross-sectional radius to the dynamic spacing of the curve points. A balanced design is found when the span of the grid of ribbon curves – which visualises the variation in the structural geometry – matches the width of the ribbon strip – which indicates the variation in the swept section radius.

7.5 Summary

In this chapter the structural geometry of curve sliceforms has been examined in detail.

Generated from an arbitrary smooth basis curve, the slice planes of a CS lack any overall symmetry and the orientation of their intersection lines is unconstrained and do not initially appear to satisfy the conditions for geometric compatibility (in which no pair of intersection lines can meet). However, because successive slices of each set are closely aligned, the array of intersections is locally well-behaved and a compatible set of slices can be generated within this local domain.

Globally, the array of slice planes can be described by the set of curve points and normal vectors, and the array of intersections can be described by an array of aligned vectors and intersection points. As for an RS, a set of aligned vectors can be generated by taking the vector product of the normal vectors to each pair of intersecting slice planes. A suitable set of intersection points is less well-defined, but one option is to take the midpoint of a pair of points on each intersection which are found by projecting a perpendicular line (to the intersection) through the curve point on each plane.

These intersection lines form a set of non-congruent, non-concurrent fans upon each slice plane. Each intersection line has an origin point on the midline of each slice and an elevation angle from this reference line Successive pairs of intersections span a facet, the apex of which lies at their point of intersection. Each slice comprises a series of facets constructed outward from the midline (which may not be consistent with the 'direction' of each intersection for slot-generation purposes), and each intersection is 'clipped' by those preceding it (corresponding to the line of self-intersection between the slices of the opposing-set).

From an intrinsic perspective, a CS comprises an array of open-faced four-sided *skew cells*. Opposing facets of each cell converge on the 'inside' of the basis curve, but these pairs do not converge concurrently, causing the cell to inscribe a 'wedge' in which with one set of facets is truncated along the 'spine' of the cell. The edges of the cell (which are the lines of intersection) form a major and minor pair, spanning the cell in lengthwise and transverse senses, respectively, but are skew, for which these cells are so termed. This skewness is captured by construction of the *skew frame* which consists of the major edges and their their mutually perpendicular 'skew axis'.

With non-concurrent facet apexes, each skew cell is the geometric dual of a tetrahedron which lies just beyond the roof of the cell. The facets of this tetrahedron subtend the same facet angles as the corresponding facets of the skew cell and its vertexes locate the facet

apexes. For a primary cell, these vertexes are the origin of the minor intersections on each slice plane; the facet angles their in-plane inclination. These are computed in this local frame (*i.e.* relative to the curve points) by geometric construction of the tetrahedron. The origin and in-plane elevation of each subsequent intersection line are determined by construction of the appropriate skew 'super-cell', spanning the (non-adjacent) curve points of the intersecting planes, and corresponding 'super-tetrahedron'.

The structural geometry a CS is a projection from this array of tetrahedra. The roof of each cell is well defined and the geometrically feasible domain of the sliceform projects outward toward the basis curve. Two approaches to constructing a curve sliceform directly from the structural geometry have been developed; by location of a set of 'outer points' on each intersection line, or by projection of each cell to a ribbon surface generated from the basis curve. Where an LS embeds a planar scissor grid, and an RS a spherical scissor grid, a CS is scissor grid upon a ribbon – though note that the axis of rotation of each joint is not perpendicular to this ribbon surface.

As shall be explored in the following chapter, one consequence of the skew geometry of each cell is that each is now intrinsically rigid. This is unlike an LS or an RS where the prismatic and pyramidal cells are mobile in isolation, yet a CS retains the same global deployable characteristic. Now that their structural geometry has been formalised, the nature of their articulation can be investigated.

Chapter 8

Kinematics of a curve sliceform

8.1 Introduction

In Chapter 6 the generalised synthesis of deployable *curve sliceforms* from a prescribed basis curve was developed. The robustness and flexibility of this synthesis technique has been demonstrated by the generation of a range of illustrative examples, all of which are flat-foldable via a collapsing mode that is characteristically similar to the deployable motion of an RS. In Chapter 7 their structural geometry of a CS was investigated, determining their generalised form to be of an array of four-sided skew cells projected from an array of tetrahedra. The kinematics of their articulation is now investigated.

8.1.1 Deployable motion of a CS: Small-scale physical models

The small-scale models of the curve sliceforms synthesised in Chapter 6 are readily collapsed and deployed from a flat-folded stack of parallel slices. This deployable motion is characteristically similar to that of an LS or RS with the slices rotating synchronously about each slotted intersection as the sliceform is expanded and contracted, Figs. 6.9 (Helix), 6.10 (Ellipse), 6.17 (Planar spiral), 6.18 (Conical spiral), 6.19 (Line), 6.20 (Kink), 6.21 (S-curve) & 6.22 (Twisted line).

Under axial tension, a flat-folded CS deploys smoothly and reversibly along a well-defined motion path, then stiffens once the design expansion is reached. During motion, the cells generally expand and contract in unison, though this is not quite as coherent as an RS with some ‘lag’ in the articulation of each cell observed along some examples. Of course the CS along a line is simply an LS and flat-folds in both directions.

When collapsed, the alignment of the slices echoes the twist of the basis curve with the slices of the helix, conical spiral and intrinsically-twisted-line visibly turning toward alignment without fully resolving, the intermediary slices interposing their misalignment. Significantly, Some sliding and scissor-twisting of the slot pairs (explained later) is visible along many intersections though this does not seem to impair their usual rotational mobility.

For practical reasons, these models are constructed at smaller scale and from much thinner card than the toroidal designs in Part I. Consequently, the slices are more flexible which allows the sliceforms to be expand beyond their design expansion under transverse pressure[1]. The elasticity of the slices permits expansion until the outer cells become triangulated, the slices bending in line with the kinking mode modelled in Part 1, Fig. 8.1. The curve sliceforms follow suit, though some twisting of the slices is evident in the examples synthesised from non-planar curves. Interestingly the S-curve is the most readily over-expanded and can actually be flat-folded in the expanded sense, though there is significant misalignment of the slots and each slice pair visibly separate. The intrinsically-twisted-line provides the most resistance, the slices twisting significantly with only slight over-expansion, causing the sliceform to seize-up well before any cell triangulation can occur.

From fully collapsed, the deployment and over-expansion modes have a distinct character. The first phase of expansion proceeds smoothly with no apparent resistance until the design configuration, whilst the over-expansion mode requires deliberate action to first activate the bending of each slice, the sliceforms tending to spring back to the design configuration when released. There is also an audible ‘clicking’ of each intersection at the transition point as the slots reconfigure to accommodate the reversal in sense of rotation. This over-expansion is clearly compliant, but the first phase of deployment, which remains smooth and resistance-free, and is the primary focus of the investigations in this chapter.

8.1.2 Chapter outline

This chapter begins with an examination of the mobility of a CS and the additional modes of freedom required to admit the flat-folded condition. The folding motion of a single skew cell is then investigated by construction of a modified bar linkage model in which the necessary additional mobilities are explicitly incorporated. This informs the construction of a model of the compliant articulation of the cell and discussion of the overall folding motion of a CS.

[1] The deployable motion of the larger scale CS helix constructed from mountboard, Fig. 6.2, is as well-defined as the toroidal RS of the same scale and the sliceform cannot be over-extended.

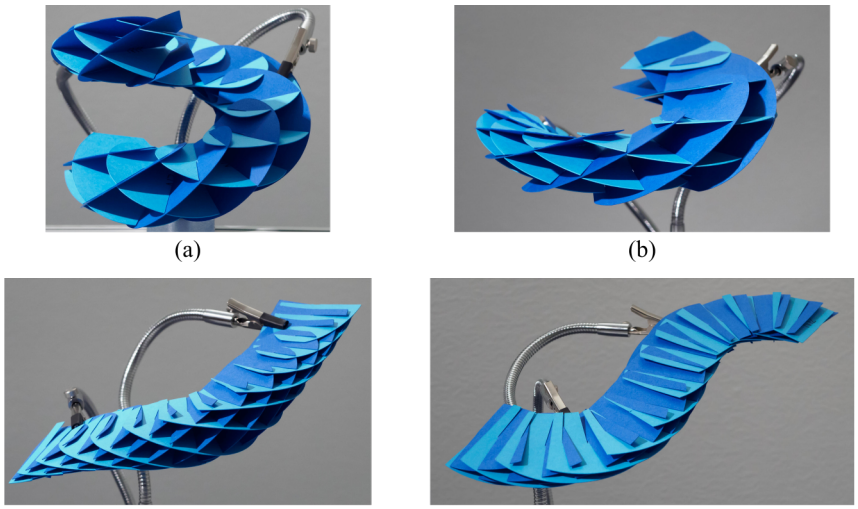

(a) (b) (c) (d)

Fig. 8.1 Maximum expansion of the CS constructed at small-scale. Under transverse compression (rather than longitudinal tension) the sliceforms may be forced to over-expand with the helix, (a), conical spiral, (b), and kink, (c), expanding until the outer cells are triangulated. Note that for the kink the straight segments expand until flat-folded, the curved portion cannot. The S-curve, (d), flat-folds on expansion with clearly visible misalignment of the slots.

8.2 Mobility of a CS

The smoothness of mobility of a CS, which echoes that of an RS, is somewhat unexpected owing to the generalised 'skew' geometry of each cell. Supposing that each slotted intersection behaves as a pure rotational hinge, each cell embeds a spatial 4R linkage. Unlike an LS or RS, the structural geometry of a skew cell has neither parallel nor concurrent edges and is therefore a three-dimensional 4R linkage, Fig. 8.2. Recalling that the mobility of a spatial linkage is given by the Grübler–Kutzbach mobility criterion in three-dimensions (Section 3.2, Eqn. 3.1), this linkage is determined to be degree 2 overconstrained.

$$m = 6(N - j - 1) + \sum_{i=1}^{j} f_i = 6(4 - 4 - 1) + 4 \times 1 = -2$$

Each link (*i.e.* facet) is coplanar to the edges it joins, has zero twist and, therefore, cannot meet the conditions for a Bennet linkage which is the only other condition under which a spatial 4R linkage is rigid-foldable[40], and so each skew cell is kinematically rigid[2]. Compliance which simply releases the frustration between cells, *e.g.* via the 'kinking' proposed for the

[2]The rigidity of a skew cell can also be deduced by noting that the roof of an extended contains a pair of degree-3 vertices at either end of the split 'spine'. Though the facets on either side of the spine are not directly

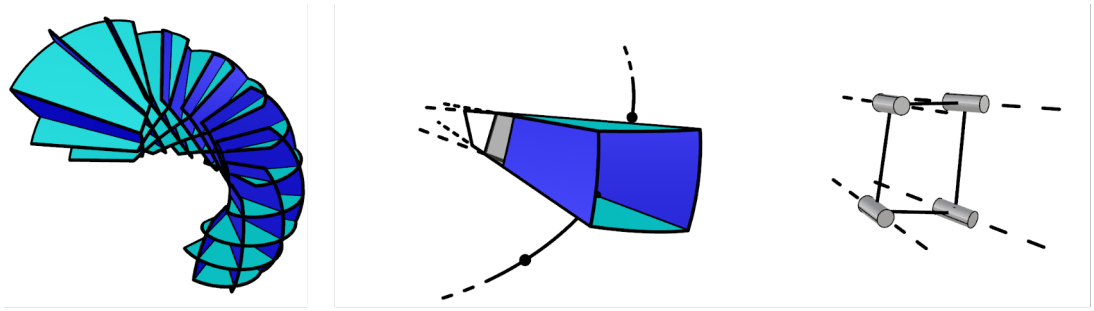

(a) (b) (c)

Fig. 8.2 A CS embeds an array of skew cells, (a)-(b). If each intersection admits revolute action, each cell embeds a 4R linkage, (c). However, the axes are neither parallel, concurrent, nor do they meet the conditions for a Bennet linkage and so each skew cell is rigid.

independently mobile pyramidal cells of an RS, is insufficient to enable mobility of a CS. Both the global compatibility of the array and local articulation of the each skew cell itself must be wrought by one or more, possibly compliant, modes of motion.

8.2.1 Flat-foldability of a CS

Similarly, the lack of symmetry would also seem to preclude the flat-foldability of a CS whose non-congruent, in-plane layouts of intersection lines cannot be aligned when they are coplanar (at best they are identical within each set but differ between them – helix – or mirror symmetric between them and variable along the curve – planar curves). When overlaid, the slices cannot be oriented to align all pairs of intersection lines simultaneously and many are misaligned, yet this apparently incompatible flat-folded condition it is readily admitted without any apparent strain of the slices.

As already identified, the 'kinking' mode which enables the mobility of a RS does not affect the structural geometry of each cell and only serves to release the frustration between them. It does not affect the mobility of each individual cell. Nevertheless, it remains likely that such a mode is active, particularly given that characteristically similar bending of the slices is visible on over-expansion. In practice, the continuous bending of each slice will have a second order effect on the geometry of each cell but this will not affect their rigidity[3]. More significantly, bending modes cannot contribute to the flat-folded condition in which the slices are evidently planar. It is clear, then, that the flat-folded condition must be enabled by

connected, permitting each vertex to be mobile in isolation, the other vertex prevents their separation and so the pair of vertices are rigid. Truncating the cell so that it is open-ended does not alter this kinematic geometry.

[3]the angle spanned by each facet facet may reduce slightly under conical bending but the cell will remain skew

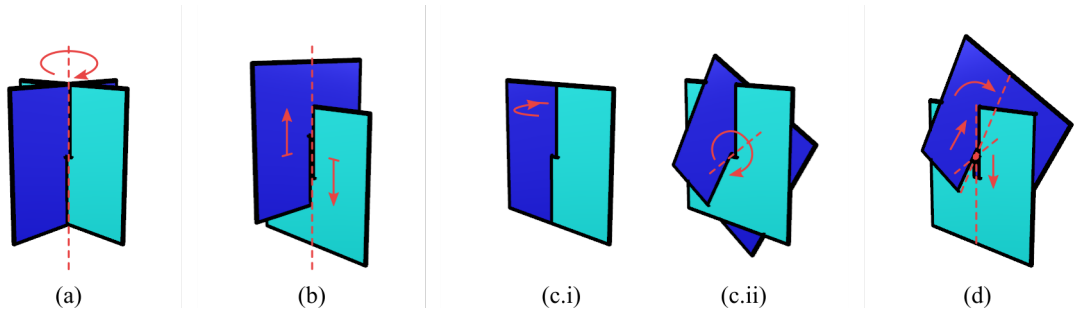

Fig. 8.3 The usual mode of freedom permitted by each pair of interlocking slots is rotation about their line of intersection, (a). Of course the slices may also slide apart, (b). However, when the slices are rotated to coplanar, (c.i), the rotation mode bifurcates and rotation may instead be admitted about the slices' common normal in a *scissor-twist* mode, (c.ii). By combination of sliding and scissor-twisting a pair of coplanar but misaligned slots can remain interlocked, (d), requiring only that their slot axes overlap.

additional mobility of the interlocking slots themselves which have so far been presumed to act as revolute joints.

Insight is provided by focusing on the flat-folded condition of a CS. From examination of the misaligned slots in a physical model, two additional mobilities are revealed: *slot-sliding*, and *scissor-twisting*. Slot-sliding is simply the partial disengagement of any pair of interlocking slots, as illustrated in Fig. 8.3(b). The second mode, scissor-twisting may occur when the slots become coplanar and can then rotate about their common normal, Fig. 8.3(c). By combination of these these modes enable any pair of misaligned slots in coplanar slices can remain interlocked provide that they overlap, Fig. 8.3(d). As these modes also do not incur any bending strains in the slices (other than the slight 'stepping' needed to accommodate their finite thickness), the flat-folded condition is geometrically compatible and a CS is, at least, bistable.

8.3 Articulation of a skew cell

When flat-folded with coplanar slices, the sliding and scissor-twist modes identified in the preceding section accommodate the misalignment of the slots. However, neither slot-sliding nor scissor-twisting are compatible at any expanded configuration – slot-sliding is prevented by the convergence of each pair of adjacent intersections and scissor-twisting is a bifurcation of the motion of each pair of slots which only occurs when the slots are coplanar. Even with these modes a CS remains kinematically rigid. It might be expected, then, for a CS to undergo a strongly bistable transition from deployed to flat-folded in which the slotted

slices suddenly snap into their scissor-twisted condition. However this is not the case, the sliceforms deploy smoothly and without resistance, the misfit of the slots seeming to accrue steadily throughout motion.

To demonstrate how this is able to proceed a simplified model of the deployment of a CS is now constructed. It is clear that the articulation of a complete sliceform is a complex motion with the compliances acting to resolve multiple geometric incompatibilities. Even determination of the slice positions in the flat-folded condition is non-trivial with the slices sliding and rotating just enough to accommodate whichever pair of slots are the worst-fit. Construction of a kinematic model of a full sliceform is therefore beyond the scope of this thesis but the motion of a single skew cell can be examined to elucidate some basic insights into the nature of the compliance required.

To further aid tractability, a primary cell of a helical sliceform is chosen for study. The helix is the natural first extension of a two-dimensional circle (an RS) to a three-dimensional spatial curve and the constant curvature and twist along its length means that the cells in each row are identical, and each primary cell anti-symmetric. As will be shown, this symmetry greatly reduces the degrees of compliance required for flat-folding of that cell in isolation enabling this model to be analysed by geometric construction.

The specific helix used in this section here has radius $R = 6$ and pitch $c = 10$, with a structural architecture of 12 slices per turn and $\theta^{\pm} = 45°$, and (constant) swept section radius $r = 4$. For each primary cell – *i.e.* where $j = i + 1$ – the skew parameters are:

$$\left.\begin{aligned} &\phi_{i\to j} = 30° \\ &s_{i\to j} = s_{j\to i} = R = 6 \\ &\alpha_{i\to j} = \alpha_{j\to i} = \tan^{-1}\left(\frac{c}{2\pi R}\right) = \tan^{-1}\left(\frac{10}{12\pi}\right) = 14.86° \end{aligned}\right\}$$

yielding facet angles:

$$\eta^{+}_{i,i} = \eta^{+}_{j,i} = 25.67°$$
$$\eta^{-}_{i,j} = \eta^{-}_{i,i} = 14.56°$$

8.3.1 Misfit model of a helical skew cell

Given the structural geometry of a helical skew cell, derived in Chapter 7, an equivalent bar linkage in which each facet is a rigid bar and each intersection is a revolute joint can be immediately constructed, Fig. 8.4(a)-(c). As identified above, this linkage is kinematically rigid and by application of the Grübler–Kutzbach mobility criterion[40] the skew cell is

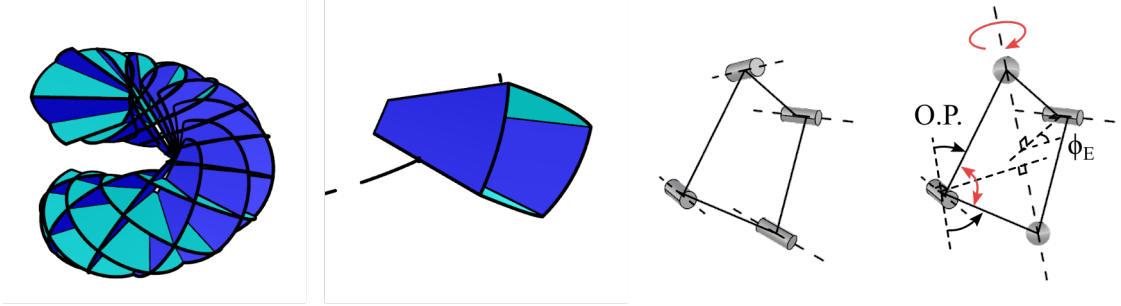

(a) (b) (c) (d)

Fig. 8.4 Modified-linkage model of the compliant articulation of a skew cell. A primary cell of a helical sliceform, (a) - (b), is skew and its embedded linkage, (c), is rigid. To model the additional mobility afforded by the slots, the revolute joints along the minor intersections are replaced with spherical joints, (d). This is sufficient to capture the flat-folded condition of this anti-symmetric linkage, which now has two degrees of freedom: a shear-mode articulation as the cell opens and closes, and relative rotation of the left and right halves about the *swivel axis* through the two ball joints. For tractability these are parameterised by an *opening proportion*, 'OP', which describes the proportional rotation of each bar from flat-folded, (OP= 0 when flat-folded, OP= 1 in the design configuration), and ϕ_E which is the signed angle subtended by the pair of lines drawn across the face of each half of the cell, each mutually perpendicular to the major intersection and swivel axis.

shown to be overconstrained by degree 2:

$$m = 6(N-j-1)+\sum_{i=1}^{j} f_i = 6(4-4-1)+4 = -2 \tag{8.1}$$

This means that three additional degrees of freedom must be added for the skew-cell linkage to become mobile.

It might be considered that sufficient sliding could enable the skew cell to become pyramidal, and thus rigid-foldable, but the required sliding distance (equal to the corresponding edge lengths of the tetrahedron located at the cell roof) is both significantly more than observed in any physical model and cannot enable folding of the array of cells because this condition cannot be met for adjacent cells simultaneously. Instead, some additional mobility is added by replacing the revolute joints along the minor edges with spherical joints, Fig. 8.4(d). Each allows three degrees of rotational freedom, adding two to the linkage. From examination of physical sliceforms, scissor-twisting is observed to be most prominent at the outer intersections, and so the revolute links along the minor edges are replaced with spherical joints for a total of four additional degrees of freedom overall. This modified linkage, which remains anti-symmetric, has two degrees of freedom: a shear-mode articulation as the cell opens and

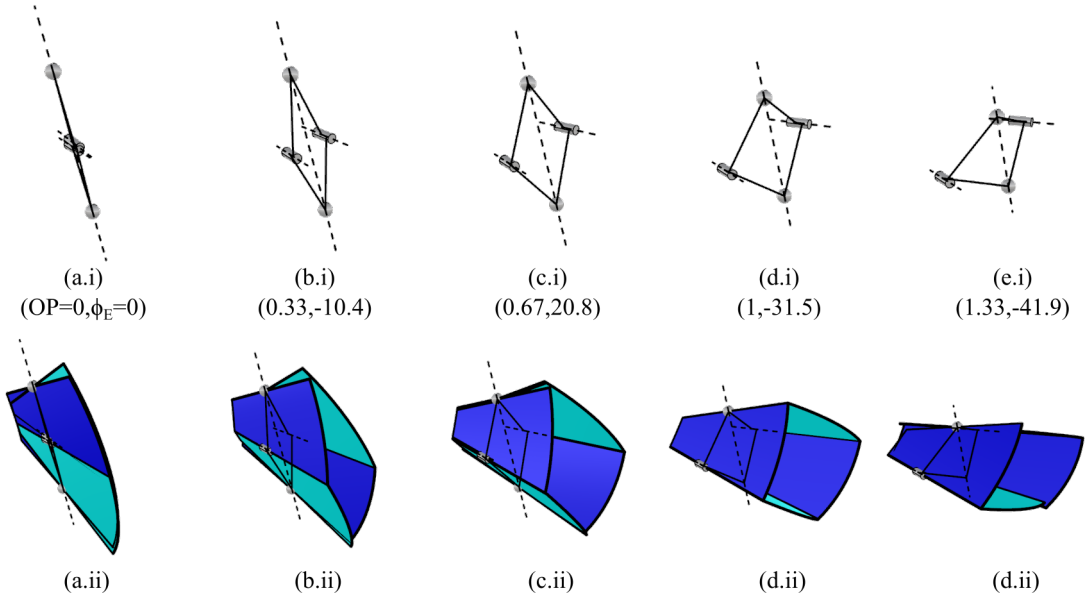

Fig. 8.5 Articulation of the modified linkage and corresponding skew cell. Top: Sequence of articulation of the modified bar linkage along a linear path from flat-folded, (a), to the design configuration, (c), and over-expanded, (d). Bottom: The facets are mapped onto the corresponding bars to reconstruct the skew cell at each configuration.

closes, and relative rotation of the left and right halves about the *swivel axis* through the two modified ball joints.

The configuration of this modified linkage is parameterised by the opening proportion of the left hand links, OP, which is the proportional rotation of each link from vertical toward the design inclination (when $OP = 0$ the links are vertical, when $OP = 1$ the links align to the orientation of the slice planes in the design configuration, $OP > 1$ corresponds to rotation beyond the design configuration toward horizontal); and the angular offset of the two halves about the swivel axis, ϕ_E, defined as the angular offset of the lines spanning from each major axis to the swivel axis and mutually orthogonal to both (this does not quite coincide with the skew angle of the cell, which is the angle between the major axes, but has a similar value and is a more tractable input parameter).

This modified linkage can articulate freely through its two-dimensional configuration space (enacted by geometric construction using Grasshopper for Rhino), and, at each configuration, the facets of the original skew cell are mapped back onto their corresponding bars to reconstruct the (now articulated) skew cell, Fig. 8.5. The facets are placed onto each bar so that the major intersection axes remain in-plane. In essence, this models a cell with pure revolute actuation of the major intersections and off-axis rotation along the minor

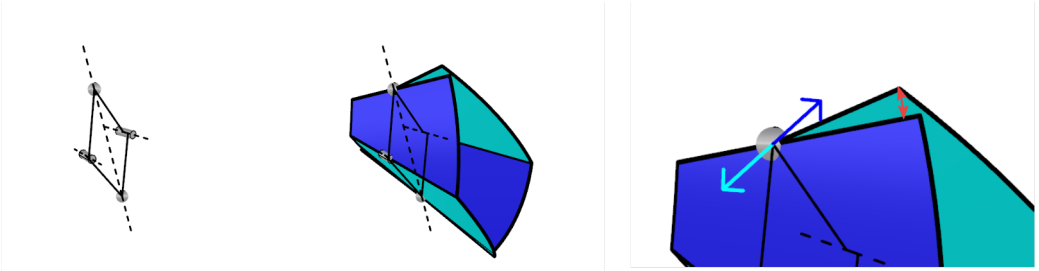

(a) (b) (c)

Fig. 8.6 At each configuration of the modified linkage – shown here for $(\text{OP}= 0.5, \phi_E = -15°)$ – the cell facets are mapped onto their corresponding links to reconstruct the articulated cell and determine the misalignment of their minor edges, (a)-(b). The edges are in contact so this misalignment is captured by the rotation between them, (c), with the (equal-and-opposite) rotation vectors indicating the rotation of each facet's minor edge from the adjoining facet.

intersections where the geometric compatibility of the cell is revealed by the (mis-)alignment of the facet edges.

Note that the motion of the modified linkage is dependent on the position of the joints along the minor edges of the skew cell. To capture pure scissor-twisting, they are placed at the midpoint of each intersection line to coincide with the contact point between the two slots.

Facet edge misalignment

The additional degrees of freedom afforded by the spherical joints along the minor edges allow the facets of the reconstructed cell to rotate independently, as can be seen in Fig. 8.5. However, the slots are only aligned when these edges are flush with their misalignment corresponding to the geometric misfit of the cell. The edges remain in contact at each spherical joint, so the misalignment can be described by the rotation from one edge to the other, Fig. 8.6. By symmetry, the upper and lower halves of this anti-symmetric helical skew cell are identical, so it is sufficient to examine the misfit along only one of the minor intersections.

Mapping the variation in this misfit throughout the configuration space confirms that the cell is compatible (with zero misfit) in the design configuration only, Fig. 8.7. The edges and slots are otherwise misaligned. The misfit landscape does feature a relatively steep 'valley', which is suspected to affect the well-defined motion of a CS. This valley follows a curve that deviates only slightly from a straight line from flat-folded to expanded configurations, so the rotation between the two cell halves varies broadly in proportion with the opening proportion. However, though the offset of the two halves about the twist axis is zero at the collapsed

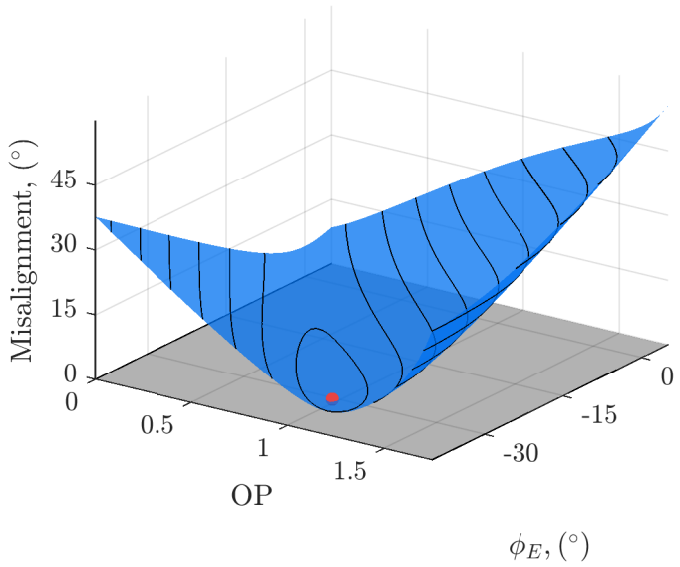

Fig. 8.7 Variation in the magnitude of the misalignment of the facet edges along the minor intersections of the reconstructed helical skew cell throughout the configuration space of the modified bar linkage. The facet edges are aligned at only the deployed, design configuration – highlighted by the dot – confirming that the skew cell is rigid and monostable if only revolute action is allowed by each slotted intersection.
Data collected and plot generated using MATLAB[50] to iterate through the configuration space, at each iteration: writing the configuration to an text file, which is read into Grasshopper/Rhino via a custom Python script in the Python component (which sets the configuration of the model causing the linkage geometry to be recomputed, facets remapped and edge offsets measured), and recording the edge offset results received via an output text file generated by secondary Python script in Grasshopper.

configuration, Fig. 8.5(a) so that the major edges and twist axes are coplanar, the major axes are not parallel, remaining offset, and the slices have not simply unwound along the basis curve to a configuration where all major axes are coincident. The major intersections between adjacent pairs of slices are rotationally staggered and the stack of slice remains twisted.

Further insight is gained by examining the misfit from the perspective of each slice. Extending the facets so that the slots can be formed, the misalignment of each slot from the interlocked slice can be decomposed into two orthogonal components, Fig. 8.8: an in-plane component in which the interlocked slice rotates within its plane, and thus through the slot; and an out-of-plane component in which the interlocked slice rotates out of its plane, 'through' the material of the first slice. The in-plane component can be accommodated by the slot (notwithstanding that the other slot may no longer be compatible), the out-of-plane component cannot. It follows that compatibility is dictated solely by the out-of-plane

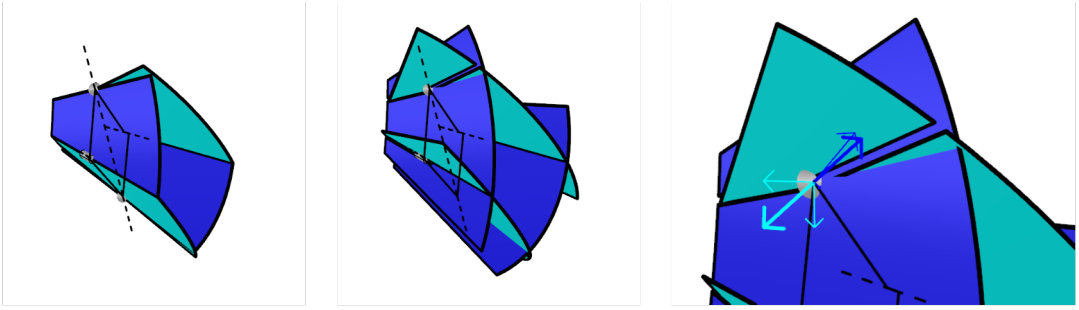

(a) (b) (c)

Fig. 8.8 The misfit along the minor edges can be decomposed into compatible and incompatible components. Extending the facets so that the slots can be formed, (a)-(b), the misfit can then be decomposed into two orthogonal components which describe the fit of the opposing slice through each slot: an in-plane component which is the scissor-twist of the slice through; and an out-of-plane component which is the misalignment of the opposing slice to the slot, (c). In this configuration the out-of-plane misfit of the light blue slice from the slot in the dark blue slice is very small (the light blue slice is almost aligned to the axis of the slot in the dark blue slot); the out-of-plane misfit of the dark blue slice from the slot in the light blue slice is non-zero and this slot is misaligned.

components, with compatible configurations of the interlocking slots (whether aligned or not) located wherever the out-of-plane misfits are simultaneously zero.

Plotting surfaces of out-of-plane misfit for each slot, Fig. 8.9, compatible configurations are located at the intersection of their contours of zero out-of-plane misfit. Reassuringly, this model predicts two geometrically compatible configurations for the primary helical skew cell: the design configuration where the slots are aligned; and the flat-folded condition where the slices are coplanar and only in-plane misalignment is required, *i.e.* scissor-twisting. At all intermediate and over-extended configurations, one or both out-of-plane components of the misalignment are non-zero, confirming that no rigid-folding transition path exists for this model. Also plotted are the zones of $\pm 3^\circ$ of out-of-plane misalignment, the areas contained within these extended boundaries do overlap, indicating that, for this cell, only a small amount of additional compliance is required to enable the bistable transition between deployed and flat-folded, scissor-twisted configurations.

8.3.2 Accommodation of out-of-plane misfit by ‘slot splaying’

The misfit model constructed in the previous section captures the bistability of an isolated primary helical skew cell by demonstrating that the slots are compatible at the flat-folded and design configurations, with (strain-free) scissor-twisting in the former. However, this model

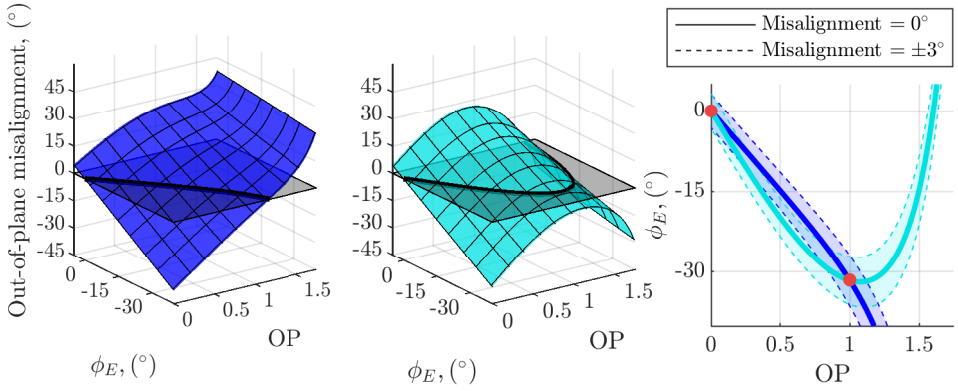

Fig. 8.9 Surfaces of out-of-plane misalignment of the interlocking slice from each slot. The zero-contours describes a motion path along which the interlocked slice remains aligned to the slot and only scissor-twists, and is therefore geometrically compatible. The contours for each slot intersect at two points, the flat-folded and design configurations in which both slots are geometrically compatible. The contours diverge between these points, indicating that scissor-twisting is insufficient to enable the deployable transition. Also indicated is the range of motion that can be achieved with only a slight misalignment, with just a few degrees of misalignment sufficient to enable the folding action.

does not provide much insight into how the transition actually proceeds. As highlighted, the contours diverge only slightly at intermediate configurations, and only a small degree of out-of-plane misfit is required to form a deployment path. However, the out-of-plane misfit is still only a relatively rudimentary measure of the incompatibility and some mechanism by which this can be accommodated is still required. Consideration must also be given to the fact that the motion path of a complete sliceform will likely be a compromise across the cells and that this may not follow the lowest-misfit solution for this cell.

Re-examining a physical CS, the scissor-twist in the flat-folded condition is clear but we can also observe that it accrues steadily through motion. This is possible partly due to some inherent ‘play’ in the slots, but principally accommodated by some slight ‘splaying’ of the flaps flanking them under action of the impinging slice. This out-of-plane bending allows the slot to achieve the necessary out-of-plane misfit, ultimately becoming the ‘stepping’ mode required to accommodate the finite thickness of the slices. The misfit model is now extended to include this out-of-plane bending and capture a realistic model of the compliant collapse and deployment of the cell. This serves as an ‘upper bound’ solution in which other modes of compliance, notably slot-sliding (which is not included), will act to reduce the compliance required by this splaying mode.

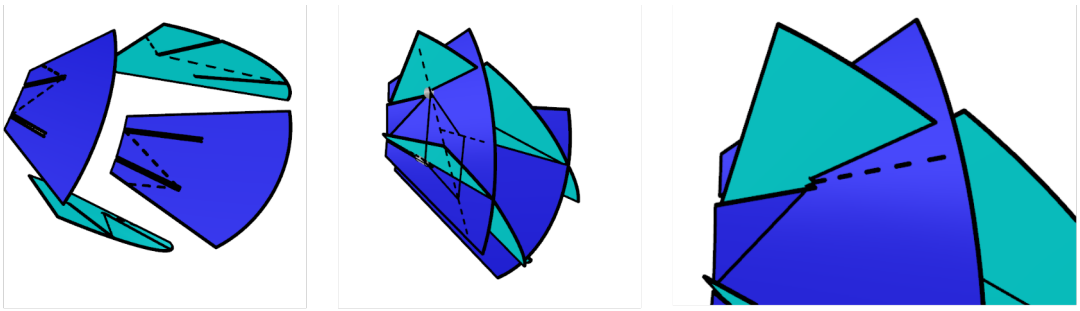

(a) (b) (c)

Fig. 8.10 A simplified model of the 'splaying' action of each slot is construed by placing a diagonal *twist line* across each flap and extension, shown in exploded view in (a). At intermediate configurations, the out-of-plane misalignment of the slices and slots is accommodated by splaying of each slot under action of the impinging slice, (b) and detail in (c) where the dashed line is the slot axis in the blue slice. Note the out-of-plane deflection of the dark blue flap at back-left and light blue flap at front-right.

Addition of flap twisting to kinematic model

Inspired by an approach to modelling the bending-activated modes of a pleated sheet[73], a simplified model of this slot splaying mode is achieved by placing a crease across each flap to allow it to be deflected out-of-plane by the impinging slice. From observation of our physical models, a *flap twist line* that runs diagonally across each flap is realistic, allowing the slot edge to deflect according to the out-of-plane misalignment of the interlocked slice whilst preserving the geometry of each major slot, Fig. 8.10.

Of course, depending on the direction of the misfit, the inner flap may actually remain planar, with the flap on the outside of the slot being deflected instead. These are included in the model by simply extending the planform of each facet to include a portion of the next facet – a 'tab' – with a realistic *tab twist line* generated by mirroring the flap twist line across the minor intersection.

Though the orientation of these twist lines is somewhat arbitrary, they produce a reasonable, discrete representation of the distributed bending mode from which to capture the variation in bending throughout motion. These flaps are also dependent on the orientation of the slots. If the slots are reversed, the flaps lie on opposite sides of each slice and the twist lines follow suit. Characteristically similar results are attained if this is the case.

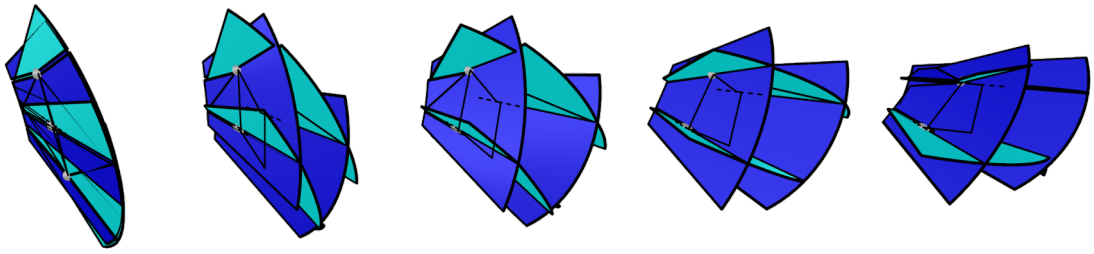

(a) (OP=0,ϕ_E=0) (b) (0.33,-10.4) (c) (0.67,20.8) (d) (1,31.5) (e) (1.33,-41.9)

Fig. 8.11 Sequence of articulation of the helical skew cell with the out-of-plane misfit of each slice from each slot accommodated by splaying of the slots under action of the impinging slice. Note the pure scissor-twist in the flat-folded condition, (a), and reversal of sense of deflection from (c)-(e).

Facet twist

At each intermediate configuration of the misfit linkage, the cell is reconstructed and each deflected flap rotated so that its slot edge lies on the surface of the impinging slice[4]. This can be achieved by rotation of the deflected flap in either sense, but it is usually clear from the relative orientation of the slices which solution is physically likely: the impinging slice deflecting the flap toward the exterior (and not interior) dihedral angle with the other deflection usually having a much greater magnitude[5]. Importantly, this extended model qualifies that folding is kinematically admissible via compliant action of the slots (with reasonable deflections compared to observations) and captures a realistic motion of the cell throughout the configuration space, Fig. 8.11.

For completeness, the flap deflection demanded at each configuration is plotted in Figure. 8.12. Each facet remains planar when the corresponding out-of-plane misalignment is zero, so the contours of zero-deflection are identical to the contours of zero out-of-plane misfit. On one side of this contour, the facets are undeflected; on the other the deflection maps to a curved surface. The sense of the deflection inverts when the slices are orthogonal, which is in the vicinity of the design configuration. This corresponds to the 'snapping' phenomenon

[4]The deflection angle is computed automatically in Rhino/Grasshopper by locating the points of intersection of the circle that is swept about the speculated twist line by a single point on the slot edge of the flap (the slot edge sweeping out a cone) with the adjacent slice plane in that configuration. This usually produces two solutions. When they span 'zero' deflection the flap is deflected, otherwise not.

[5]Strictly, the deflection sense is set when the distortion is initiated and is thus dependent on the path taken to reach each configuration. It is possible for the initial 'exterior' deflection of the flap to become the 'interior' sense on further rotation but without first flattening. This is only of practical consequence when the slices are close to orthogonal, when both solutions are then realistic and similar in magnitude, with the dihedral-based approach valid for most of the configuration space.

wherein the splaying of the slots must first reverse before the cell can expand beyond the design configuration.

Generalisation to non-helical skew cell

This mode of twisting compliance can be constructed for any skew cell geometry to determine an estimate of the bending requirement throughout a similar two-dimensional, twisting-only configuration space. In fact, the combination of the scissor-twisting and slot-splaying modes allow each intersection to act much as a ball joint over a small range of motion. Any skew cell will therefore be mobile via this compliance. However, without (anti-)symmetry, the left and right halves are unlikely to have the same span and scissor-twisting alone will not be able to enable flat-foldability and the cell will triangulate. From our physical sliceforms, it seems that this is resolved in the collapsing sense by a small amount of slot-sliding. The addition of both additional twisting modes along the major intersections and some slot-sliding significantly increases the freedoms of the cell, and our simple parameter-space mapping approach rapidly becomes infeasible.

It also seems that sliding and off-axis rotation of all four slot pairs ought to enable any skew cell to be bidirectionally-flat-foldable in isolation. However, the majority of our models are not. It is suspected that the one-way deployability of a CS likely arises from a similar variation in the compatibility of the interaction between cells to that exhibited by an RS, especially given the visible bending of the slices on over-expansion.

8.3.3 Discussion of a kinematic model of a complete CS

As identified in section 8.2, a curve sliceform is both locally rigid (due to the skewness of each cell) and globally overconstrained. Yet, the small scale models constructed in Chapter 6 are self-evidently deployable, arising from the imperfect action of each intersection and the compliant deflection of the slices.

The model developed in this section has sought to interrogate the nature and scale of the imperfect action which is required for folding of each cell and verifies that the local deformations are realistic and reasonable in magnitude. However, the overall folding motion of a CS is much more complex. Even with addition of out out-of-plane bending, the continuity of each slice enforces identical in-plane action (sliding and rotation) of contiguous facets. This couples the motion of adjacent cells so that their action no longer simply follows the path which minimises deformations locally, but instead the path which minimises the overall strain energy penalty incurred across the array of cells.

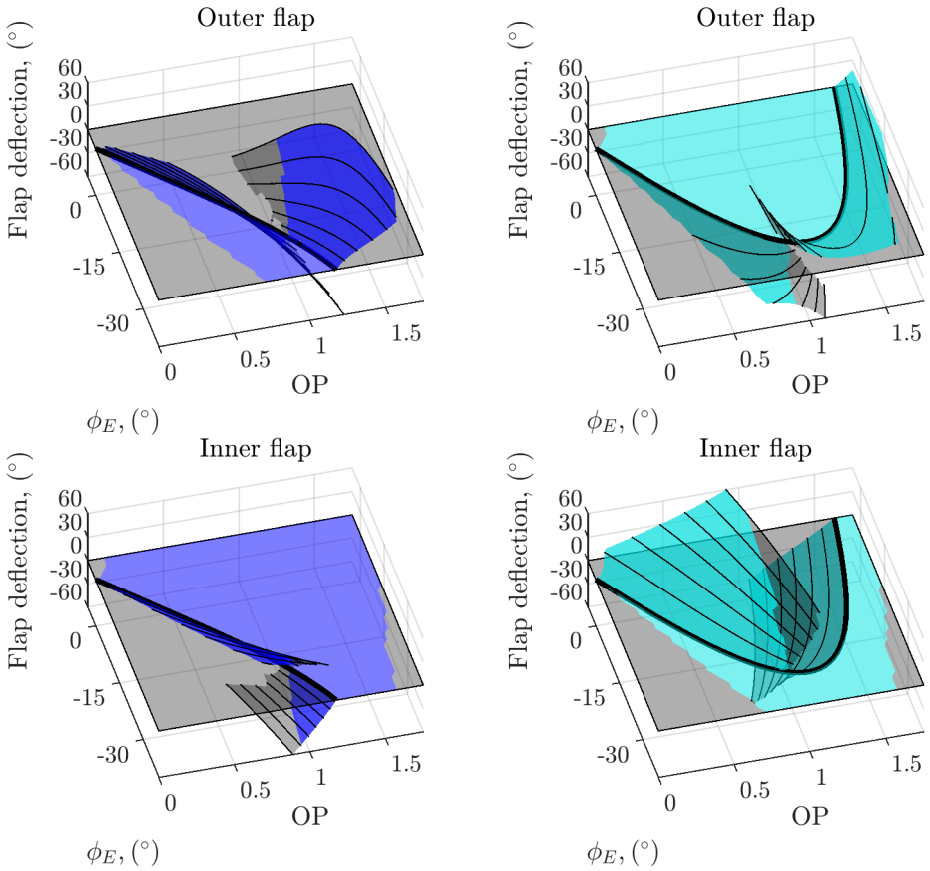

Fig. 8.12 Surfaces of flap deflection to accommodate the out-of-plane misfit of the slices and slots at each configuration. The contours of zero deflection are identical to the contours of zero out-of-plane misfit in Figure 8.9, as expected. Each flap is only deflected when the misfit causes the interlocking slot to impinge upon it, and therefore remains undeflected on one side of the contour. The sense of each deflection inverts from contraction to over-expansion, corresponding to the 'clicking' observed in the small-scale models. The coloured solutions indicate the deflection in an 'exterior' sense, the greyed solutions are viable with deflection occurring in the unexpected sense (depending on the path taken to reach that configuration).

A similar, purely geometric model of a complete sliceform would be intractable due to the large number of degrees of motion that must be resolved. A stiffness-based formulation, such as that used by Schenk and Guest to model the out-of-plane action of a folded shell structure[73], via analysis of an equivalent bar structure with appropriate spring stiffnesses, is likely to be required. Further consideration would also be required to determine how to capture the off-axis twisting and slot-sliding of the intersections within the equivalent bar mechanism, which is beyond the scope of this thesis. The true motion is further complicated by friction which generates dynamic internal forces but does not incur a strain energy penalty.

Nonetheless, slice bending surely plays a significant role in enabling global folding, as for an RS, and this is suspected to be the likely cause of the resistance of each CS to over-extension, particularly given that visible bending of the slices is observed in this mode.

8.4 Summary

A curve sliceform is kinematically rigid. This stems from both the overconstrained nature of the array of slices and also the intrinsic rigidity of each skew cell. Despite this, small scale models are readily flat-folded and deploy smoothly under longitudinal tension.

Examination of the flat-folded condition, which is geometrically incompatible due to the misalignment of the overlaid layouts of intersection lines, reveals that this state is enabled by scissor-twisting (in-plane rotation of a pair of coplanar slices about their common normal) and slot-sliding, which allow pairs of misaligned slots to remain interlocked without incurring elastic deformations. Hence, the flat-folded condition, which is geometrically incompatible under the theoretical articulation of a sliceform by revolute action of the intersections, is nonetheless strain-free. A CS is, at least, bistable.

The articulation of a single skew cell – specifically an anti-symmetric primary helical skew cell – has been examined by construction of an equivalent linkage modified to model off-axis rotation about each minor intersection. The geometric misfit of the cell is assessed by mapping the facets onto the modified linkage, demonstrating that scissor-twisting of the minor edges is sufficient to admit the flat-folded condition. To enable the transition, each slot must admit some out-of-plane rotation of the interlocking slice, which is achieved in practice by ‘splaying’ of the slots via deflection of the flaps flanking them. A simplified model of this action is constructed by addition of a ‘twist’ line across each flap. This model demonstrates that local deflection is sufficient to enable a compliant transition from flat-folded to deployed, and *vice versa*, in turn verifying that cell folding is admissible by some slight, localised, compliant action.

The model constructed in this investigation only captures the flat-foldable behaviour of an anti-symmetric cell, which requires scissor-twisting about only two of the intersection lines. The action of a more general cell would involve scissor-twisting about all intersection lines, and realistic motion likely also includes slot-sliding. These additional modes make a purely geometric approach intractable.

Overall, it has been demonstrated that the articulation of a curve sliceform is a compliant, bistable transformation between collapsed and deployed configurations, enabled by off-axis rotation and sliding along each intersection line. This informal 'play' has been examined and verified for a simple case via a simplified but realistic mode of action, demonstrating that local deformations are sufficient to enable a large range of articulation of each skew cell.

It is intuitively clear that the compliance required by each cell is dependent on the proximity of each cell's geometry to its rigid-folding pyramidal counterpart. A more robust approach to the design and parameterisation of a CS – versus the aesthetic proxy used to generate 'balanced' designs here – could perhaps be based on an objective measure of the skewness of each cell.

Chapter 9

Summary, Conclusions and Future Work

Sliceforms are volumetric, honeycomb-like, papercraft structures assembled from an array of interlocking, cross-sectional, planar slices. They have an interesting threefold geometric hierarchy – the *global volume* describes the overall shape, the spatial layout of slice planes is the *structural architecture*, and the in-plane *slice geometry* comprises the cross-sectional planform with slots along and to the midpoint of each intersection line – and are typically used to make simple sculptural models. With slotted intersections acting as revolute joints, a sliceform embeds a spatial mechanism, and a lattice sliceform is bi-directionally flat-foldable. Inspired by the discovery that a particular sliceform torus is deployable at mid-assembly with an unusual one-way flat-foldable characteristic, the central objective of this thesis has been the investigation of this folding behaviour and synthesis of new folding sliceforms toward the design of novel deployable structures. Deriving from the torus, *Rotational sliceforms*, *RS*, which (when disconnected) can be articulated about their central axis of rotational symmetry, have been investigated in Part I. In Part II this has been generalised to the design of deployable *curve sliceforms*, *CS*, which are generated from a spatial curve. The main findings are now summarised.

9.1 Rotational sliceforms

The torus is an example of a rotational sliceform whose structural architecture consists of two sets of inclined slices arranged at regular intervals about a central axis of symmetry. The *structural geometry* of an RS comprises a spherical array of intersection lines. With rotational mobility about each intersection line, the sliceform, therefore, embeds a spherical linkage – a spherical single-layer scissor grid. The flat-foldability of an incomplete RS is dependent on the intrinsic flat-foldability of each constituent pyramidal cell: a symmetric

RS is flat-foldable; an asymmetric RS is not. The extrinsic motion of each slice plane is captured by the symmetric articulation of the row of midplane cells, which form a chain of spherical scissor links. However, this articulation is incompatible with the intrinsic geometry of each slice, establishing that rigid-folding is not viable. A compliant-folding mode in which the slices bend out-of-plane is suspected. A simplified geometric model of this mode is constructed by removing the coplanarity constraint on contiguous facets, allowing the slices to 'kink' across each intersection line and preserving, instead, the intrinsic geometry of each cell. The geometrical compatibility of a symmetric RS when flat-folded and deployed is verified, indicating that an RS is bistable. The characteristic features of the deployment are captured by the variation in each planar defect: the shallow variations in each defect from flat-folded to deployed are readily accommodated by the slices, the initial expansion therefore proceeding smoothly; much larger deformation of the slices is required to accommodate the rapid increase on over-expansion, this causes a rapid increase in stiffness and the structure to 'locks-out'. An asymmetric RS is monostable, though slice compliance can enable some mobility. The range of mobility that can be achieved within a given deflection limit of the slices decreases with increased asymmetry.

A set of representative rotational sliceforms with volumetric, shell-like and hollow geometries have been designed and manufactured to illustrate the range of deployable structures that can be synthesised using the symmetric RS architecture.

9.1.1 Future work

The analysis conducted in Part I verifies that a symmetric RS is flat-foldable, articulating via a bistable transition between strain-free collapsed and deployed configurations. This can be translated to the design of a deployable structure with a more conventional structural form by collapsing the slices to a set of curved, scissor-jointed bars, as has been achieved by Muñoz-Vidal et al[61] (Fig. 4.9). They have only considered the construction of a hemispherical dome, but deployable bar structures of more general shape could be generated by design of the equivalent RS shell of zero thickness. Before such structures could be used in real-world scenarios, careful detailed design and analysis of their performance under loading would be required.

When constructed at a tabletop-scale, these structures are readily deployed by manual action. An avenue for practical development would be the design of a distributed deployment system, perhaps composed of pneumatic pockets or wires spanning each cell, to enable the structure to be deployed and collapsed automatically. Alternatively, a system of appropriately

tuned spring elements might be used to produce a pop-up effect in which the RS requires constraint in the flat-folded configuration but automatically deploys to the design configuration when these are released.

In this work the slices have been planar by default. However, with an RS embedding a spherical scissor-grid, an intriguing direction for future investigation would be the design of RS-derived structures composed of slices (or, more practically, bars) with an initial (fixed) curvature or sequence of kinks so that adjacent facets($\tilde{\text{b}}$ars) are no longer coplanar. Such structures would be analogous to angulated elements for scissor structures and would cease to be flat-foldable, but this may enable the bistable characteristic to be tuned, either to mitigate or to emphasise it, or might even result in a different mode of deployment, perhaps akin to the radial motion of Hoberman's Iris dome (Fig. 3.11(d)).

Alternatively, the initially-kinked elements could be designed such that they must be flattened as they are interlocked, introducing a pre-stress to the structure which might be designed so to increase or decrease the bistable effect, and/or improve the rigidity of the deployed sliceform. Analysis of the folding action of such a structure would require introduction of the associated strain energy into the simplified model, which could be readily achieved by inclusion of a representative rotational spring across each intersection.

9.2 Curve sliceforms

The key to the compliant-deployability of a symmetric RS is that their structural geometry embeds a grid of scissor links whose symmetry assures flat-folding and which, though kinematically rigid, sufficiently approximates a rigid-folding linkage so that only small deflections of each slice are required to enable the bistable transition across a large range of motion. That such designs perform so effectively as folding structures suggests that it might be possible to generate other 'almost-rigid-folding', deployable structures with more general geometric forms.

This has been explored in Part II through the development of a technique for synthesising a sliceform along a smooth basis curve inscribing a corresponding swept tube, so-called curve sliceforms. The synthesis of a CS along a simple curve, such as a helix or an ellipse, is relatively straightforward, though steps must be taken to ensure the geometric feasibility of the slices explicitly. If the curve has a large variation in curvature, additional parameters are required to generate a well-conditioned design in which the slices and array of cells remains relatively self-similar along the length of the curve, which is pursued in anticipation of minimising any misfit during folding of the assembled model. This approach is robust,

though care must be taken when synthesising a CS from any curve with straight segments or any reversal of curvature. Small-scale models of sliceforms generated along a helix, an ellipse, a planar spiral, a conical spiral, a 'kink', an 's-curve' and a 'twisted line' are all found to retain the one-way deployability of an RS, functioning as viable deployable structures.

Examination of the structural geometry of a CS reveals their general form to be of an array of four-sided *skew cells*, each a projection from the tetrahedron inscribing the non-coincident apexes of its facets. The local structural geometry of the array of intersection lines and cells is found by geometric construction of the appropriate tetrahedron. With neither parallel nor concurrent edges, each cell is intrinsically rigid under revolute articulation about along each intersection line, indicating that the self-evident foldability of a CS must involve additional off-axis mobilities of each pair of slots. Examination of small-scale models reveals that the flat-folded condition is admitted by sliding and scissor-twisting of each pair of interlocking slots as required, in combination enabling pairs of misaligned slots in coplanar slices to remain engaged without incurring any elastic strain: a CS is, at least, bistable though this requires imperfect articulation of the slots.

Insight into the compliant folding motion is gained by examination of the articulation of a single skew cell – an anti-symmetric midplane cell from a helix whose symmetry reduces the additional compliances required – via a modified equivalent bar linkage in which additional mobilities are incorporated along the minor edges. The articulated cell is reconstructed upon the linkage, and the misalignment of the facet edges is decomposed into two orthogonal components for each slot: an in-plane rotation of the interlocking slice through the slot, which does not incur any elastic deformation; and an out-of-plane rotation of the interlocking slice, which is incompatible. This model verifies that the cells undergo a bistable, compliant transition with each slot required to accommodate some out-of-plane rotation of the interlocked slice during motion. Examination of the physical models reveals that this is accommodated by out-of-plane deflection of each 'flap' which 'splays' the slots as necessary. A simple model of this action is incorporated into the reconstructed cell by the addition of a diagonal 'twist line' across each flap. This captures a realistic articulation of the cell and demonstrates that local deformation is sufficient to enable the full range of folding motion. This model is an upper-bound on the deformation required for this cell because it does not include off-axis rotation of the major intersections nor sliding along any intersection, both of which will reduce the total elastic deformation required.

This geometric model of an anti-symmetric, midplane helical cell is viable because its symmetry reduces the configuration space to two dimensions, and the misfit is identical at both minor intersections. A purely geometric model of a general skew cell would be

significantly more complex due to the increased number of degrees of freedom required, with sliding and off-axis rotation necessary along each intersection. The motion of the complete sliceform is yet more complex and is likely to include out-of-plane bending of the slices, much as in an RS. However, it is clear that the combination of the intrinsic deformations of each cell – slot-splaying to enable scissor-twisting and slot-sliding – and the extrinsic deformations of each slice – slice-bending – is sufficient to enable the folding motion.

Two approaches to construction of the 'inherent' geometry of a CS have been designed based on projection of the cells outward from the array of tetrahedra, either to a set of concordantly generated points along each intersection line or to a 'ribbon' surface generated directly from the basis curve. This was pursued in the interest of translating the structural geometry of a CS to a more conventional form as a scissor-grid, but it is evident that the deployable motion would not be replicated by such a linkage, even with elastic deformation of the links, due to imperfect articulation (scissor-twisting and sliding) required of the interlocking slots along each intersection line.

9.2.1 Future work

Although the design of a CS is not readily translated to the design of an equivalent deployable linkage, the CSs synthesised in this thesis demonstrate that a large range of folding structures can be generated as sliceforms.

The 'aesthetic proxy' utilised to drive the selection of a well-conditioned parameterisation which enhances the deployability of each CS (by pursuing a 'balanced' design in which the structure is relatively self-similar and consistent in form along its length) is merited by the insight that symmetry is the key requirement for flat-foldability of an RS. Though such symmetry is not forthcoming for all but the simplest CS designs, it is clear that the basic scheme produces ill-conditioned results for more complex basis curves and the balanced designs generated through this aesthetic approach are a significant improvement, as evidenced by the ready foldability of the small-scale physical models (and are aesthetically pleasing too). Parameter selection is aided by evaluation of more objective heuristics – *e.g.* the variation in angle subtended between successive pairs of slices – but is ultimately reliant on the designer's judgment and a more concrete metric for foldability remains desirable. Now that some insights into the compliant articulation have been derived, in particular that an anti-symmetric cell is flat-foldable without requiring sliding, it would be interesting to explore whether a design process might be developed which sets the parameterisation to minimise the misfit required during folding and/or when flat-folded. For instance, a more

objective approach may be possible in which, for a given curve, the parameterisation of the structural architecture is set such that the primary row of cells are all anti-symmetric, even if the curve is non-uniform.

Alternatively, inspired by these designs, a simpler folding structure could be generated from each curve by generating a staggered series of pyramidal cells forming a single row where the apex of each is offset along their mutual contact edge such that the polyline connecting them traces the basis curve, each pyramid sweeping the angle subtended between successive segments. Such an approach would guarantee rigid-folding, and flat-folding may also be viable.

9.3 Wider implications

The investigations conducted in this research add to the growing body of literature demonstrating the influence of local compliances on the overall structural behaviour of some folding structures, in this case being essential to the folding action of both an RS and a CS. The representative degrees-of-freedom introduced into the simplified model may not capture the exact articulation of the real-world system, but, through careful selection, enable deep insights to be drawn from purely geometric analyses – in particular a clear understanding of the folding behaviour of an RS and characterisation of the influence of both the initial design parameterisation and the component compliance in enabling it.

These insights are sufficient to directly inform the design of a range of folding rotational sliceforms and guide the exploration of the wider design space for sliceform structures through development of the generalised protocol for curve sliceforms. This conceptual approach could readily be extended to drive innovations in other deployable technologies, particularly discovery of other compliant-folding systems by geometric generalisation of existing rigid-folding forms.

Similarly, the use of an algorithmic design method enables an interactive exploration of a wide parameter space of possible designs. Use of rapid fabrication methods to manufacture a sample of designs at small scale enhances this, with informal observations of the resulting structural behaviour guiding their analysis. Further, by linking their analysis directly to their structural geometry through simplified representative models, design principles and limits are readily inferred and implemented. Such an integrated approach could prove useful in the development of other highly geometric folding and non-folding structural technologies in which deformations are critical to their function – such as metamaterial-like origami-architectured structures designed for impact absorption devices, *for example*.

References

[1] Arnouts, L. I., Massart, T. J., de Temmerman, N., and Berke, P. Z. (2019). Computational design of bistable deployable scissor structures: Trends and challenges. *Journal of the International Association for Shell and Spatial Structures*, 60(1):19–34.

[2] Balkcom, D. J. and Mason, M. T. (2008). Robotic origami folding. *The International Journal of Robotics Research*, 27(5):613–627.

[3] Calladine, C. (1978). Buckminster Fuller's "Tensegrity" structures and Clerk Maxwell's rules for the construction of stiff frames. *International Journal of Solids and Structures*, 14(2):161–172.

[4] Calladine, C. R. (1983). *Theory of Shell Structures*. Cambridge University Press, Cambridge, 1st edition.

[5] Callens, S. J. and Zadpoor, A. A. (2018). From flat sheets to curved geometries: Origami and kirigami approaches. *Materials Today*, 21(3):241–264.

[6] Cheung, K. C., Tachi, T., Calisch, S., and Miura, K. (2014). Origami interleaved tube cellular materials. *Smart Materials and Structures*, 23(9):094012.

[7] Cignoni, P., Pietroni, N., Malomo, L., and Scopigno, R. (2014). Field-aligned mesh joinery. *ACM Transactions on Graphics*, 33(1):1–12.

[8] Conn, A. T. and Rossiter, J. (2012). Smart Radially Folding Structures. *IEEE/ASME Transactions on Mechatronics*, 17(5):968–975.

[9] Connelly, R. and Guest, S. (2015). Finite Mechanisms. In *Frameworks, Tensegrities and Symmetry: Understanding Stable Structures*, chapter 8, page 151. Cornell Univ., College Arts Sci.

[10] Connelly, R., Sabitov, I., and Walz, A. (1997). The Bellows Conjecture. *Beiträge zur Algebra und Geometrie*, 38(1):1–10.

[11] Coxeter, H. S. M. (1989). *Introduction to Geometry*. Wiley, 2nd edition.

[12] Cundy, H. M. and Rollett, A. P. (1954). *Mathematical Models*. Clarendon Press, 1st edition.

[13] Davis, L., Rippmann, M., Pawlofsky, T., and Block, P. (2011). Efficient and Expressive Thin-tile Vaulting using Cardboard Formwork. In *Proceedings of the IABSE-IASS Symposium*, London, UK.

[14] De Temmerman, N. (2007). *Design and Analysis of Deployable Bar Structures for Mobile Architectural Applications*. PhD, Vrije Universiteit Brussel.

[15] Dudte, L. H., Vouga, E., Tachi, T., and Mahadevan, L. (2016). Programming curvature using origami tessellations. *Nature Materials*, 15(5):583–588.

[16] Escrig, F. (1985). Expandable Space Structures. *International Journal of Space Structures*, 1(2):79–91.

[17] Escrig, F., Sánchez, J., and Valcarcer, J. P. (1996). Two Way Deployable Spherical Grids. *International Journal of Space Structures*, 11(1-2):257–274.

[18] Escrig, F. and Valcarcel, J. (1993). Geometry of Expandable Space Structures. *International Journal of Space Structures*, 8(1-2):71–84.

[19] Fei, L. J. and Sujan, D. (2013). Origami Theory and its Applications: A. *Computer Science, Engineering*, 7(1):1131–1135.

[20] Filipov, E., Liu, K., Tachi, T., Schenk, M., and Paulino, G. (2017). Bar and hinge models for scalable analysis of origami. *International Journal of Solids and Structures*, 124:26–45.

[21] Filipov, E. T., Paulino, G. H., and Tachi, T. (2016). Origami tubes with reconfigurable polygonal cross-sections. *Proceedings of the Royal Society A: Mathematical, Physical and Engineering Sciences*, 472(2185).

[22] Filipov, E. T., Paulino, G. H., and Tachi, T. (2019a). Deployable Sandwich Surfaces with High Out-of-Plane Stiffness. *Journal of Structural Engineering*, 145(2).

[23] Filipov, E. T., Tachi, T., and Paulino, G. H. (2015). Origami tubes assembled into stiff, yet reconfigurable structures and metamaterials. *Proceedings of the National Academy of Sciences*, 112(40):12321–12326.

[24] Filipov, E. T., Tachi, T., and Paulino, G. H. (2019b). Coupled Origami Tubes for Stiff Deployable Cantilevers. In *Proceedings of the ASME 2019 International Design Engineering Technical Conferences and Computers and Information in Engineering Conference.*, volume 5B, pages 1–9. American Society of Mechanical Engineers.

[25] Gantes, C. and Konitopoulou, E. (2004). Geometric design of arbitrarily curved bistable deployable arches with discrete joint size. *International Journal of Solids and Structures*, 41(20):5517–5540.

[26] Gantes, C. J., Connor, J. J., Logcher, R. D., and Rosenfeld, Y. (1989). Structural analysis and design of deployable structures. *Computers & Structures*, 32(3):661–669.

[27] García-Mora, C. J. and Sánchez-Sánchez, J. (2020). Geometric method to design bistable and non - bistable deployable structures of straight scissors based on the convergence surface. *Mechanism and Machine Theory*, 146.

[28] García-Mora, C. J. and Sánchez-Sánchez, J. (2021). The convergence surface method for the design of deployable scissor structures. *Automation in Construction*, 122.

[29] Gattas, J. and You, Z. (2015). Geometric assembly of rigid-foldable morphing sandwich structures. *Engineering Structures*, 94:149–159.

[30] Grey, S. W., Scarpa, F., and Schenk, M. (2021). Embedded actuation for shape-adaptive origami. *Journal of Mechanical Design, Transactions of the ASME*, 143(8):1–8.

[31] Guest, S. D. and Fowler, P. W. (2014). Symmetry-extended counting rules for periodic frameworks. *Philosophical Transactions of the Royal Society A: Mathematical, Physical and Engineering Sciences*, 372(2008).

[32] Hanaor, A. and Levy, R. (2001). Evaluation of Deployable Structures for Space Enclosures. *International Journal of Space Structures*, 16(4):211–229.

[33] Hart, G. W. (2004). "Slide-Together" Geometric Paper Constructions. In Alagic, M. and Sarhangi, R., editors, *Bridges for Teachers, Teachers for Bridges*, pages 31–42.

[34] Hart, G. W. (2007). Modular Kirigami. In *Bridges Donostia: Mathematics, Music, Art, Architecture, Culture*. Stony Brook University.

[35] Hildebrand, K., Bickel, B., and Alexa, M. (2012). crdbrd: Shape Fabrication by Sliding Planar Slices. *Computer Graphics Forum*, 31(2):583–592.

[36] Hoberman, C. (1991). Patent 5,024,031. Radial expansion/retraction truss structures.

[37] Howell, L. L. and Midha, A. (1994). A Method for the Design of Compliant Mechanisms With Small-Length Flexural Pivots. *Journal of Mechanical Design*, 116(1):280–290.

[38] Howell, L. L., Midha, A., and Norton, T. W. (1996). Evaluation of Equivalent Spring Stiffness for Use in a Pseudo-Rigid-Body Model of Large-Deflection Compliant Mechanisms. *Journal of Mechanical Design*, 118(1):126–131.

[39] Hudert, M., Scholte-Wassink, J., and Kotnik, T. (2018). Interlocking Particle Structures: Design and Fabrication of a Medium Scale Demonstrator. In *Form and Force: Proceedings of the IASS Symposium*, Boston.

[40] Hunt, K. H. (1978). *Kinematic Geometry of Mechanisms*. Clarendon Press, Oxford.

[41] Kassabian, P. E., You, Z., and Pellegrino, S. (1999). Retractable Roof Structures. *Proceedings of the ICE - Structures and Buildings*, 134(1):45–56.

[42] Krishnan, S. and Liao, Y. (2020). Geometric Design of Deployable Spatial Structures Made of Three-Dimensional Angulated Members. *Journal of Architectural Engineering*, 26(3):04020029.

[43] Lam, C. D. (2008). Make a sliceform prototype. *Computer Arts Magazine*, pages 102–107.

[44] Langbecker, T. (1999). Kinematic Analysis of Deployable Scissor Structures. *International Journal of Space Structures*, 14(1):1–15.

[45] Le-Nguyen, T.-V., Low, K.-L., Ruiz, C., and Le, S. N. (2013). Automatic Paper Sliceform Design from 3D Solid Models. *IEEE Transactions on Visualization and Computer Graphics*, 19(11).

[46] Lebée, A. (2015). From Folds to Structures, a Review. *International Journal of Space Structures*, 30(2):55–74.

[47] Lu, Y. and Demaine, E. D. (2015). A Pattern Tracing System for Generating Paper Sliceform Artwork. In Delp, K., Kaplan, C. S., McKenna, D., and Sarhangi, R., editors, *Proceedings of Bridges 2015: Mathematics, Music, Art, Architecture, Culture*, pages 367–370, Baltimore.

[48] Luecking, S. (2006). Creating Sliceforms with 3D Modelers. In *Bridges London: Mathematics, Music, Art, Architecture, Culture*, pages 631–638.

[49] Lusk, C. (2013). Using Pseudo-Rigid Body Models. In Howell, L. L., Magleby, S. P., and Olsen, B. M., editors, *Handbook of Compliant Mechanisms*, chapter 5. John Wiley & Sons, Incorporated, 1 edition.

[50] MathWorks (2019). Matlab R2019a.

[51] Maxwell, J. C. (1864). On reciprocal figures and diagrams of forces. *Philosophical Magazine Series 4*, 27(182):250–261.

[52] Mccrae, J., Mitra, N. J., and Singh, K. (2013). Surface perception of planar abstractions. *ACM Transactions on Applied Perception*, 10(3):1–20.

[53] McCrae, J. and Singh, K. (2016). Patent 10,262,457. System and method for generating planar section 3d shape representations.

[54] McCrae, J., Umetani, N., and Singh, K. (2014). FlatFitFab. In *Proceedings of the 27th annual ACM symposium on User interface software and technology*, pages 13–22, New York, NY, USA. ACM.

[55] McNeel, R. and Associates (2015). Rhinoceros5.

[56] Mitani, J. and Suzuki, H. (2003). Computer Aided Design for 180-degree Flat Fold Origamic Architecture with Lattice-type Cross Sections. *Journal of Graphic Science of Japan*, 37 No. 3(101):3–8.

[57] Miura, K. (1970). Proposition of Pseudo-Cylindrical Concave Polyhedral Shells. In *Proc. IASS Symposium on Folded Plates and Prismatic Structures. Section I.*, Vienna, Austria.

[58] Miura, K. (1985). Method of packaging and deployment of large membranes in space. *The Institute of Space and Astronautical Science report*, 618:1–9.

[59] Monera, M. G. (2020). Cardboard Construction of the Sphere by the Stereographic Projection. In Yackel, C., Bosch, R., Torrence, E., and Fenyvesi, K., editors, *Bridges 2020 Conference Proceedings*, pages 169–174.

[60] Monera, M. G. and Monterde, J. (2011). Building a Torus with Villarceau Sections. *Journal for Geometry and Graphics*, 15(1):41–47.

[61] Muñoz-Vidal, M., López César, I. R., Pérez-Valcárcel, J. B., and Riestra, F. S. (2019). A New Approach to Expandable Structures: Crossed Expandable Frames (X-Frames). *Journal of the International Association for Shell and Spatial Structures*, 60(4):294–305.

[62] Overvelde, J. T., de Jong, T. A., Shevchenko, Y., Becerra, S. A., Whitesides, G. M., Weaver, J. C., Hoberman, C., and Bertoldi, K. (2016). A three-dimensional actuated origami-inspired transformable metamaterial with multiple degrees of freedom. *Nature Communications*, 7(1).

[63] Overvelde, J. T. B., Weaver, J. C., Hoberman, C., and Bertoldi, K. (2017). Rational design of reconfigurable prismatic architected materials. *Nature*, 541(7637):347–352.

[64] Peraza-Hernandez, E. A., Hartl, D. J., Malak Jr, R. J., and Lagoudas, D. C. (2014). Origami-inspired active structures: a synthesis and review. *Smart Materials and Structures*, 23(9).

[65] Rommers, J., Radaelli, G., and Herder, J. L. (2017). Pseudo-Rigid-Body Modeling of a Single Vertex Compliant-Facet Origami Mechanism. *Journal of Mechanisms and Robotics*, 9(3):031009.

[66] Roovers, K., Alegria Mira, L., and de Temmerman, N. (2013). From Surface to Scissor Structure. In *Proceedings of the First Conference Transformables 2013*, pages 275–280.

[67] Roovers, K. and de Temmerman, N. (2014). A classification of singly curved deployable scissor grids. In Brazil, R. M. and Pauletti, R. M., editors, *Proceedings of the IASS-SLTE 2014 Symposium: "Shells, Membranes and Spatial Structures: Footprints"*, Brazilia, Brazil.

[68] Roovers, K. and de Temmerman, N. (2015). Digital design of deployable scissor grids based on circle packing. In *Proceedings of the International Association for Shell and Spatial Structures (IASS) Symposium 2015: Future Visions*, Amsterdam.

[69] Roovers, K. and De Temmerman, N. (2017). Deployable scissor grids consisting of translational units. *International Journal of Solids and Structures*, 121:45–61.

[70] Roovers, K. and de Temmerman, N. (2017). Geometric design of deployable scissor grids consisting of generalized polar units. *Journal of the International Association for Shell and Spatial Structures*, 58(3):227–238.

[71] Rutten, D. (2014). Grasshopper v0.9.0076.

[72] Sánchez-Cuenca, L. (1996). Geometric models for expandable structures. *WIT Transactions on The Built Environment*, 21:93–102.

[73] Schenk, M. and Guest, S. D. (2011). Origami Folding: A Structural Engineering Approach. In *Origami 5 Fifth International Meeting of Origami Science Mathematics and Education*.

[74] Schenk, M. and Guest, S. D. (2013). Geometry of Miura-folded metamaterials. *Proceedings of the National Academy of Sciences*, 110(9):3276–3281.

[75] Schwartzburg, Y. and Pauly, M. (2011). Design and Optimization of Orthogonally Intersecting Planar Surfaces. In *Computational Design Modelling*, pages 191–199. Springer Berlin Heidelberg, Berlin, Heidelberg.

[76] Schwartzburg, Y. and Pauly, M. (2013). Fabrication-aware Design with Intersecting Planar Pieces. *Computer Graphics Forum*, 32(2):317–326.

[77] Seffen, K. (2004). Bi-stable Concepts for Reconfigurable Structures. In *45th AIAA/ASME/ASCE/AHS/ASC Structures, Structural Dynamics & Materials Conference*, pages 236–249, Reston, Virigina. American Institute of Aeronautics and Astronautics.

[78] Sharp, J. (1998). Sliceform Sculptures-a Bridge between Art and Mathematics. In *Bridges: Mathematical Connections in Art, Music, and Science*, pages 275–276.

[79] Sharp, J. (1999). *Sliceforms: Mathematical Models from Paper Sections*. Tarquin Group, Norfolk.

[80] Sharp, J. (2002). Sliceform Surfaces and a Serendipitous Discovery. *The Quarterly of the International Society for the Interdisciplinary Study of Symmetry [Special Issue] Symmetry: Art and Science*, 2(1-4):123–130.

[81] Sharp, J. (2004). *Surfaces: Explorations with Sliceforms*. Tarquin Group, Norfolk.

[82] Surabhi, A. (2011). KRANIUM: Research and Methodology. Technical report, Royal College of Art, Imperial College London.

[83] Tachi, T. (2009a). One-DOF Cylindrical Deployable Structures with Rigid Quadrilateral Panels. In Domigo, A. and Lazaro, C., editors, *Proceedings of the International Association for Shell and Spatial Structures (IASS) Symposium 2009: Evolution and Trends in Design, Analysis and Construction of Shell and Spatial Structures*, pages 2295–2305.

[84] Tachi, T. (2009b). Simulation of Rigid Origami. In *Origami 4*, volume 4, pages 175–187. A K Peters/CRC Press.

[85] Tachi, T. (2010). Origamizing Polyhedral Surfaces. *IEEE Transactions on Visualization and Computer Graphics*, 16(2):298–311.

[86] Tachi, T. (2019). Introduction to Structural Origami. *Journal of the International Association for Shell and Spatial Structures*, 60(No. 1 March n. 199):7–18.

[87] Tachi, T., Filipov, E. T., and Paulino, G. H. (2015). Deployable Folded-core Sandwich Panels Guided by a Generating Surface. In *The International Association for Shell and Spatial Structures (IASS): Future Visions*.

[88] Tachi, T. and Miura, K. (2012). Rigid-Foldable Cylinders and Cells. *Journal of the International Association for Shell and Spatial Structures*, 53(no.4 December n.174):217–226.

[89] Tarnai, T. (2001). Infinitesimal and Finite Mechanisms. In Pellegrino, S., editor, *Deployable Structures*, chapter 7, pages 112–142. Springer-Verlag Wien GmbH.

[90] TodHunter, I. (1863). *Spherical Trigonometry for the use of Colleges and Schools*. Macmillan, Cambridge, 2nd edition.

[91] Turner, N., Goodwine, B., and Sen, M. (2016). A review of origami applications in mechanical engineering. *Proceedings of the Institution of Mechanical Engineers, Part C: Journal of Mechanical Engineering Science*, 230(14):2345–2362.

[92] You, Z. and Chen, Y. (2011). *Motion Structures*. Spon Press, Abingdon, Oxon, 1st edition.

[93] You, Z. and Pellegrino, S. (1996). Cable-stiffened pantographic deployable structures Part 1: Triangular mast. *AIAA Journal*, 34(4):813–820.

[94] You, Z. and Pellegrino, S. (1997). Foldable bar structures. *International Journal of Solids and Structures*, 34(15):1825–1847.

[95] Yu, H., Guo, Z., and Wang, J. (2018). A method of calculating the degree of freedom of foldable plate rigid origami with adjacency matrix. *Advances in Mechanical Engineering*, 10(6):1–20.

[96] Zanardo, A. (1985). Patent 4,557,083. Extensible Arm, Paricularly for Space Modules or Vehicles.

[97] Zeigler, T. R. (1976). Patent 3,968,808. Collapsible self-supporting structure.

Appendix A

Synthesis of a rotational sliceform

Digital models and slice templates for the rotational sliceforms featured in Part I are cultivated within Rhino via the Grasshopper plug-in for algorithmic modelling [55, 71]. This appendix provides additional details on the implementation of the 'sliceforming' process within this software.

A.1 Details of implementation

Details of the generation of an RS from a prescribed volumetric geometry are now provided. The core function is to provide a boundary representation of the target global volume and generate the sets of slice planes according to the structural architecture parameterisation so that the plane-brep intersection component can be used to generate the sets of cross-sectional planforms. These planforms are then processed by clipping when necessary and addition of slots along each line of intersection to generate the requisite set of slice templates by which the slices can be manufactured and a physical model of the sliceform then assembled.

A.1.1 Definition of geometric inputs

Global geometry

The volumetric target global geometry is specified by its exterior surface as a boundary representation ('B-Rep' or 'Brep'). Dedicated components are available for a few primitive shapes (spheres, cylinders, cuboids, cones) but more complex shapes can be specified as NURBS surfaces by other operations, such as by sweeping a curve about an axis of revolution (which is of particular use for generating rotational sliceforms), or by lofting through a set of curves (themselves specified using a variety of curve tools).

Structural architecture

The structural architecture of an RS consists of two sets of slice planes. Within Rhino/Grasshopper, planes are handled as a geometric object consisting of an origin point and set of orthogonal basis vectors. The sets of slice planes are generated by placing a *yz*-basis plane at an offset point from the origin, and then replicating the rotations illustrated in Fig. 4.2 using the rotation component to generate the first plane in each set and the polar array component to complete each set. The parameterisation of the architecture (number of planes per set, rotation from vertical – both specified by user-modifiable sliders) are direct inputs to these operations.

A.1.2 Generation of slice planforms and post-processing

The raw cross-sectional planforms corresponding to each slice plane are generated using the plane-brep intersection tool which returns a set of closed planar curves which can be filled to form each cross-section. For each slice plane, secondary portions are immediately discarded by keeping only those sections which lie at the origin of each slice plane – determined by finding the closest point on each section to the origin (curve closest point component) and keeping only the section with the smallest offset (a strict section-must-be-coincident-with-origin filter will discard all sections if the global geometry happens not to overlap these points, such as for the shell-like sliceforms of Section 4.4.5). These local sections are then clipped against the preceding and following slices to prevent self-intersection, essentially 'masking' each slice to maintain only those portions which remain within the semi-infinite area illustrated in Fig. 4.5(b). This is performed by splitting each slice along both its 'forward' and 'backward' limit lines (which are the lines of self-intersection with the preceding and following slices of the same set – generated using the plane-plane intersection tool after use of the 'relative item' output of the list item component to generate the appropriate pairs) to remove excess areas – achieved for each limit by using the line-curve intersection tool to find any points at which the slice outline crosses the limit, splitting the planform along a line drawn through these points (surface split) and then discarding the portion which does not cross the midline of the slice and closing the now open curve which remains – and then uniting the remaining portions (region union).

A separate routine is required for clipping the slices along the 'vertical' line (perpendicular to the axis about which the slice planes are initially rotated) which passes through the origin of the sliceform if the RS is parameterised with symmetrically inclined sets of slices and an even number of slices in each set. The 'dispatch' component enables an 'if-else' conditional

statement to be effected by supplying the planforms to this routine instead of the standard routine when these conditions are met.

Generating slots

With the slice planforms excised and clipped where necessary, the three-dimensional representation of the sliceform is complete. All that remains is to generate a suitable layout of slots upon each planform to complete the slice templates. The brep-brep intersection tool is again used to generate the array of intersection lines, which are then (re-)oriented to a consistent (outward) sense by aligning them to the vector product of the normal vectors to each corresponding slice pair. Each intersection is then split at its midpoint (or otherwise if the user desires) – by finding the midpoint by vector operation on the end points and then use of the 'shatter' component to split it into two segments – and slots are placed along the outer set of segments in one set, and *vice-versa*. The slots are created by using the region difference component to remove a rectangle corresponding to the slot (extended slightly beyond the planform of the slice to account for the inclination of the perimeter of the slice to the intersection at the open end of the slot) from the slice planform.

Layout for cutting

Finally, the completed slice templates are rotated to the *xy*-plane and laid-out for manufacture using a computer driven cutting tool. Most commercial equipment use proprietary software to setup each 'print', into which the templates can be imported as a DXF file (Drawing Exchange Format).In this project a Laserscript laser cutter was used to manufacture the larger RS designs from mountboard, and a Cricut tabletop cutting plotter used to manufacture the smaller RS and CS designs from card. For some designs a grid layout is sufficient, but in the interest of maximising material usage and thus manufacturing the largest possible model from a given sheet, a more efficient result is often obtained by 'nesting' the slices onto the cuttable area. Neither the of the cutting tool used offered sufficiently effective nesting tools to generate an efficient arrangement of the slices within their control software and so, the 'OpenNest' plugin is utilised to generate a layout of the templates within the Grasshopper/Rhino suite. Starting with a random slice, this plug-in sequentially places the slices into the cuttable area at arbitrary orientations until either all of the templates are in place or they overspill the maximum defined area, then repeats for a user specified number of iterations in search of an improved solution. If this is unsuccessful, the user can either re-run the tool with a different input 'seed' (a numerical value that feeds a pseudo-random-number-generator which then

defines the initial nesting order and rotation of each slice) to generate a different result which may then fit into the area (usually multiple runs are required to get a satisfactory solution if the efficiency required is high), or reduce the size of the model and re-try the layout operation until the templates have been fitted.

A.1.3 Tube-like sliceforms

A modified version of the standard script was required for generation of the 'tube-like' sliceform in Section 4.4.6. Specifically the challenge is that each cross-sectional planform contains a hole and is therefore defined by multiple curves. The methodology remains unchanged but modifications are required to the script to enable it to handle this increased geometric complexity. Modification is also required to the slot-generation routine which must now generate multiple, alternately oriented pairs of slots along each intersection line which spans the internal void.

Appendix B

Synthesis of a curve sliceform

Generation of a CS follows broadly the same principles and approaches as generation of an RS, though ensuring robustness is significantly more involved owing to their generalised geometric form.

B.1 Input parameters

The approach developed in this project has been designed with the objective of minimising user input – indeed only specification of the basis curve and parameterisation of the sliceform are required with all subsequent steps up until layout of the completed slice templates fully automated – whilst seeking to maximise the variety of basis curves along which sliceforms can be generated by taking as general and robust an approach as possible. Within the Rhino/Grasshopper algorithm the user is required to set:

- Any of the parameters for generation of each particular basis curve, *e.g.* radius, amplitude, angle subtended, length (these are specific to each design),
- The parameterisation of the swept-section: the target average radius, curvature exponent, and aspect ratio,
- The parameterisation of the structural architecture: the number of slice pairs, the rotation of each set of slices from the curve planes, a curvature attraction factor and exponent which control the distribution of curve points along the basis curve, the maximum number of cells that are to be formed (trim level)[1], and the facet extension factor (which sets the position of the trim line across each facet),

[1]The trim level sets the maximum number of facets enclosed cells to be formed above and below the basis curve. If set to '0' then the slices are not trimmed, if set to '-1' the slices are trimmed across their outermost

- The width of the slots and their orientation (used to invert the direction of the slots upon each set of slices)

Some other parameters relating to the implementation must also be provided:

- An overall scale factor (which allows for adjustment of the size of the design when seeking to fit the slice templates onto a given area of material),
- The number of cross-sections to be used when lofting the swept global volume along the basis curve,
- Inputs pertaining to the nesting routine (the dimension of the cutting area, a 'seed' which controls the pseudo-random order in which the slices are nested, the number of discrete rotations that are permitted (setting this to '4' dictates that the slices can be randomly rotated in increments of 90°, and so forth), the minimum spacing between the slices, and a margin between the layout and the border of the cutting area)

B.2 Details of implementation

The overall synthesis of a CS follows the four stages detailed in Section 6.4.1. Further details are now provided.

B.2.1 Fundamental geometry

Basis curve

The basis curve can be generated however the user wishes. Rhino/Grasshopper components are available for various primitive curves (circle, ellipse, arc, polygon with rounded vertices) or a more general curve can be defined as a NURBS curve (non-uniform rational b-spline) (by setting the control points, from which the curve is generated) or an interpolate curve (by setting the points through which the curve should pass). The latter approach is useful for setting an algebraic curve from its parametric equation, *e.g.* for the helix and spirals, by generating a series of closely-spaced points along its length through which the curve is generated. It is also possible to construct a curve by joining multiple segments, which may be NURBS curves, circular arcs or lines.

(dangling) facet which removes unnecessary area whilst preserving the natural connectivity of the sliceform at the given parameterisation

Structural architecture

The basic parameterisation of the structural architecture (N, θ^+, θ^-) is specified by the user as usual, and the curve points are generated along the basis curve at curve parameters ($0 \leq t \leq 1$) which may be evenly spaced or 'skewed' toward regions of high curvature according to the user-specified parameters using the method described in the main text.

The Frenet-Serret curve frames are generated directly from the basis curve using the 'curve frame' component at each curve point. The basis planes follow by inverting all curve planes following any inversion of curvature of the basis curve, located wherever the scalar product between consecutive normal vectors is negative. This apparently iterative procedure is achieved deterministically by first finding the scalar product between successive normal vectors and checking whether these are greater-than-or-equal-to zero (which returns a boolean list in binary form indicating where inversions have occurred), converting this to a series of corresponding ± 1's, and taking their cumulative product using the 'mass multiplication' component to yield a list of positive and negative 'ones' indicating whether each basis frame should be oriented to the curve frame (+1) or reversed from it (-1). The basis frame vectors follow by multiplying the curve frame basis vectors by these indicators, and the modified tangent and binormal vectors are rotated by $\theta^{\pm}$ about the local (adjusted) normal vector to generate each set of slice planes.

To accommodate the degenerate cases described in Section 6.4.2, curve frames at points of zero curvature are discarded prior to generation of the slice frames. Then, after correcting for reversals of curvature, curve frames at these points are generated by interpolating their basis vectors (or extrapolating if at the end of a curve) from the nearest slice frames that are well-defined. A subtlety here is that a straightforward interpolation of the normal and binormal vectors will not generally produce a perpendicular frame at intermediate points because the bracketing points that are well-defined usually lie slightly along the next curved section and so their normal vectors are not aligned to the straight segment. Therefore, the interpolated basis vectors are actually generated from the component of the basis vectors of the preceding/following frames that are perpendicular to the tangent vector at the interpolation point (which remains well-defined).

Swept section global geometry

The global volume is constructed by sweeping a surface through a series of cross-sections placed on perpendicular planes spaced along the length of the curve (inverted as necessary in

the same manner as the slice frames to account for reversals of curvature)[2]. A significantly larger number of swept-section points (versus slices in each set) are required to ensure overall smoothness. In principle any simple shape may be used to generate a swept global volume, but an elliptical section is suitably neutral whilst allowing the user to adjust its aspect ratio to refine the overall connectivity and conditioning of the resulting sliceform. The dimension of each cross-section is set in accordance with the curvature at each point along the length of the curve according to the user-defined 'section-skew' parameters.

B.2.2 Slice geometry

The basic cross-sectional slices of a CS are generated in much the same way as those of an RS – using the plane-brep intersection component to excise each cross-sectional planform, then discarding portions which are not coincident with the curve point – but the post-processing steps now require much more careful specification.

Slice clipping

Unlike an RS, the clip lines for slices of a CS (which lie along the lines of intersection between adjacent slices of the same set) are only coincident at their intersection with the major axis of each slice if the curve is planar. When they are not, the simple approach outlined for an RS is insufficient because the masking shape is no longer a simple chevron but includes the portion of the midline spanning the points where each clip line intersects with it (as in the first few slices of the ill-conditioned sliceform along the conical spiral in Fig. 6.12). Construction of the clipping routine therefore requires a more precise approach.

Firstly the clip lines are generated by locating the lines of intersection between each planform and the previous and following slice planes of the same set, locating the 'origin' of each clip line on the midline of the slice and generating the 'outward' unit vector by the vector product of the slice normals.

Then the points of intersection of this line and the perimeter curve are located. Points lying at a 'negative' position along the clip line are discarded and the perimeter curve is split at the points that remain (and at the point at which the perimeter curve crosses the midline of the slice on the inside of the curve if an odd number of points were indicating that the slice is clipped against both forward and backward neighbours). Then, only the main portion of the

[2]The 'sweep' component enables a surface to be generated from a single cross-section placed at the start of a 'rail' curve, but this provides no functionality to vary the cross-sectional dimension along the length of the curve and will also follow the intrinsic twist of the basis curve whereas the structural architecture does not, generating an ill-conditioned result if a a non-circular (elliptical) section is used.

planform perimeter (identified by checking which segment crosses the midline of the slice on the outside of the curve) and alternate sections thereon are retained with lines drawn between consecutive pairs of points to form the newly clipped edges of the slice. If an odd number of points were generated, an extra line is drawn from the remaining point to the 'origin' of the clip line. This is repeated for the clip line in the opposite sense, and the segment of the midline joining the clip line. Finally the remaining curve segments and newly drawn clip line segments are 'merged', yielding a multi-segment curve defining the clipped perimeter of the slice. This operation is robust to all viable geometric options and thereby does not require user interaction to account for the different cases that may arise depending on the input global geometry.

Intersection geometry

The intersection lines themselves are generated using the brep-brep intersection tool as for an RS, with 'sided' intersection vectors generated via the vector product of each pair of intersecting slices. Careful interrogation of the in-plane orientation of each intersection line is required to determine whether this is consistent with the 'outward' direction of each intersection line from the midplane of each slice (which is determined independently for each set of slices), and, by comparison of the inclination of successive intersection lines, the 'outward' direction relative to the facet enclosed (again, independently for each set of slices). This is necessary to know for later slice trimming operations.

It is also necessary to determine the domain of each intersection line which is well-formed – *i.e.* exclusive of segments which now form the edge of a trimmed slice – so that slots can be generated from the midpoint of this section. If the apex of a facet is contained within the planform of the slice, the intersection at its inner edge will span beyond the inner edge of the facet and construction of slots to the midpoint of its complete span may lead to segments of the slice becoming disconnected. Similarly those intersections that do not fully span the slice so that the apex of the enclosed facet lies within the planform are noted because generating slots along these intersections requires careful treatment later on.

B.2.3 Slice trimming

Slice 'trimming' involves the removal of excess portions of each planform if requested by the user. This is intuitive but again requires careful specification. The trimming procedure follows a similar approach to the clipping scheme with each trim line defined as the line subtending the facet outside the outermost intersection specified (or at a user specified

proportion at its facet angle, calculated by weighted sum of the corresponding intersection vectors). The intersections of this line with the planform perimeter define the trim points, through which the trim line is drawn and at which the planform curve is split, with the extraneous portion (which does not span the midline) then discarded. If the apex of the split facet lies within the slice, the trim line is drawn to that point, and then joined to the exposed segment of the next intersection line, and so forth until reaching the far side of the slice. This is not common and occurs only when the sliceform is parameterised so that the slices self-intersect significantly and are severely clipped. It is necessary to ensure that this operation is robust though so that ill-conditioned designs can be visualised and then improved.

A special case arises if a slice is trimmed through a facet spanning parallel intersection lines whose apex is not defined. This is readily resolved by generating a 'pseduo-apex' at the midpoint of the intersection of those lines with the clip line of the slice (which usually lies outside the slice planform), from which the trimming routine proceeds as usual.

For the outermost slices along an open curve where the array of intersections is not fully formed due to the lack of slices beyond the curve end, trim-lines are generated by rotating the outermost intersection outward by half (or other specified proportion) of the enclosed facet angle about that facet's apex, and proceeding as usual. This is particularly useful for removing excess portions of the slices at the CS ends.

B.2.4 Preparation for manufacture

Slot generation

Similarly to the clipping operation, generation of the slices in a CS requires a more delicate approach than for an RS. The problem is that the rectangular patches used for an RS must be extended beyond the planform of the slice to ensure that the slot opening is fully formed (otherwise a 'burr' remains whenever the perimeter is concave at the slot opening). However, if adjacent intersections meet within the planform of a slice so that the outer intersection terminates on a preceding intersection (as is the case at the outer edges of many ill-conditioned CS designs) any extension of the slot patch cuts into the inner facet. The slots must, instead, be constructed by drawing their outline directly. Firstly, a short line perpendicular to the intersection is constructed at the midpoint of the intersection line, forming the 'roof' of the slot (this direction determined by vector product of the intersection line and the slice plane normal). The slot edges are then projected from each end of this line, the slot 'shoulders', parallel to the intersection until reaching the perimeter of the slice planform (or an inner

intersection line) – this latter step is achieved by using the line-curve intersection tool to find the points where the slot edges cross the slice planform (usually one corresponding to either end of the intersection line) and selecting the point in the positive direction from the shoulder, or the line-line intersection tool when the intersection is known to be clipped against the preceding intersection line (as determined in the intersection geometry stage previously). Finally the segment of the boundary curve spanning the open ends is removed from the planform and replaced by the slot outline.

Layout for cutting

Layout of the slices proceeds as for an RS, using the OpenNest plugin to nest the templates within a defined cutting area. The Cricut desktop cutting plotter used to manufacture the CS models also has functionality to draw using a pen so labels are added to each slice to assist in selecting the correct slice during sequential assembly.